2012

Application of geosynthetic vertical drains under cyclic loads in stabilizing tracks

Jing Ni
University of Wollongong

Application of Geosynthetic Vertical Drains under Cyclic Loads in Stabilizing Tracks

A thesis submitted in fulfillment of the

requirements for the award of the degree

Doctor of Philosophy

from

University of Wollongong, NSW Australia

by

Jing Ni

School of Civil, Mining and Environmental Engineering

2012

Certification

I, Jing Ni, declare that this thesis, submitted in fulfillment of the requirements for the award of Doctor of Philosophy, in the Department of Civil Engineering, University of Wollongong, is wholly my own work unless otherwise referenced or acknowledged. The document has not been submitted for qualifications at any other academic institution.

_____

Jing Ni

10th May 2012

Abstract

Railways have technical and economic advantages, and therefore, railway traffic has gained a specific and irreplaceable position in recent years. With this background, and to satisfy their rapid development, railways will inevitably be constructed on soft soil subgrade such as soft clay subgrade. It is desired to understand the behaviour of soft clay subgrade subjected to cyclic loads when a new rail track is designed or an existing one is under maintenance. When the soft clay subgrade is subjected to the cyclic loading, excess pore pressures and axial strains keep developing with the increasing number of cycles, resulting in a decreased bearing capacity of the subgrade and excessive settlement. To improve the subgrade, prefabricated vertical band drains (PVDs) is used increasingly in popularity among a variety of techniques. With the installation of PVDs, a short radial drainage path is introduced to dissipate the excess pore pressure so that the soft clay subgrade becomes more stable subjected to train loads. This thesis covers the laboratory tests and numerical modelling. The behaviour of soft clays under cyclic loading with or without radial drainage is investigated.

A series of undrained cyclic triaxial tests were conducted on specimens of reconstituted Kaolinite. Three cyclic stress ratios and four loading frequencies were used in the laboratory tests to study the performance of soft subgrade soil subjected to cyclic loading. The effects of cyclic stress ratio and loading frequency on the generation of excess pore pressures and axial strains were investigated. The roles of cyclic stress ratio and loading frequency play in influencing the stability of soft clay subgrade were discussed. The effect of strain rate for a stress controlled test on the performance of soft clays under cyclic loading was investigated. The relationship between the strain rate and either cyclic stress ratio or loading frequency were figured out, and in this way, the influence of cyclic stress ratio and loading frequency on the progressive shear failure and excessive plastic deformation were justified. Furthermore, due to a high strain rate varying from 150 to 550 %/h for a stress controlled test, the slope of q/p' at failure for cyclic loading could increase compared to the condition of monotonic loading.

An undrained cyclic model has been proposed based on the modified Cam-clay model. A modified yield surface function during elastic unloading was proposed to capture the soil behaviour under cyclic loading. Only two additional cyclic degradation parameters ξ_1 and ξ_2 were introduced to present the yield surface during elastic unloading, in addition

to the parameters adopted in the modified Cam-clay model. These two cyclic degradation parameters controlled how much the size of the yield surface would shrink during an elastic unloading and how this reduction in the size of the yield surface would change with loading cycles. This model was verified against the laboratory experiments conducted. The cyclic degradation parameters ξ_1 and ξ_2 from the back calculation indicated that ξ_1 was a soil property which was independent of both the cyclic stress ratio and loading frequency, while ξ_2 depended on the loading frequency. This undrained cyclic model was further analysed by investigating the effects of consolidation stress ratio, parameters ξ_1 and ξ_2 on the predictions of the proposed model.

Large scale cyclic triaxial tests were conducted on specimens of reconstituted Kaolinite using the cylindrical dynamic triaxial equipment (accommodating 300 mm diameter and 600 mm height samples) which was designed and built at the University of Wollongong. To allow for radial drainage during and after the cyclic tests, a single PVD was installed in the centre of the soil cylinder. The effectiveness of radial drainage in dissipating the excess pore pressure was examined. It was found that for a high cyclic stress ratio, the radial drainage decelerated the rate of excess pore pressure build up to its critical value, so the soil could undergo more loading cycles prior to failure. With a low cyclic stress ratio, radial drainage could prevent the excess pore pressure from accumulating to its critical value, so the soil would not fail. The test results also suggested that for newly constructed railway lines, a train with a lower speed is preferred initially, until the track becomes stable for the next loading stage.

A radial consolidation model under cyclic loading has been proposed to capture the behaviour of soft clays subjected to cyclic loading when radial drainage is allowed during the loading period. This was achieved by combining the theory of radial consolidation with the undrained cyclic model. The effects of the stress history and dissipation of excess pore pressure on the generation of excess pore pressure were considered in the proposed model. This model was verified against the large scale cyclic triaxial tests conducted at the University of Wollongong. Analysis of this new model was carried out to investigate the effects of coefficient of radial consolidation, parameters ξ_1 and ξ_2 on the predictions of the proposed model. This model was further verified against a field case history in Sandgate, between Maitland and Newcastle. It is indicated that the stability of the soft soil subgrade could be improved effectively by the installation of PVDs.

Acknowledgements

Ten years ago, when I came to the University of Shanghai for undergraduate study, I thought probably it would be the highest education I could receive. Ten year later, when I have finished my thesis in University of Wollongong, I still can't believe that I will be granted the degree of Doctor of Philosophy in the near future. I would like to thank the following people for their help, cheerfulness, approachability, and enthusiasm during my postgraduate study.

Firstly, I would like to thank my principal supervisor, Prof. Buddhima Indraratna, who graciously welcomed me into the Centre for Geomechanics and Railway Engineering in University of Wollongong, provided me with a project that was challenging, and never gave up on me. Secondly, I would like to thank my co-supervisor, Cholachat Rujikiatkamjorn, who discussed with me in detail after each progress meeting, patiently checked every sentence in my program, and corrected my English for my papers and thesis. I would also like to thank Dr. Xue-Yu Geng, who is my co-supervisor, my friend and like my elder sister. I thank you for your insightful suggestions on how to make my model more understandable and acceptable. I will always remember the happy time we got together playing yoga in the Gym, learning to swim in the swimming pool, surfing at the beach in Kiama, and enjoying the flower show (Floriade 2011) in Canberra.

I would like to thank all the technicians, who helped in the lab so that I could finish all the small scale and large scale triaxial tests on time. I would like to thank Zhuo Wang, who started his postgraduate study at the same time as I did and will also get his PHD degree shortly. I will never forget the 1,000 cups of coffee we had together in Piccasso, talking about the research work, and our dreams for life and work, and getting me through those days of stress and self-doubt. I would also like to thank my friends Yi Wang, Zhen-Yu Zhang, Yu Han, Guang-Hui Meng, Lei Zhang, Da-Lin Cai, Zhong-Wei Wang, Qi-Deng Sun who brought me laugh when I was in sadness, and gave me cheerfulness when I was disappointed.

At lastly, I would like to thank my parents, who gave me the biggest support and understanding all the way here. While my parents' friends already played with their grandson or granddaughter, my parents were concerned about whether I was used to the life in Australia and whether I could finish my study. Thank you for allowing me to trace my dream and I feel very fortunate to have parents like you.

Publications

Published work

Ni, J., Indraratna, B., Geng, X. Y., and Rujikiatkamjorn, C. (2012). "The effect of the strain rate on soft soil behaviour under cyclic loading." *11th Australia New Zealand Conference on Geomechanics: Ground Engineering in a Changing World*, 15-18 July, Melbourne, Australia.

Indraratna, B., Rujikiatkamjorn, C., and Ni, J. (2011). "Cyclic behaviour of soft soil subgrade improved by prefabricated vertical drains." *International Symposium on Deformation Characteristics of Geomaterials*, 1-3 Septembe, Seoul, Korea.

Indraratna, B., Ni, J., and Rujikiatkamjorn, C. (2010). "Investigation on effectiveness of a prefabricated vertical drain during cyclic loading." *Materials Science and Engineering*, 10, 1–8.

In preparation

Ni, J., Indraratna, B., Geng, X. Y., and Carter, J. P. "Radial consolidation of soft soils under cyclic loads."

Table of Contents

List of Figures

List of Tables

List of Symbols

a	width of prefabricated vertical drain
a_{ex} , a_{re}	modified width of PVD for experimental test and real width of PVD, respectively
b	PVD thickness
b_{ex} , b_{re}	modified thickness of PVD for experimental test and real thickness of PVD, respectively
c_h	horizontal coefficient of consolidation
$\bar{c}_h$	horizontal coefficient of consolidation under cyclic loading
c_v	vertical coefficient of consolidation
C_c	compression index
C_s	swelling index
CSL	critical state line
CSR	cyclic stress ratio
CSR^*	critical cyclic stress ratio
d_e	diameter of influence zone
d_w	equivalent diameter of drain
$d\varepsilon_s^e$, $d\varepsilon_s^p$	incremental elastic and plastic shear strains
$d\varepsilon_v^e$, $d\varepsilon_v^p$	incremental elastic and plastic volumetric strains
dq	incremental deviator stress
du_p , du_u	internal excess pore pressure generated during partially drained and undrained cyclic loading
D	wheel diameter
$D_{granular}$	density of granular layer
$D_{subgrade}$	density of subgrade layer
e	void ratio
e_0	initial void ratio
E_r	resilient modulus
f	cyclic loading frequency
G	shear modulus
G_s	specific gravity
G_{s1}	cyclic secant shear modulus in the first cycle of shearing with a constant shear strain
G_{sN}	cyclic secant shear modulus after N cycles of shearing with a constant shear strain
$H_{granular}$	thickness of granular layer
k_0	horizontal permeability at the boundary of drain and soil
k_h	undisturbed horizontal permeability

k_s	smear zone permeability
k_v	vertical permeability
K	bulk modulus
K_s^z	stress coefficient of uniform distribution
K_t^z	stress coefficient of triangle distribution
l	length of drain
$l_{sleeper}$	length of sleeper
m	slope of the $q_{u,s}/\sigma'_{vc}$ versus OCR relation on a log-log plot
$m_{sleeper}$	mass of sleeper
m_v	coefficient of compressibility
$m_{vp'}$	coefficient of compressibility in triaxial condition
M	slope of critical state line in $q-p'$ space
M_c	slope of critical state line in $q-p'$ space for cyclic loading
M_m	slope of critical state line in $q-p'$ space for monotonic loading
N	number of loading cycles
N_f	number of loading cycles at failure
NCL	normal compression line
OCR	overconsolidation ratio
p'	mean effective stress
p'_0	initial mean effective stress
p'_{c0}	pre-consolidation stress
p'_{cl}	yield stress corresponding to peak deviator stress
p'_{cu}	yield stress after unloading part of each cycle
P_d	design wheel load
P_s	static wheel load
P_u	unsprung weight at one wheel
p'_y	loading parameter
PI	plastic index
PVD	prefabricated vertical drain
q_a	average deviator stress
p'_y	loading parameter
q_0	initial deviator stress
q_{cyc}	cyclic deviator stress
q^*_{cyc}	critical cyclic deviator stress
q_w	drain discharge capacity
$q_{u,c}$	undrained shear strength for cyclic loading

$q_{u,s}$	undrained shear strength for static loading
$q_{u,s}^0$	value of $q_{u,s}$ at the reference strain rate, $\dot{\varepsilon}_{a,s}^0$
$q_{yielding}$	yield stress for each cycle
r_e	radius of influence zone
$r_{e,ex}$, $r_{e,re}$	radius of influence zone of experimental and real soil cylinders, respectively
r_w	equivalent radius of drain
$r_{w,ex}$, $r_{w,re}$	equivalent radius of modified and real PVDs, respectively
r_u	normalised excess pore pressure
S_d	drain spacing
S_{OCR}	value of $q_{u,s} / \sigma_{vc}^{'}$ when $\mathrm{OCR} = 1$
$S_{sleeper}$	sleeper spacing
s_q	sensitivity of the strain rate
t	time
t_f	time at failure
t_f^0	reference time at failure
t_δ	degradation parameter of cyclic shear modulus
t_{total}	total time
T_h	time coefficient for vertical consolidation
T_v	time coefficient for horizontal consolidation
u	excess pore pressure
u_a	average excess pore pressure
u_{cyc}	cyclic excess pre pressure
u_p	internal generation of excess pore pressure in partially drained test
U_h	average degree of consolidation due to radial drainage
$U_{h,ex}$, $U_{h,re}$	average degree of consolidation for experimental and real soil cylinder, respectively
U_v	average degree of consolidation due to vertical drainage
v	specific volume, vehicle speed
v_0	initial specific volume
v_z	flow velocity in the z direction
w	water content
w_L	liquid limit
w_p	plastic limit
$W_{sleeper}$	weight of sleeper
W_{rail}	weight of rail
z	depth

Greek symbols

α	experimental parameter for predicting the relationship between u/u_f and N/N_f
β	experimental parameter for predicting the relationship between u/u_f and $\varepsilon_a/\varepsilon_{af}$
δ	degradation index of cyclic shear modulus
Δu_d	dissipation of excess pore pressure in partially drained test
Δu_p	incremental internal generation of excess pore pressure in partially drained test
Δu_u	incremental internal generation of excess pore pressure in undrained test
ε_a	axial strain
ε_{af}	axial strain at failure
$\dot{\varepsilon}_a$	axial strain rate
$\varepsilon_{a,a}$	average axial strain
$\varepsilon_{a,cyc}$	cyclic axial strain
$\varepsilon_{a,cycle}$	axial strain for half cycle
$\dot{\varepsilon}_{aL,s}$	strain rate for stress controlled cyclic loading
$\dot{\varepsilon}_{aL,s}$	strain rate for static loading
$\dot{\varepsilon}^0_{aL,s}$	reference strain rate for static loading
ε_s	shear strain
ε_v	volumetric strain
ϕ	impact factor for static wheel load
$\varphi_{p'}$	effective stress friction angle
$\phi_{subgrade}$	coefficient of the axle load on the subgrade
Γ	slope of critical state line in $v - \ln p'$ space
γ_{cyc}	cyclic shear strain
γ^*_{cyc}	cyclic threshold shear strain
γ_w	unit weight of water
η	material parameter for predicting the relationship between ψ and CSR
κ	slope of unloading-reloading line in $v - \ln p'$ space
λ	slope of normal compression line in $v - \ln p'$ space
λ_h	coefficient of finite difference method for radial consolidation
λ_z	coefficient of finite difference method for vertical consolidation
θ	cyclic loading parameter
θ^*	modified cyclic loading parameter
ϑ	material parameter for predicting the relationship between ψ and CSR

ρ_{rail}	mass unit length of rail
$\sigma_1^{'}$, $\sigma_2^{'}$, $\sigma_3^{'}$	principal effective stress
$\sigma_{3c}^{'}$	minor principle stress for consolidation
σ_d	dynamic stress at the surface of the subgrade
σ_{track}	vertical stress from track structure
$\sigma_{granular}$	vertical stress from granular layer
$\sigma_h^{'}$	horizontal effective stress
$\sigma_v^{'}$	vertical effective stress
$\sigma_{vc}^{'}$	vertical effective stress for consolidation
τ_1	cyclic shear stress in the first cycle of shearing with a constant shear strain
τ_N	cyclic shear stress after N cycles of shearing with a constant shear strain
ω	cyclic load angular frequency
ξ_1, ξ_2	cyclic test related constant
ψ	experimental parameter for predicting the relationship between axial strain rate and time
ζ	decay constant for predicting the relationship between axial strain rate and time

1 Introduction

1.1 Background

Trains have a history of about 200 years, ever since Stephenson created the first train in Britain in 1814. Over the following decades the train has gradually become an important means of transport. In recent years, railway traffic has gained a specific and irreplaceable position for the following three reasons:

(a) Transportation capacity and price. It enables and facilitates the transportation of goods, which by a different mode would be too expensive and therefore inefficient. And it enables the transportation of larger quantities of goods for long or medium distances at relatively low costs.

(b) Direct access to the city centre. While air transport for a typical journey includes time for checking in, a security screen and transfer of goods from the city centre, the entire journey by high speed rail can take much less time.

(c) Safety. A comparison between rail traffic with other modes of transport shows that it is undoubtedly the most reliable mode, but this is not only the result of less traffic accidents, there are also fewer losses incurred from these accidents. The high level of safety makes rail traffic one of the most favourable modes of transport.

Railways have technical and economic advantages that are consistent with a sustainable development strategy, which is why many countries around the world are giving more and more attention to developing them. Indeed there is a worldwide wave of railway reform. With this background, and to satisfy their rapid development, railways will inevitably be constructed on undesired soft soils. Take the newest railway system in Australia for example, most train lines are located along the east coast where there are plenty of soft clays characterised by low bearing capacity, high compressibility, and low permeability. Thus it is of great importance to understand the performance of soft clays under train induced cyclic loading for the purpose of either constructing new lines or maintaining existing ones.

1.2 Statement of the problem

Studies on cyclic loading were first conducted on sands because the liquefaction of sands causes ground failure during earthquakes. As cyclic loading progresses, excess pore pressure increases and the mean effective stress ($p' = \left(\sigma_1' + \sigma_2' + \sigma_3'\right)/3$, where σ_1', σ_2', and σ_3' are principle stresses) is correspondingly reduced. When the normalised excess pore pressure ($r_u = u/\sigma_{3c}'$ for triaxial tests, where σ_{3c}' is the minor principle stress for consolidation, or $r_u = u/\sigma_{vc}'$ for field conditions, and where σ_{vc}' is the vertical effective stress for consolidation) increases to a maximum value of 100%, soils have zero effective stress, which has been defined as liquefaction. However, recent site investigations on ground failure in low-plasticity silts and clays during strong earthquakes have illustrated the fact that the development of significant strains and loss of strength can be triggered by earthquake loading in a wide range of saturated soils, from sands to clay (Chu et al. 2004; Bray et al. 2004a). To evaluate whether the true behaviour of the soil is best described as liquefaction (i.e., sand-like soil behaviour) or cyclic softening (i.e., clay-like soil behaviour), some detailed studies have been conducted (Seed and Idriss 1982; Koester 1992; Andrews and Martin 2002; Bray et al. 2004b; Seed et al. 2003; Boulanger and Idriss 2006).

The results of the cyclic stress-strain and stress path responses of the majority of clays indicated that undrained cyclic shear results in a progressive increase in excess pore pressure to some limiting level $r_u < 100\%$, at which time dramatic strains with each subsequent loading cycle develop. For simplicity, the soils referred to in the following studies are only those that have clay-like behaviour.

When the soft clay subgrade is subjected to the cyclic loading, excess pore pressures and axial strains keep developing with the increasing number of cycles, resulting in a decreased bearing capacity of the subgrade and excessive settlement. Thus, the accumulation of excess pore pressure and excessive plastic deformation of the soft clay subgrade under repeated loading is always a grave concern for highway pavements and railway tracks (Yamanouchi et al. 1975; Kutara et al. 1980; Li and Selig 1996; Chai and Miura 2002; Wilson and Green-wood 1974; Lee and Focht 1976).

This situation seems to be getting worse as heavy axle loads and high speed trains are going to be used to satisfy the transport of passengers and freights both in quantity and speed. The magnitude and frequency of the resulting dynamic stress will be increased and the deterioration of the subgrade will be exacerbated. To improve the foundations, the installation of vertical drains is a widely used method to enable the short radial drainage path to accelerate the dissipation of excess pore pressure, effectively transferring the external load from the pore water to the skeleton of the foundation. Among the different types of vertical drains, the use of prefabricated vertical drains (PVDs) is increasing because their construction is cheaper and their installation has the least disturbance of the surrounding soils (See Fig. 1.1). Recently, the installation of PVDs has been found useful in improving the subgrade under cyclic loading (Indratana et al. 2009; Indraratna et al. 2010), in addition to its conventional application under static loading during the construction stage.

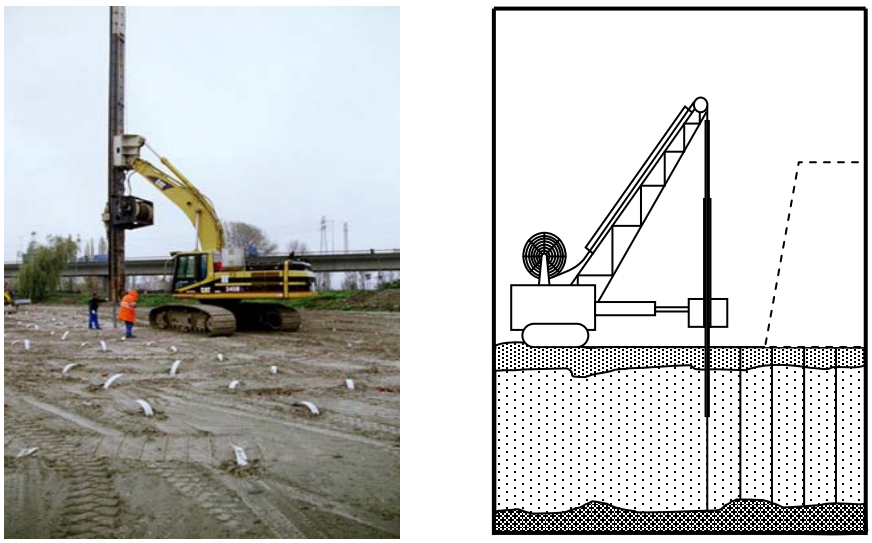

(a) (b)

Fig. 1.1 The installation of prefabricated vertical drains: (a) In site photograph, (b) Schematic drawing

The scope of this thesis covers the laboratory tests, including the undrained cyclic loading tests and partially drained cyclic loading tests with a single PVD installed in the centre of the soil cylinder, and models which can predict the behaviour of soft clays with or without drainage under cyclic loading.

This chapter explains the properties of train induced dynamic stress which subgrade is subjected to, the fundamental behaviour of soft subgrade soils under this dynamic stress through laboratory tests, and how prefabricated vertical drains accelerate cyclic consolidation and therefore increase the stability of the subgrade. The objectives and content of this thesis are presented at the end of this chapter.

1.2.1 Dynamic stress from train load

Conventional railway structure consists of rail track structure and substructure, as shown in Fig. 1.2. The configuration of rail track structure is characterised by two parallel rail beams resting on regularly spaced sleepers through elastic fastening or resilient pads (Cai and Raymond 1994). Substructure usually has layers of ballast, subballast, and subgrade.

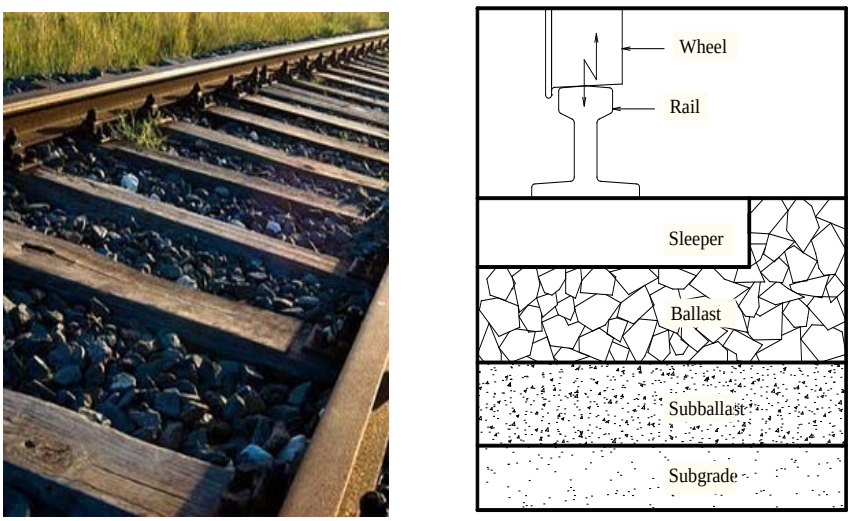

(a) (b)

Fig. 1.2 Configuration of rail track system: (a) Photograph of ballast railway structure, (b) Profile of railway structure

When railway structures are designed the various sources of their loads must be considered. In addition to the dead load of the structure itself, live loads from the traffic being carried must be taken into account. In a typical railway structure, live loads dominate all of the other design considerations.

When subgrade is subjected to the dynamic stress transferred from the track structure through the granular layers (ballast and subballast), it deforms and deteriorates, which results in a worse support for the structure above it. This is why subgrade can have a

significant influence on the performance of a railway structure. Differences in the conditions of the subgrade can cause variations in the characteristics of the track and granular layers, hence it is necessary to investigate how subgrade is affected under various operating conditions so that the ballast and subballast materials selected can provide a cost effective and technically acceptable support. In addition, selecting the appropriate materials for the track structure can minimise maintenance costs.

1.2.2 Performance of soft clay subgrade under cyclic load

Subgrade usually has plenty of soft soils such as soft clays which are characterised by high compressibility, low bearing capacity, and low permeability. To investigate the performance of soft clay subgrade under train induced cyclic loading, Laboratory testing is the primary method used by researchers and engineers (Ladd et al. 1977; Jamiolkowski et al. 1985; Mesri and Choi 1985), as shown in Fig. 1.3.

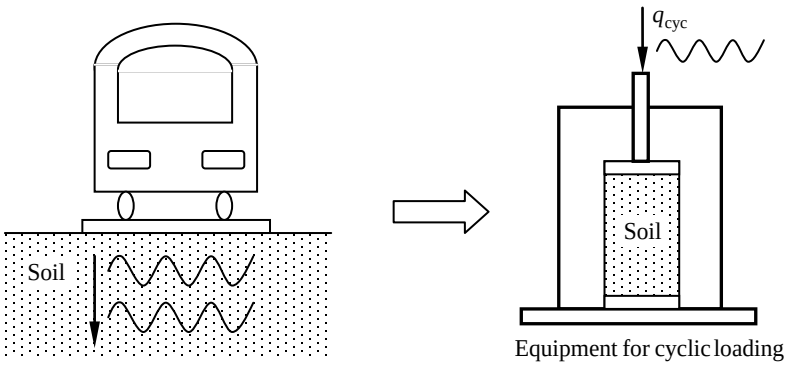

Fig. 1.3 Laboratory test to simulate soft clay under train induced cyclic loading

Among various methods, triaxial testing is the one of most widely used procedures to determine the stress-strain relationship and strength characteristics of soils (Sheng et al. 1997; Wang 2005). The outstanding advantages of this method include:

- The control of drainage conditions, where both undrained and drained tests can be performed.
- Excess pore pressures can be measured during the tests.
- The control of different types of loading conditions, where different combinations of confining and axial stress can be applied.
- Relatively simple preparation and testing procedures.

In such a triaxial test, a cylindrical soil specimen is subjected to an axial compression stress and a radial pressure stress. It is assumed that the soil specimen deforms uniformly during the test so that the axial strain which is determined based on the measured displacement represents the true material behaviour of a single soil element. Nevertheless, it is not often the case that a specimen deforms uniformly during the triaxial test. Non-uniformity can be caused by many factors, e.g. end restraint, insufficient drainage, membrane effects and self weight. How much effect such non-uniformity has on the strength and stress-strain properties has investigated by numerous researchers (Casagrande and Poulos 1964; Rowe and Barden 1964; Bishop and Green 1965; Duncan and Dunlop 1968; Lee 1978; Saada and Townsend 1981; Carter 1982; Wood 1990; Airey 1991; Schanz and Gussman 1994; Zhang and Garga 1997).

The response of excess pore pressure to a change of total stress in fine-grained soils during cyclic tests is somehow inaccurate due to various factors, among which time lag in pore pressure measuring system is probably the major problem. In the fifties and sixties of the last century, the effect of the time lag on laboratory measurements of excess pore pressure was initially recognized (Hvorslev 1951; Kallstenius and Wallgren 1956; Penman 1961; Whitman et al. 1961; Bishop and Henkel 1962; Gibson 1963). Another problem contributing to the inaccurate measurement of excess pore pressure is the non-uniform distribution of the excess pore pressure within the soil specimen. Generally, the measurements are made from top or bottom pedestals and sometimes from the middle. Also, for the equalization of excess pore pressure throughout the specimen, tests must be conducted at slow rates, like between 0.001 to 0.1Hz. However, cyclic loading can be conducted at frequencies much higher than these values and as a result the equalization of excess pore pressure throughout the specimen is prevented. Consequently, excess pore pressure may not be a reliable parameter in evaluating the cyclic performance of fine-grained soils under high loading rates. During the last five decades, numerous research activities have been carried out to develop advanced triaxial equipment, testing techniques and interpretation methods (Tatsuoka 1988; Baldi et al. 1988).

Various types of cyclic stress have been used to simulate the train load (see Fig. 1.4) such as the sinusoidal wave (Yang et al. 2007; Gong et al. 2001; Zhu et al. 1998; Zhou et al. 1996; Yang et al. 2008; Yang et al. 2007; Geng et al. 2007; Wang and Chen 2007; Zhu et al. 2007; Yang 2003; Yang and Guan 2001; Shahu et al. 1999; Suiker et al. 2005;

Yildirim and Ersan, 2007), the triangular wave (Huang et al. 2006; Ling et al. 2005; Liu and Mo 2008), the trapezoid wave (Miller et al. 2000), and the rectangular wave (Frost et al. 2004).

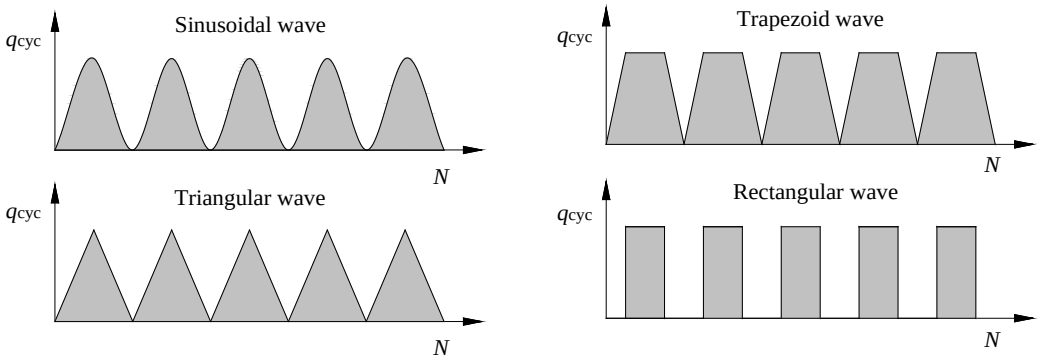

Fig. 1.4 Different types of cyclic loading

It has been found that excess pore pressure and strain keep increasing with the number of loading cycles under cyclic loading. The variations of stress, excess pore pressure, and strain are shown in Fig. 1.5. q_{cyc}, u_{cyc} and $\varepsilon_{\mathrm{a,cyc}}$ are cyclic deviator stress, excess pore pressure, and axial strain, while q_{a}, u_{a} and $\varepsilon_{\mathrm{a,a}}$ are the average deviator stress, excess pore pressure, and axial strain. It can be seen that under cyclic deviator stress with constant amplitude, the average excess pore pressure and strain develop with an increasing number of cycles, while the amplitudes of cyclic excess pore pressure and strain remain almost constant, showing a cycle independent characteristic.

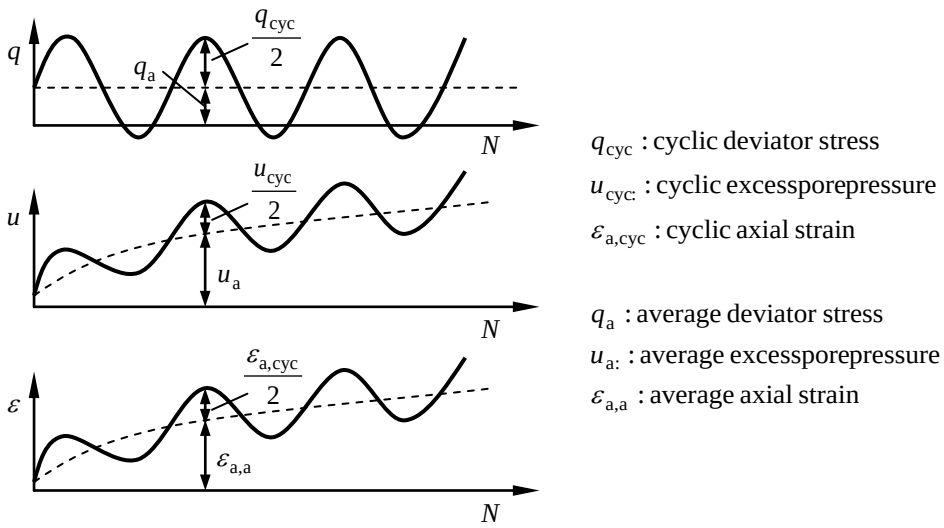

Fig. 1.5Shear stress, excess pore pressure and shear strain under cyclic loading (after Yasuhara et al. 1992)

There are many factors affecting the cyclic behaviour of soft soils, for example, the magnitude of cyclic stress, the loading period of each cycle, the number of loading cycles, static pre-shearing, and the over consolidated ratio. Details of their influence on soil performance will be discussed in Chapter 2.

1.2.3 The gain in strength stemming from Consolidation

To improve the stability of soft ground, the voids must be reduced under load, i.e. consolidation. Usually soils have three phases: solid, water, and air. In the scope of this thesis, only saturated soil (voids full of water) was considered. The composition of saturated soil is shown in Fig. 1.6 (a). The reduction of voids associated with settlement occurred during consolidation. The process of consolidation can be illustrated by Fig. 1.6 (b) where the solid skeleton is represented by a spring. Immediately after an external load has been applied the pressure is taken up by the water because there is no displacement for the spring. As water seeps out, the excess pore pressure dissipates and the pressure is transferred to the soil skeleton, which is known as primary consolidation. However, compression does not cease when the excess pore pressure has dissipated to zero, it continues at a gradually decreasing rate under constant effective stress. This is called secondary consolidation which is thought to be due to the gradual readjustment of the clay particles into a more stable configuration following a structural disturbance caused by a decrease in the void ratio.

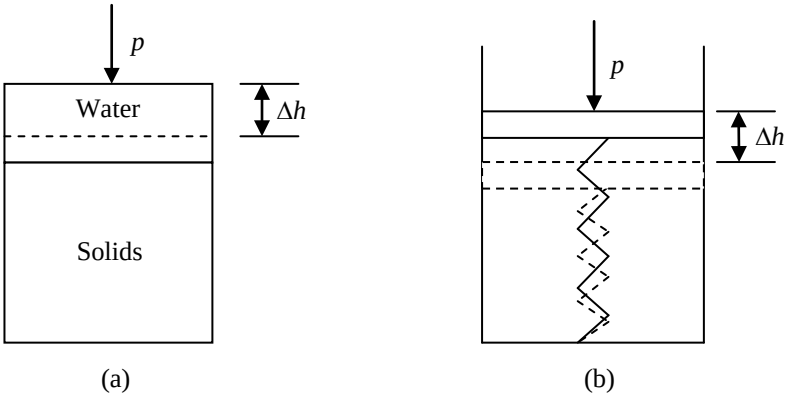

Fig. 1.6 Soil composition: (a) Two phases, (b) Spring structure

To accelerate the dissipation of excess pore pressure, prefabricated vertical drains (PVDs) can be installed to introduce a short radial drainage path. Prefabricated vertical drains (PVDs) combined with surcharge loading have been used in construction, and have proven to be an effective method for shortening the consolidation period, and hence decreasing the following undesirable settlement (see Fig. 1.7).

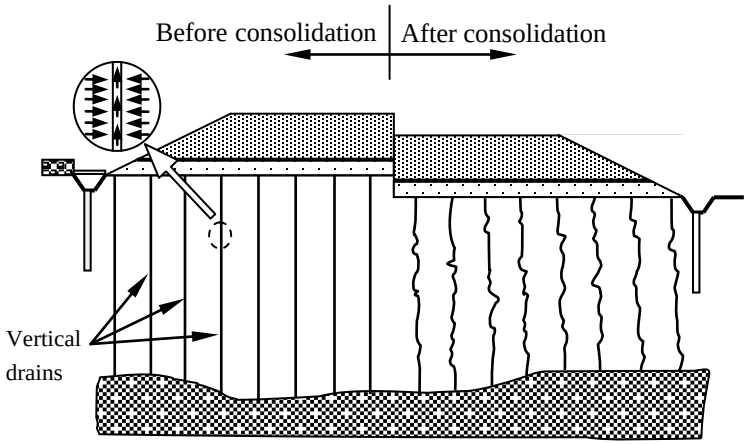

Fig. 1.7 Consolidation with prefabricated vertical drains (PVDs)

The ability of prefabricated vertical drains (PVDs) to reduce the excess pore pressure induced by cyclic loading, and subsequently increase the stability of soft soils, has not really been understood comprehensively. When prefabricated vertical drains are installed, some of the excess pore pressure due to cyclic loading can dissipate when the pore water drains out through the radial drainage paths, and thus less excess pore pressure is generated than under undrained conditions (see Fig. 1.8).

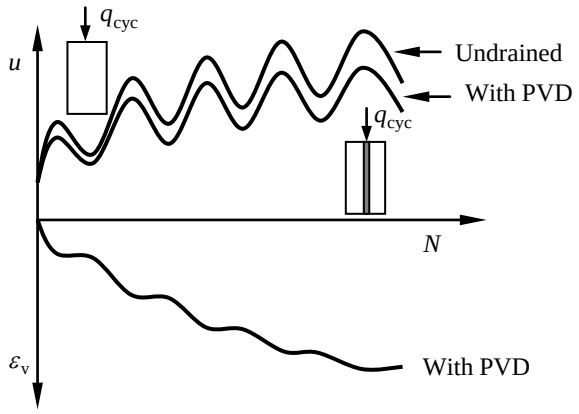

Fig. 1.8 Sample with or without PVD under cyclic loading

1.3 Objectives and content of present study

This thesis is aimed to investigate the performance of soft clay under cyclic loading with or without radial drainage. A modified undrained cyclic model is proposed based on Carter et al. (1982) to more precisely predict the development of excess pore pressures and strains under cyclic loading. Furthermore, a model of radial consolidation under cyclic loading is proposed based on the modified undrained cyclic model. The motivations for the two proposed models are given:

- **New model for undrained cyclic loading**

  Most of the existing cyclic models are empirical, with excess pore pressure or strain expressed in terms of loading cycles. Because the critical state has not been included in these models, it is impossible for them to predict failure; they can only predict the pre-failure performance.

  Carter et al. (1982) proposed a cyclic model based on a modified Cam clay model. Only one additional cyclic loading parameter was introduced to indicate how the yield surface changes during elastic unloading. However, the generation of excess pore pressure predicted by Carter et al. (1982) is not suitable for all the specimens under cyclic loading, so a modified cyclic loading based on Carter et al. (1982) is proposed, where Carter et al. (1982)'s model is also included as a special case.

- **New model for partially drained cyclic loading**

  A model of radial consolidation under cyclic loading based on the modified undrained cyclic loading is proposed. This model will combine the generation of internal excess pore pressure with radial drainage to simulate the condition where soft ground has been installed with PVD and is under train induced cyclic loading. For models considering the internal excess pore pressure and radial drainage separately, predicting the internal excess pore pressure lies at the heart of these models. The proposed model has advantage over existing models which assume that the internal generation of excess pore pressure in partially drained conditions is equal to that under undrained conditions. This simplification stems from the fact that the internal excess pore pressure is predicted by empirical equations which cannot consider the stress history and drainage conditions. However, the internal excess pore pressure is predicted in the proposed model, for partially drained conditions.

1.4 Organisation of Dissertation

There are 9 chapters in this dissertation. Following the Introduction in Chapter 1, Chapter 2 presents a review of prominent literatures related to two aspects: (a) the performance of soft ground under train induced cyclic loading; (b) PVD associated radial consolidation. Rail track structures are first illustrated and the factors influencing the performance of soft ground are demonstrated. The experimental tests with changing variables that correspond to the in situ condition are summarised and then the properties of prefabricated vertical drains and theoretical analysis of radial consolidation are described.

Chapter 3 illustrates the undrained cyclic loading tests conducted on the soft clay specimens with varying cyclic stress ratios and loading frequencies. The development of excess pore pressure and axial strain are analysed against either time or cycles. It has been found that the cyclic stress ratio rather than the loading frequency governs the stability of soft clay subgrade under cyclic loading. A critical cyclic stress ratio exists, above which failure will occur after a certain number of cycles, while below it a stable state can be reached. The loading frequency is only responsible for how many cycles the specimens will undergo before failure occurs at a high cyclic stress ratio, or before it reaches a stable state for a low cyclic stress ratio. Finally, the concept that the behaviour of soils depends on the cyclic stress level rather than the loading frequency is

investigated through strain rate during cyclic loading, which is considered to be responsible for the cyclic response of soft clays under various loading conditions. For loading frequencies ranging from 0.1 to 5 Hz, it was found that the strain rate depended on the cyclic stress ratio rather than the loading frequency, which implies that the cyclic stress level plays a more important role in influencing the cyclic performance of soft soil subgrade.

Chapter 4 presents a new cyclic model based on Carter et al. (1982)'s model to predict the behavior of soft clays under undrained cyclic loading. This theory was developed in terms of the modified Cam-clay soil model where attention was largely restricted to triaxial conditions. A modified yield surface function during elastic unloading is proposed to capture the behaviour of soil under cyclic loading. Only two additional parameters which characterise cyclic behaviour were used, together with the traditional parameters associated with the modified Cam-clay soil model. The establishment of parameters for soil properties, initial states, and cyclic loading conditions are presented, and a detailed computational procedure for determining the effective stresses and strains is demonstrated. The new model was used to simulate the cyclic triaxial tests on kaolin and then make a comparison. Predictions from the new model agreed with the measured values of excess pore pressures and axial strains, so in this way, the new cyclic model was verified. Furthermore, many factors which influenced the cyclic performance of soft soils such as cyclic stress ratios, pre-shearing, and loading frequencies, can be considered in the new model. The critical cyclic stress ratio is predictable using the new cyclic model by detecting the development of excess pore pressures and axial strains.

Chapter 5 describes the partially drained cyclic loading tests conducted on large scale (300 mm diameter by 600 mm high) clay specimens. The cylindrical specimen with a single PVD is to simulate the equivalent circular zone converted from the square or hexagonal influence zone under in situ conditions. Three types of partially drained tests were conducted to investigate the usefulness of PVD in cyclic loading: (a) cyclic loading without a rest period, (b) cyclic loading with a rest period, and (c) cyclic loading with a changing amplitude. For a high cyclic stress ratio, radial drainage decelerates the rate of excess pore pressure build up to its critical value, so the soil can undergo more loading cycles prior to failure. With a low cyclic stress ratio, radial drainage can prevent the excess pore pressure from accumulating to its critical value. In addition, the dissipation of excess pore pressure during the rest period can increase the resistance of the soil to the following cyclic loading.

Chapter 6 proposes a model of radial consolidation under cyclic loading. The internal generation of excess pore pressure predicted by the modified undrained cyclic model described in Chapter 4, and radial drainage, are combined as an analytical method in this new model. The parameters of radial consolidation are needed, in addition to soil properties, initial states, and cyclic loading conditions. This proposed model makes it possible to predict the behaviour of soil under partially drained cyclic loading even after a limited number of cycles that represent undrained cyclic loading. An acceptable agreement was found between the prediction and the test data of large scale laboratory tests described in Chapter 5. This clearly suggests that under cyclic loading conditions such as high speed rail, the failure of soft subgrade soil can be prevented by the use of vertical drains.

Chapter 7 provides a case history at Sandgate between Maitland and Newcastle, in the lower Hunter Valley of New South Wales, where two new railway lines were constructed adjacent to the existing working track to meet the requirements of demanding freight and passenger train schedules. The field data of settlement and lateral displacement were compared with the values predicted by a multi-layered cyclic consolidation model incorporating vertical and horizontal drainage.

Chapter 8 lists the conclusions and highlights in the current research, and provides discussion and recommendation for future research work.

Lists of references and appendices follow Chapter 8.

2 Literature Review

2.1 Rail track structures

2.1.1 Rail track response under passing train

A traditional rail track consists essentially of rails and sleepers that are laid in and fixed by ballast and sub-ballast on a layer of subgrade, as shown in Fig. 2.1. Many attempts have been made over the past 200 years to develop other designs, and the slab track is a recent preference. A slab track means a reinforced concrete (RC) slab laid on a viaduct, or some other rugged bed, to which is secured with cement asphalt. Due to its light weight it can be used for high speed rail, however, because a traditional railway track is an economical and rational structure well able to support heavy fast trains on soft ground, it is usually chosen on the basis of experience and as such, has remained virtually unchanged, irrespective of other subsequent technical progress.

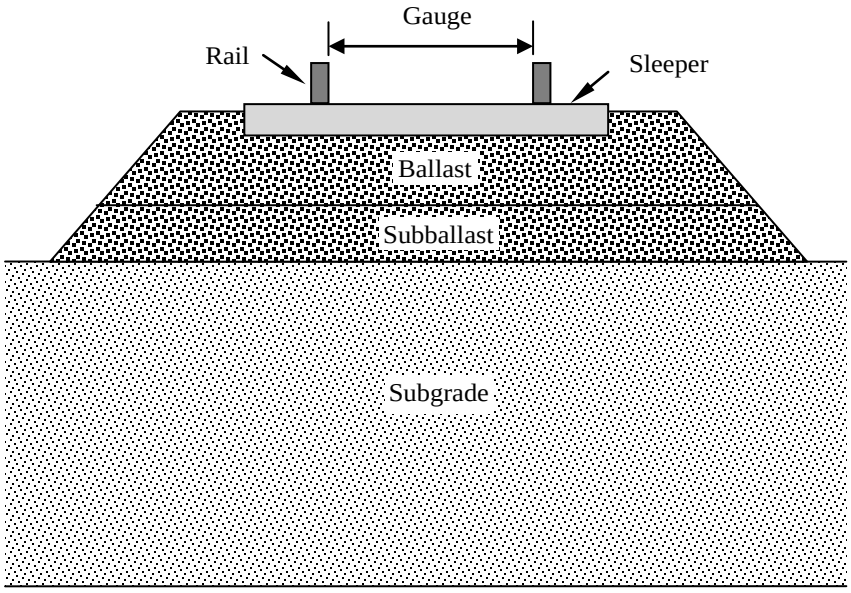

Fig. 2.1 The components of the railway track

The properties of rails, sleepers/ties, ballast, sub-ballast, and subgrade vary hugely, with Table 2.1 only giving some general ideas of what these properties are. Rail is classified by mass over a standard length. By using heavier rails, greater axle loads and higher train speeds can be supported without causing damage, but at a greater cost. Railway sleepers

or ties are rectangular objects onto which the rails are supported and fixed. Sleepers transfer the loads from the rails to the track ballast and the formation underneath, and also maintain the rail gauge by holding the rails the correct distance apart (their width). Sleepers/ ties are usually classified by three dimensions and spacing. Both the ballast and sub-ballast are included in the granular layer. The thickness of the granular layer is defined as the combined thickness of the ballast and sub-ballast, between the bottom of the sleepers and the surface of the subgrade. It is required that H_{granular} be larger than 0.15 m because if the granular layer is not thick enough, the subgrade will be subjected to higher repeated stresses, excessive deformation, and eventual failure (Li and Selig 1998a). The last structural part of a rail track is the formation of the track which supports the granular layer. This formation comprises the subgrade and a layer of sand or stone dust, known as the blanket, which restricts the upward migration of wet clay or silt. The data in Table 2.1 indicates that the compressive strength of the subgrade is very low and its resilient modulus is much smaller than the granular layer, which means that the deformation of rail track structure is mainly caused by the layer of subgrade. It is therefore necessary to understand the cyclic behaviour of subgrade to ensure the safety of train operations and organise track maintenance.

Table 2.1 Variable track values

Components of rail track structure		Value
Rail	Mass (ρ_{rail}), kg/m	30, 36, 40, 47, 50, 53, 60, 68
	Gauge, mm	1067, 1435, 1600
Sleeper/tie	length × Width × Depth (m×mm×mm)	2. 3×230×115
		2.45×230×115
		1.5×200×110
	Spacing (S_{sleeper}), mm	667, 685
Granular layer	Thickness (H_{granular}), m	> 0.15
	Resilient modulus (E_{r}), MPa	20 (poor), 40 (intermediate), and 80 (good)
Subgrade layer	Resilient modulus (E_{r}), MPa	1-4 (poor), 4-10 (intermediate), and 10-20 (good)
	Compressive strength,kPa	5-15 (poor), 15-30(medium), and 30-50 (good)

How railway tracks respond to a moving train is a complex problem that depends on a great number of factors. The transmission of train induced dynamic force is described in Fig. 2.2. Once dynamic stresses are excited by the contact between train wheels and rails, they will be transmitted from the rails, through the sleepers to the granular layer, and finally to the subgrade. This thesis will focus on the response of the subgrade under train induced dynamic stress.

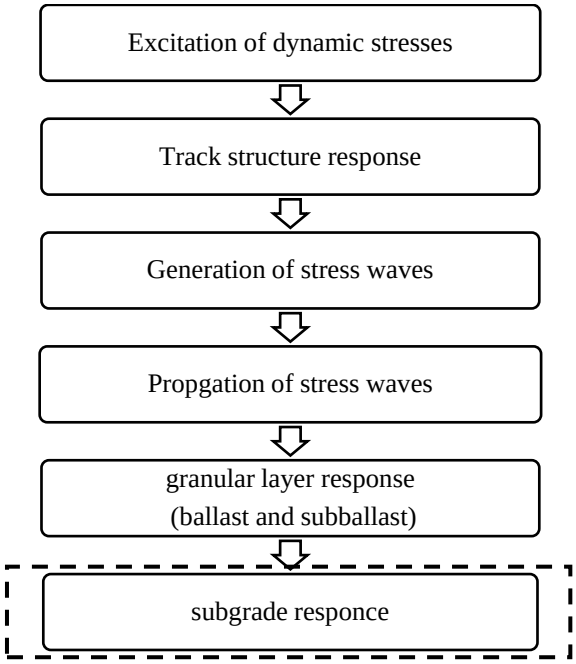

Fig. 2.2 A schematic description of different stages in the transmission of train induced dynamic force

2.1.2 Properties of dynamic stresses in the subgrade

The static weight of a train generates the stress field, while the characteristics of the vehicle allied to speed will determine how the track and its foundations enhance this stress field. Thus, the design axle load imposed by the vehicle moving at speed rather than the static axle load is the one from which actual dynamic stresses in various components of the track structures must be determined. An increase in rail stress above the static condition stemming from the design axle load may be attributed to several factors:

- Lateral bending of the rail.
- Eccentric vertical loading.
- Transfer of the wheel loads due to the rolling action of the vehicles.
- Vertical impact of wheel on rail due to speed.
- Irregularities in the track and non-uniform wheel and rail profiles.

The method generlly used to determine the design axle load is to express it empirically as a function of the static axle load:

$$P_{\mathrm{d}} = \phi P_{\mathrm{s}} \tag{2.1}$$

where P_{d} is the design wheel load (kN), P_{s} is the static wheel load (kN) and ϕ is the dimensionless impact factor.

Various parameters are always considered when the expression for calculating the impact factor is empirically determined. These parameters are for a vehicle, e.g. the speed of the train, diameter of the wheel, static wheel load, unsprung wheel mass, centre of gravity of vehicle, and the maintenance condition of the locomotive, and for the track, e.g. the modulus of the track, track stiffness at the rail joint, track joint dip angle, cant deficiency in curves, curve radius, and condition of the track maintenance. Table 2.2 shows five main types of formulae for the impact factor, and Table 2.3 shows other expressions.

Table 2.2 Main types of formula for impact factor

Formula		Impact factor ϕ	Vehicle						Track					
			Train speed	Wheel diameter	Static wheel load	Unsprung wheel mass	Centre of gravity of vehicle	Locomotive maintenance condition	Track modulus	Track stiffness at rail joint	Track joint dip angle	Cant deficiency in curves	Curve radius	Track maintenance condition
Main types	AR[a]	$1+5.4\frac{v}{D}$, where v is vehicle speed (km/h) and D is wheel diameter (mm)	√	√										
	AREA[b]	$1+5.21\frac{v}{D}$, where v is vehicle speed (km/h) and D is wheel diameter (mm)	√	√										
	Eisenmann	$1+\delta\eta t$, where δ and η are determined by the quality of the track and speed of the vehicle respectively, and t depends upon the chosen upper confidence limits	√											√
	ORE[c]	$1+\alpha'+\beta'+\gamma'$, where α' and β' relate to the mean value of the impact factor and γ' to the standard deviation of the impact factor	√				√	√				√	√	√
	BR[d]	$1+\frac{8.784(\alpha_1+\alpha_2)v}{p_s}\sqrt{\frac{D_j P_u}{g}}$, where v is vehicle speed (km/h), p_s (kN) is static wheel load, P_u is unsprung weight at one wheel (kN), D_j is track stiffness at the joints (kN/mm), g is gravitational constant (m/s^2) and $(\alpha_1+\alpha_2)$ are total rail joint dip angle (radians)	√		√	√				√	√			

[a] AR is the abbreviation of Australia Railways, [b] AREA is the abbreviation of American Railroad Engineering Association, [c] ORE is the abbreviation of Office of Research and Experiments of the International Union of Railways and [d] BR is the abbreviation of British Railways

Table 2.3 Other types of formula for impact factor

Formula		Impact factor ϕ	Vehicle						Track					
			Train speed	Wheel diameter	Static wheel load	Unsprung wheel mass	Centre of gravity of vehicle	Locomotive maintenance condition	Track modulus	Track stiffness at rail joint	Track joint dip angle	Cant deficiency in curves	Curve radius	Track maintenance condition
Other types	IR[a]	$1+\frac{v}{58.14\sqrt{k}}$, where v is vehicle speed (km/h) and k is track modulus (MPa)	√						√					
	German	$1+\frac{v^2}{3\times10^4}$ (For speeds up to 100km/h) $1+\frac{4.5v^2}{10^5}-\frac{1.5v^3}{10^7}$ (For speeds above 100km/h), where v is vehicle speed (km/h)	√											
	SAR[b]	$1+4.92\frac{v}{D}$, where v is vehicle speed (km/h) and D is wheel diameter (mm)	√											
	Clarke	$1+\frac{19.65v}{D\sqrt{k}}$, where v is vehicle speed (km/h), D is wheel diameter (mm) and k is track modulus (MPa)	√	√					√					
	WMATA[c]	$\left(1+3.86\times10^{-5}v^2\right)^{2/3}$, where v is vehicle speed (km/h)	√	√										

[a] IR is the abbreviation of Indian Railways, [b] SAR is the abbreviation of South African Railways and [c] WMATA the abbreviation of the Washington Metropolitan Transit Authorit

After the design axle load is obtained the dynamic stresses in various components of the track structures can be determined. It is well known that once dynamic stress is produced in the sub-structure beneath the sleepers, it will propagate away from the source and decrease in intensity with distance due to both material and geometric damping. Geometric damping occurs because the vibration spreads over a larger area as the wave front moves away from the source, whereas material damping is caused by friction in the transmitting medium. Some of this wave energy is then transformed into heat energy. The dynamic stress at the surface of the subgrade can be expressed using the following empirical equations:

$$\sigma_{\mathrm{d}} = \phi_{\mathrm{subgrade}} P_{\mathrm{d}} \tag{2.2}$$

where ϕ_{subgrade} is the coefficient of the axle load on the subgrade that depends on the structure of the track, especially the thickness of the ballast (Han and Zhang, 2005).

Furthermore, field measurements of the attenuation factor of dynamic stress within the subgrade caused by a passing train are also shown in Fig. 2.3. It can be seen here that the dynamic stress attenuates rapidly relative to depth, dropping to 20% of the surface mean at a depth of 1.5 m.

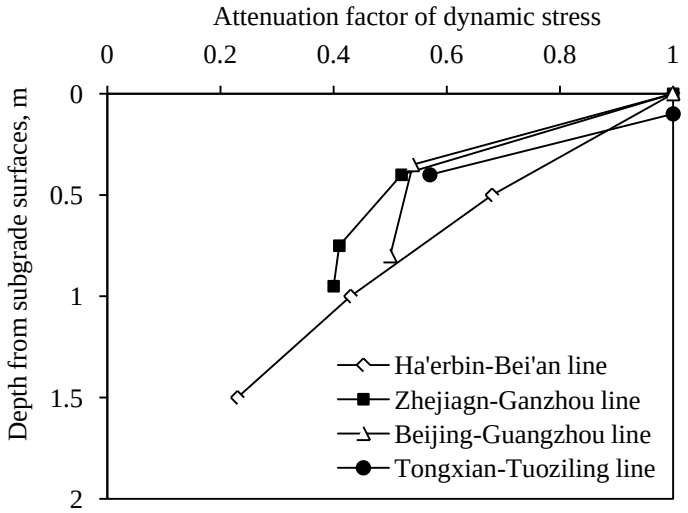

Fig. 2.3 The attenuation factor of dynamic stress in the subgrade (original data from Liu and Xiao 2010)

2.2 Factors influencing the cyclic performance of soft clays

2.2.1 Cyclic stress ratio

Early investigations of cyclic loading tests (Seed et al. 1955; Larew and Leonards 1962; Seed and Chan 1966) have shown that the performances of soft soils under static loading and cyclic loading are different mainly in two aspects:

- At particular levels of stress that are well below the maximum static deviator stress, cyclic loading leads to a much larger deformation than would be obtained for a single cycle of loading and cause collapse.
- There are levels of repeated stresses at which no ultimate collapse was observed.

Therefore, Larew and Leonards (1962) defined a critical level of repeated stress as the minimum level of repeated stress that will lead to failure. Above this value the loading cycle leads to non-recoverable deformation, until the effective stress failure envelope, and ultimate failure is reached. This idea was confirmed by Sangrey et al. (1969) (see Fig. 2.4). Cyclic triaxial tests were conducted on normally consolidated specimens of Yew York clay. Two levels of cyclic stress were used, i.e., 0.8 and 0.5 times the maximum static deviator stress ($q_{u,s}$) determined in a single cycle. The results shown in Fig. 2.4 (a) indicate that at a level of high stress the residual excess pore pressure and non-recoverable deformation increase with the increasing number of loading cycles until on the tenth cycle, when the specimen was unable to sustain the deviator stress and a dramatic increase in axial strain was observed. On the other hand, at a low cyclic stress level (see Fig. 2.4 (b)), the stress-strain and excess pore pressure-strain curves showed different patterns. Here the recoverable rather than the non-recoverable excess pore pressure and axial strain dominated. At around six cycles, maximum values of excess pore pressure and axial strain were reached and additional loading cycles caused no further obvious net changes in excess pore pressure and axial strain.

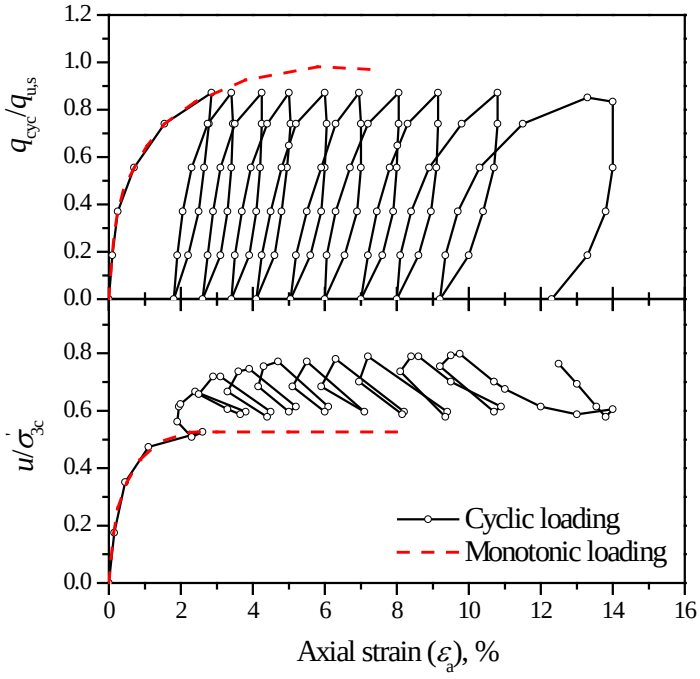

(a)

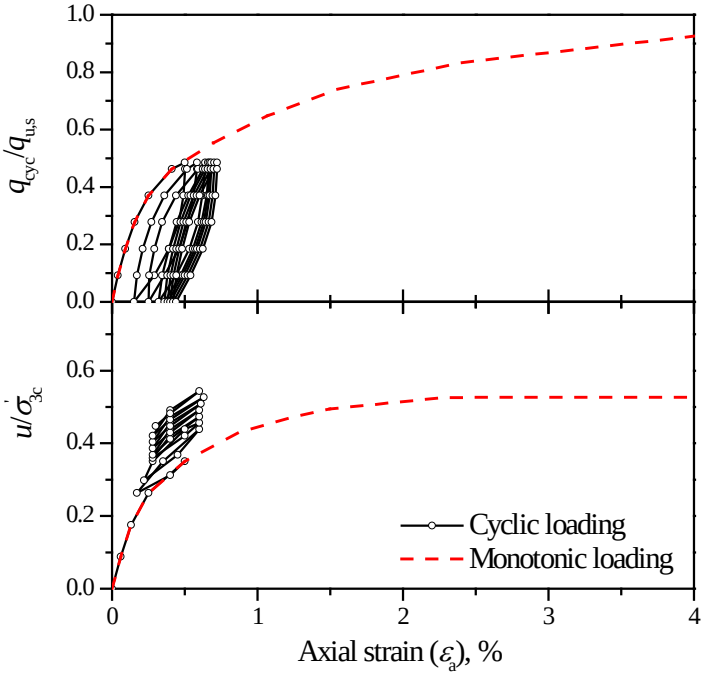

(b)

Fig. 2.4 Response of specimens under cyclic loading: (a) Failed specimen, (b) Stable specimen (original data from Sangrey et al. 1969)

Therefore, instead of using the absolute value of cyclic stress, the cyclic stress ratio (CSR) was used to show the level of cyclic stress (Brown et al. 1975), taking the form of:

$$\mathrm{CSR} = \frac{q_{\mathrm{cyc}}}{q_{\mathrm{u,s}}} \tag{2.3}$$

where q_{cyc} is the cyclic deviator stress and $q_{\mathrm{u,s}}$ is the static deviator stress at failure. Generally, under identical conditions, the larger the cyclic stress ratio (CSR), the higher the level of excess pore pressure and strain. For the critical cyclic stress ratio (CSR^*), the following equation holds:

$$\mathrm{CSR}^* = \frac{q^*_{\mathrm{cyc}}}{q_{\mathrm{u,s}}} \tag{2.4}$$

where q^*_{cyc} is the critical cyclic deviator stress. The value of the critical cyclic stress ratio can be determined for a particular soil by conducting cyclic loading tests at different cyclic stress ratios (see Fig. 2.5). At a low cyclic stress ratio (CSR = 0.2, 0.35, and 0.5), excess pore pressure develops slowly with the increasing number of cycles, and failure will probably occur after a large number of cycles. But at a high cyclic stress ratio (CSR = 0.6), the excess pore pressure increased significantly at the initial stage of the test and failure occurred after the first few cycles. The results of the excess pore pressures shown in Fig. 2.5 indicate there was a sudden change in the curves of excess pore pressure - number of cycles relationship when the cyclic stress ration increased from below the critical value to the critical value, or above the critical value (CSR increased from 0.5 to 0.6). In other words, without a critical stress ratio there would not be a sudden change in the relationship between excess pore pressure and number of cycles (CSR increased from 0.2 to 0.5). Thus the critical cyclic stress ratio for the Hanzhou clay in Zhou and Gong (2001) can be determined as between 0.5 and 0.6. The collected critical cyclic stress ratios in the literature varied from 0.5 to 0.8 (Sangrey et al. 1969; Lashine 1971; France and Sangrey 1977; Sangrey et al. 1978; Ausal and Erken 1989; Zhou and Gong 2001; Pillai et al. 2011).

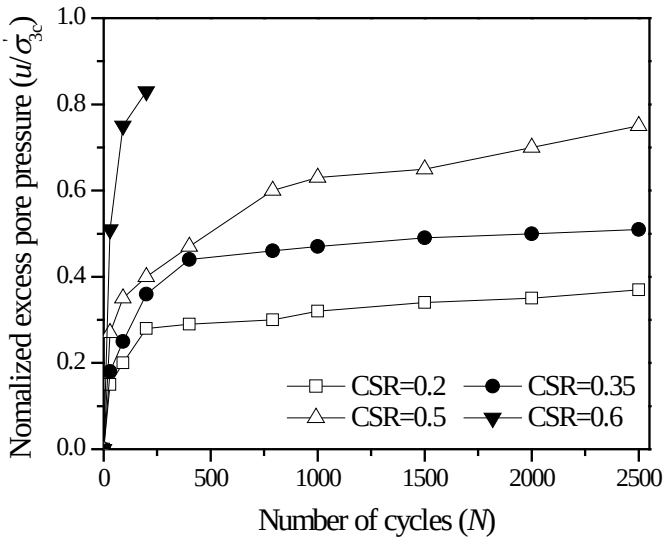

Fig. 2.5 Excess pore pressures at different cyclic stress ratios (original data from Zhou and Gong 2001)

2.2.2 Cyclic shear strain

As the cyclic stress ratio is important for stress controlled cyclic loading tests, the cyclic shear strain (γ_{cyc}) is a key parameter for strain controlled cyclic loading. The cyclic properties of soils loaded at small cyclic shear strains have mainly been investigated with resonant column tests (Andreasson 1979, 1981; Woods 1991, 1994; Turan et al. 2011), while cyclic tri-axial tests (Dobry et al. 1981; Dyvik et al. 1984; Hynes-Griffin 1988; Ladd et al. 1989) and cyclic simple shear tests (Vucetic et al. 1985; Ohara and Matsuda 1988; Vucetic and Dobry 1988; Vucetic et al. 1998; Hsu and Vucetic 2006) were used for cyclic shear tests at larger cyclic shear strain.

As with the critical cyclic stress ratio, there is a cyclic threshold shear strain (γ^*_{cyc}). Dobry et al. (1982) proposed that the cyclic threshold shear strain divides the domains of the significant development of excess pore pressure, and no accumulation at all. For $\gamma_{cyc,2} > \gamma^*_{cyc}$ or $\gamma_{cyc,3} > \gamma^*_{cyc}$ (see Fig. 2.6), the permanent excess pore pressure kept accumulating and developed relatively rapidly with the number of loading cycles, whereas for $\gamma_{cyc,1} < \gamma^*_{cyc}$ (see Fig. 2.6), the accumulation of excess pore pressure was negligible. It should be noted that the critical cyclic stress ratio domains the non-failure equilibrium (there is still an accumulation of excess pore pressure) and failure, while

cyclic threshold shear strain domains no accumulation of excess pore pressure or significant accumulation.

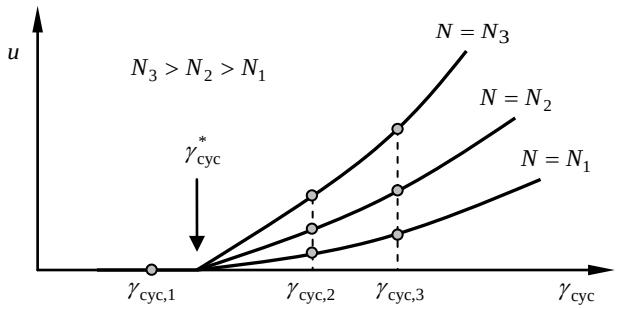

Fig. 2.6 Typical results of undrained excess pore pressures for defining the cyclic threshold shear strain (after Hsu and Vucetic 2006)

The previous studies of the strain controlled cyclic loading tests on either cohesive or non-cohesive soils are given in Table 2.4. The test results indicate that the cyclic threshold strain in cohesive soils (clays or silts) varied from 0.024 to 0.1%, which was larger than for non-cohesive soils (sand), which ranged from 0.005 to 0.028%. In addition, the cyclic threshold shear strain increased with the plasticity index for cohesive soils. Hsu and Vucetic (2006) found that for clays and silts with a plasticity index ranging from 14 to 30, the cyclic threshold shear strain varied from 0.024 to 0.06%.

Table 2.4 Stain-controlled cyclic loading tests

Resources	Soil type	Test type	Description	Plasticity index (PI), %	Cyclic shear strain (γ_{cyc}), %	cyclic threshold shear strain (γ_{cyc}^{*}), %
Andreasson (1979, 1981)	Clay	Resonant-column	–	40-50	–	0.04-0.1
Dobry et al. (1981)	Clean sand	Tri-axial	OCR =1-8	NP[b]	–	0.012-0.028
Dyvik et al. (1984)	Clean sand	Tri-axial	D_r = 45-80%	NP	–	0.007-0.015
Hynes-Griffin (1988)	Gravel	Tri-axial	D_r = 25-45%	NP	–	0.005-0.02
Ohara and Matsuda (1988)	Kaolin clay	Direct simple shear	OCR =1-6	25	0.05-3	0.08-0.1
Vucetic and Dobry (1988)	Venezuelan	Direct simple shear	OCR =1-4	39-51	0.59-5.09	
Ladd et al. (1989)	Clean sand	Tri-axial	D_r = 45-80%	NP	–	0.01-0.015
Vucetic et al. (1998)	Santa Monica sand	Direct simple shear	–	NP	0.001-0.04	–
	Antelope Valley sand			NP		
	Clay A, Clay B, and Clay C			22, 38, and 75		
Turan et al. (2011)	Glyben[a]	Tri-axial	OCR =1	–	0.1-2	–
		Resonant-column	OCR =1	–	0.001-0.2	–
Hsu and Vucetic (2006)	Nevada sand	Direct simple shear	Wet compaction	NP	–	0.012-0.016
	Irvine silt		Intact sample	14	–	0.04-0.06
	Kaolin clay		–	20	–	0.024-0.04
	Southern California clay		Wet compaction	30	–	0.03-0.06

[a]Glyben is prepared by mixing bentonite mixed with water and glycerine. [b]NP represents non-plastic soil.

2.2.3 Loading rate

Experimental studies have been carried out by a number of researchers on the response of soil to various loading rates (Taylor 1943; Casagrande and Wilson 1951; Richardson and Whitman 1963; Perzyna 1966; Kutter and Sathialingam 1992; Sheahan et al. 1996; David and Campanella 1997). In the following two sections, the influence of loading rate on soil behaviour in monotonic loading and cyclic loading will be demonstrated respectively.

2.2.3.1 Static loading

It has been well recognised that the undrained strength of saturated clays can be significantly affected by the rate of loading applied. Generally the undrained strength increases as the strain rate increases (Richardson and Whitman 1963; Ladd et al. 1972; Crooks and Graham 1976; Vaid and Campanella 1977; Vaid et al. 1979; Baracos et al. 1980; Andersen and Stenhamar 1982; Craig 1982; Graham et al. 1983; Adachi et al. 1985; Lefebvre and LeBoeuf 1987; Sheahan et al. 1996). To quantify this increment in undrained strength with an increasing loading rate, the sensitivity of the strain rate (s_q), defined as the change in undrained strength ($\Delta q_{u,s}$), either per log cycle of strain rate ($\dot{\varepsilon}_{aL,s}$), or per log time to failure (t_f) may be used:

$$s_q(\%) = \left[\left(\frac{\Delta q_{u,s}}{q^0_{u,s}}\right)\log\left(\frac{\dot{\varepsilon}_{aL,s}}{\dot{\varepsilon}^0_{aL,s}}\right)\right]\times 100 \tag{2.5}$$

or

$$s_q(\%) = \left[\left(\frac{\Delta q_{u,s}}{q^0_{u,s}}\right)\log\left(\frac{t_f}{t^0_f}\right)\right]\times 100 \tag{2.6}$$

where $q^0_{u,s}$ is the value of $q_{u,s}$ at the reference strain rate ($\dot{\varepsilon}^0_{aL,s}$), or reference time to failure (t^0_f). It should be noted that the sensitivity of the strain rate is related to the referenced strain rate or referenced time to failure. It has been pointed out by (Sheahan et al. 1996) that the rate dependence is a function of the range in the strain rates being tested. That is, the nature of the rate dependence changes as the strain rate increases.

The collected results of strain rate sensitivity from the literature are given in Table 2.5. There are only limited results for high OCR soils (Richardson and Whitman 1963; Hight 1983; Sheahan et al. 1996), while there are comprehensive data available for low OCR soils, ranging from 1.0 to 2.4. The value of these strain rates varies from 0.0014 to 470 %/h. It can be seen from Table 2.5 that although variations exist in the values of strain rate sensitivity, the undrained shear strength increased by 0-20% for a tenfold increment in strain rate regardless of the type of soil, overconsolidated ratio, and range of strain rates.

Table 2.5 Strain rate sensitivity

Resources	Soil type	OCR	Range of strain rates ($\dot{\varepsilon}_{a,s}$), %/h	Strain rate sensitivity (s_q), %
Bjerrum et al. (1958)	Fornebu clay	1	0.0036-10	13
Richardson and Whitman (1963)	Mississippi Valley alluvial clay	1-16	0.12- 60	0-12
Graham (1969)	Mastemyr marine clay	1.2	0.05-0.3	9.4-14.9
Ladd et al. (1972)	Atchafalaya clay	1	0.5-60	10-17
Alberro and Santoyo (1973)	Mexico City clay	1	0.045-94	9
Berre and Bjerrum (1973)	Drammen clay	1	0.0014-35	0-16
Graham (1974)	Lyndhurst clay	1.5	0.015-0.3	19.4
Crooks and Graham (1976), Bell (1977)	Belfast organic estuarine clay	1.2-2.0	0.05-5	9.7-13.4
Vaid and Campanella (1977)	Haney clay	1	0.01-670	0-10
Baracos et al. (1980)	Winnipeg clay	2.4	0.003-10	12.5
Hight (1983)	Lower Cromer Till	1-7	0.04-470	6-9
Sheahan et al. (1996)	Boston blue clay	1-8	0.05- 50	0-11.5

For the combined effects of the strain rate and overconsolidation ratio on the undrained shear strength of soils, the following conclusions have been addressed by Sheahan et al. (1996):

- For the same increment in strain rate, the gain in undrained shear strength drops with an increasing overconsolidation ratio.
- For highly overconsolidated specimens, the effective stress envelope at peak strength depends on the strain rate, and therefore any increase in strength is due to a decrease in the shear induced excess pore pressure.
- For normally consolidatedor slightly overconsolidated specimens, the increase in undrained shear strength was caused by the suppression of shear induced pore pressures and an increase in the effective stress envelope at peak strength.

The mechanisms responsible for this increase in the undrained shear strength with an increasing strain rate can be summarised as follows (see Fig. 2.7):

- **Single mechanism**. For example the curves OA, OB, and OC represent the stress paths under undrained monotonic loading with increasing strain rate. Since points A, B, and C are on the initial effective stress envelope defined at a standard strain rate, the increase in undrained shear strength was caused only by decreased shear induced excess pore pressure with unchanged (initial) effective stress envelope/unchanged effective stress friction angle ($\varphi_{p'}$).
- **Combined mechanisms**. For example the curves OA', OB', and OC' represent the stress paths under undrained monotonic loading with an increasing strain rate. Since points A', B', and C' are on the new effective stress envelope, the increase in undrained shear strength was caused by a decreased shear induced pore pressure and an increased effective stress friction angle.

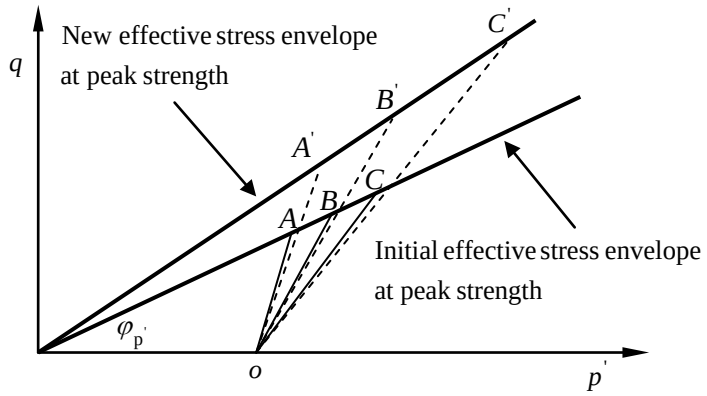

Fig. 2.7 The mechanism of an increase in undrained shear strength due to the strain rate

The strain rate dependent behaviour can be explained by the visco-plasticity of soft clays. The simple explanation is as follows. There are two loading rates for the same designed load, one is *OA* that reaches the designed load within a time $t_{A,n}$, while the other one is *OB* that reaches this load within a time $t_{B,n}$, as shown in Fig. 2.8 (a). For simplicity, divide both loading stages into n steps. Now consider the first step, the loads $p_{A,1} = p_{B,1}$ are applied during the period $t_{A,1}$ and $t_{B,1}$ for *OA* and *OB* respectively.

For very small time intervals $t_{A,1}$ and $t_{B,1}$, the loads applied during this period can be replaced by the step load. After the step load $p_{A,1} = p_{B,1}$ is applied, the state point of mean effective stress p_h' and the corresponding volume strain $\varepsilon_{v,h}$ for both loading rates are at a point h. The corresponding mean total stress for point *h* is p_h. The broken line m–m in Fig. 2.8 (b) has a volumetric strain $\varepsilon_{v,h}$. Since this is undrained cyclic loading, there is no drainage of pore water and the volume remains the same as $\varepsilon_{v,h}$. Due to the creep (viscous) nature of the clay, which causes volumetric compression for a certain period of time, the volumetric strain intends to increase from $\varepsilon_{v,h}$ to $\varepsilon_{v,k}$ and from $\varepsilon_{v,h}$ to $\varepsilon_{v,k'}$ considering that creep is time dependent. Obviously, the state point k and k' cannot be maintained due to incompatible volumetric strains, so to maintain compatibility or equilibrium in stress and volumetric changes, the state point must move to point l and l' with unloading or the mean effective stress must be reduced from p_k' to p_l' and from p_k' to $p_{l'}'$ with a total mean stress of p_h. According to the principle of effective stress

for saturated soils, during the first loading steps, the increment of excess pore pressure can be expressed by:

$$\Delta u_{hkl} = u_l - u_k = \left(p_h - p_l^{'}\right) - \left(p_h - p_k^{'}\right) = p_h^{'} - p_l^{'} \tag{2.7}$$

$$\Delta u_{hk^{'}l^{'}} = u_{l^{'}} - u_{k^{'}} = \left(p_h - p_{l^{'}}^{'}\right) - \left(p_h - p_{k^{'}}^{'}\right) = p_h^{'} - p_{l^{'}}^{'} \tag{2.8}$$

Since the mean effective stress $p_{l^{'}}^{'}$ is smaller than $p_l^{'}$, and Δu_{hkl} is smaller than $\Delta u_{hk^{'}l^{'}}$. This is why less excess pore pressure is caused by a higher loading rate.

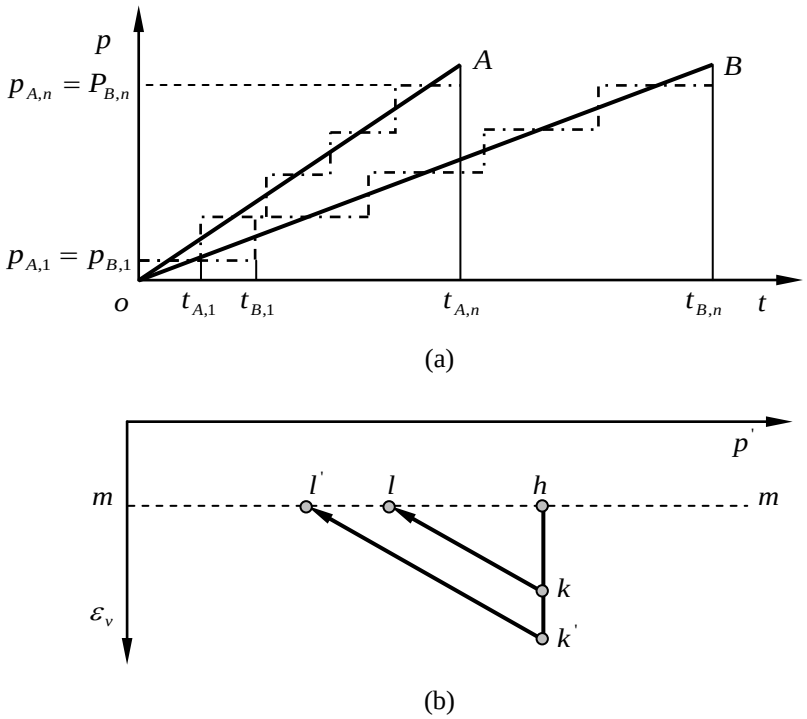

Fig. 2.8 Visco-plasticity of soft clays: (a) Loading scheme, (b) Interpretation of time dependent behaviour

2.2.3.2 Cyclic loading

The cyclic loading frequency in the laboratory test was quite low in the early stage, e.g., the research by Sangrey et al. (1969) took 10 hours for each cycle to load and unload. The loading frequency was deemed to be a cyclic loading associated property to which not enough attention was paid. Another reason was that a reliable measurement of cyclic shear induced excess pore pressure could only be obtained in the tests with relatively long cycles because conventional pore pressure transducers have a slow response time.

However, the strain rate could be very important when interpreting cyclic tests on soft clays at high frequencies (Matsui et al. 1980; Takahashi et al. 1980), even though it has never been found to have any significant effect on the strength of granular materials (Peacock and Seed 1968). With the application of new technology in transducers, cyclic loading tests have been conducted with higher loading frequencies and the influence of loading frequency over the cyclic behaviour of soils has been studied by more researchers (Hyde and Brown 1976; Yasuhara et al. 1982; Procter and Khaffaf 1984; Lefebvreand LeBoeuf 1987; Hyde et al. 1993; Lefebvre and Pfendler 1996; Liu and Xiao 2010; Zhou and Gong 2001; Jiang et al. 2010).

The types of soil and test conditions for the collected literatures are described in Table 2.6. Most of the cyclic tests were tri-axial apart from the tests by Lefebvre and Pfendler (1996). The cyclic loading frequency ranged from 0.0005 to 10 Hz. It was noted that in the cyclic loading frequency column, some cells only have one value. This is because there are two ways to check the frequency dependent behaviour in existing literatures: (a) One is to change the cyclic loading frequency in a series of cyclic loading tests (Matsui et al. 1980; Yasuhara et al. 1982; Takahashi et al. 1980; Procter and Khaffaf 1984; Hyde et al. 1993; Zhou and Gong 2001; Liu and Xiao 2010); (2) The other is to maintain a constant frequency and investigate any change in the soil from a high strain rate accompanied with cyclic loading in comparison to monotonic loading where the strain rate was quite low.

Table 2.6 Range of cyclic loading frequency from the literatures

Resources	Soil type	Test type	OCR	Cyclic loading frequency (f), Hz
Hyde and Brown (1976)	Keuper Marl clay	Triaxial	4-20	10
Takahashi et al. (1980)	Lower Cromer Till	Triaxial	1-7	0.0005-0.01
Yasuhara et al. (1982)	Ariake clay	Triaxial	1	0.1-1
Procter and Khaffaf (1984)	Derwent clay	Triaxial	1	0.008-5
Hyde et al. (1993)	Ariake clay	Triaxial	1	0.1-3
Konrad and Wagg (1993)	Clayey silt	Triaxial	1	0.05-0.5
Lefebvreand LeBoeuf (1987)	Northwestern Quebec clay	Triaxial	–	0.1
Lefebvre and Pfendler (1996)	St. Lawrence valley clay	Direct simple shear	2.2	0.1
Zhou and Gong (2001)	Hangzhou clay	Triaxial	1.2-8	0.01-1
Liu and Xiao (2010)	Southwest Shandong clay	Triaxial	–	1-2

Compared to static loading, a comprehensive understanding of the effect of cyclic loading frequency on soil behaviour has not yet been achieved, probably because this problem is complex and sometimes the results are expressed somewhat ambiguously. The outcomes are provided as follows:

- The high strain rate in stress controlled cyclic tests could result in a higher cyclic shear strength compared to an undrained shear strength determined in monotonic tests at standard strain rates of 0.5-1.0 %/h. For example, Lefebvre and Pfendler (1996) conducted direct simple shear tests and found that at a strain rate equivalent to a 0.1 Hz cyclic load of about 300 % per hour, the clay could mobilise an undrained shear strength that was about 40% higher than that determined at a standard strain rate. This was equivalent to a 12% increase per log cycle of strain rate. Lefebvre and LeBoeuf (1987) presented an equivalent

strain rate that corresponded to 0.1 Hz as 3,500% per hour, and the cyclic shear strength was 43% higher than that determined at a traditional monotonic test.

- In cyclic tests the high strain rate partially compensates for a degrading shear strength with the number of cycles, such that at 12 cycles (Lefebvre and Pfendler 1996) and 300 cycles (Lefebvre and LeBoeuf 1987), the cyclic shear strength can be taken as equal to the undrained shear strength determined in monotonic tests at standard strain rates.

- The relationship of excess pore pressure and number of loading cycles showed that samples loaded more slowly took 450 seconds to achieve maximum shear stress and generated higher excess pore pressure, and so migrated more rapidly than samples loaded to their maximum shear stress in 50 seconds (Takahashi 1980). The generation rate of excess pore pressure showed a corresponding dependence on the period of each cycle. It should be noted that the expression "more rapidly" corresponds to the number of loading cycles, i.e., for identical cycles, more excess pore pressure generated at a lower loading rate. If the conclusion regarding the loading time is going to be made, the loading cycles should be transferred to time ($t = N / f$).

- The relationship of normalised excess pore pressures by the confining pressure and axial strains can be expressed by a unique hyperbolic function independent of the loading frequency, for a loading frequency ranging from 0.1 to 1 Hz (Yasuhara et al. 1982). In addition, the cyclic strength and deformation modulus were not influenced by the different frequencies of repeated loading.

- For stress controlled cyclic testing, the value of the limiting minimum stress ratio below which any load controlled cycling would have no weakening effect, appears to increase with frequency when examined in terms of $q_{cyc} / q_{u,s}$, but it can be assumed to be constant, i.e., independent of frequency, if the data are analysed in terms of $q_{cyc} / q_{u,c}$, where $q_{u,c}$ is the shear strength considering the strain effect under cyclic loading condition (Procter and Khaffaf 1984). While for displacement controlled cyclic testing, the value of the limiting minimum stress ratio depends on the frequency no matter if it's examined in terms of $q_{cyc} / q_{u,c}$ or $q_{cyc} / q_{u,s}$.

2.2.4 Overconsolidation ratio

The overconsolidation ratio (OCR) is defined as the ratio of the pre-consolidation pressure ($p_{c0}^{'}$), i.e., the maximum value of effective stress in the past, to the present effective consolidation stress ($p^{'}$):

$$\mathrm{OCR} = \frac{p_{c0}^{'}}{p^{'}} \tag{2.9}$$

If the present effective stress is the maximum to which the soil has ever been subjected, i.e., $\mathrm{OCR} = 1$, the soil is said to be normally consolidated. On the other hand if the effective stress in the past was greater than the present value, i.e., $\mathrm{OCR} > 1$, the soil is said to be overconsolidated.

The monotonic undrained shear strength was found to be closely related to the consolidation stress history (Ladd and Foott 1974; Ladd 1991) and can be expressed as:

$$\frac{q_{u,s}}{\sigma_{vc}^{'}} = \mathrm{OCR}^{m} S_{\mathrm{OCR}} \tag{2.10}$$

where S_{OCR} is the value of $q_{u,s} / \sigma_{vc}^{'}$ when $\mathrm{OCR} = 1$, and m is the slope of the $q_{u,s} / \sigma_{vc}^{'}$ versus OCR relation on a log-log plot. When the values of S and m are determined, the monotonic undrained shear strength can be evaluated. Since the different overconsolidation ratios can be due to either different values of either pre-consolidation pressures ($p_{c0}^{'}$) (see Fig. 2.9(a)) or present effective consolidation stresses ($p^{'}$) (see Fig. 2.9(b)), then an opposite conclusion can be obtained. For those specimens swelled back from different pre-consolidation ratios, as shown in Fig. 2.9(a), the monotonic undrained shear strength increased with an increasing overconsolidation ratio, but for those specimens swelled back from the same pre-consolidation ratio as shown in Fig. 2.9(b), the monotonic undrained shear strength decreased with an increasing overconsolidation ratio.

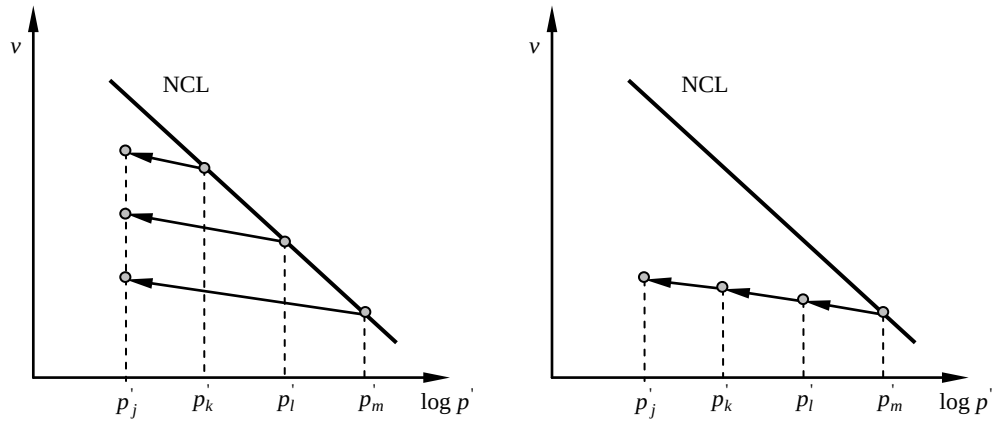

(a) (b)

Fig. 2.9 Overconsolidation ratio: (a) With the same (p'), (b) With the same (p'_{c0})

Referring to previous investigations (Sangrey et al. 1969; Brown et al. 1975; Andersen 1976; Andersen et al. 1980; Takahashi et al. 1980; Vucetic and Do bry 1988; Yasuhura 1995; Sheahan et al. 1996; Zhou and Gong 2001; Katti et al. 2003; Wang and Cai 2008), the undrained cyclic behaviour of fine-grained soils can be largely affected by overconsolidation ratios, especially in the following aspects:

- The development of excess pore pressures for specimens with various OCRs by stress release from the same maximum consolidation pressure were fundamentally different. Takahashi et al. (1980) found that at a low OCR the excess pore pressure gradually increased with an increasing number of cycles and the effective stress path kept moving towards the failure envelope, whereas the first effective stress cycle of specimens loaded under a high cyclic stress ratio at a sufficiently high OCR lay close to the failure envelope, and any further migration of the cycles was restricted. However there are bound to be differences in the rate that effective stress paths migrate under cyclic loading that correspond to different overconsolidation ratios.

- The degradation of the undrained secant shear modulus, which can be represented by a degradation index δ, is related to the overconsolidation ratio, and thus for strain controlled cyclic loading tests, the degradation index can be defined by:

$$\delta = \frac{G_{sN}}{G_{s1}} = \frac{\left(\frac{\tau_N}{\gamma_{\text{cyc}}}\right)}{\left(\frac{\tau_1}{\gamma_{\text{cyc}}}\right)} = \frac{\tau_N}{\tau_1} \tag{2.11}$$

where G_{sN} and τ_N are the cyclic secant shear modulus and shear stress after N cycles of shearing with a constant shear strain of γ_{cyc} respectively , and G_{s1} and τ_1 are the cyclic secant shear modulus and shear stress in the first cycle. The test results presented by Zhou and Gong (2001) indicated that the degradation of the undrained secant shear modulus decreased with the increasing OCR . To take into account the rate of degradation, the negative slope of the degradation index versus N line was introduced by Idriss et al. (1976, 1978) as the degradation parameter t_δ :

$$t_\delta = -\frac{\log \delta}{\log N} \tag{2.12}$$

It was also found that the degradation parameter decreased with an increasing OCR as well (Vucetic and Do bry 1988; Matasovic and Vucetic 1995).

- A reduction in the undrained shear strength directly after the undrained cyclic loading was more marked for normally consolidated and lightly over consolidated specimens than for heavily over consolidated specimens (Hyde and Ward 1986). This was because specimens with a high OCR do not generate large excess pore pressures under cyclic loading and therefore do not exhibit large changes in post-cyclic monotonic strength.

- The results of post-cyclic undrained shear strength after the cyclic induced excess pore pressure had drained away were different from those that had not drained away. For normally consolidated and lightly overconsolidated specimens, the soils consolidated with the drainage of positive excess pore pressure and the void ratios were decreased, which resulted in increased resistance to the following shearing. The heavily overconsolidated specimens were found softened due to swelling after the negative excess pore pressure had dissipated Yasuhara (1995).

2.2.5 Initial static shear stress

Initial static shear stresses may be applied under undrained and drained conditions. The application of an undrained initial static stress is to dissociate the effect of the initial static shear stress from the drainage that occurs during the application of a drained static shear stress. This condition is used to simulate a cyclic load applied shortly after the initial static shear stress has been applied, and before the excess pore pressure has dissipated, e.g., at the end of the construction of an embankment on a soft soil subgrade. The application of a drained initial static stress, also referred to as anisotropic consolidation, is to simulate the condition where enough time has elapsed after the embankment has been constructed and before cyclic loading has been applied, so that excess pore pressure has dissipated and the soft soil subgrade has gained sufficient strength.

The test results (Lefebvre and Pfendler 1996) from a series of direct, simple, cyclic shear tests conducted on intact sensitive clay from the St. Lawrence valley that was subjected to undrained initial static shear stress, indicated that an undrained static shear stress before cyclic loading decreases the cyclic shear strength but increases the total shear strength, which is from combined static and cyclic shear stress. For an undrained initial shear stress of 0.3 to 0.8 times the undrained shear strength, the total shear strength was increased by 30% if 12 cycles are considered as the number of cycles to failure.

The results from the cyclic loading tests on anisotropically consolidated soft clay specimens indicated that a similar rule was observed for specimens with undrained initial static shear stress, where a drained initial static shear stress decreases the cyclic resistance but it may increase the total shear strength (a combination of static and cyclic shear stress). In addition, the total shear strength is proportional to the initial static shear stress (Seed and Chan 1966; Goulois et al. 1985; Zimmie and Lien 1986; Andersen 1988; Ishihara et al. 1993; Hyodo et al. 1994), and the relationship of normalised excess pore pressure and axial strain for clays with and without initial static shear stress are in different hyperbolic curves (Yasuhara et al. 1982). The test results indicated that the pre-shear effect induces less build up of excess pore pressure in anisotropically consolidated specimens than in isotropicallly consolidated specimens.

2.2.6 Drainage effect on post-cyclic loading

Normally consolidated clay subjected to undrained cyclic loading undergoes a reduction in effective stress, such that it may behave in a similar manner to overconsolidated clay produced by unloading (Yasuhara et al. 1983; Yasuhara 1985). The undrained strength of an apparently overconsolidated clay may decrease depending on the OCR associated with unloading. The undrained strength of an overconsolidated clay due to stress release can be estimated using the relationship proposed by Mitachi and Kitago (1976) and Mayne (1980):

$$\left(q_{\mathrm{u,s}} / \sigma_{\mathrm{c}}^{'}\right)_{(\mathrm{OC})} / \left(q_{\mathrm{u,s}} / \sigma_{\mathrm{c}}^{'}\right)_{(\mathrm{NC})} = (\mathrm{OCR})^{\Lambda_0} \tag{2.13}$$

where $\left(q_{\mathrm{u,s}} / \sigma_{\mathrm{c}}^{'}\right)_{(\mathrm{OC})}$ and $\left(q_{\mathrm{u,s}} / \sigma_{\mathrm{c}}^{'}\right)_{(\mathrm{NC})}$ are the undrained static strength ratios of overconsolidated and normally consolidated clays, $\left(q_{\mathrm{u,s}}\right)_{(\mathrm{OC})}$ and $\left(q_{\mathrm{u,s}}\right)_{(\mathrm{NC})}$ are the undrained strengths of overconsolidated and normally consolidated clays without any previous cyclic loading history, and Λ_0 is an experimental parameter.

The undrained strength after undrained cyclic loading can be estimated using the relationship proposed by Yasuhara et al. (1983):

$$\left(q_{\mathrm{u,s}}\right)_{(\mathrm{cy})} / \left(q_{\mathrm{u,s}}\right)_{(\mathrm{NC})} = \left[1 / \left(1 - \Delta u / \sigma_{\mathrm{c}}^{'}\right)\right]^{\left[\Lambda_0 / (1 - C_{\mathrm{S}} / C_{\mathrm{c}}) - 1\right]} \tag{2.14}$$

where Δu is the excess pore pressure generated by undrained cyclic loading and C_{s}, C_{c} are the sweeling and compression indices, respectively.

If drainage is allowed after undrained cyclic loading, then the resistance to further undrained cyclic loading for normally consolidated clay can be improved, according to studies previously carried out using triaxial equipment (Brown et al., 1977; Matsui et al., 1978), and using simple shear apparatus (Andersen et al. 1976; France and Sangrey 1977; Ohara and Matsuda 1986, 1988; Yasuhara et al. 1988; Yasuhara and Hirao 1989c).

Previous studies by authors (Yasuhara et al. 1983; Yasuhara 1985; Yasuhara and Hirao 1989) showed that the undrained strength of clay after the dissipation of the excess pore pressure induced by undrained cyclic loading increases in proportion to the amount of excess pore pressure developed during undrained cyclic loading, while its gain in strength

is assumed to be due to a decrease in the void ratio. The undrained strength ratio of clay followed by drainage after cyclic loading is given by:

$$\left(q_{\mathrm{u,s}}\right)_{(\mathrm{dcy})} / \left(q_{\mathrm{u,s}}\right)_{(\mathrm{NC})} = \left[1 / \left(1 - \Delta u / \sigma_{\mathrm{c0}}^{'}\right)\right]^{\Lambda_0 [(C_\mathrm{S}/C_\mathrm{c})/(1-C_\mathrm{S}/C_\mathrm{c})]} \tag{2.15}$$

The above relationship can be simply illustrated by Fig. 2.10 (a). While soil elements are subjected to undrained cyclic loading, an excess pore pressure (Δu) is induced by the path AB. If the excess pore pressure is allowed to dissipate, then the soil will undergo a decrease in the void ratio via the path BC and the undrained strength at points A, B, and C are $\left(q_{\mathrm{u,s}}\right)_{(\mathrm{NC})}$, $\left(q_{\mathrm{u,s}}\right)_{(\mathrm{cy})}$ and $\left(q_{\mathrm{u,s}}\right)_{(\mathrm{dcy})}$ respectively.

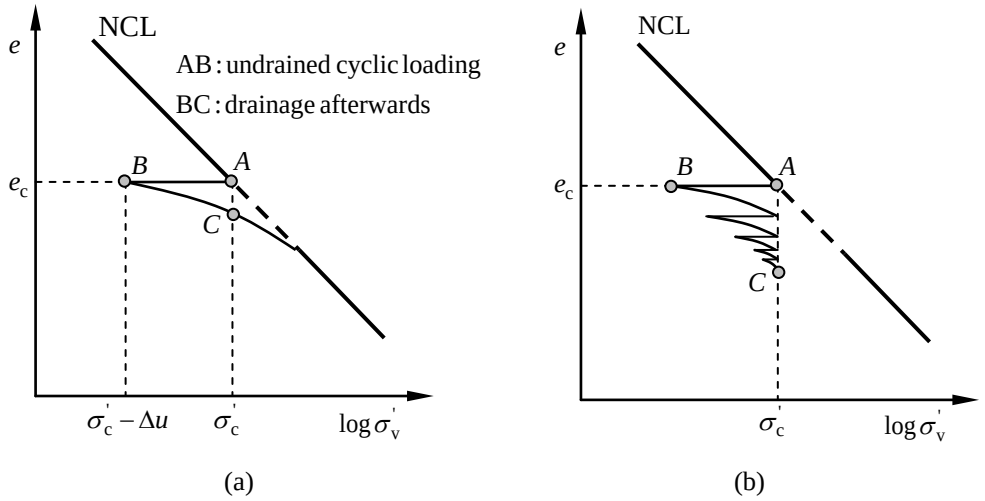

Fig. 2.10 Schematic illustration of $e - \log \sigma_{\mathrm{v}}^{'}$ relations: (a) One series of undrained cyclic loading followed by drainage, (b) Five series of undrained cyclic loading followed by drainage (after Yasuhara and Andersen 1991)

France and Sangrey (1977) found that with a cyclic deviator stress of approximately 75% of the specimen's original undrained monotonic strength, the undrained monotonic strength after several cycles of undrained loading and drained unloading was approximately 30% (for isotropically consolidated specimens) and 15% (for anisotropically consolidated specimens) higher than its original undrained monotonic strength. A similar conclusion was obtained by O'Reilly et al. (1991) and Yasuhara and Andersen (1991) in that during the fifth loading period, none of the specimens showed any significant development of permanent shear strain, irrespective of the level of stress applied, indicating that the soil was behaving in an essentially elastic manner (see Fig. 2.10 (b)).

2.3 Consolidation theories

Before facilities on soft soil formations were constructed, ground improvement was deemed necessary to control the generation of excess pore pressure, as well as vertical and lateral displacement. Surcharging or preloading is one of the most effective and widely used techniques to pre-consolidate weak compressible soft soils and gain strength. Two major aims are achieved by pre-consolidation via surcharging or preloading (Aldrich 1965; Johnson 1970; Stamatopoulos and Kotzias 1985; Lo and Mesri 1994; Yeung 1997):

- To improve the shear strength of soft soil foundations by decreasing the pore space or void ratio by draining out the pore water.
- To eliminate settlement due to the construction of the embankments, buildings, highways, railways, abutments, and tanks by increasing the effective stress in the compressible foundation soils.

However, if only vertical drainage is allowed, then in many cases the time needed to achieve the required compression can be excessive and the preload needed for the time available can be quite large and the rate at which strength is gained can be too slow to allow for a rapid application of a new construction load to the soft soil foundations. This is because the layer of soft soils can be quite deep and the consolidation time required is inversely proportional to the square of the drainage length. In this context, vertical drains, which introduce shorter drainage paths, can be used to accelerate the dissipation of excess pore pressure and rate of consolidated settlement. In addition, most compressible soft soils are alluvial deposits which are more pervious in the direction of the bedding plane than in a perpendicular direction (Barron 1948), i.e., most geologic deposits have larger hydraulic conductivity horizontally than vertically. Thus, horizontal flows can accelerate the consolidation of soft soil foundations quite considerably. Theories of vertical consolidation, radial consolidation, and combined vertical and radial consolidation will be reviewed in the following sections.

2.3.1 Vertical consolidation theory

The most famous vertical consolidation theory is Terzaghi's theory of one-dimensional consolidation (Terzaghi 1943), which states that all quantifiable changes in stress to a soil (compression, deformation, shear resistance) are the direct result of a change in effective stress. The assumptions made in Terzagh’s theory of one-dimensional consolidation are:

(a) The soil is homogeneous and fully saturated.
(b) The solid particles and water are incompressible.
(c) The flow of pore water is solely in the vertical direction.
(d) Strains are small.
(e) The flow of pore water is governed by Darcy's law.
(f) There is a linear relationship between the void ratio and effective stress that is independent of time and stress history.
(g) The coefficient of soil permeability is assumed to be constant during consolidation.

Though the first 4 assumptions are either likely to hold, or any deviation will have no discernible effect, experimental results contradict the final 3. Darcy's Law does not seem to hold at low hydraulic gradients and both the coefficients of permeability and volume compressibility decrease during consolidation. This is due to the non-linearity of the relationship between the void ratio and effective stress although for small increments of stress an assumption of 6 is reasonable. Finally, the relationship between the void ratio and effective stress is not independent of time, again proven by experimental results. The theory relates the following three quantities:

- The excess pore pressure (u).
- The depth (z) below the top of the clay layer.
- The time (t) from the instantaneous application of a total stress increment.

Consider an element with dimensions dx, dy, dz and a layer of clay with a thickness H, as shown in Fig. 2.11. An increment of total vertical stress p is applied to the element. The flow velocity through the element is given by Darcy's law as:

$$v_z = ki_z = k\frac{\partial h}{\partial z} \tag{2.16}$$

Since any change in head (h) is due to a change in pore water pressure:

$$v_z = \frac{k}{\gamma_w}\frac{\partial u}{\partial z} \tag{2.17}$$

The condition of continuity can therefore be expressed as:

$$\frac{\mathrm{d}V}{\mathrm{d}t} = q - \left(q + \frac{\partial q}{\partial z}\mathrm{d}z \right) = -\frac{\partial q}{\partial z}\mathrm{d}z = -\frac{\partial}{\partial z}\left(v_z \mathrm{d}x\mathrm{d}y\right)\mathrm{d}z = -\frac{k}{\gamma_\mathrm{w}}\frac{\partial^2 u}{\partial \mathrm{z}^2}\mathrm{d}x\mathrm{d}y\mathrm{d}z \tag{2.18}$$

The rate of volume change can be expressed in terms of m_v:

$$\frac{\mathrm{d}V}{\mathrm{d}t} = m_\mathrm{v}\frac{\partial \sigma'}{\partial t}\mathrm{d}x\mathrm{d}y\mathrm{d}z \tag{2.19}$$

where m_v is the coefficient of compressibility.

The total stress increment is gradually transferred to the soil skeleton which increases the effective stress as the excess pore water pressure decreases. Hence the rate of volume change can be expressed as:

$$\frac{\mathrm{d}V}{\mathrm{d}t} = -m_\mathrm{v}\frac{\partial u}{\partial t}\mathrm{d}x\mathrm{d}y\mathrm{d}z \tag{2.20}$$

Combining above two equations:

$$m_\mathrm{v}\frac{\partial u}{\partial t} = \frac{k}{\gamma_\mathrm{w}}\frac{\partial^2 u}{\partial \mathrm{z}^2} \tag{2.21}$$

or

$$\frac{\partial u}{\partial t} = c_\mathrm{v}\frac{\partial^2 u}{\partial \mathrm{z}^2} \tag{2.22}$$

This is a differential equation of consolidation in which:

$$c_\mathrm{v} = \frac{k}{m_\mathrm{v}\gamma_\mathrm{w}} \tag{2.23}$$

where c_v is defined as the coefficient of consolidation.

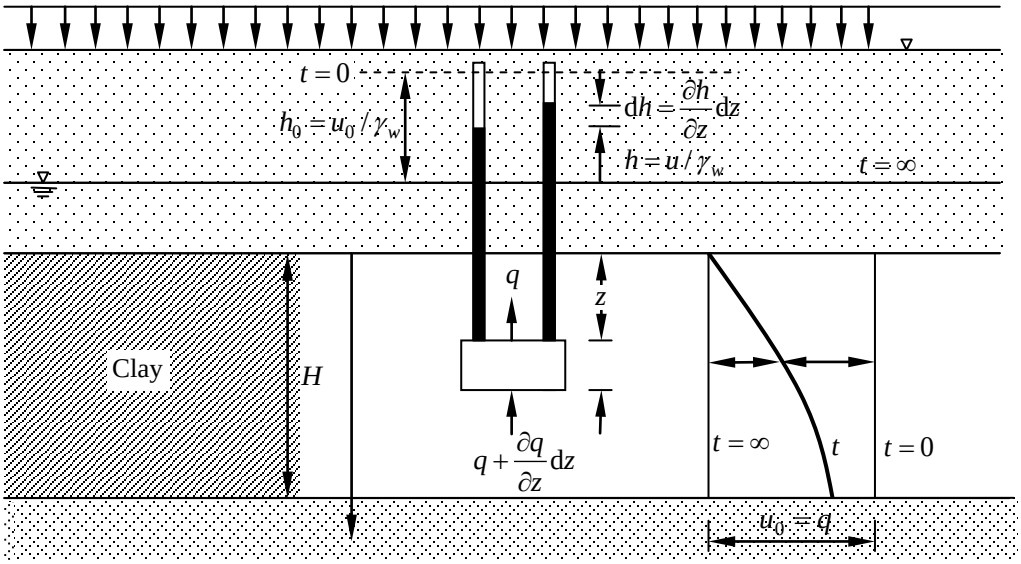

Fig. 2.11 Element within a clay layer

The solution for excess pore water pressure at depth z after time t is:

$$u = \sum_{\varpi=0}^{\varpi=\infty} \frac{2u_0}{\mu}\left(\sin\frac{\mu z}{d}\right)\exp\left(-\mu^2 T_{\mathrm{v}}\right) \tag{2.24}$$

where $\mu = \frac{\pi}{2}(2\varpi+1)$, $T_v = \frac{c_v t}{H^2}$, u_0 is the initial excess pore water pressure and H is the length of the drainage path.

The average degree of consolidation (U_{v}) at time (t) for constant u_0 is given by:

$$U_{\mathrm{v}} = 1 - \sum_{\varpi=0}^{\varpi=\infty} \frac{2}{\mu^2}\exp\left(-\mu^2 T_{\mathrm{v}}\right) \tag{2.25}$$

where the symbols have the meanings mentioned above.

In addition, the equation for average degree of consolidation can be represented by the following empirical equations:

For $U_{\mathrm{v}} < 0.6$, $T_{\mathrm{v}} = \frac{\pi}{4}U_{\mathrm{v}}^2$ (2.26)

For $U_{\mathrm{v}} > 0.6$, $T_{\mathrm{v}} = -0.933\log(1-U_{\mathrm{v}}) - 0.085$ (2.27)

The consolidated curves for the distribution of initial pore pressure that varied linearly across the layer of soil is shown in Fig. 2.12.

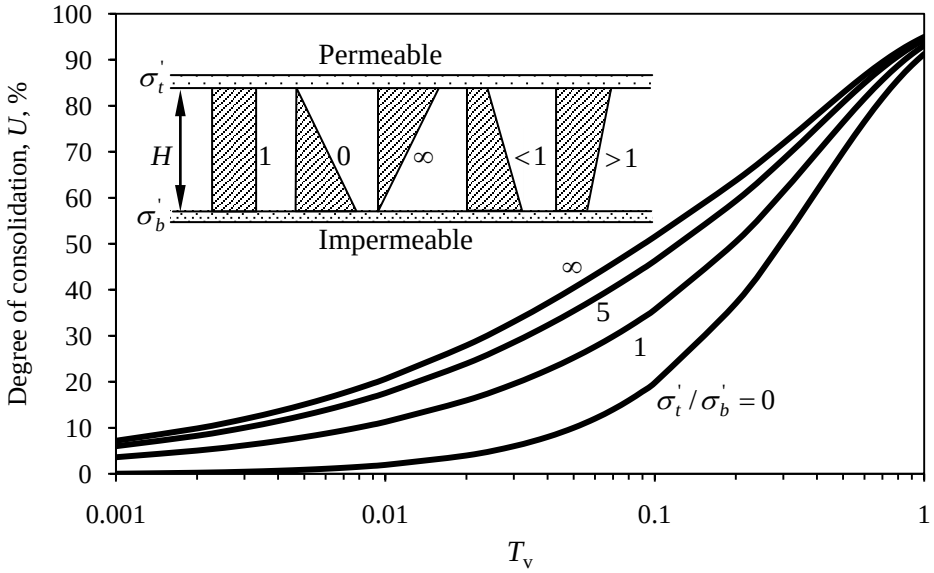

Fig. 2.12 Consolidation curves (after Walker 2006)

2.3.2 Radial consolidation theory

A theory for radial consolidation was initially proposed by Carrillo (1942), and Barron (1948). Further studies considering the effects of smear and well resistance attributed to vertical drains were conducted by Richart (1959), Rowe (1964), Olson et al. (1974); Yoshikuni and Nakanodo (1974), Hansbo (1981), Jamiolkowski et al. (1983); Onoue (1988), Zeng and Xie (1989), Zhu and Yin (2004), Basu et al. (2006), Walker and Indraratna (2006), Walker and Indraratna (2007), and Rujikiatkamjorn and Indraratna (2009). Solutions based on free strain and equal strain hypotheses were developed. The details of these two hypotheses are as follows:

- **Free strain**. In this case it is assumed that the surcharge loading applied is uniform over the circular zone of influence. As consolidation progresses, the soil adjacent to the vertical drain consolidates and compresses faster than soil farther away from the drain, for a shorter drainage path. This difference in the rate of consolidation results in a differential settlement of the upper surface of the soil. The effect on the stress distribution by this variation of vertical strains is neglected.

- **Equal strain**. In this case it is assumed that the surcharge loading applied is rigid and an equal vertical strain occurs at the surface. This assumption is based on the fact that the arching that develops in the material above the consolidating soils results in some distribution of stress. An extreme case would be that all the vertical strains are equal and no differential settlement develops due to the redistribution of stress processed by arching.

For a symmetrical flow to a central vertical drain, a unit cell of a soil cylinder with a vertical drain is usually used for analysis, as shown in Fig. 2.13. d_w is the diameter of the drain, d_s is the diameter of the smear zone, d_e is the diameter of the soil cylinder, and l is the length if the drain. k_h and k_v are the coefficient of permeability in the horizontal and vertical directions, and k_s is the coefficient of permeability in the smear zone.

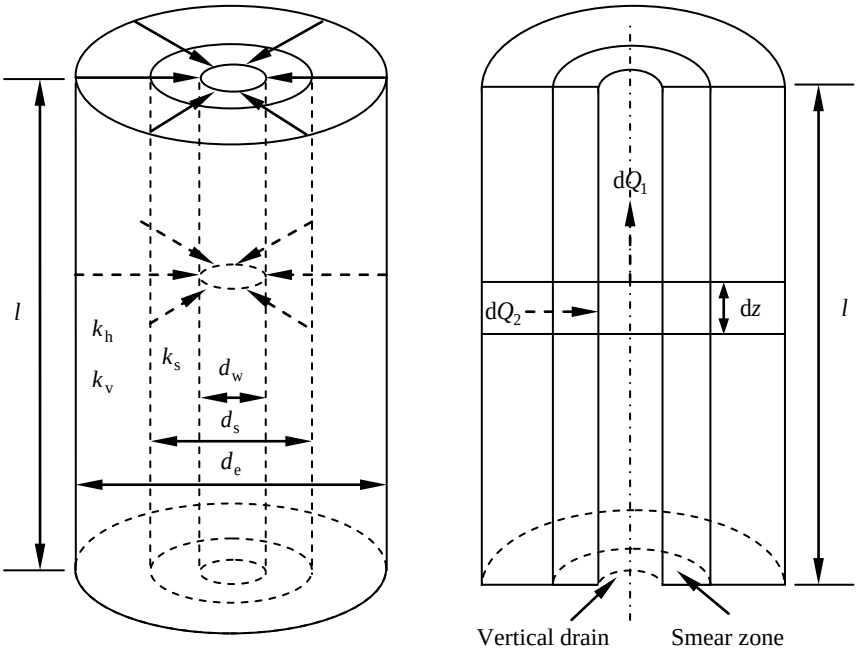

Fig. 2.13 Soil cylinder with vertical drain (after Walker and Indraratna 2006)

Under free strain conditions the governing equation for consolidation by radial drainage (Barron, 1948) is given by:

$$c_h\left(\frac{\partial^2 u}{\partial r^2}+\frac{1}{r}\frac{\partial u}{\partial r}\right)=\frac{\partial u}{\partial t} \tag{2.28}$$

where t is the time elapsed after the load is applied and u is the excess pore pressure at a radius r and a depth z.

Under equal strain conditions the following equation can be obtained:

$$c_h\left(\frac{\partial^2 u}{\partial r^2}+\frac{1}{r}\frac{\partial u}{\partial r}\right)=\frac{\partial \bar{u}}{\partial t} \tag{2.29}$$

where $\bar{u}$ is the average excess pore pressure.

Details of this general approach to equal strain radial consolidation with Darcian flow was given by Walker (2006), with the main idea shown below. By considering the vertical flow in a drain, the change in flow from the entrance to the exit face of the slice with a thickness $\mathrm{d}z$ is given by:

$$\mathrm{d}Q_1=\frac{\pi r_w^2}{\gamma_w}\left(\frac{\partial^2 w(z)}{\partial z^2}\right)\mathrm{d}z\mathrm{d}t \tag{2.30}$$

where $w(z)$ represents the excess pore pressure in the drain at a depth z.

The radial flow into the slice is determined from:

$$\mathrm{d}Q_2=\pi\left(r_e^2-r_w^2\right)\frac{\partial \varepsilon}{\partial t}\mathrm{d}z\mathrm{d}t \tag{2.31}$$

Assuming no sudden drop in excess pore pressure at the boundary of drain and soil, then for continuity:

$$\mathrm{d}Q_1=\mathrm{d}Q_2 \tag{2.32}$$

Then the average excess pore pressure and average degree of consolidation can be obtained:

$$\bar{u} = \bar{u}_0 \exp\left[-8T_h / \mu\right] \tag{2.33}$$

$$U_h = 1 - \exp\left[-8T_h / \mu\right] \tag{2.34}$$

where the time factor T_h can be expressed as:

$$T_h = \frac{c_h t}{4r_e^2} \tag{2.35}$$

The μ parameter is extremely important for this equal strain approach. The smear zone and well resistance effect the determination of the μ parameter. If the smear effect and well resistance are not considered then the drains are called ideal drains. Solutions for such drains show the fastest dissipation of excess pore pressure. Ideal drains over predict short term settlement and dissipation of excess pore pressure (Indraratna and Redana 1998), which may be realistic for a long term performance greater than 400 days (Indraratna et al. 1992). When water is restrained from exiting the soil the increased duration of higher excess pore pressure will result in greater mobilisation of shear strains, which leads to greater lateral deformation than if its escape was unrestricted. Therefore, ideal drains lead to underestimated predictions of lateral deformation (Indraratna and Redana 2000). When the smear effect and well resistance were included in the modelling the predictions were improved but settlement was still slightly over predicted (Indraratna et al. 1999). To take the smear effect into account a reduced horizontal permeability in the smear zone is incorporated in most analytical models.

In the early stage, the horizontal permeability was held constant throughout the smear zone (Hansbo 1981; Zhu and Yin 2004), however the horizontal permeability resulting from large scale experimental tests showed a substantial nonlinear decrease towards the drain within the smear zone (Onoue et al. 1991; Madhav et al. 1993; Indraratna and Redana 1998; Sharma and Xiao 2000). The nonlinear horizontal permeability in the smear zone was considered in linear or parabolic distribution (Walker and Indraratna 2007; Walker and Indraratna 2006). The classic solutions for ideal drains and drains with well resistance and smear effect are given below. It is noted that if well resistance is ignored then μ can be expressed without $\pi z(2l - z)(k_h / q_w)$.

- For an ideal drain (Hansbo, 1981)

$$\mu_I = \ln(n) - 0.75 \tag{2.36}$$

where $n = r_e / r_w$.

- For constant permeability in the smear zone (Hansbo, 1981)

$$\mu_C = \ln(n/s) + \kappa_C \ln(s) - 0.75 + \pi z(2l - z)(k_h / q_w) \tag{2.37}$$

where $s = r_s / r_w$, $\kappa_C = k_h / k_s$, and q_w is the drain discharge capacity.

- For a linear distribution of permeability in the smear zone (Walker and Indraratna 2007)

$$\mu_L = \ln(n/s) + \frac{\kappa_L(s-1)}{s-\kappa_L}\ln\left(\frac{s}{\kappa_L}\right) - 0.75 + \pi z(2l - z)(k_h / q_w) \tag{2.38}$$

where $\kappa_L = k_h / k_0$, and k_0 is the permeability at the boundary of drain and soil.

- For parabolic permeability in the smear zone (Walker and Indraratna 2006):

$$\begin{aligned}\mu_P = {} & \ln(n/s) + \frac{\kappa_P(s-1)^2}{\left(s^2 - 2\kappa_P s + \kappa_P\right)}\ln\left(\frac{s}{\sqrt{\kappa}}\right) \\ & - \frac{s(s-1)\sqrt{\kappa_P(\kappa_P - 1)}}{2\left(s^2 - 2\kappa_P s + \kappa_P\right)}\ln\left(\frac{\sqrt{\kappa_P} + \sqrt{\kappa_P - 1}}{\sqrt{\kappa_P} - \sqrt{\kappa_P - 1}}\right) - 0.75 + \pi z(2l - z)(k_h / q_w)\end{aligned} \tag{2.39}$$

where $\kappa_P = k_h / k_0$.

2.3.3 Combined vertical and radial consolidation

The scheme of combined vertical and radial flow is given in Fig. 2.14. When the soil being considered is far from the top drainage, the contribution of vertical flow to consolidation is smaller than radial flow, and as a result the consolidation due to vertical flow is ignored in many cases. However, when the soil is near the top drainage, vertical drainage becomes important and must be considered in the analysis.

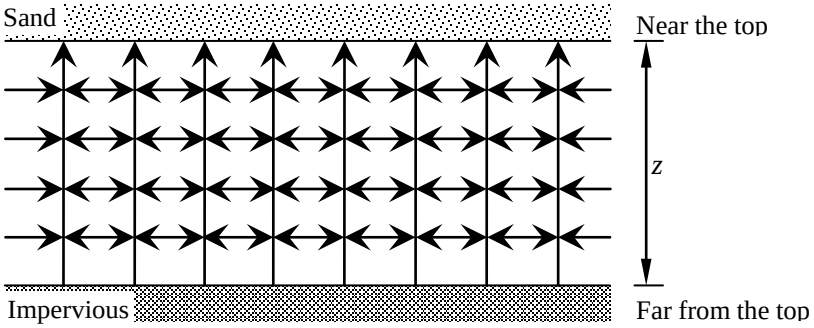

Fig. 2.14 Combined vertical and radial flow

The governing equation for combined vertical and radial consolidation can be written as:

$$\frac{\partial u}{\partial t} = c_{\mathrm{v}}\left(\frac{\partial^2 u}{\partial z^2}\right) + c_{\mathrm{h}}\left(\frac{\partial^2 u}{\partial r^2} + \frac{1}{r}\frac{\partial u}{\partial r}\right) \tag{2.40}$$

Solutions given by Zhu and Yin (2001), Tang and Onitsuka (2000), and Leo (2004) are lengthy and can be difficult to implement.

For simplicity, the method proposed by Carillo (1942) is often used, where the total degree of consolidation is related to the radial and vertical degrees of consolidation considered separately by the expression:

$$(1-U) = (1-U_{\mathrm{v}})(1-U_{\mathrm{h}}) \tag{2.41}$$

The discrepancy between this approximation and the solutions mentioned above is small, usually within 10%.

2.4 Properties of Prefabricated vertical drains

With early theoretical formulations developed for radial flow, when vertical sand drains and drain wells were first introduced for ground improvement, it was assumed that the drain had a circular cross section. However, sand drains have some disadvantages (McGown and Hughes 1981; Hausmann 1990; Hansbo 1993; Koener 1994):

- To have sufficient drainage capacity, the sand should be carefully selected, and the proper materials are not always found around a construction site.

- Discontinuity and bulking may occur due to the manner of their installation, or excessive lateral displacement, which may reduce the efficiency of the drainage system.
- The large diameter (from 150 to 750 mm) (Landau 1966) required for sand drains may cause an installation issue. In addition, a reduced hydraulic conductivity in the disturbed soils surrounding the sand drains can result from the installation process.

By contrast, various types of prefabricated vertical drains, also known as prefabricated band-shaped drains can overcome most of defects of sand drains (Rixner et al. 1986). Prefabricated vertical drains usually consist of a core of plastic covered by a filter sleeve or jacket of non-woven geotextile, paper, fibrous material, or porous material (see Fig. 2.15). Most available drains are from 90 to 100 mm wide and 3 to 10 mm thick. They are commonly used to accelerate the process of consolidation or to de-water fine grained soils (Li and Rowe 2001; Bergado et al. 2002; Chu et al. 2004; Lorenzo et al. 2004; Shen et al. 2005; Rowe and Li 2005; Abuel-Naga et al. 2006; Sinha at al. 2007; Rowe and Taechakumthorn 2008; Chai et al. 2008).

(a)

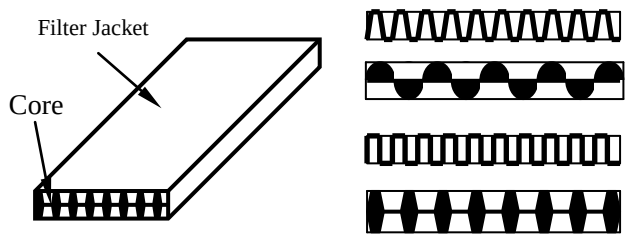

(b)

Fig. 2.15 Prefabricated vertical drains: (a) PVD consists of a plastic drainage core surrounded by a geotextile filter, (b) different shapes of plastic cores

2.4.1 Influence Zone

Square or triangular patterns are always used for vertical drains, as shown in Fig. 2.16. It was noted by Rixner et al. (1986) that while a square pattern can be laid out in the field, a triangular pattern provides more uniform settlement. The influence zone can be defined as the area covered by pore water flowing to a single drain. A circle of equal area is calculated to convert the square or hexagonal influence zones to equivalent circular zones for use in analytical solutions. The influence radius (r_e), for square and triangular spacing arrangements can be expressed in terms of the drain spacing (S_d) by Eqs. (1) and (2) respectively:

$$r_e = \frac{S_d}{\sqrt{\pi}} = 0.564 S_d \tag{2.42}$$

$$r_e = S_d \sqrt{\frac{\sqrt{3}}{2\pi}} = 0.525 S_d \tag{2.43}$$

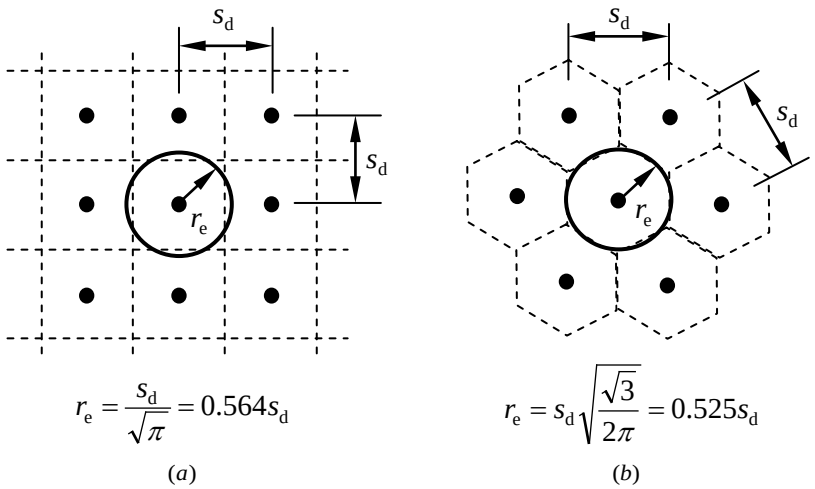

Fig. 2.16 Installation patterns for vertical drains: (a) Square pattern, (b) Triangular pattern (after Basu et al. 2008)

2.4.2 Equivalent diameter of prefabricated vertical drains

Most analytical solutions to vertical drain problems assume that pore water flows into drains with a circular cross section. If band shaped drains are to be analysed with such solutions then the rectangular cross section must be converted to an equivalent circular one, as shown in Fig. 2.17

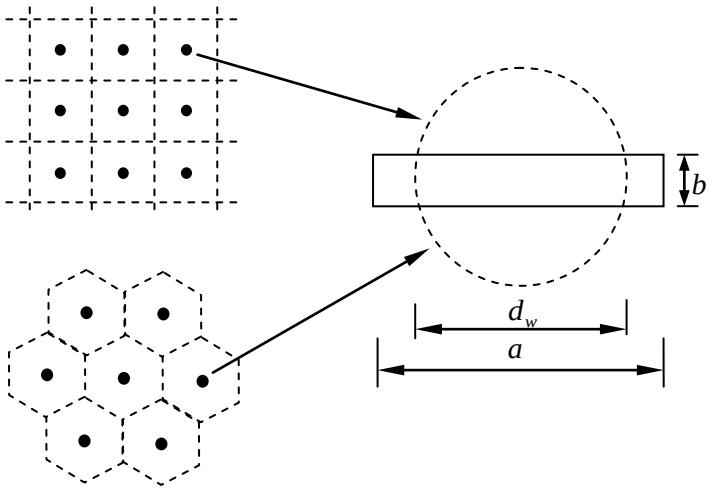

Fig. 2.17 Equivalent drain diameter

Conversion relationships have been proposed for a rectangular drain with width a and thickness b in Table 2.7. Walker et al. (2000) and Indraratna and Redana (2002) found that the difference in consolidation rates calculated using any of the equations was limited. The equations proposed by Hansbo (1979) and Atkinson and Eldred (1981) are mostly used although there is no definitive answer as to which of the above equations are the best. Some studies have been carried out to calculate the equivalent diameter for band shaped drains by comparing the consolidation rate for areas in which both band shaped drains and sand drains were installed in the same soft clay formation (Hansbo and Torstensson 1977; Fellenius and Wager 1977; Hannon 1986). The computed equivalent band diameter varied from 100 to 150 mm, which was much larger than the physical dimensions of the band shaped drains. These observations were probably caused by the different smear effects due to the drain installation. The mandrel used for installing the band shaped drains may cause less smear than the larger mandrel required for installing sand drains. Therefore, an over estimated equivalent diameter drain would result from not considering the different smear effects when the equivalent drain diameter is calculated.

Table 2.7 Equivalent drain diameter

Resources	Equivalent diameter of prefabricated vertical drains
Hansbo (1979) and Koerner (1994)	$d_w = 2(a+b)/\pi$
Atkinson and Eldred (1981)	$d_w = (a+b)/2$
Fellenius and Castonguay (1985)	$d_w = (4ab/\pi)^{0.5}$
Pradhan et al. (1993)	$d_w = d_e - 2\sqrt{s^{-2}} + b$ where $s^{-2} = \frac{1}{4}d_e^2 + \frac{1}{12}a^2 - \frac{2a}{\pi^2}d_e$
Long and Covo (1994)	$d_w = 0.5a + 0.7b$

2.4.3 Smear zone properties

2.4.3.1 Formation of the smear zone

The smear zone is a disturbed area surrounding the drain when vertical drains are installed in the soft ground with mandrels that are inserted and then withdrawn. The soil adjacent to the drains restructures immediately, and the soil further away from the drain consolidates caused by the dissipation of excess pore pressure created by cavity expansion when the mandrel is pushed into the soil (Sharma and Xiao, 2000). Usually the influence of the smear zone is considered with an idealized two-zone model, where the smear zone is the disturbed region in the immediate vicinity of the drain, and the outer zone is the intact (undisturbed) region.

2.4.3.2 Smear zone properties and extent

Compared to undisturbed soil, the permeability, water content, and void ratio in the smear zone are reduced. The variation of the horizontal and vertical coefficient of permeability with radial distance for various mean applied consolidation pressures (Indraratna and Redana 1998) is shown in Fig. 2.18. The significant reduction of horizontal permeability observed in the vicinity of the drain indicates that the radius of the smear zone can be taken to be 100 mm, or estimated to be a factor of four to five times the radius of the mandrel. As can be seen, horizontal permeability can be reduced to the same value as vertical permeability when approaching the drain, while the vertical permeability remains relatively unchanged along the radial distance. In addition, the change in horizontal permeability increases with the decreasing mean consolidation pressure.

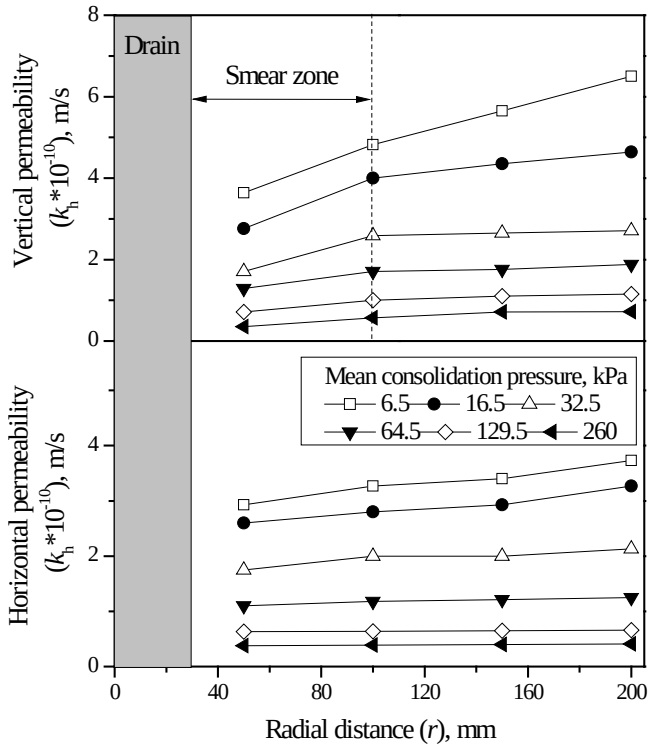

Fig. 2.18 Permeability along radial distance from central drain: (a) horizontal, (b) vertical (original data from Indraratna and Redana 1998)

As discussed by various researchers (Taylor 1948; Samarasinghe et al. 1982; Tavenas et al. 1983a, b; Babu et al. 1993), the permeability depends on the water content and void ratio of the soil, and therefore the extent of the smear zone can be examined based on variation in the water content and void ratio measurements. The relationship between water content and radial distance (Sathananthan and Indratana 2006) is shown in Fig. 2.19. As expected, the water content decreased towards the drain. Based on these curves, the extent of the smear zone can be estimated to be around 2.5 times the equivalent radius of the mandrel. The relationship between the void ratio and radial distance is shown in Fig. 2.20. Similarly to the water content, the void ratio reduces towards the drain. The smear zone parameters proposed for a constant permeability smear zone are given in Table 2.2 (Xiao 2002).

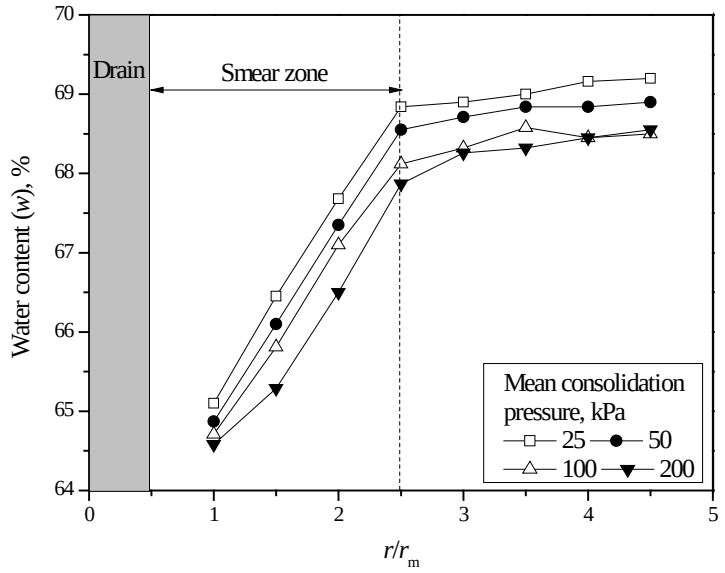

Fig. 2.19 The variation of water content with radial distance (original data from Sathananthan and Indratana 2006)

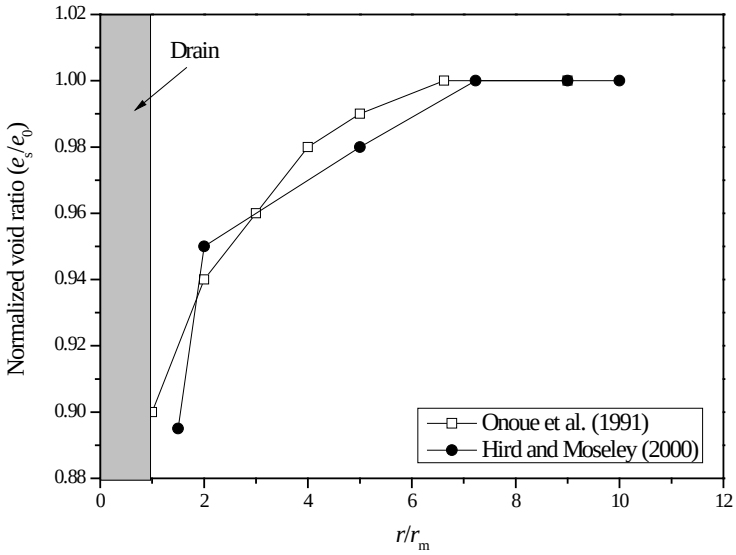

Fig. 2.20 The variation of normalised void ratio with radial distance after drain installation

Table 2.8 Smear zone parameters

Resource	Extent	Permeability
Barron (1948)	$r_s = 1.6r_w$	$k_h / k_s = 3$
Hansbo (1981)	$r_s = 1.5r_w$	$k_h / k_s = 3$
Bergado et al. (1991)	$r_s = 2r_w$	$k_h / k_s = 1$
Onoue (1991)	$r_s = 1.6r_w$	$k_h / k_s = 3$
Almeida et al. (1993)	$r_s = 1.5 \sim 2r_w$	$k_h / k_s = 3 \sim 6$
Indraratna and Redna (1998)	$r_s = 4 \sim 5r_w$	$k_h / k_s = 1.15$
Chai and Miura (1999)	$r_s = 2 \sim 3r_w$	$(k_h / k_s)_{field} = C_f (k_h / k_s)_{lab}$
Hird and Moseley (2000)	$r_s = 1.6r_w$	$k_h / k_s = 3$
Xiao (2001)	$r_s = 4r_w$	$k_h / k_s = 1.3$
Sathananthan and Indratana (2006)	$r_s = 2.5r_w$	$k_h / k_s = 1.5$

2.5 Conclusions

A comprehensive review of the behaviour of soft soils under cyclic loading is provided in Chapter 2. The factors which affect the performance of the soils such as amplitude of cyclic load or cyclic stress ratio, loading rate (strain rate for static loading and loading frequency for cyclic loading), overconsolidation ratio, initial shear stress (drained or undrained), drainage during or after cyclic loading are analysed. In addition, theories of consolidation have been reviewed. Vertical consolidation (Terzaghi's theory of one-dimensional consolidation), radial consolidation (Barron's theory including hypotheses of free strain and equal strain), and the combination of vertical and radial consolidation (Carillo's expression) have been presented. The modification of these theories from other researchers is provided as well. Finally, the properties of prefabricated vertical drains such as influence zone, equivalent diameter of prefabricated vertical drain, smear zone properties and extent have been studies.

3 Undrained Cyclic Triaxial Test

3.1 Introduction

This Chapter describes the undrained cyclic triaxial tests carried out on soft clay specimens. Varying cyclic stress ratios (CSR = 0.4, 0.6 and 0.8) and frequencies (f = 0.1, 1, 2, and 5 Hz) were chosen as the experimental variables to investigate the performance of soft subgrade soil subjected to cyclic loading. The development of excess pore pressures and axial strains were investigated against either a number of loading cycles or loading time, and the primary factors influencing the stability of clay subgrade are discussed. A critical level of cyclic stress was determined by distinguishing failure from stable specimens, and the effect of the strain rate on the cyclic behaviour of soft clays was investigated.

3.2 Test schedule

3.2.1 Soil properties

Specimens of reconstituted Kaolinite 38 mm in diameter by 76 mm high were used in this undrained cyclic triaxial test. The soil had the following properties:

- A specific gravity of $G_s = 2.7$.
- A liquid limit of $w_L = 55\%$. This liquid limit is the moisture content at which the soil passes from a plastic to a liquid state, as determined by the liquid limit test. A Cone Petrometer or Casagrande Apparatus can be used to determine the value of the Liquid Limit, and in this study, the Cone Penetrometer Method was chosen. As can be seen in Fig. 3.1, the moisture contents were plotted against their corresponding penetration values on a linear graph, with the water content on the horizontal axis and the penetration value on the vertical axis. A straight line of best fit was drawn through the plotted points. The liquid limit can then be determined from the intersection of the line of best fit, and the 20 mm penetration coordinate: $w_L = 0.0206 \times 20 + 0.1371 = 0.55$.

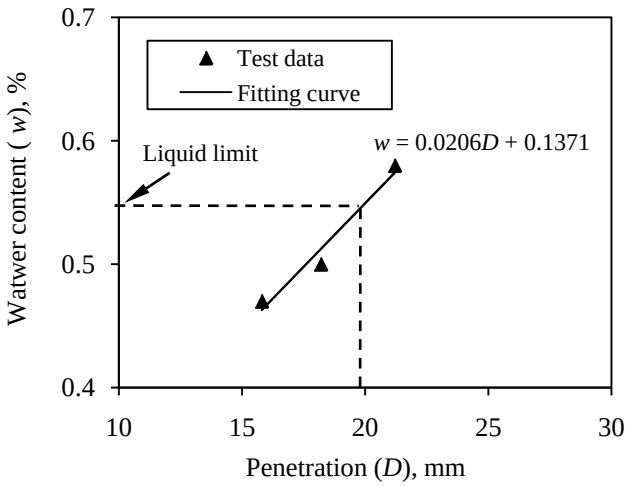

Fig. 3.1 Determination of liquid limit

- The plastic limit is $w_p = 27\%$. The plastic limit is the water content where soil transitions between brittle and plastic behaviour, and it can be determined as the one where a thread of soil begins to crumble when rolled into a 3 mm diameter. The results of three plastic limit tests are given in Table 3.1. The plastic limit can then be calculated as the average value of three water contents: $w_p = (0.26 + 0.27 + 0.28)/3 = 0.27$.

Table 3.1 Water content data for plastic limit test

Can no.	K-B	K87	E1
Mass of cup & wet soil, g	9.35	15.41	22.4
Mass of cup & dry soil, g	9.21	15.09	21.99
Mass of can, g	8.66	13.9	20.54
Mass of dry soil, g	0.55	1.19	1.45
Mass of water, g	0.14	0.32	0.41
Water Content, %	0.26	0.27	0.28

- A plastic index of $\mathrm{PI} = 28\%$. The plasticity index is a measure of the plasticity of a soil. It is the size of the range of water contents where the soil exhibits plastic properties and can be determined as $\mathrm{PI} = w_{\mathrm{L}} - w_{\mathrm{P}} = 0.55 - 0.27 = 0.28$.

- The compression index is $C_{\mathrm{c}} = 0.42$ and swelling index is $C_{\mathrm{s}} = 0.06$. The relationship between the void ratio (e) and vertical pressure (σ_{v}) is given in Fig. 3.2. The compression index is the slope of the linear portion of the $e - \log\sigma_{\mathrm{v}}$ plot, while the swelling index is the slope of the swelling part of the $e - \log\sigma_{\mathrm{v}}$ plot.

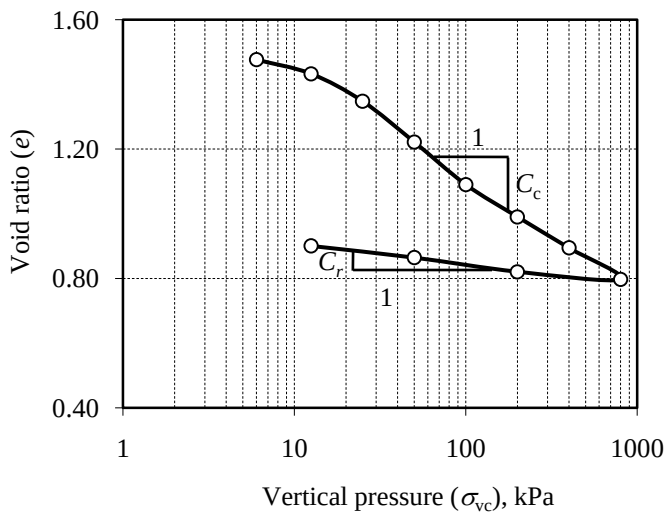

Fig. 3.2 Relationship between the void ratio (e) and vertical pressure (σ_{vc})

3.2.2 Triaxial equipment

The undrained cyclic loading tests were carried out using the cyclic triaxial loading equipment shown in Fig. 3.3. This apparatus is mainly comprised of the axial loading unit, the air pressure and water control unit, the pore pressure measurement system, and the volumetric change measurement device. Excess pore pressures were measured through the bottom base.

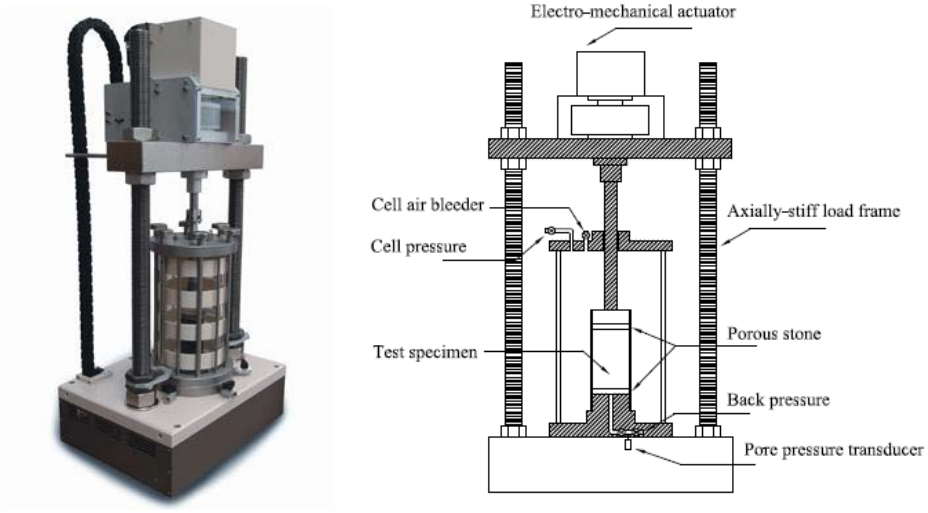

(a) (b)

Fig. 3.3 Triaxial cyclic loading equipment: (a) Photograph and, (b) Schematic diagram

3.2.3 Consolidation condition

The consolidation pressure was chosen to simulate an in situ condition and therefore it was necessary to work out the typical in situ effective vertical stress $\sigma_{\mathrm{v}}^{'}$ and effective horizontal stress $\sigma_{\mathrm{h}}^{'}$ based on $\sigma_{\mathrm{h}}^{'} = k_0 \sigma_{\mathrm{v}}^{'}$. The components of the rail track structure are given in Fig. 3.4.

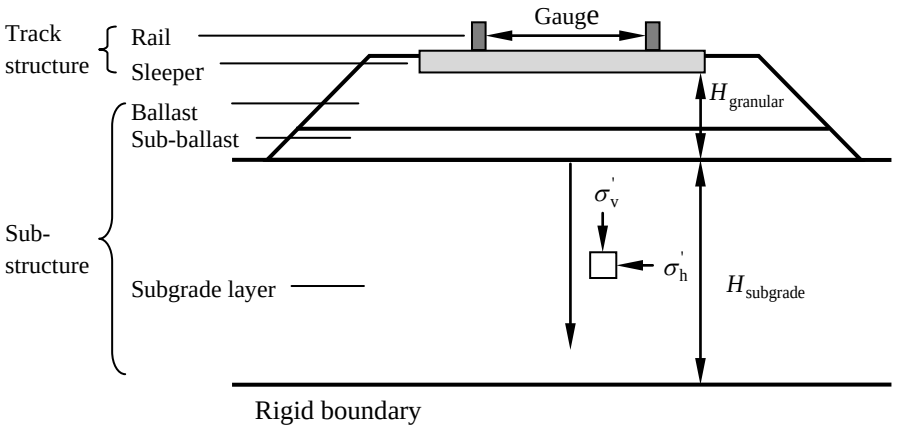

Fig. 3.4 The structure of a rail track system

The additional vertical stress in the subgrade layer consisted of two parts from the track structure (rectangular shape) and granular layer (trapezoidal shape) respectively, as shown in Fig. 3.5 (a). To make the calculation easier, the stress from the granular layer was further divided into one rectangle and two triangles.

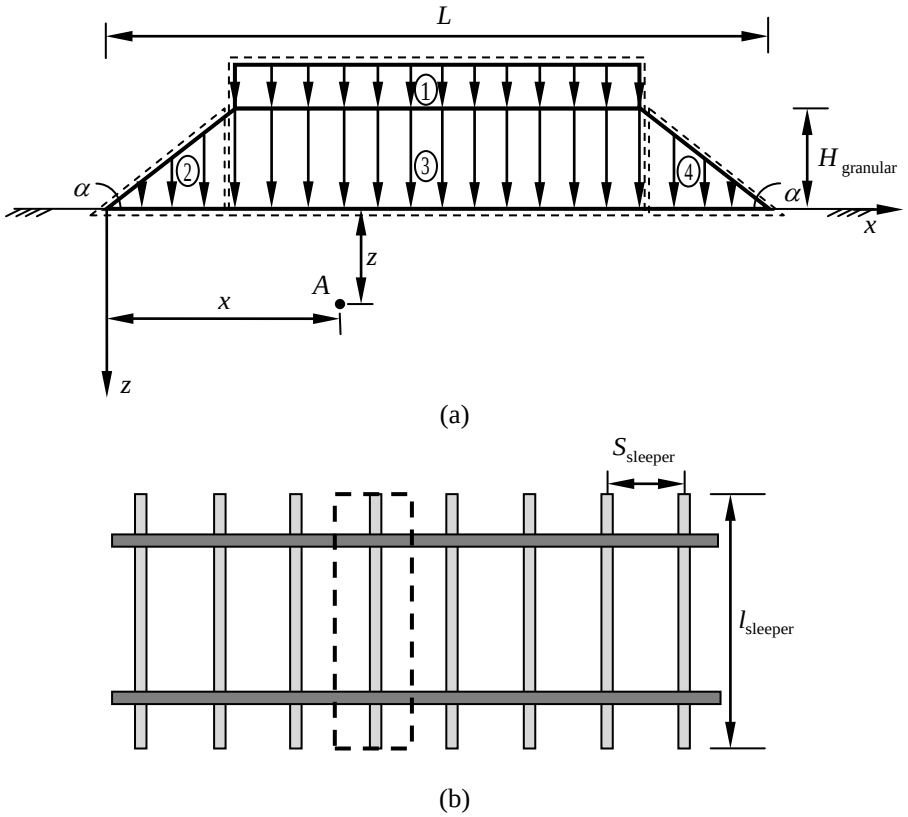

Fig. 3.5 The calculation of the consolidation pressure in the subgrade: (a) Vertical stress in the subgrade, (b) Area being considered

Elastic theory and the principle of superposition were used to calculate the vertical stress at point *A* . The details are shown below:

- **Stress for shape ①**: The chosen area for this analysis is shown in Fig. 3.5 (b). The weight of the rail can be expressed as:

$$W_{\text{rail}}(\text{N}) = 2 \times \rho_{\text{rail}}(\text{kg/m}) \times S_{\text{sleeper}}(\text{m}) \times 9.81(\text{m/s}^2) \tag{3.1}$$

The weight of the sleeper can be expressed as:

$$W_{\text{sleeper}}(\text{N}) = m_{\text{sleeper}}(\text{kg}) \times 9.81(\text{m/s}^2) \tag{3.2}$$

Then the vertical stress from the track structure can be obtained by:

$$\sigma_{\text{track}}(\text{kPa}) = \frac{W_{\text{rail}}(\text{N}) + W_{\text{sleeper}}(\text{N})}{S_{\text{sleeper}}(\text{m}) \times L_{\text{sleeper}}(\text{m})} / 1000 \tag{3.3}$$

- **Stress for shape ②**: The stress intensity at the vertical side can be given by:

$$\sigma_{\text{granular2}}(\text{kPa}) = D_{\text{granular}}(\text{kg/m}^3) \times 9.81(\text{m/s}^2) \times H_{\text{granular}}(\text{m}) / 1000 \tag{3.4}$$

- **Stress for shape ③**: The stress intensity can be given by:

$$\sigma_{\text{granular3}}(\text{kPa}) = D_{\text{granular}}(\text{kg/m}^3) \times 9.81(\text{m/s}^2) \times H_{\text{granular}}(\text{m}) / 1000 \tag{3.5}$$

- **Stress for shape ④:** The stress intensity at the vertical side can be given by:

$$\sigma_{\text{granular4}}(\text{kPa}) = D_{\text{granular}}(\text{kg/m}^3) \times 9.81(\text{m/s}^2) \times H_{\text{granular}}(\text{m}) / 1000 \tag{3.6}$$

- Then the additional vertical stress in the subgrade can be calculated by:

$$\begin{aligned} \sigma_{\text{z,additional}}(\text{kPa}) &= K_{\text{t2}}^{\text{z}} \sigma_{\text{granular2}}(\text{kPa}) \\ &+ K_{\text{s}}^{\text{z}} \left(\sigma_{\text{track}} + \sigma_{\text{granular3}}\right)(\text{kPa}) + K_{\text{t4}}^{\text{z}} \sigma_{\text{granular4}}(\text{kPa}) \end{aligned} \tag{3.7}$$

where $K_{\text{t2}}^{\text{z}} = \frac{1}{\pi}\left\{ m_2 \left[\text{arctg}\left(\frac{m_2}{n_2}\right) - \text{arctg}\left(\frac{m_2 - 1}{n_2}\right)\right] - \frac{(m_2 - 1)n_2}{(m_2 - 1)^2 + n_2^2} \right\}$,

$m_2 = x/\left(H_{\text{granular}} \text{c}\tan(\alpha)\right)$, $n_2 = z/\left(H_{\text{granular}} \text{c}\tan(\alpha)\right)$,

$K_{\text{s}}^{\text{z}} = \frac{1}{\pi}\left\{ \text{arctg}\left(\frac{m_3}{n_3}\right) - \text{arctg}\left(\frac{m_3 - 1}{n_3}\right) + \frac{m_3 n_3}{n_3^2 + m_3^2} - \frac{(m_3 - 1)n_3}{(m_3 - 1)^2 + n_3^2} \right\}$,

$m_3 = \left(x - H_{\text{granular}} \text{c}\tan(\alpha)\right)/l_{\text{sleeper}}$, $n_3 = z/l_{\text{sleeper}}$,

$K_{\text{t4}}^{\text{z}} = \frac{1}{\pi}\left\{ m_4 \left[\text{arctg}\left(\frac{m_4}{n_4}\right) - \text{arctg}\left(\frac{m_4 - 1}{n_4}\right)\right] - \frac{(m_4 - 1)n_4}{(m_4 - 1)^2 + n_4^2} \right\}$

$m_4 = \left(H_{\text{granular}} + 2H_{\text{granular}} \text{c}\tan(\alpha) - x\right)/\left(H_{\text{granular}} \text{c}\tan(\alpha)\right)$,

$n_4 = z/\left(H_{\text{granular}} \text{c}\tan(\alpha)\right)$.

- Therefore the total vertical stress at depth z can be calculated as:

$$\sigma_z\left(\text{kPa}\right) = D_{\text{subgrade}}\left(\text{kg/m}^3\right) \times 9.81\left(\text{m/s}^2\right) \times z\left(\text{m}\right)/1000 + \sigma_{z,\text{additional}}\left(\text{kPa}\right) \qquad (3.8)$$

Usually H_{granular}, ρ_{rail}, D_{granular}, m_{sleeper}, S_{sleeper}, and l_{sleeper} influence the additional vertical stress imposed in the subgrade, however the last five parameters were relatively constant and therefore only the effect of H_{granular} on the additional vertical stress was considered. The vertical stresses that changed with depth for different thicknesses of the granular layer are shown in Fig. 3.6, where H_{granular} changed through 0.3, 0.6, 0.9 to 1.2 m. As the thickness of the granular layer increased the vertical stress near the surface of the subgrade obviously increased as well, but when $H_{\text{granular}} > 4\,\text{m}$, the vertical stress was almost equal to the self-weight stress of the subgrade and was not affected by any further vertical stress. The vertical stresses that changed with depth as the densities of the rail differed, are shown in Fig. 3.7 where the ρ_{rail} changed through 30, 40, 50 to 60 kg/m. It can be seen that as the density of the rail increased, the vertical stress only increased incrementally and therefore can be omitted.

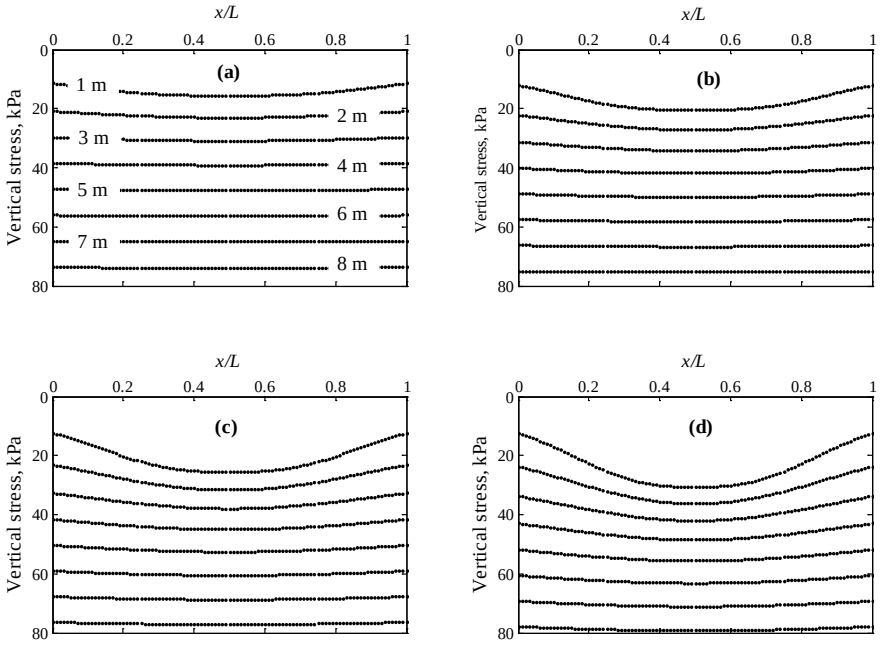

Fig. 3.6 Vertical stress at different depths from the surface of the subgrade, from one metre to eight metres, at one metre intervals ($S_{\text{sleeper}} = 0.6\,\text{m}$, $l_{\text{sleeper}} = 2.45\,\text{m}$, $m_{\text{sleeper}} = 300\,\text{kg}$, $\rho_{\text{rail}} = 60$ kg/m, $D_{\text{granular}} = 1.76$ Mg/m^3, $D_{\text{subgrade}} = 1.92$ Mg/m^3, and $\alpha = 35^o$):
(a) $H_{\text{granular}} = 0.3\,\text{m}$, (b) $H_{\text{granular}} = 0.6\,\text{m}$, (c) $H_{\text{granular}} = 0.9\,\text{m}$, (d) $H_{\text{granular}} = 1.2\,\text{m}$

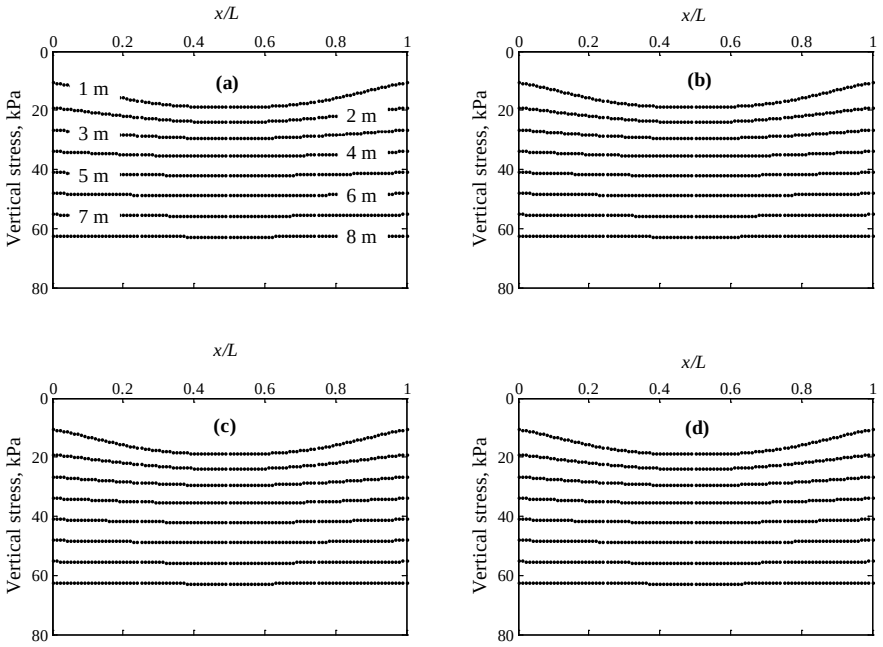

Fig. 3.7 Vertical stress at different depths from the surface of the subgrade , from one metre to eight metres, at one metre intervals ($S_{\text{sleeper}} = 0.6$ m, $l_{\text{sleeper}} = 2.45$ m, $m_{\text{sleeper}} = 300$ kg, $H_{\text{granulal}} = 0.6$ m, $D_{\text{granular}} = 1.76$ Mg/m^3, $D_{\text{subgrade}} = 1.92$ Mg/m^3, and $\alpha = 35^{\text{o}}$): (a) $\rho_{\text{rail}} = 30$ kg/m, (b) $\rho_{\text{rail}} = 40$ kg/m , (c) $\rho_{\text{rail}} = 50$ kg/m , (d) $\rho_{\text{rail}} = 60$ kg/m

Since the additional dynamic stress induced by the train attenuated rapidly relative to depth, dropping to 20% of the surface mean at a depth of 2.5 m (Liu and Xiao 2010), 3 or 4 m were deep enough for this analysis. It can be seen from Fig. 3.6 that the vertical stress at a depth of 4 m is $\sigma_{\text{v}}^{'} = 40$ kPa. Assuming that $k_0 = 0.6$, the horizontal stress is $\sigma_{\text{h}}^{'} = 24$ kPa. Therefore $\sigma_{1\text{c}}^{'} = 40$ kPa and $\sigma_{3\text{c}}^{'} = 24$ kPa were used as the consolidation pressures for the specimens used for the following tests.

3.2.4 Cyclic loading conditions

A series of undrained cyclic triaxial loading tests were carried out on specimens of soft Kaolin clay. The effect of the influencing factors on the cyclic behaviour of these specimens, such as the cyclic stress ratio (CSR = 0.4, 0.6 and 0.8) and loading frequency (f = 0.1, 1, 2, and 5 Hz) were investigated through the development of excess pore pressures and strains. All the test conditions, including the specimen name, cyclic stress ratio, and loading frequency are given in Table 3.2. These tests were stopped when either

failure occurred (axial strain began to increase dramatically) or it reached 34.466 cycles (for f = 1, 2, and 5 Hz) or 6,000 cycles (for f = 0.1 Hz). The patterns of cyclic stress at CSR = 0.8 for different loading frequencies are provided in Fig. 3.8.

Table 3.2 Test conditions and results

Sample	Mean effective stress after consolidation (p'_{c0}), kPa	Cyclic stress ratio (CSR)	Cyclic loading frequency (f), Hz	Loading cycles (N)	Time (t), min	Failed?
U_{01}	30	0.4	0.1	6,000	1,000	No
U_{02}	30	0.4	1	34,466	574	No
U_{03}	30	0.4	2	34,466	287	No
U_{04}	30	0.4	5	33,466	112	No
U_{05}	30	0.6	0.1	6,000	1,000	No
U_{06}	30	0.6	1	34,466	574	No
U_{07}	30	0.6	2	34,466	287	No
U_{08}	30	0.6	5	34,466	112	No
U_{09}	30	0.8	0.1	1,793	299	Yes
U_{10}	30	0.8	1	10,419	174	Yes
U_{11}	30	0.8	2	18,537	160	Yes
U_{12}	30	0.8	5	33,964	113	Yes

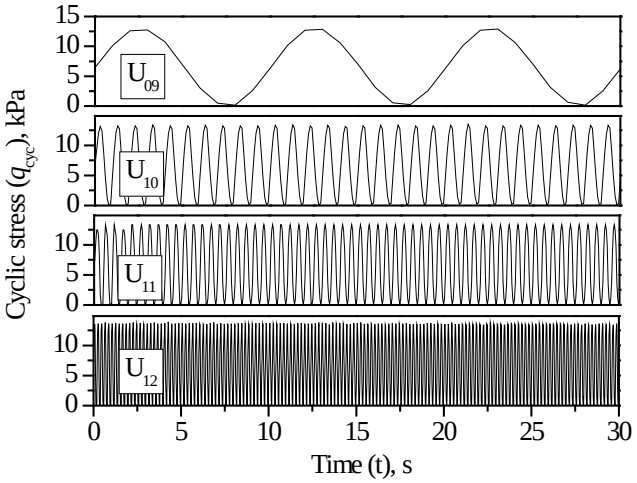

Fig. 3.8 Patterns of applied cyclic stress

3.3 The condition of the specimens after test (failed or stable)

Some of the results of the cyclic triaxial loading tests, such as the loading cycles, time, and whether they failed or not, are given in Table 3.2. Failure occurred after a number of cycles for specimens tested under a CSR of 0.8, irrespective of the loading frequency. The number of cycles at failure increased from 1,793 to 33,964 after the loading frequency was increased from 0.1 to 5 Hz. This observation was consistent with studies by Andersen (2009) and Takahashi et al. (1980) where more cycles were needed to bring the specimen to failure at a higher frequency. The time to failure can be calculated by $t_f = N_f (1/f)$ where N_f is the number of cycles at failure. In this current study t_f decreased from 299 to 113 min when the loading frequency was increased from 0.1 to 5 Hz. On the other hand, the specimens did not fail at the end of the tests and behaved in a stable manner under a CSR of 0.4 and 0.6. Therefore, the critical cyclic stress ratio was expected to be greater than 0.6.

The conditions of the failed and stable specimens are given in Fig. 3.9. It is shown in Fig. 3.9 (b) that the failure mode of soft clay was barrelling. It is well known that the original microstructure begins to be destroyed when very large strains are imposed on the specimen. No soil element is perfectly homogenous, and because of imperfections such as friction between the loading platens and the soil, the stress conditions imposed on the specimen were not uniform either. The combined effect of these factors was that after failure, shear strains tended to occur along a plane or planes of weakness, as shown in Fig. 3.10. With stiff clays and dense sand there was usually only one such slip surface, as shown in Fig. 3.10 (b), whereas for soft clays, large strains resulted in barrelling (see Fig. 3.10 (a)) with numerous slip surfaces that formed a diamond shaped pattern on the surface of the sample.

(a)

(b)

(c)

Fig. 3.9 The profile of the specimen: (a) Before the undrained cyclic triaxial test, (2) After the undrained cyclic triaxial test (failed specimen), (3) After the undrained cyclic triaxial test (stable specimen)

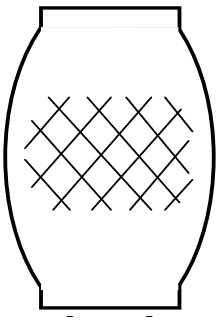

(a)

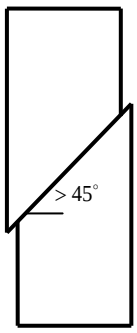

(b)

Fig. 3.10 Modes of failure of samples subjected to axial loading: (a) Barrelling of soft clay sample, (b) Single failure surface typical of stiff clay or dense sand

3.4 Excess pore pressure and strain history

Axial strains are plotted in Fig. 3.11(b) against the number of loading cycles for the first 1,000 and 10,000 cycles for specimens U_{06} and U_{10} to show the difference between a stable and a failed sample. The data for specimen U_{06} indicated that the development of axial strain was very small, at less than 0.7% after 10,000 cycles, while the specimen U_{10} had a much larger axial strain of nearly 10% after the same time period. Apart from the different values of axial strains between the failed and stable sample, the shapes of the axial strain-cycle curves were also different. While the rate of axial stain generated generally diminished during the initial 1,000 cycles of loading of both specimens, there was a significant increase in axial strain for U_{10} beyond say 8,000 cycles (following a constant rate of strain between say 2,000 and 6,000 cycles), which caused failure to occur.

A similar comparison for excess pore pressure was found between specimens U_{06} and U_{10} as shown in Fig. 3.11(a). The maximum normalised excess pore pressure for specimen U_{06} was around 0.4 after 10,000 cycles, which was lower than the failed specimen U_{06} of 0.65. Nevertheless, there was no distinct difference in the shape of the excess pore pressure-cycle curve for both the stable and failed samples. The rate of excess pore pressure build up for specimen U_{10} kept on decreasing, even after 10,000 cycles, where failure was imminent.

The cyclic stress-strain relationship for 2,000 to 10,000 cycles at 2,000 cycle intervals, for specimens U_{06} and U_{10} are shown in Fig. 3.12. While the incremental axial strain for specimen U_{06}, at each cycle decreased with the increasing number of cycles, it increased for specimen U_{10}.

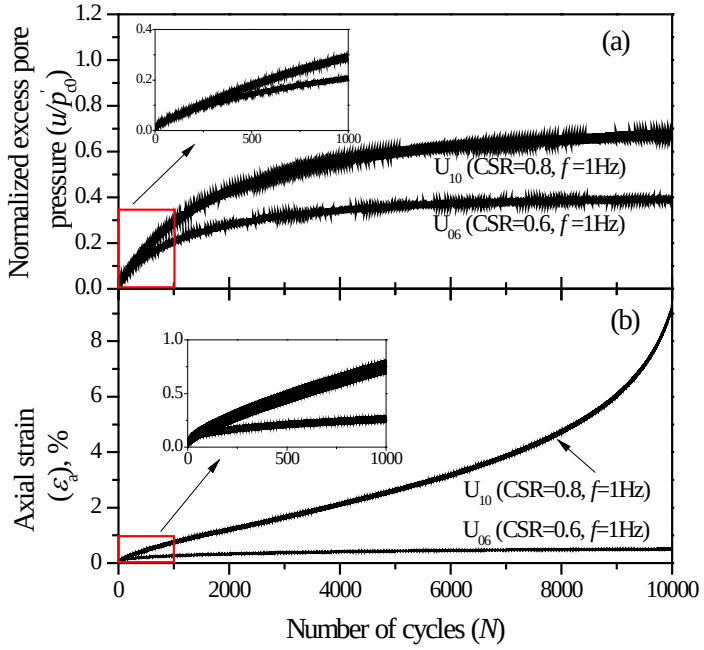

Fig. 3.11 History of excess pore pressure and axial strain during cyclic triaxial test: (a) Excess pore pressure, (b) Axial strain

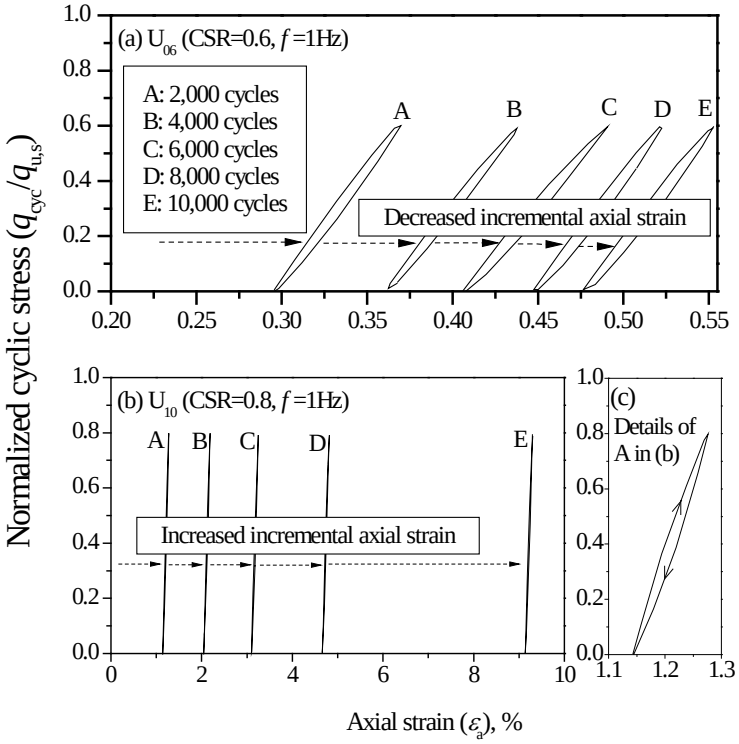

Fig. 3.12 Cyclic stress-strain behaviour

The cyclic stress-excess pore pressure for 2,000 to 10,000 cycles at 2,000 cycle intervals for specimens U_{06} and U_{10} are shown in Fig. 3.13. The data for specimens U_{06} and U_{10} indicate that for both stable and failed specimens, the incremental excess pore pressure for each cycle decreased as the number of cycles increased. Unlike with strains, specimen U_{10} did not indicate failure in view of excess pore pressure alone.

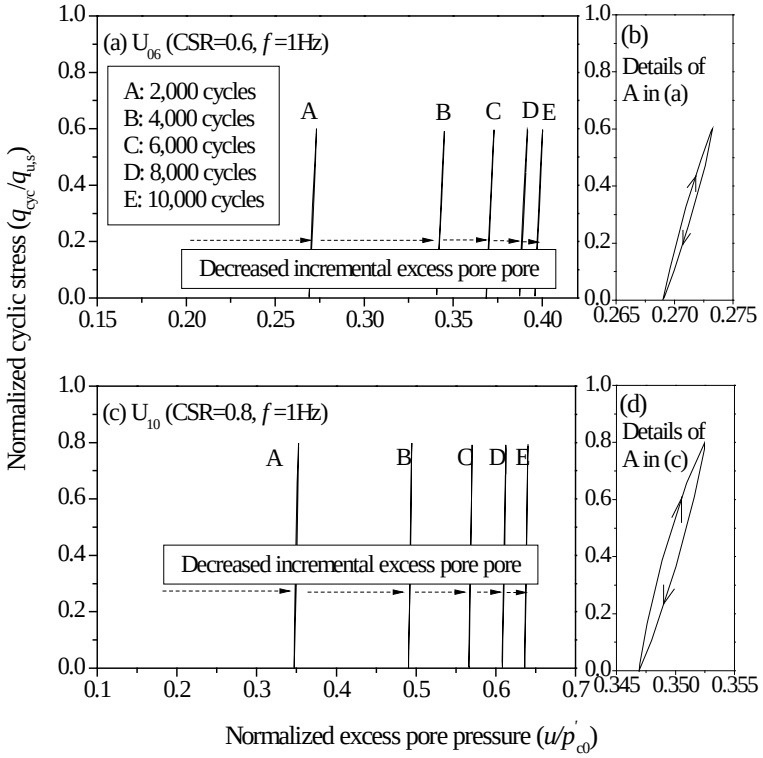

Fig. 3.13 Cyclic excess pore pressure behaviour

3.5 The effect of the cyclic stress ratio

The variations of normalised excess pore pressure and axial strain for specimens U_{01} to U_{12} against the number of cycles are plotted in Fig. 3.14 ~ Fig. 3.17. As expected, the normalised excess pore pressure and axial strains increased with the increasing cyclic stress ratio, for any loading frequency. The plots shown in Fig. 3.14(a) ~ Fig. 3.17(a) clearly suggest that the excess pore pressure rises significantly at the initial stages (N < 500) and then gradually increases with the number of cycles. For stable specimens (CSR = 0.4 and 0.6), the excess pore pressures stabilised after an initial rapid development, where the normalised excess pore pressures equalled 0.2 and 0.4 where the CSR = 0.4 and 0.6 respectively. For the failed specimens (CSR = 0.8), the excess pore pressures developed so quickly that a critical normalised value of 0.65 was reached in the first few cycles. The specimens failed before they could stabilise. It should be noted that no sample indicated failure simply by only looking at the normalised excess pore pressures.

In contrast, the results shown in Fig. 3.14(b) ~ Fig. 3.17(b) indicate that the four specimens failed because of a dramatic rise in axial strain, beyond a critical number of cycles. As can be seen, a rapid upward trajectory of axial strain occurred when a normalised excess pore pressure of 0.55 to 0.6 was attained through a comparison between the excess pore pressure and axial strains of specimens U_{09} - U_{12} (CSR = 0.8). While the failure of U_{09} (f = 0.1 Hz) occurred as N approached 2,000 cycles, for the highest frequency, i.e., U_{12} at f = 5 Hz, failure occurred as N > 30,000 cycles. However, it is important to note that if one were to convert the number of cycles to the actual time scale for a given frequency the difference in the time in which specimens U_{09} and U_{12} would fail is not as much as the number of cycles. For specimens with a CSR = 0.4 and 0.6, the axial strains at the end of the tests were less than 1%.

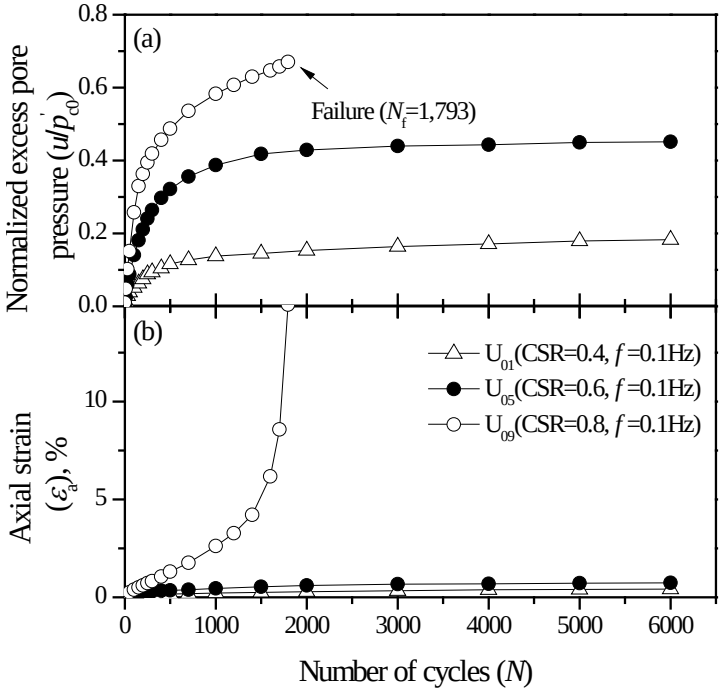

Fig. 3.14 Normalised excess pore pressures and axial strains under $f = 0.1$ Hz

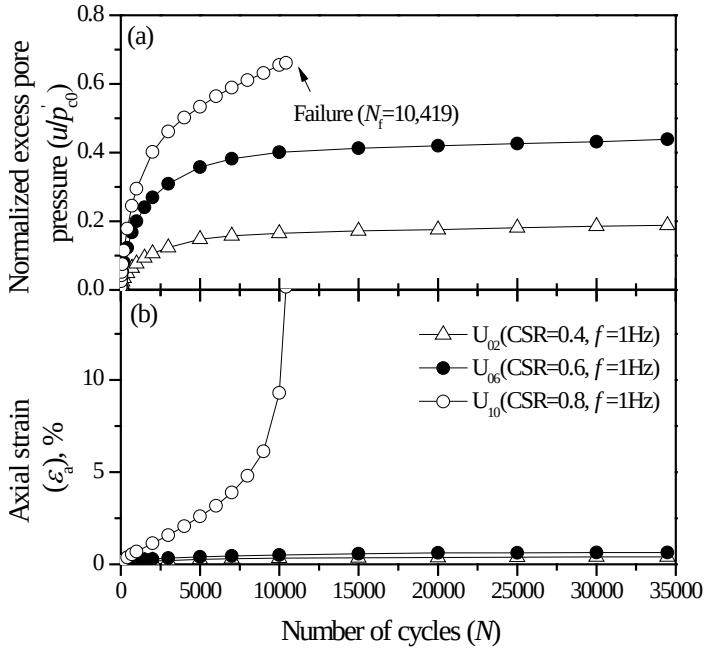

Fig. 3.15 Normalised excess pore pressures and axial strains under $f = 1$ Hz

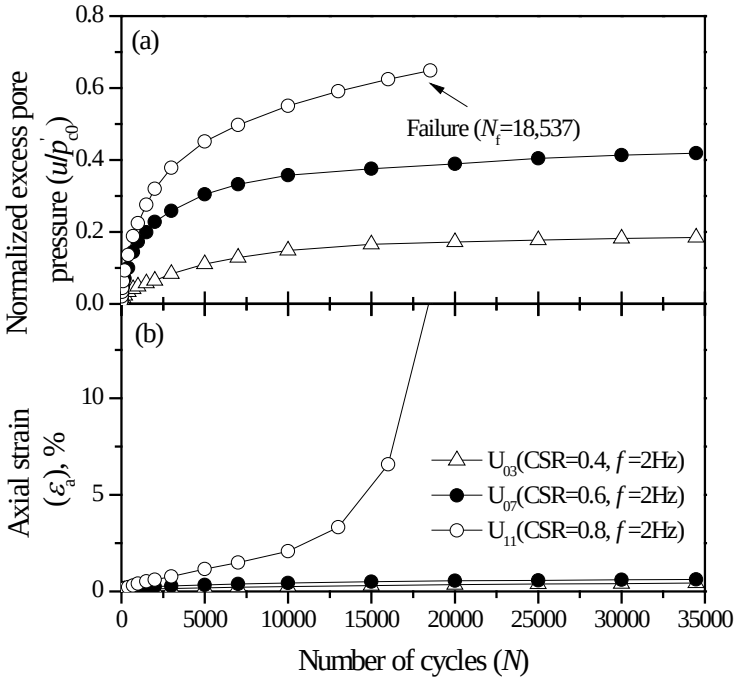

Fig. 3.16 Normalised excess pore pressures and axial strains under $f = 2$ Hz

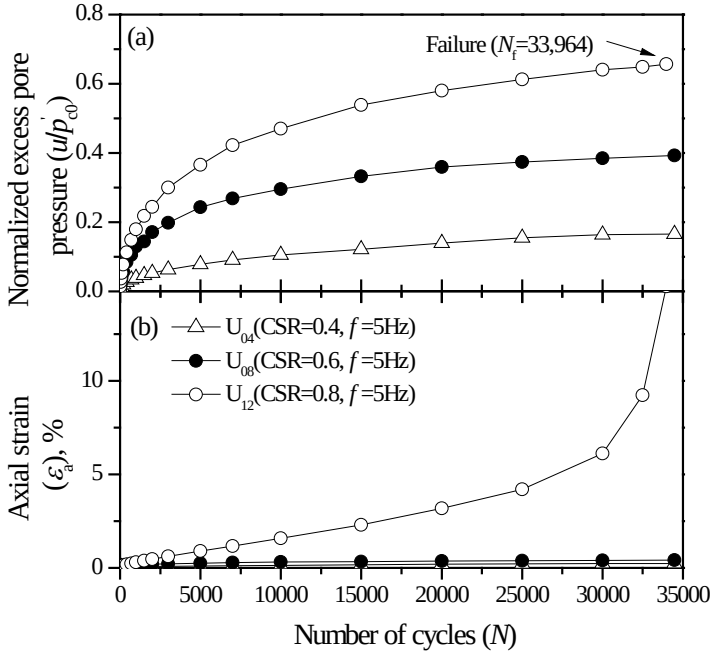

Fig. 3.17 Normalised excess pore pressures and axial strains under $f = 5$ Hz

It was proposed by Sakai et al. (1996) that there is a unique relationship between the normalised peak excess pore pressure (u/u_f) and the normalised loading cycle (N/N_f):

$$\frac{u}{u_f} = \frac{4}{\pi}\arctan\left[\left(\frac{N}{N_f}\right)^{(1/\alpha)}\right] \tag{3.9}$$

where α is an experimental parameter. The non-linear relationship for specimens U_{09} - U_{12} are shown in Fig. 3.18. The value of the experimental parameter α is 3. Sakai et al. (1996) found that the curves of u/u_f - N/N_f were dependent of neither the cyclic stress ratio nor the initial shear stress level. In the current research work, it is indicated in Fig. 3.18 that the curves of u/u_f - N/N_f are independent of the cyclic loading frequency.

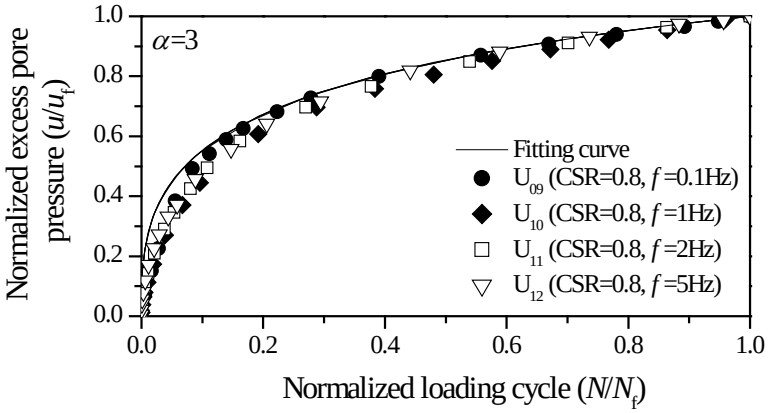

Fig. 3.18 Relationship between normalised excess pore pressure and the loading cycle

If the results of normalised excess pore pressure (u/u_f) are plotted against the normalised axial strain ($\varepsilon_a/\varepsilon_{af}$), a unique relationship will be observed as well (Sakai et al. 1996):

$$\frac{u}{u_f} = \ln\left[1+\beta\left(\varepsilon_a/\varepsilon_{af}\right)\right]/\ln\left(1+\beta\right) \tag{3.10}$$

where β is an experimental parameter. Then the development of excess pore pressure and axial strains against the number of cycles can be predicted by the u/u_f - N/N_f and u/u_f - $\varepsilon_a/\varepsilon_{af}$ relationships. For CSR = 0.4 and 0.6, where the failure did not occur, the values of u_f , ε_{af}, and N_f are replaced by the ones at the end of the test.

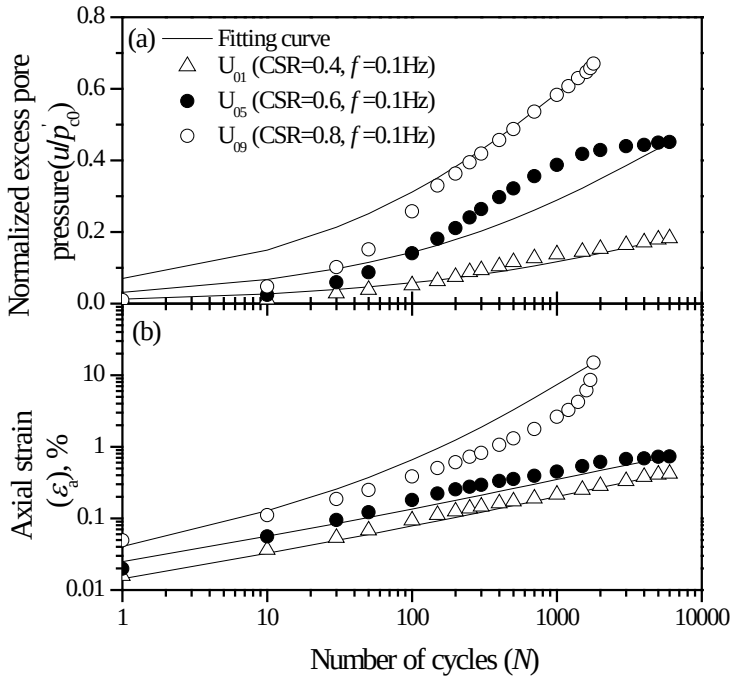

Fig. 3.19 Comparison of predicted excess pore pressures and axial strains with test data $f = 0.1$ Hz

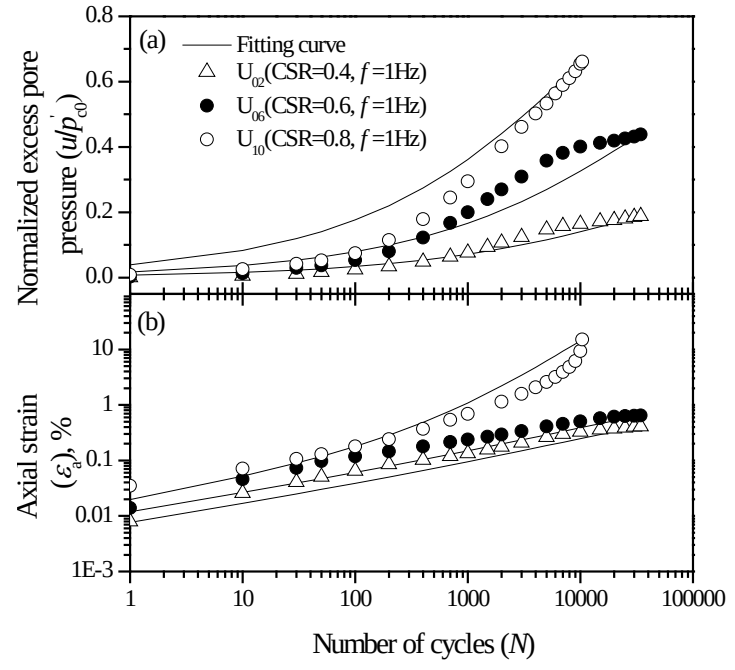

Fig. 3.20 Comparison of predicted excess pore pressures and axial strains with test data $f = 1$Hz

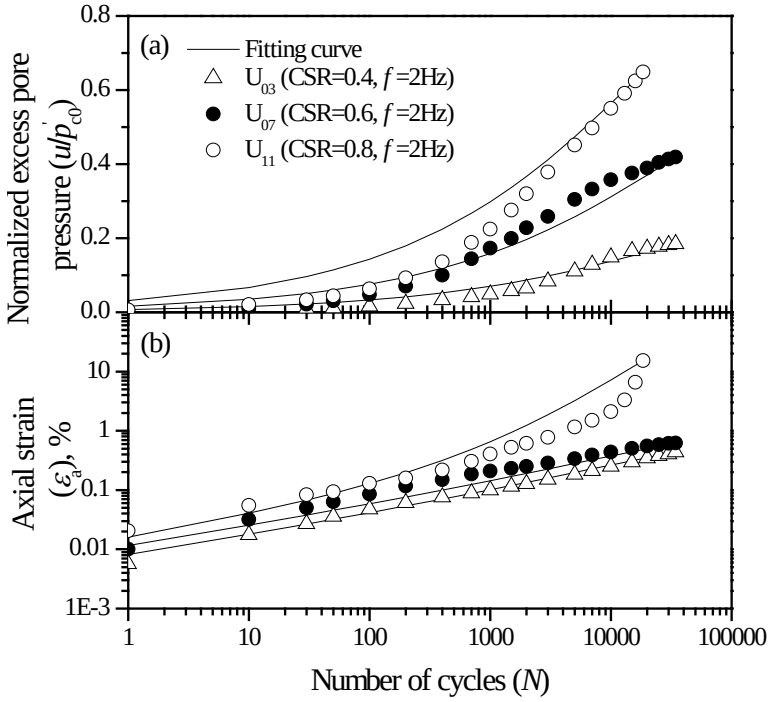

Fig. 3.21 Comparison of predicted excess pore pressures and axial strains with test data $f = 2$ Hz

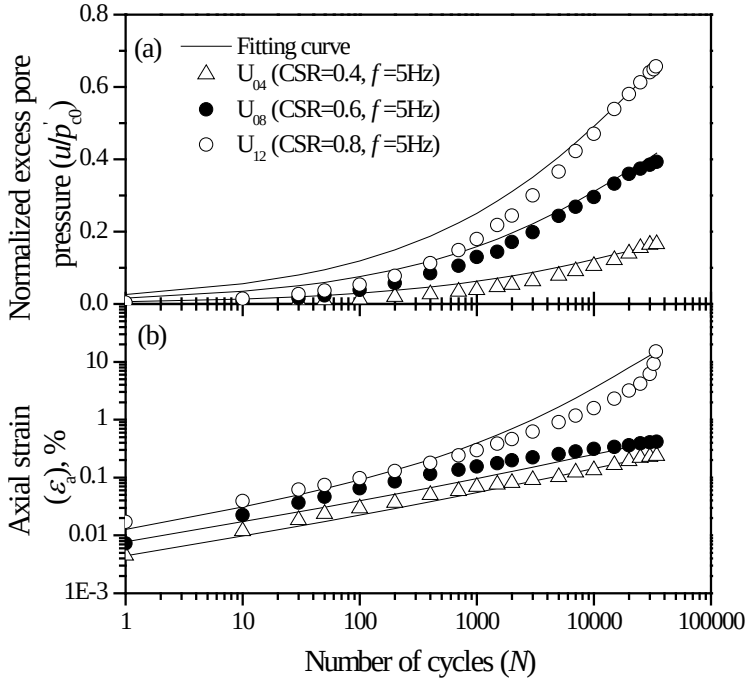

Fig. 3.22 Comparison of predicted excess pore pressures and axial strains with test data $f = 5$ Hz

3.6 The effect of cyclic loading frequency

3.6.1 Analysis based on the number of loading cycles

The effect of the cyclic loading frequency on normalised excess pore pressure and axial strains against the number of cycles is shown in Fig. 3.23 ~ Fig. 3.25. The test results given in Fig. 3.23(a) and Fig. 3.24(a) indicate that at a low cyclic stress ratio (CSR = 0.4 and 0.6), excess pore pressure developed more rapidly at a lower loading frequency in the early stage of cyclic loading (N < 5,000 cycles). The development of excess pore pressure can be roughly divided into an initial rapid development and then a stable state. The excess pore pressure at the end of the initial rapid development can be defined as the stable excess pore pressure u_s. Based on the observation of excess pore pressure, the specimens at a lower loading frequency entered a stable state within a lesser number of cycles. For example, where $CSR = 0.4$, the specimen U_{01} had u_s / p'_{c0} = 0.15 at N = 1,000 cycles while specimen U_{02} had u_s / p'_{c0} = 0.15 at N = 6,000 cycles. It was indicated that the value of u_s / p'_{c0} was fixed for a particular cyclic stress ratio while the number of cycles for reaching a stable state changed with the loading frequency. Where $CSR = 0.6$, the specimen U_{05} had u_s / p'_{c0} = 0.41 at N = 1,000 cycles while specimen U_{06} had u_s / p'_{c0} = 0.4 at N = 6,000 cycles. When the cyclic stress ratio increased from 0.4 to 0.6, the value of u_s / p'_{c0} increased from 0.15 to 0.4 correspondingly. In addition, the number of cycles needed to reach a stable state seems to be independent of the cyclic stress ratio and only related to the loading frequency, i.e., N = 1,000 cycles at f = 0.1 Hz while N = 6,000 cycles at f = 1Hz. Furthermore, a more remarkable decrease in the generation rate of the excess pore pressures is found at a lower loading frequency.

The test results given in Fig. 3.25(a) indicate that at a high stress ratio (CSR = 0.8), there was a more rapid generation of excess pore pressure at a lower loading frequency which caused failure within less cycles, i.e., N_f =1,793 cycles at f = 0.1 Hz increased to N_f 33,964 cycles at f = 5 Hz. It should be noted that where CSR = 0.8, the excess pore pressures underwent only one stage, which is initial rapid development. The excess pore pressure was high enough to cause the specimens to fail before entering the stable stage. The critical excess pore pressure (u_c) was found to be 60% of p'_{c0} where the axial strain increased dramatically.

The development of axial strains presented in Fig. 3.23(b) and Fig. 3.24(b) show similar trend to the excess pore pressures where CSR = 0.4 and 0.6. The lower loading frequency leads to a more rapid accumulation of axial strains. By way of contrast, the two stages of development which was found in excess pore pressures were not obvious in axial strains. The axial strain totally changed shape when the cyclic stress ratio increased from 0.6 to 0.8. The axial strain increased rather than decreased in rate, which indicated that the soil structure was softening and the specimens were failing.

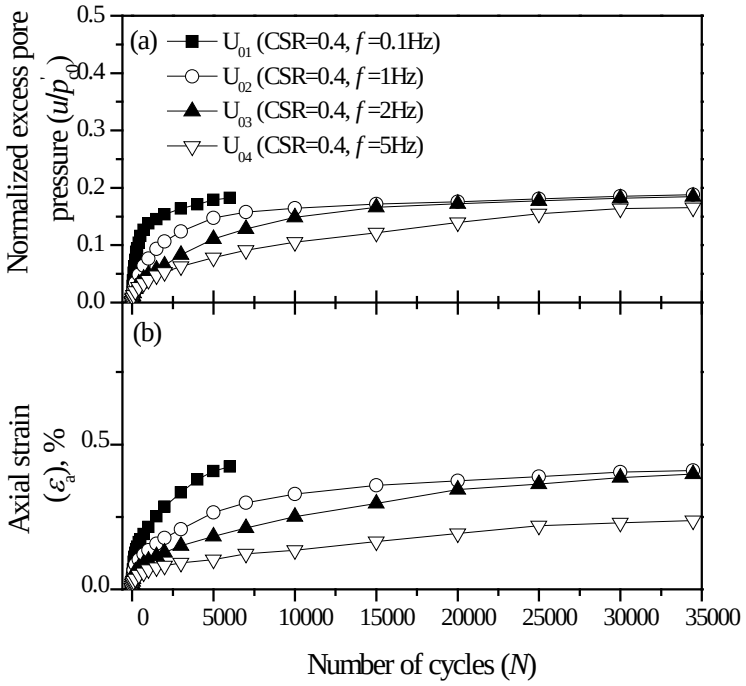

Fig. 3.23 Normalised excess pore pressures and axial strains against number of cycles under CSR = 0.4

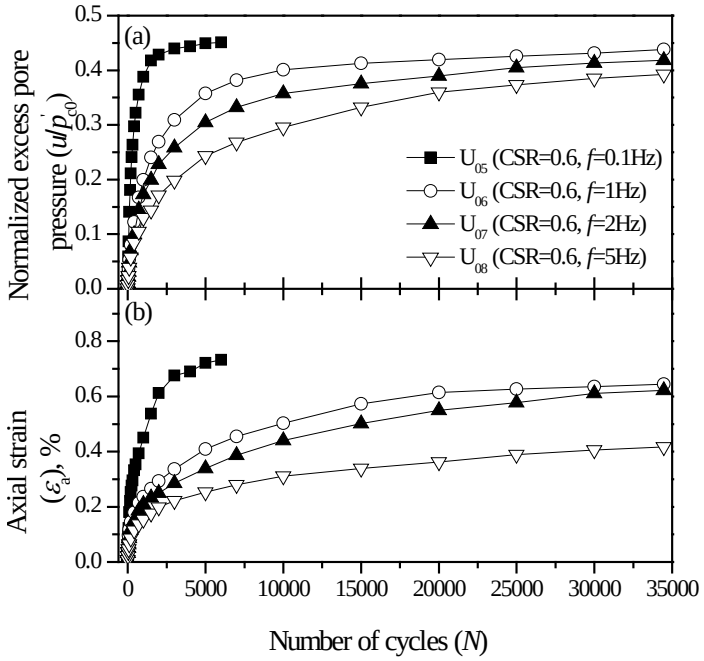

Fig. 3.24 Normalised excess pore pressures and axial strains against the number of cycles under CSR = 0.6

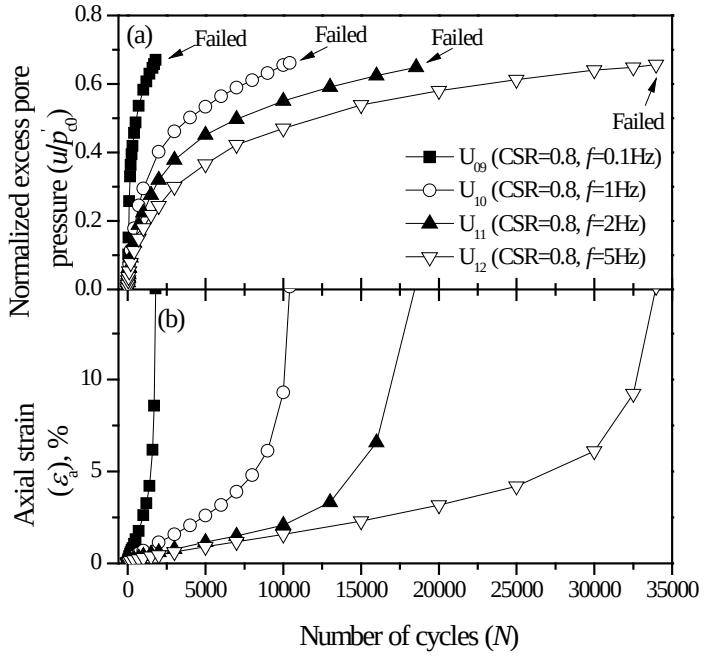

Fig. 3.25 Normalised excess pore pressures and axial strains against the number of cycles under CSR = 0.8

The variations of excess pore pressures and axial strains under an increasing loading frequency at each cyclic stress ratio are given in semi-log scale in Fig. 3.26 ~ Fig. 3.28. Using a semi-log scale means that the initial cyclic responses of the specimens were given more clearly. For the stable specimens (see Fig. 3.26 and Fig. 3.27), the majority of the excess pore pressures and axial strains develop in 100 cycles < N < 1,000 cycles for f = 0.1 Hz and 100 cycles < N < 10,000 cycles for f = 1, 2, and 5 Hz. A lowered generation rate of excess pore pressures after N =1,000 for f = 0.1 Hz and N =10,000 for f = 1, 2, and 5 Hz is given in Fig. 3.26(a) and Fig. 3.27(a), which indicates that the specimens were entering a stable state. A decreased rate of axial strains was not as obvious as observed in the excess pore pressures. For failed specimens (see Fig. 3.28), the excess pore pressures and axial strains kept developing after the initial stage. There was no reduction in the rate at which excess pore pressure was being generated, but then it reached a critical value of 0.6, the axial strains increased dramatically.

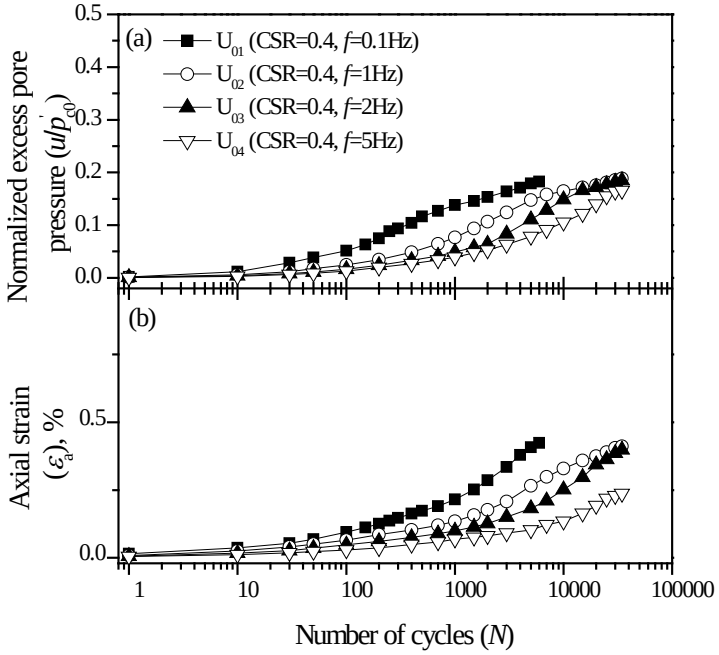

Fig. 3.26 Normalised excess pore pressures and axial strains against the number of cycles under CSR = 0.4 (semi-log scale)

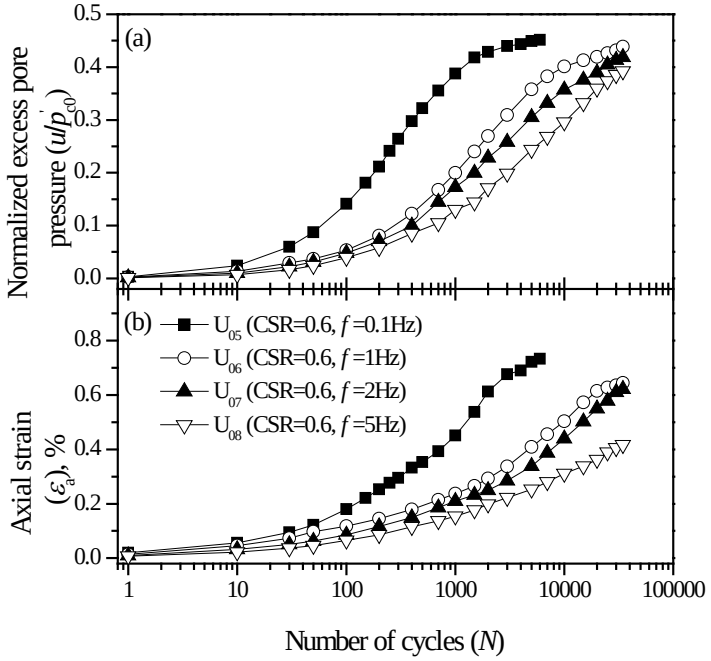

Fig. 3.27 Normalised excess pore pressures and axial strains against number of cycles under CSR = 0.6 (semi-log scale)

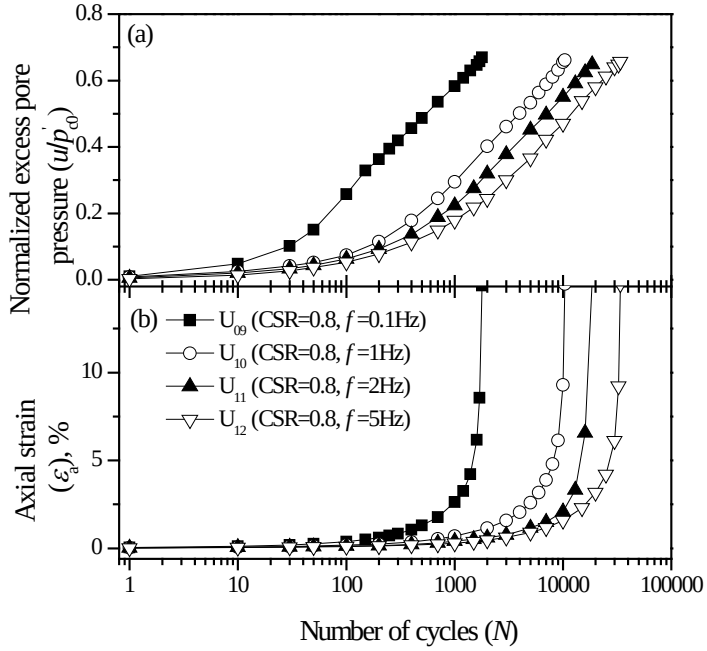

Fig. 3.28 Normalised excess pore pressures and axial strains against the number of cycles under CSR = 0.8 (semi-log scale)

3.6.2 Analysis based on time

The effect of the loading frequency on normalised excess pore pressure and axial strains against time is graphically illustrated in Fig. 3.29 ~ Fig. 3.31, where instead of the number of cycles, the x-axis was replaced with the actual time scale. It is indicated in Fig. 3.29 and Fig. 3.30 that for a CSR of 0.4 and 0.6, the axial strains and excess pore pressure data points did not deviate significantly from each other as the frequency increased from 0.1 to 5 Hz. This verified that for CSR in the range of 0.4 to 0.6, the increase in frequency had little effect on the axial strains and excess pore pressure. However, as the CSR increased to 0.8 (see Fig. 3.31), while the excess pore pressure remained similar to lesser values of, CSR as discussed earlier for Fig. 3.29 and Fig. 3.30, the axial strains showed a considerable difference when the frequency increased from 0.1 to 5 Hz, and where a rapid upward trajectory of strains represents failure. As expected, at the highest frequency 5 Hz, the failure tended to begin at a smaller time scale (i.e. t = 113 minutes), while at the smallest frequency 0.1 Hz, failure still occurred at a delayed time scale (t = 299 minutes).

In summary, the results shown in Fig. 3.29 ~ Fig. 3.31 suggest that for failure to occur, the CSR must exceed a critical value (i.e. CSR > 0.6 for this soil) irrespective of the frequency. On the other hand, at a given critical CSR where failure is inevitable, the higher the frequency the smaller the time required for failure to occur. Moreover, it was indicated in Fig. 3.29(a) ~ Fig. 3.31(a) that for a given value of CSR, the excess pore pressure for all specimens tended to converge to the same value irrespective of the frequency. For a CSR of 0.4 and 0.6 the normalised excess pore pressure after about 200 minutes approached 0.15 and 0.4 respectively. Not surprisingly, a significantly higher excess pore pressure, exceeding 0.6, was observed for the four failed specimens (U_{09} - U_{12}) having a CSR of 0.8 (see Fig. 3.31).

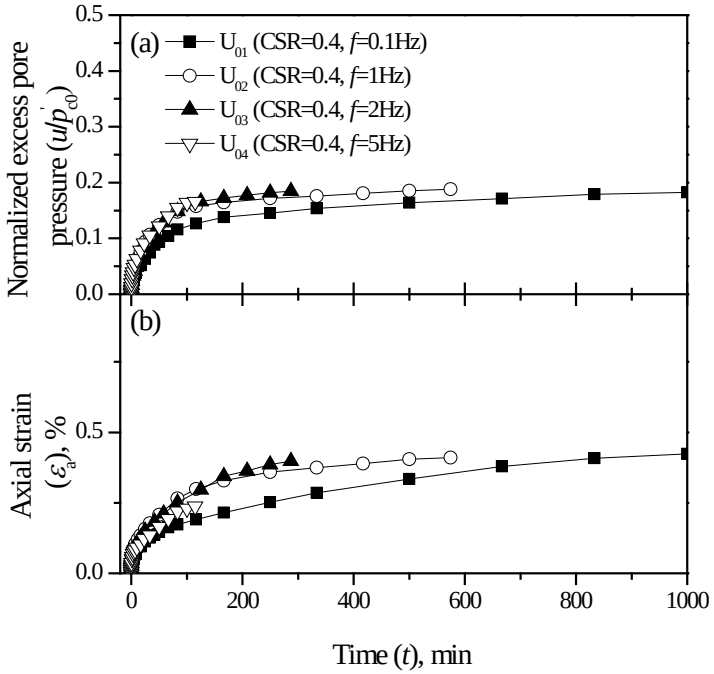

Fig. 3.29 Normalised excess pore pressures and axial strains against time under CSR = 0.4

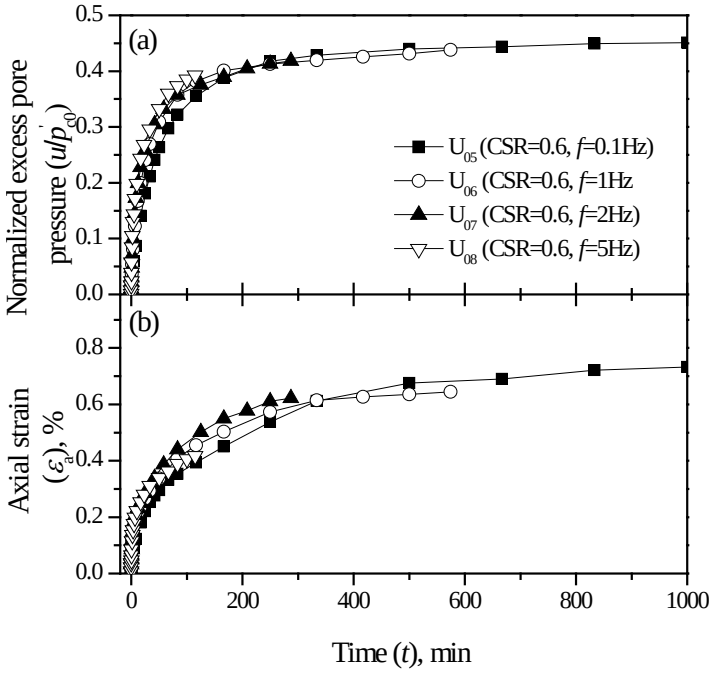

Fig. 3.30 Normalised excess pore pressures and axial strains against time under CSR = 0.6

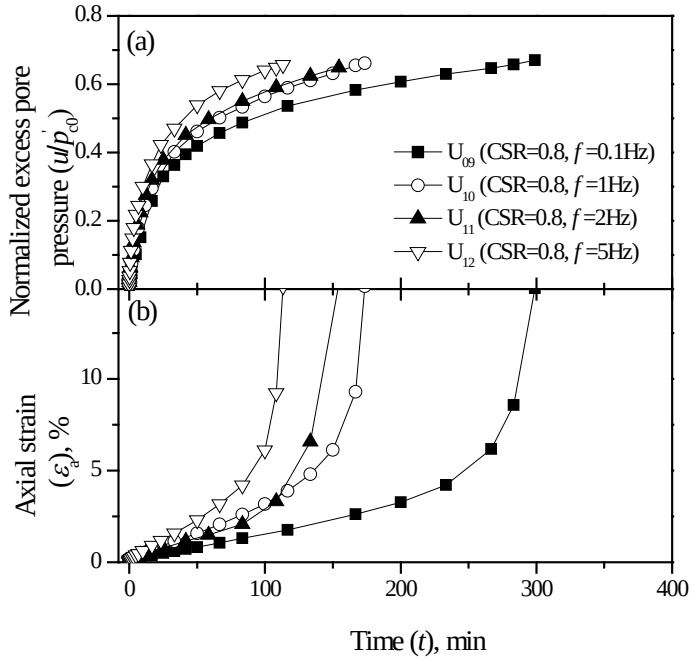

Fig. 3.31 Normalised excess pore pressures and axial strains against time under CSR = 0.8

3.7 Analysis of the test results

In this section the effects of cyclic stress ratio and loading frequency on the development of excess pore pressure and axial strains will be analysed by the creep mechanism (Singh and Mitchell 1968). The generation rate of axial strains of soft clays under creep loading can be calculated by:

$$\dot{\varepsilon}_a = \psi t^{-\zeta} \tag{3.11}$$

where $\dot{\varepsilon}_a$ is the axial strain rate, ζ is the decay constant and ψ is the parameter related to deviator stress (Li and Selig 1996), which can be assumed to have the form:

$$\psi = \eta(\mathrm{CSR})^{\vartheta} \tag{3.12}$$

where η and ϑ are material parameters.

To apply the above mentioned equations to the cyclic loading condition, the increment of q_{cyc} during a half cycle must be divided into a number of equal increments (say n) through each of which the curve can be approximated by a straight line (see Fig. 3.32(a)). Then the total axial strain can be given by:

$$\varepsilon_a = \sum_{i=1}^{n} \int_0^{t_i} \eta \left(\text{CSR}_i\right)^{\vartheta} t_i^{-\zeta} \, \text{d}t \tag{3.13}$$

where CSR_i is the cyclic stress ratio under each load step q_i:

$$\text{CSR}_i = i \frac{\text{CSR}}{n} \text{ , } i = 1, 2 \cdots\cdots, \ n \tag{3.14}$$

and t_i is the total time under load step q_i:

$$t_i = \sum \Delta t_i \text{ , } i = 1, 2 \cdots\cdots, \ n \tag{3.15}$$

where Δt_i is the time duration under load step q_i for half cycle:

$$\Delta t_i = \frac{\left[\arcsin\left(i \frac{2}{n} - 1 \right) - \arcsin\left((i-1) \frac{2}{n} - 1 \right) \right]}{2\pi} \frac{1}{f} \text{ , } i = 1, 2 \cdots\cdots, \ n \tag{3.16}$$

Therefore, the axial strain can be given by:

$$\varepsilon_a = \sum_{i=1}^{n} \eta \left(\text{CSR}_i\right)^{\vartheta} \frac{\left(t_i\right)^{1-\zeta}}{1-\zeta} \tag{3.17}$$

where t_i can be expressed by:

$$t_i = 2 t_{\text{total}} \frac{\left[\arcsin\left(i \frac{2}{n} - 1 \right) - \arcsin\left((i-1) \frac{2}{n} - 1 \right) \right]}{2\pi} \text{ , } i = 1, 2 \cdots\cdots, \ n \tag{3.18}$$

where t_{total} is the total time being considered.

Based on the above, the effect of the cyclic stress ratio and loading frequency on axial strains can be explained. It was indicated that the axial strain is related to the cyclic stress ratio, while it is independent of the cyclic loading frequency for an identical time period, but dependent on the cyclic loading frequency for an identical number of cycles. For example, for curves A and C with the same cyclic loading frequency (see Fig. 3.32 (b)), curve A has a higher axial strain than curve C because curve A has a higher cyclic stress ratio. Where curves A and B have the same cyclic stress ratio (see Fig. 3.32 (b)), there are two possibilities: If an identical time is considered, then the development of axial strains for curves A and B are the same, but if identical cycles are considered, then less time is available for a higher frequency than a lower frequency, which results in less axial strain at a higher frequency compared to a lower frequency. Moreover, as excess pore pressure is intimately related to axial strain (Wilson and Green wood 1974; Lee and Focht 1976), the effect of the cyclic stress ratio and loading frequency on excess pore pressure is similar to axial strain.

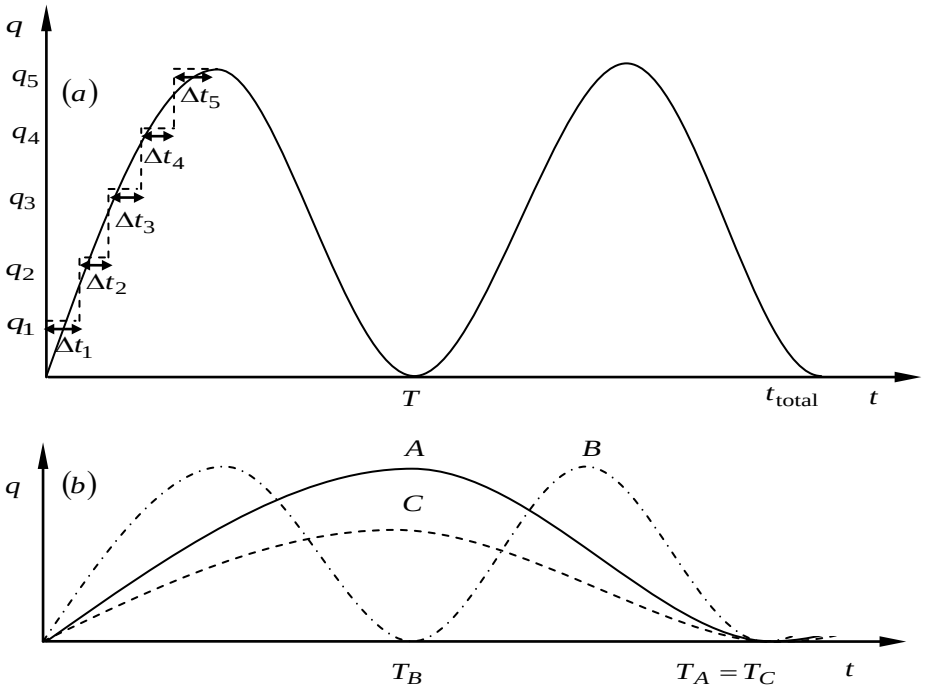

Fig. 3.32 Step loading to simulate cyclic loading

For simplicity, the effects of the cyclic stress ratio and loading frequency on the performance of soft soils can be explained by the areas covered by the cyclic stress curves and time axis (see Fig. 3.33). It is shown in Fig. 3.33(a) that the areas covered by curves A and B under different cyclic loading frequencies, are roughly the same for identical time, which implies that the axial strains and excess pore pressures are independent of the loading period of each cycle. If an identical number of cycles are considered, the areas covered by curve A is larger than that covered by curve B (see Fig. 3.33 (b)), which implies that more axial strain and excess pore pressure develop under lower cyclic loading frequency than higher cyclic loading frequency. Where curves A and C have the same cyclic loading frequency (see Fig. 3.33(c)), a larger area is covered by curve A than curve C , no matter whether identical time or number of cycles is considered.

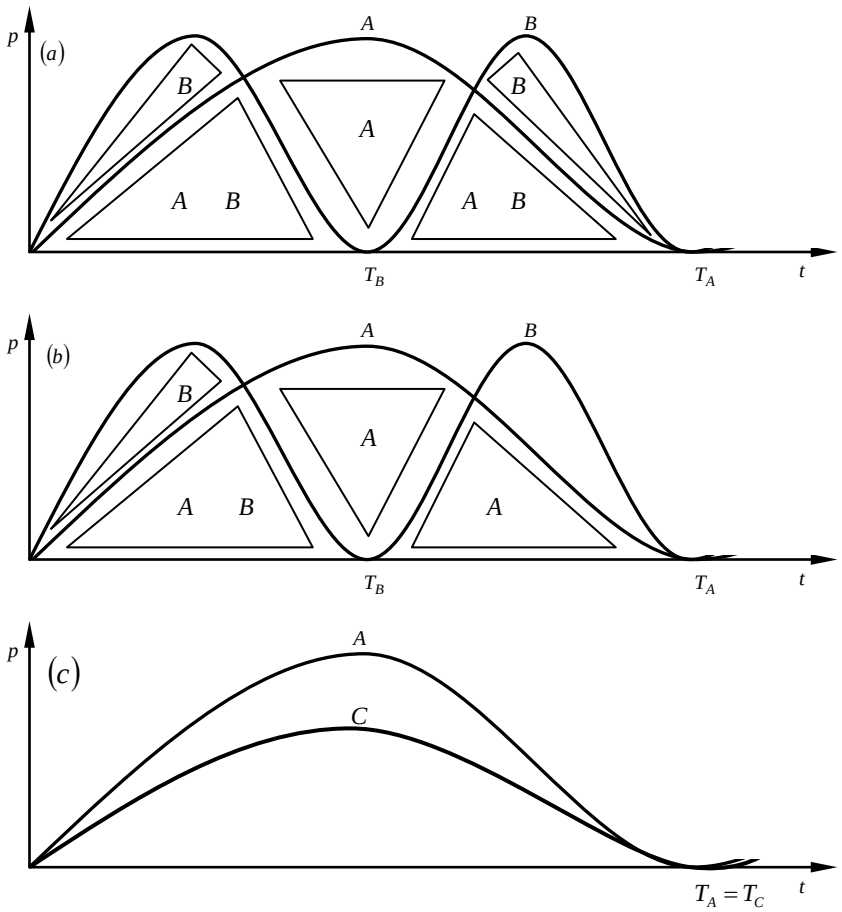

Fig. 3.33 Area method

3.8 The effect of the strain rates

As mentioned above, the level of cyclic stress plays a more important role than the loading frequency. So some fundamental questions arise, especially, what is the mechanism that leads to this cyclic stress dependent behaviour? Why does the loading frequency have almost no influence on the development of excess pore pressure and axial strain?

To answer these questions it should be noted first that the cyclic triaxial tests conducted in this research work were stress controlled. Therefore, the applied stress rates were different for specimens loaded at the same stress level but different loading frequencies. It seems that the stress rate cannot explain the independent behaviour of the loading frequency, e.g. the stress rate ratio of specimens U_{01} to U_{04} was 1 to 50 but their performances were similar. If the stress rate is not the reason, what about strain rate? The effect of the strain rate in static loading has already been investigated very well, and it has been found that the excess pore pressures and undrained shear strength are intimately related to the strain rate (Richardson and Whitman 1963; Ladd et al. 1972; Crooks and Graham 1976; Vaid and Campanella 1977; Vaid et al. 1979; Baracos et al. 1980; Andersen and Stenhamar 1982; Graham et al. 1983; Adachi et al. 1985; Lefebvre and LeBoeuf 1987; Sheahan et al. 1996). However, a comprehensive understanding of the effect of the strain rate in stress controlled cyclic loading has not yet been obtained. Indeed the only results related to this aspect were made by Lefebvre and LeBoeuf (1987) Lefebvre and Pfendler (1996), who reported that the strain rates for stress-controlled tests under 0.1 Hz were roughly 300 and 3,500 %/h for Eastern Canada clay and St. Lawrence valley clay, respectively. Because they only used 0.1 Hz as the loading frequency in their tests, the relationship between the strain rate and loading frequency was not considered.

In the following part, the relationship between the strain rate - cyclic stress ratio - loading frequency will be investigated and the questions raised earlier in this section will hopefully be answered. To calculate the strain rate, it is assumed that during the whole cycle a constant strain rate was applied, therefore the strain rate ($\dot{\varepsilon}_{aL,c}$) for stress controlled cyclic loading can be given by:

$$\dot{\varepsilon}_{aL,c} = 2 \times \varepsilon_{a,cyc} \times f \tag{3.19}$$

where $\varepsilon_{a,cyc}$ is the axial strain for a half cycle.

The strain rate for each cyclic loading condition, with an increasing number of cycles is shown in Table 3.3. The strain rate for each value of CSR seemed to be constant during the whole process of cyclic loading for each condition. The average value of the strain rate was calculated and then tabulated in Table 3.3.

Table 3.3 Strain rate for cyclic tests

Strain rate ($\dot{\varepsilon}_{aL,c}$), %/h							
N	0.1 Hz			*N*	1 Hz		
	CSR=0.4	CSR=0.6	CSR=0.8		CSR=0.4	CSR=0.6	CSR=0.8
150	178	287	578	1,500	199	250	513
500	185	290	580	5,000	198	260	574
1,000	186	282	585	10,000	192	256	564
3,000	186	265		30,000	198	240	
6,000	120	270					
Average	171	278	581	Average	192	251	550
N	2 Hz			*N*	5 Hz		
	CSR=0.4	CSR=0.6	CSR=0.8		CSR=0.4	CSR=0.6	CSR=0.8
1,500	172	274	532	1,500	216	291	566
5,000	167	255	548	5,000	220	291	575
10,000	163	296	527	10,000	217	288	572
30,000	165	290		30,000	217	289	580
Average	167	279	536	Average	218	290	573

The relationship between strain rate and cyclic stress ratio for specimens at four loading frequencies is shown in Fig. 3.34. The results shown in Fig. 3.34 indicate that an increase in the cyclic stress ratio raises the strain rate and this increment was also influenced by the value of the cyclic stress ratio, e.g., the difference in strain rate was 100 %/h between CSR =0.4 and 0.6, whereas the difference in strain rate between CSR = 0.6 and 0.8 was 300 %/h. This sharp rise in the strain rate when the CSR increased from 0.6 to 0.8 suggests that the cyclic resistance decreased dramatically at a high cyclic stress level, which further confirmed previous observations that failure would occur at CSR = 0.8. Therefore, the mechanism that leads to cyclic stress dependent behaviour can be described as: higher strain rate at CSR = 0.8 caused a higher strain rate and a subsequently higher excess pore pressures and axial strains. It should be noted that all four plots for f = 0.1 to 5 Hz were close together, indicating that the strain rate did not depend on the frequency. That is why the loading frequency had very little influence on the development of excess pore pressure and axial strains.

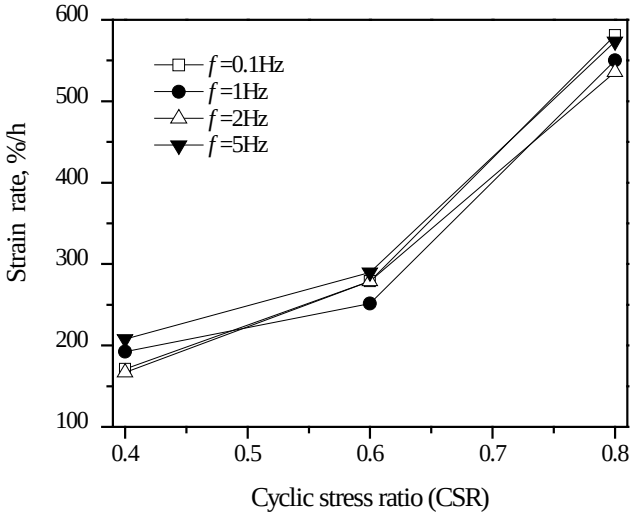

Fig. 3.34 Strain rate for cyclic tests

The relationship of normalised excess pore pressures at t =100 min, when all the specimens did not fail, and strain rates is shown in Fig. 3.35. When the strain rate increased from 200 %/h to 300 %/h the excess pore pressure increased from 0.15 to 0.35, whereas when the strain rate increased from 300 %/h to 600 %/h, the excess pore pressure increased from 0.35 to 0.6. The frequency did not seem to influence the excess pore pressure because all four curves do not show large deviations. The relationship between the axial strains and strain rates is shown in Fig. 3.36. The results indicate that the higher the strain rate, the greater the axial strain generated during cyclic loading. Divergence occurs when the strain rate increased from 300 %/h to 600 %/h, because the axial strains were slightly different when failure occurred at different loading frequencies.

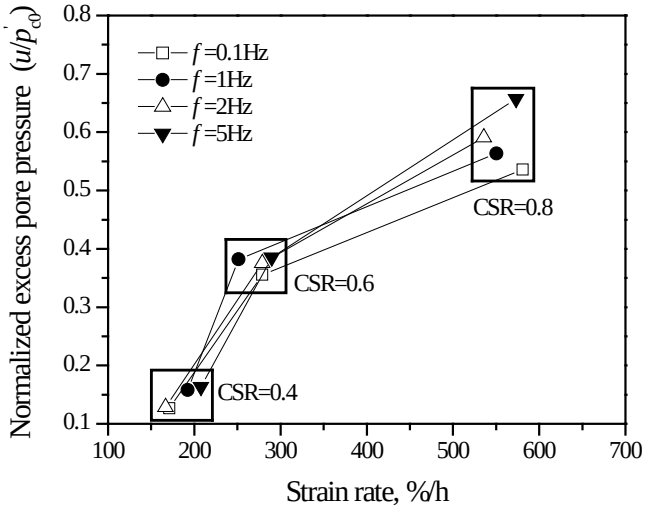

Fig. 3.35 Relationship between normalised excess pore pressures and strain rates

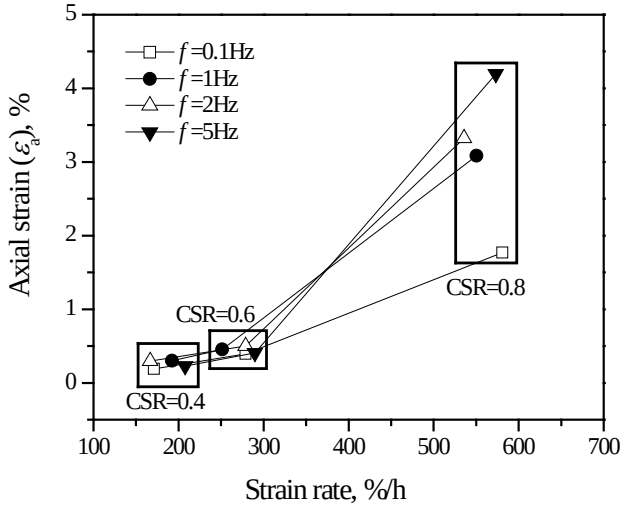

Fig. 3.36 Relationship between axial strains and strain rates

As mentioned in Chapter 2 Literature Review, the undrained shear strength increases with the strain rate; there was an approximately 7% to 14% increase in undrained shear strength per each log cycle of strain rate, therefore the undrained shear strength ratio of cyclic loading to static loading can be given as:

$$\log\left(\frac{q_{\mathrm{u,c}}}{q_{\mathrm{u,s}}}\right)=\log\left(\frac{\dot{\varepsilon}_{\mathrm{aL,c}}}{\dot{\varepsilon}_{\mathrm{aL,s}}}\right)\log\left(1+s_{\mathrm{q}}\right) \tag{3.20}$$

where $q_{\mathrm{u,c}}$ and $q_{\mathrm{u,s}}$ are the undrained shear strength for cyclic loading and static loading respectively, s_{q} is the increment in undrained shear strength per log cycle of strain rate, and $\dot{\varepsilon}_{\mathrm{aL,s}}$ is the strain rate for static loading with a value of 0.5 %/h.

If $s_{\mathrm{q}}=10\,\%$ is assumed, then the undrained shear strength for three levels of cyclic stresses considering the effect of strain rate can be calculated by:

$$q_{\mathrm{u,c}}=q_{\mathrm{u,s}}\left(1+s_{\mathrm{q}}\right)^{\log\left(\frac{\dot{\varepsilon}_{\mathrm{aL,c}}(\mathrm{CSR})}{\dot{\varepsilon}_{\mathrm{aL,s}}}\right)} \tag{3.21}$$

where $\dot{\varepsilon}_{\mathrm{aL,c}}(\mathrm{CSR})$ is the average strain rate for each cyclic stress ratio. The calculated $q_{\mathrm{u,c}}$ is equal to $1.27q_{\mathrm{u,s}}$, $1.3q_{\mathrm{u,s}}$, and $1.33q_{\mathrm{u,s}}$ for CSR = 0.4, 0.6, and 0.6 respectively.

It has been discussed that the increase in undrained shear strength can be caused by decreased shear induced excess pore pressure or increased effective stress friction angle, or a combination of both. If the mechanism is a single decreased shear induced excess

pore pressure, then the slope of q/p' at failure (M_c) for cyclic loading will be the same as that for monotonic loading (M_m). If the mechanism is a single increased effective stress friction angle, then the slope of q/p' at failure (M_c) is a boundary value which is related to the cyclic stress ratio. It can be obtained from calculations that $M_{0.4}^b = 2.15$, $M_{0.6}^b = 2.22$, $M_{0.8}^b = 2.30$ for CSR =0.4, 0.6, and 0.8 respectively. If the mechanism is combined decreased shear induced excess pore pressure and increased effective stress friction angle, then the slope of q/p' at failure (M_c) is between M_m and boundary value. The slopes of q/p' at failure for cyclic and monotonic loading are given in Fig. 3.37, along with the boundary value. The results shown in Fig. 3.37 indicate that the slope of q/p' at failure (M_c) for cyclic loading lies between M_m and the boundary values. Therefore, the effect of strain rate of cyclic loading is caused by the combined mechanism. In addition, it can be seen in Fig. 3.37 that the excess pore pressure at failure decreased as the cyclic stress ratio increased.

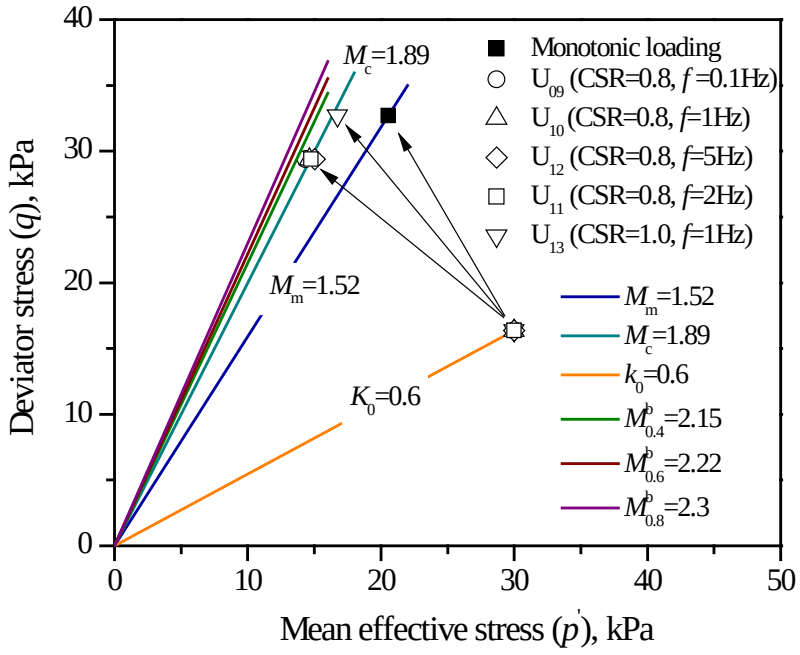

Fig. 3.37 Critical state lines for monotonic loading and cyclic loading

3.9 Conclusions

A series of cyclic loading tests under undrained condition were conducted on the soft clay specimens. The cyclic stress ratio changed from 0.4, 0.6, to 0.8 while the loading frequency changed from 0.1, 1, 2, to 5 Hz. The obtained conclusions are as follows:

- Specimens tested under a CSR of 0.8 failed after a number of cycles, irrespective of the loading frequency, while specimens tested under a CSR of 0.4 and 0.6 did not fail at the end of the tests and behaved in a stable manner. Therefore, the critical cyclic stress ratio was expected to be greater than 0.6.

- The number of cycles at failure increased from 1,793 to 33,964 when the loading frequency was increased from 0.1 to 5 Hz, which indicated that more cycles were needed to bring the specimen to failure at a higher frequency.

- Failed specimens showed that the failure mode was barrelling with numerous slip surfaces that formed a diamond shaped pattern on the surface of the sample, which is different from stiff clays and dense sand, where there is usually one such slip surfaces.

- The effect of cyclic stress ratio on the development of excess pore pressure and axial strain has been investigated. As expected, the normalised excess pore pressure and axial strains increased with the increasing cyclic stress ratio irrespective of the loading frequency. The excess pore pressure rose significantly at the initial stages ($N < 500$) and then gradually increased with the number of cycles. For stable specimens with a CSR of 0.4 and 0.6, the excess pore pressures stabilised after an initial rapid development, where the normalised excess pore pressures equalled 0.2 and 0.4 respectively. For failed specimens with a CSR of 0.8, the excess pore pressures developed so quickly that the critical normalised value of 0.65 was reached in the first few cycles, therefore specimens failed before they could stabilise. Nevertheless, there was no distinct difference in the shape of the excess pore pressure-cycle curve for both the stable and failed samples. In contrast, failed specimens showed a significant difference in axial strain from stable specimens. For specimens with a CSR of 0.8, when a normalised excess pore pressure of 0.55 to 0.6, rapid upward trajectory of axial strain occurred. While for specimens with a CSR of 0.4 and 0.6, the axial strains

developed at a very low generation rate and at the end of the tests were less than 1%.

- The effect of cyclic loading frequency on the development of excess pore pressure and axial strain has been analysed against both number of cycles and time. In the first case, the loading frequency was only responsible for how many cycles the specimens underwent before failure occurred at a high cyclic stress ratio, or before it reached a stable state for a low cyclic stress ratio. In the second case, the axial strains and excess pore pressure data points did not deviate significantly from each other as the frequency increased from 0.1 to 5 Hz.

- The test results suggest that for failure to occur, the CSR must exceed a critical value (i.e. CSR > 0.6 for this soil) irrespective of the frequency. On the other hand, at a given critical CSR where failure is inevitable, the higher the frequency the smaller the time required for failure to occur. Moreover, it was indicated that for a given value of CSR , the excess pore pressure for all specimens tended to converge to the same value irrespective of the frequency. Therefore the cyclic stress ratio rather than the loading frequency governs the stability of soft clay subgrade under cyclic loading.

- Finally, the concept that the behaviour of soils depends on the level of cyclic stress rather than the loading frequency was investigated through strain rate during cyclic loading, which is considered to be responsible for the cyclic response of soft clays under various loading conditions. For loading frequencies ranging from 0.1 to 5 Hz, it was found that the strain rate depended on the cyclic stress ratio rather than the loading frequency, which implies that the cyclic stress level plays a more important role in influencing the cyclic performance of soft soil subgrade.

4 Undrained Cyclic Model

4.1 Introduction

Cyclic models have been developed using a considerable body of data obtained from laboratory tests. Indeed, most of the theories are devoted to one specific interest, or a combination of two, and therefore it is better if a cyclic model can be established in which various cyclic loading conditions can be considered. Some attempts have been carried out by Ramsamooj and Alwash (1990), and Li and Meissner (2002), but these models are complex whereby the parameters associated with them cannot be easily determined, which makes using them in practical situations quite difficult. A less complicated model was proposed by Carter et al. (1982) based on a modified Cam-clay framework in which only one additional parameter is needed, in addition to the parameters adopted in the modified Cam-clay model. This parameter can conveniently be determined by conducting cyclic triaxial loading tests. Since the modified Cam-clay model can capture the behaviour of soft soils and the determination of the additional parameter is feasible, Carter et al. (1982)'s model is potentially applicable to soft clays subjected to cyclic loading although its predictions of excess pore pressures show some divergences with the test data (Takahashi et al. 1980; Miller et al. 2000; Zhou and Gong 2001; Sakai et al. 2003). The predicted generation rate of excess pore pressure increases until the soil ultimately fails, which is contrary to the fact that excess pore pressure develops at a decreasing rate, especially for soils in a stable state.

Therefore, a new cyclic model based on Carter et al. (1982)'s model is presented in this chapter. In this new model only two additional cyclic degradation parameters are introduced to present the yield surface during elastic unloading. The cyclic stress level, static pre-shearing, and over consolidation ratio can be represented by the cyclic load, the initial state of the soil, and the pre-consolidation condition respectively. The loading frequency can be included by the additional cyclic degradation parameters ξ_1 and ξ_2.

4.2 Modified Cam-clay model

The first critical state models for describing the behaviour of soft soils such as clays are the Cam-clay (CC) and Modified Cam-clay (MCC) models formulated by researchers at Cambridge University. Both models describe three important aspects of soil behaviour, its strength, compression or dilatancy, and critical states in which soil elements can

experience infinite deformation without any changes in stress or volume. In this chapter, attention will largely be restricted to the Modified Cam-clay model and triaxial conditions.

4.2.1 State of the soil

Three parameters for describing the state of a soil element are characterised by:

- **Effective mean stress**

$$p' = \frac{1}{3}\left(\sigma_1' + \sigma_2' + \sigma_3'\right) \tag{4.1}$$

where σ_1', σ_2', and σ_3' are the principal effective stresses.

- **Deviator (shear) stress**

$$q = \frac{1}{\sqrt{2}}\sqrt{\left(\sigma_1' - \sigma_2'\right)^2 + \left(\sigma_2' - \sigma_3'\right)^2 + \left(\sigma_3' - \sigma_1'\right)^2} \tag{4.2}$$

- **Specific volume**

$$v = 1 + e \tag{4.3}$$

where e is the voids ratio.

4.2.2 Normal compression and unloading-reloading lines

The model assumes that when a soft soil element is slowly compressed under isotropic stress and perfect drained conditions, the relationship between the specific volume (v) and ln p' consists of a straight normal compression (virgin consolidation) line and a set of straight unloading-reloading (swelling) lines (Fig. 4.1). When a soil element is first loaded to an isotropic stress p_B', in the v-ln p' space, it moves down the virgin consolidation line from point A to point B. If the sample is unloaded the specific volume-mean stress behaviour moves up the unloading-reloading line BC to point C.

If the sample is now reloaded to a stress p_D', it will first move down the unloading-reloading line for stress values up to p_B', but once p_B' has been exceeded the sample will again move down the virgin consolidation line to point D. If the sample is then unloaded to a stress value of p_A' it will move up the unloading-reloading line DE. The virgin consolidation line in Fig. 4.1 can be defined by:

$$v = N - \lambda \ln p' \tag{4.4}$$

where the values of N and λ are characteristic properties of a particular soil. λ is the slope of the normal compression line in v-ln p' space, and N is known as the specific volume of normal compression line at unit pressure, and is dependent on the units of measurement. The equation for an unloading-reloading line has the form:

$$v = v_k - \kappa \ln p' \tag{4.5}$$

where the value of κ is a characteristic property of a particular soil as well. κ can be defined as slope of unloading-reloading line in v-ln p' space.

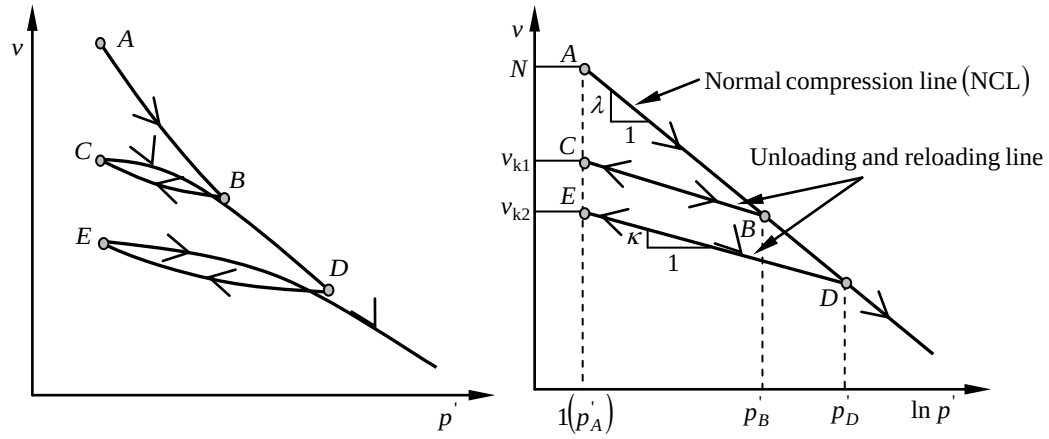

(a) (b)

Fig. 4.1 Normal compression line and unloading-reloading line: (a) In v-p' space, (b) In v-lnp' space

4.2.3 The Critical State Line

Sustained shearing of a soil element eventually leads to a state in which further shearing can occur without any changes in stress or volume. This is also known as the critical state condition where the soil is distorting at a constant state ($\frac{\delta v}{\delta \varepsilon_s} = \frac{\delta q}{\delta \varepsilon_s} = \frac{\delta p'}{\delta \varepsilon_s} = 0$). This state is characterised by the Critical State Line (CSL). The location of this line relative to the normal compression line is shown in Fig. 4.2. As can be seen, the CSL is parallel to the normal compression line in v-ln p' space. The parameter Γ is the specific volume of the CSL at unit pressure. Like N, its value depends on the units of measurement, and there is a relationship between the parameter N of the normal compression line and Γ given by :

$$\Gamma = N - (\lambda - \kappa)\ln 2 \tag{4.6}$$

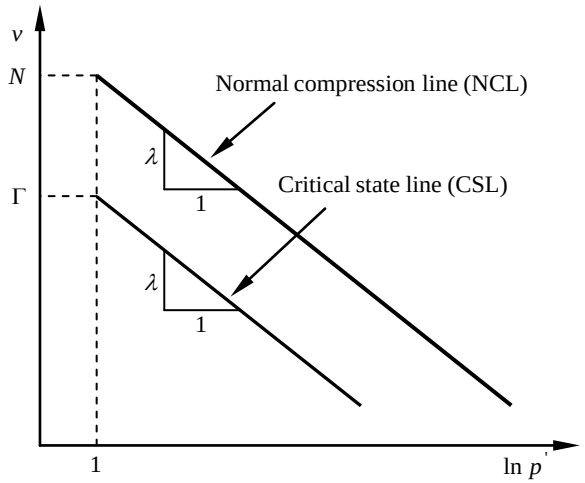

Fig. 4.2 Location of CSL relative to normal compression line

4.2.4 Yield function

Under increasing triaxial shear loading, MCC soils behave elastically until a yield value of q is attained. The yield values are determined from the following equation:

$$p_{c0}^{'} = p^{'} + \frac{1}{M^2 p^{'}} q^2 \tag{4.7}$$

where the parameter $p_{c0}^{'}$ (known as the yield stress or pre-consolidation pressure) controls the size of the yield surface, and is different for each unloading-reloading line. The parameter M is the slope of the CSL in $p^{'}$ - q space. In $p^{'}$ - q space, the MCC yield surface plots as an elliptical curve, as shown in Fig. 4.3.

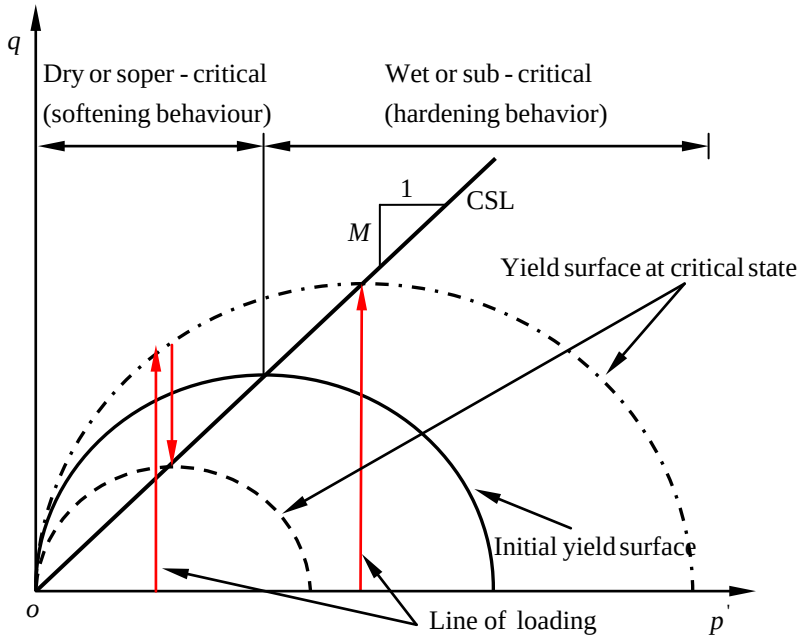

Fig. 4.3 Evolution of the yield curve on the wet or dry side of the modified Cam-Clay model under shearing

4.2.5 Hardening behaviour

If yielding occurs to the right of the point at which the CSL intersects a yield surface, then hardening and compression takes place. This side of the yield surface is known as the wet or sub-critical side. The behaviour of soil on the wet side, in the case of simple shearing, is illustrated in Fig. 4.3. When a specimen is sheared it behaves elastically until it hits the initial yield surface. From then on the yield surface begins to grow (become enlarged) and become harder (yielding and plastic strain is accompanied by an increase in yield stress). When the yield surface at a critical state is reached the specimen will continue to distort without any accompanying changes in stress or volume.

If yielding occurs to the left of the intersection of the CSL and yield surface (called the dry or super-critical side), the soil begins to soften, accompanied by dilatancy. In softening, the yield stress curve decreases after the stress state touches the initial envelope, and the yield curve and sustained load move downwards until the specimen reaches the critical state.

4.3 Framework of the new cyclic model

4.3.1 Assumption of the new cyclic model

The assumption made for this model is based on experimental data or field data collected for soft soils under cyclic loading. For normally consolidated soils, permanent excess pore pressures and strains only occur in the first cycle if the modified Cam-clay model is used to simulate the cyclic performance. This occurs because the yield surface remains unchanged after the first cycle, which means that afterwards the soils become elastic and consequently no permanent excess pore pressures and strains develop. However, when saturated soft clays are repeatedly unloaded and reloaded, the permanent excess pore pressures and strains keep increasing during the whole process of cyclic loading. One way of interpreting this real behaviour is to assume that the position and perhaps the shape of the yield surface have been influenced in some way by the elastic unloading. For simplicity, the form of the yield surface is assumed to remain unchanged, but with a reduced size in an isotropic manner by the elastic unloading. The function of the yield surface when soils are elastically unloaded can be defined as:

$$\frac{\mathrm{d}p_{\mathrm{c}}^{'}}{p_{\mathrm{c}}^{'}} = \theta^{*} \frac{\mathrm{d}p_{\mathrm{y}}^{'}}{p_{\mathrm{y}}^{'}} \tag{4.8}$$

where $p_{\mathrm{c}}^{'}$ is a hardening parameter which can be considered as pre-consolidation pressure, and $p_{\mathrm{y}}^{'}$ is a variable defined as:

$$p_{\mathrm{y}}^{'} = p^{'} + \left(\frac{q}{M}\right)^{2} \frac{1}{p^{'}} \tag{4.9}$$

where M is the slope of the critical state line in $p^{'}$ - q space, and $p^{'}$ and q are the effective mean stress and deviator stress taking the form of:

$$p^{'} = \frac{1}{3}\left(\sigma_1^{'} + 2\sigma_2^{'}\right) \tag{4.10}$$

$$q = \sigma_1^{'} - \sigma_3^{'} \tag{4.11}$$

where $\sigma_1^{'}$ and $\sigma_3^{'}$ are the major and minor principle stresses respectively.

The cyclic degradation parameter θ^* is introduced in this new model. It is assumed that θ^* decreases with the increasing number of cycles during cyclic loading rather than remaining constant, taking the form of:

$$\theta^* = \frac{1}{\xi_1 N + \xi_2} \tag{4.12}$$

where ξ_1 and ξ_2 are experimental constants. If $\xi_1 = 0$, then the above mentioned equation can be simplified to Carter et al. (1982), assuming $\theta = 1/\xi_2$:

$$\frac{\mathrm{d}p_{\mathrm{c}}^{'}}{p_{\mathrm{c}}^{'}} = \theta \frac{\mathrm{d}p_{\mathrm{y}}^{'}}{p_{\mathrm{y}}^{'}} \tag{4.13}$$

4.3.2 Effective stresses and strains during cyclic loading

A calculation of the effective stresses and strains are demonstrated against the stress path for normally and isotropically consolidated soils under cyclic loading, as shown in Fig. 4.4. $p_{\mathrm{cl},i}^{'}$ (i=1, 2……, n) is the yield stress after the loading part of each cycle, $p_{\mathrm{cu},i}^{'}$(i=1, 2……, n) is the yield stress after the unloading part of each cycle, and $p_{\mathrm{y},i}^{'}$(i=1, 2……, n) is the loading parameter after each cycle.

When the soil element starts from point $A^{'}$ to point A during the first loading period, the excess pore pressure increases and effective mean stress decreases. $p_{\mathrm{cl},1}^{'}$ is the yield stress corresponding to point A, which can be expressed as:

$$p_{\mathrm{cl}}^{'} = p_A^{'} + \left(q_A / M\right)^2 p_A^{'} \tag{4.14}$$

where q_A is equal to the cyclic stress q_{cyc} and the effective mean stress at point A can be given by:

$$\frac{p_A^{'}}{p_{A^{'}}^{'}} = \left(\frac{M^2 + \left(q_A / p_A^{'}\right)^2}{M^2 + \left(q_{A^{'}} / p_{A^{'}}^{'}\right)^2} \right)^{\frac{\lambda - \kappa}{\lambda}} \tag{4.15}$$

where λ and κ are the slopes of the normally compression line and swelling line in v-$\ln p^{'}$ space respectively.

During the following unloading period, the stress path travels from point A to point A^*, the effective mean stress remains constant, and $p'_{y,1}$ is the loading parameter corresponding to point A^*. The yield stress for the second cycle, or the yield stress after unloading can be calculated as:

$$p'_{cu,1} = p'_{cl,1}\left(\frac{p'_{y,1}}{p'_{cl,1}}\right)^{\theta^*} \tag{4.16}$$

For the first half of the second cycle, the stress path travels from point A^* to point B' and the soil behaves elastically when $q < q_{yielding}$. The deviator stress $q_{yielding}$ causes the soil to yield and may be given by:

$$q_{yielding} = \sqrt{\left(p'_{cu,1} - p'_{y,1}\right)M^2 p'_{y,1}} \tag{4.17}$$

Afterwards the stress path goes from point B' to B ($q_{yielding} < q < q_{cyc}$) and the effective mean stress decreases. During this period, the soil behaves plastically.

The incremental elastic stress-strain relationship is used to calculate the incremental strains within the current yield surface. The incremental elastic shear and volumetric strains can be given by:

$$\mathrm{d}\varepsilon_s^e = \frac{\mathrm{d}q}{3G} \tag{4.18}$$

and

$$\mathrm{d}\varepsilon_v^e = \frac{\mathrm{d}p'}{K} \tag{4.19}$$

where G is the shear modulus and K is the bulk modulus given by:

$$K = \frac{(1+e)}{\kappa}p' \tag{4.20}$$

The incremental plastic stress-strain relationship is used to calculate the incremental strains on the current yield surface. The incremental plastic shear and volumetric strains can be given by:

$$\mathrm{d}\varepsilon_{\mathrm{s}}^{\mathrm{p}} = C_{21}\mathrm{d}p' + C_{22}\mathrm{d}q \tag{4.21}$$

and

$$\mathrm{d}\varepsilon_{\mathrm{v}}^{\mathrm{p}} = C_{11}\mathrm{d}p' + C_{12}\mathrm{d}q \tag{4.22}$$

where $C_{11} = \left(\frac{\lambda-\kappa}{1+e}\right)\frac{a}{p'} + \left(\frac{\kappa}{1+e}\right)\frac{1}{p'}$.

$$C_{12} = C_{21} = \left(\frac{\lambda-\kappa}{1+e}\right)\left(\frac{1-a}{p'}\right),$$

$$C_{22} = \left(\frac{\lambda-\kappa}{1+e}\right)\frac{b}{p'} + \frac{1}{3G},$$

$$a = \frac{M^2-\eta^2}{M^2+\eta^2},$$

$$b = \frac{4\eta^2}{M^2-\eta^2},$$

$$\eta = \frac{q}{p'}.$$

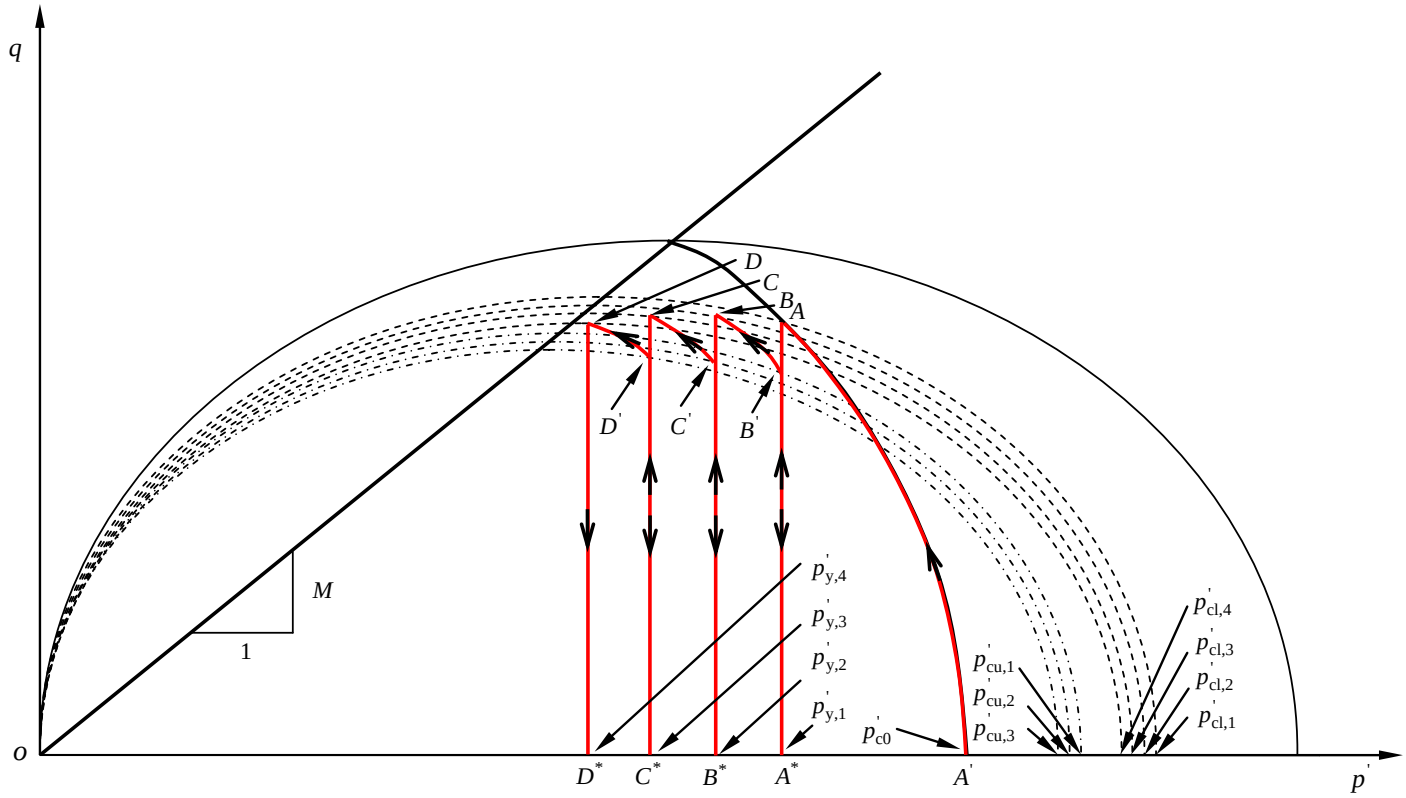

Fig. 4.4 The stress path for soil element under undrained cyclic loading

4.3.3 Computational procedure

The procedure for calculating the excess pore pressures and axial strains under undrained cyclic loading is summarised in Fig. 4.5. The details are described in the following sections.

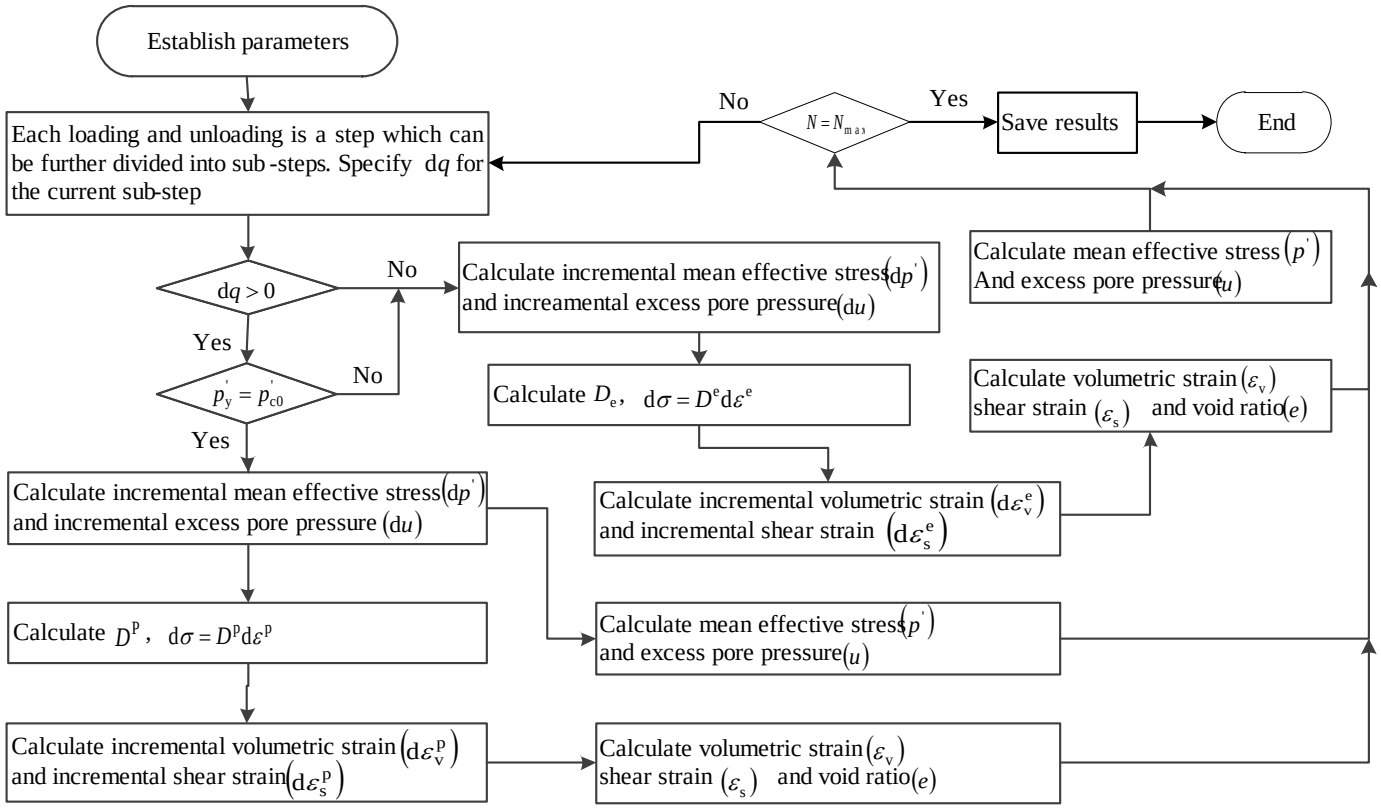

Fig. 4.5 Computational Procedure

4.3.3.1 Establish parameters for the new cyclic model

First of all, the parameters for the cyclic model should be established.

- Soil properties:
  - The slope of the normal compression line (λ)
  - The slope of the unloading-reloading line (κ)
  - The slope of the Critical State Line in $p' - q$ space (M_c)
  - Shear modulus (G)
  - Pre-consolidation stress (p'_{c0})

- Initial soil state:
  - Effective mean stress (p'_0)
  - Deviator stress (q'_0)
  - Specific volume ($v_0 = 1 + e_0$)

- cyclic loading:
  - Cyclic deviator stress (q_{cyc})
  - Cyclic loading frequency (f)
  - Cyclic degradation parameters (ξ_1 and ξ_2)

4.3.3.2 Set up steps and sub-steps

Each loading and unloading can be deemed to be a step which can also be divided into sub-steps, e.g., q_{cyc} can be divided into a number of increments (say n) where each step has an incremental deviator stress (dq_i) (i =1, 2, 3… n). Based on the notation of the deviator stress (dq_i) (i =1, 2, 3… n) and state of the soil, the process of cyclic loading can be divided into three categories and the corresponding process can be applied to calculate the stresses and strains.

- $dq_i < 0$, soil is unloaded and corresponds elastic.
- $dq_i > 0$ and $p'_y < p'_c$, soil is reloaded and corresponds elastic.
- $dq_i > 0$ and $p'_y = p'_c$, soil is reloaded and corresponds plastic.

4.3.3.3 **Soil is elastic**

When soil is elastic, the computational procedures are as follows:

(a) Calculate the deviator stress (q_{i+1}): $q_{i+1} = q_i + \mathrm{d}q_{i+1}$

(b) Calculate the effective mean stress (p'_{i+1}): $p'_{i+1} = p'_i$

(c) Calculate the excess pore water pressure (u_{i+1}): $u_{i+1} = u_i + \left(p'_i - p'_{i+1}\right) + \dfrac{\mathrm{d}q_{i+1}}{3}$

- Calculate the compliance matrix for $\begin{bmatrix} \mathrm{d}p'_{i+1} \\ \mathrm{d}q_{i+1} \end{bmatrix} = \begin{bmatrix} K_{i+1} & 0 \\ 0 & 3G \end{bmatrix} \begin{bmatrix} \mathrm{d}v_{i+1} \\ \mathrm{d}\varepsilon_{i+1} \end{bmatrix}$
- $K_{i+1} = \dfrac{(1+e_i)}{\kappa} p'_i$
- G is a constant

(d) Calculate the volumetric strain ($\varepsilon_{\mathrm{v},i+1}$) and shear strain ($\varepsilon_{\mathrm{s},i+1}$):

- $\mathrm{d}p'_{i+1} = K_{i+1}\mathrm{d}v_{i+1}$

$$\int_{p'_i}^{p'_{i+1}} \mathrm{d}p'_{i+1} = \int_{e_i}^{e_{i+1}} K_{i+1}\left(-\frac{\mathrm{d}e_{i+1}}{1+e_{i+1}}\right)$$

$$\ln(1+e_{i+1}) = \ln(1+e_i) - \frac{p'_2 - p'_1}{K_{i+1}}$$

$$e_{i+1} = (1+e_i)\exp\left(-\frac{p'_2 - p'_1}{K_{i+1}}\right) - 1$$

$$v_{i+1} = 1 + e_{i+1}$$

- $\varepsilon_{v,i+1} = \dfrac{e_{i+1} - e_0}{1+e_0}$
- $\varepsilon_{s,i+1} = \varepsilon_{s,i} + \dfrac{\mathrm{d}q_{i+1}}{3G}$

4.3.3.4 Soil is plastic

When soil is plastic, the computational procedures are as follows:

(a) Calculate the deviator stress (q_{i+1}): $q_{i+1} = q_i + \mathrm{d}q_{i+1}$

(b) Calculate the effective mean stress (p'_{i+1}): p'_{i+1} can be calculated from the expression:

$$\frac{p'_i}{p'_{i+1}} = \left(\frac{M^2 + \left(q_{i+1} / p'_{i+1}\right)^2}{M^2 + \left(q_i / p'_i\right)^2} \right)^{\frac{\lambda-\kappa}{\lambda}}$$

- The method for finding p'_{i+1} is the Newton-Raphson Method (see Appendix A):

$$f\left(p'_{i+1}\right) = \frac{p'_i}{p'_{i+1}} - \left(\frac{M^2 + \left(q_{i+1} / p'_{i+1}\right)^2}{M^2 + \left(q_i / p'_i\right)^2} \right)^{\frac{\lambda-\kappa}{\lambda}} = 0$$

$$f'\left(p'_{i+1}\right) = -\frac{p'_i}{\left(p'_{i+1}\right)^2} + \frac{\lambda-\kappa}{\lambda} \left(\frac{M^2 + \left(q_{i+1} / p'_{i+1}\right)^2}{M^2 + \left(q_i / p'_i\right)^2} \right)^{\frac{-\kappa}{\lambda}} \frac{2\left(q_{i+1}\right)^2 / \left(p'_{i+1}\right)^3}{M^2 + \left(q_i / p'_i\right)^2}$$

$$p'_{i+1}(1) = p'_i$$

$$p'_{i+1}(j+1) = p'_{i+1}(j) - \frac{f\left(p'_{i+1}(j)\right)}{f'\left(p'_{i+1}(j)\right)},\ 1 \le j \le n_{\text{iteration}}$$

where $n_{\text{iteration}}$ is the value of iteration. The value of p'_{i+1} can be obtained by:

$$p'_{i+1} = p'_{i+1}\left(n_{\text{iteration}} + 1\right)$$

(c) Calculate the excess pore water pressure (u_{i+1}): $u_{i+1} = u_i + \left(p'_i - p'_{i+1}\right) + \frac{\mathrm{d}q_{i+1}}{3}$

(d) Calculate the compliance matrix for $\begin{bmatrix} \mathrm{d}v_{i+1} \\ \mathrm{d}\varepsilon_{i+1} \end{bmatrix} = \begin{bmatrix} C_{11,i+1} & C_{12,i+1} \\ C_{21,i+1} & C_{22,i+1} \end{bmatrix} \begin{bmatrix} \mathrm{d}p'_{i+1} \\ \mathrm{d}q_i \end{bmatrix}$

- $C_{11,i+1} = \left(\frac{\lambda - \kappa}{1 + e_i}\right)\frac{a_i}{p_i^{'}} + \left(\frac{\kappa}{1 + e_i}\right)\frac{1}{p_i^{'}}$

- $C_{12,i+1} = C_{21,i+1} = \left(\frac{\lambda - \kappa}{1 + e_i}\right)\left(\frac{1 - a_i}{p_i^{'}}\right)$

- $C_{22,i+1} = \left(\frac{\lambda - \kappa}{1 + e_i}\right)\frac{b_i}{p_i^{'}} + \frac{1}{3G}$

  where $a_{i+1} = \frac{M^2 - \eta_i^2}{M^2 + \eta_i^2}$, $b_{i+1} = \frac{4\eta_i^2}{M^2 - \eta_i^2}$, and $\eta_i = \frac{q_i}{p_i^{'}}$

(e) Calculate the volumetric strain ($\varepsilon_{v,i+1}$) and shear strain ($\varepsilon_{s,i+1}$):

- $\mathrm{d}v_{i+1} = C_{11,i+1}\mathrm{d}p_{i+1}^{'} + C_{12,i+1}\mathrm{d}q_{i+1}$

  $$\int_{e_i}^{e_{i+1}}\left(-\frac{\mathrm{d}e}{1+e}\right) = \int_{p_i^{'}}^{p_{i+1}^{'}} C_{11}\mathrm{d}p^{'} + \int_{q_i}^{q_{1+1}} C_{12}\mathrm{d}q$$

  $$-\left(\ln(1+e_{i+1}) - \ln(1+e_i)\right) = C_{11}\left(p_2^{'} - p_1^{'}\right) + C_{12}(q_2 - q_1)$$

  $$\ln(1+e_{i+1}) = \ln(1+e_i) - \left(C_{11}\left(p_2^{'} - p_1^{'}\right) + C_{12}(q_2 - q_1)\right)$$

  $$e_{i+1} = (1+e_i)\exp\left(-C_{11}\left(p_2^{'} - p_1^{'}\right) - C_{12}(q_2 - q_1)\right) - 1$$

  $$v_{i+1} = 1 + e_{i+1}$$

- $\varepsilon_{v,i+1} = \frac{e_{i+1} - e_0}{1 + e_0}$

- $\varepsilon_{s,i+1} = \varepsilon_{s,i} + \frac{\mathrm{d}q_{i+1}}{3G}$

4.4 Verification of the new undrained cyclic model

To verify this new cyclic model, comparisons were made between the predictions of this proposed model and the test results of undrained cyclic loading given in Chapter 3. The parameters for the new model, including soil properties, initial states, and cyclic loading conditions are provided in Table 4.1 and Table 4.2. The values of cyclic degradation parameters ξ_1 and ξ_2 given in Table 4.2 indicate that ξ_1 is a soil property which is independent of both the cyclic stress ratio and loading frequency, while ξ_2 depends on the loading frequency in the way that ξ_2 increases with an increasing loading frequency.

Table 4.1 Parameters for Soil properties and initial states

Soil properties				Initial states		
λ	κ	M_c	p'_{c0} (kPa)	p'_0 (kPa)	q_0 (kPa)	e_0
0.18	0.03	1.89	30	30	16	1.32

Table 4.2 Parameters for cyclic loading

Cyclic loading conditions			
f (Hz)	Specimen	ξ_1	ξ_2
0.1	U_{01}, U_{05}, and U_{09}	2.8	50
1	U_{02}, U_{06}, and U_{10}	2.7	280
2	U_{03}, U_{07}, and U_{11}	2.7	400
5	U_{04}, U_{08}, and U_{12}	2.8	550

The simulation, together with the test data of normalised excess pore pressure and axial strains, against the number of cycles for specimen U_{01} - U_{12} are given in Fig. 4.6 ~ Fig. 4.9. There was a good agreement between the predicted results and the actual trends. As expected, both the normalised excess pore pressures and axial strains increased with the increasing cyclic stress ratio.

The plots shown in Fig. 4.6(a) ~ Fig. 4.9(a) clearly suggest that the excess pore pressures rise quickly at the initial stages and continue to increase gradually with the number of cycles. For stable specimens (CSR = 0.4 and 0.6), the excess pore pressures reach a stable state after an initial rapid development, with normalised excess pore pressures equal to 0.15 and 0.35 for CSR = 0.4 and 0.6, respectively. With the failed specimens, the excess pore pressures developed so quickly that the critical normalised value of 0.65 was reached in the first few cycles. The specimens failed before they reached a stable state. It should be noted that the samples gave no indication of failure merely by looking at these normalised excess pore pressures.

In contrast, the results shown in Fig. 4.6(b) ~ Fig. 4.9(b) indicate that the failure of the four specimens U_{09}, U_{10}, U_{11}, and U_{12} (CSR = 0.8) is clearly characterised by a dramatic rise in axial strain beyond a critical number of cycles. While the failure of U_{09} (f = 0.1 Hz) occurred as N approached 2,000 cycles, at the highest frequency, i.e. U_{12} at f = 5 Hz, failure occurred as N > 30,000 cycles. For specimens with a CSR = 0.4 and 0.6, the axial strains were quite small at less than 1%, at the end of the tests. This indicated that a rapid upward trajectory of axial strains occurred when a normalised excess pore pressure of 0.6 was reached through a comparison between the excess pore pressures and axial strains for specimens U_{09}, U_{10}, U_{11}, and U_{12} (CSR = 0.8).

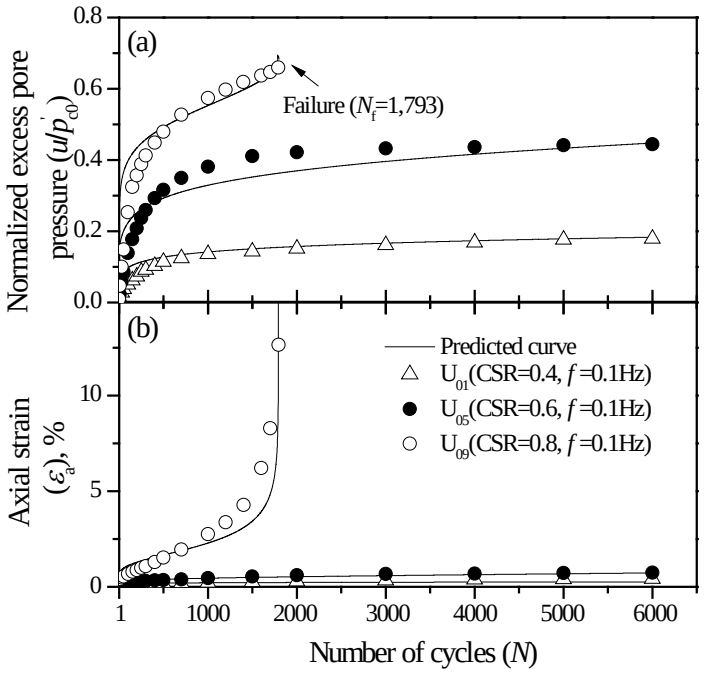

Fig. 4.6 Comparison of predicted results and test data under $f = 0.1\text{Hz}$: (a) Excess pore pressure, (b) Axial strain

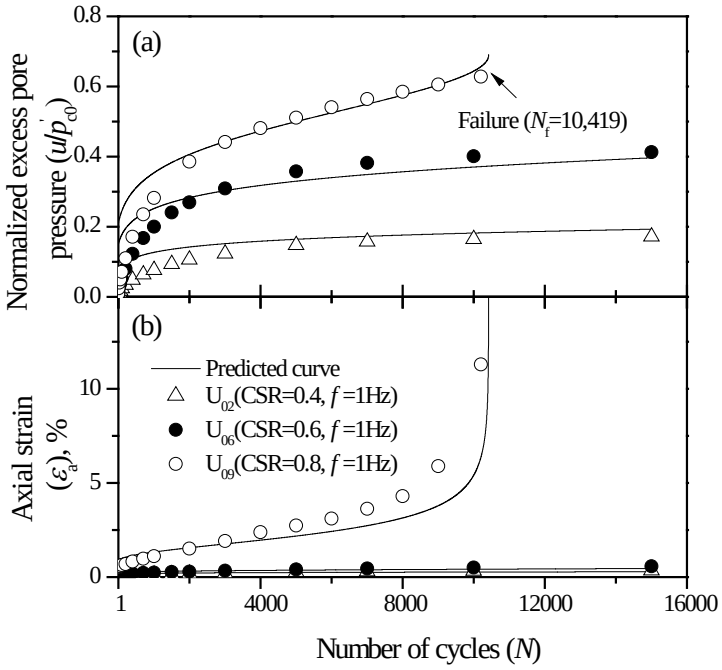

Fig. 4.7 Comparison of predicted results and test data under $f = 1\text{Hz}$: (a) Excess pore pressure, (b) Axial strain

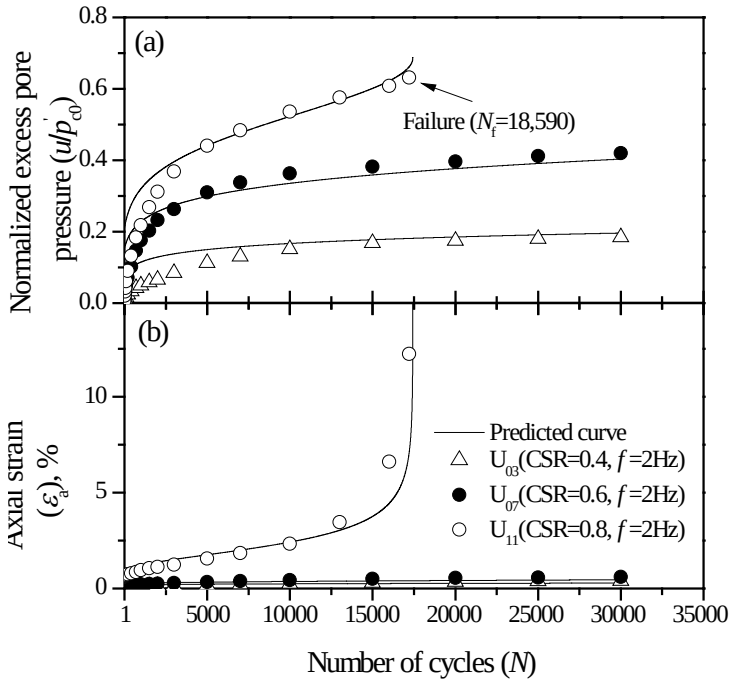

Fig. 4.8 Comparison of predicted results and test data under f = 2Hz : (a) Excess pore pressure, (b) Axial strain

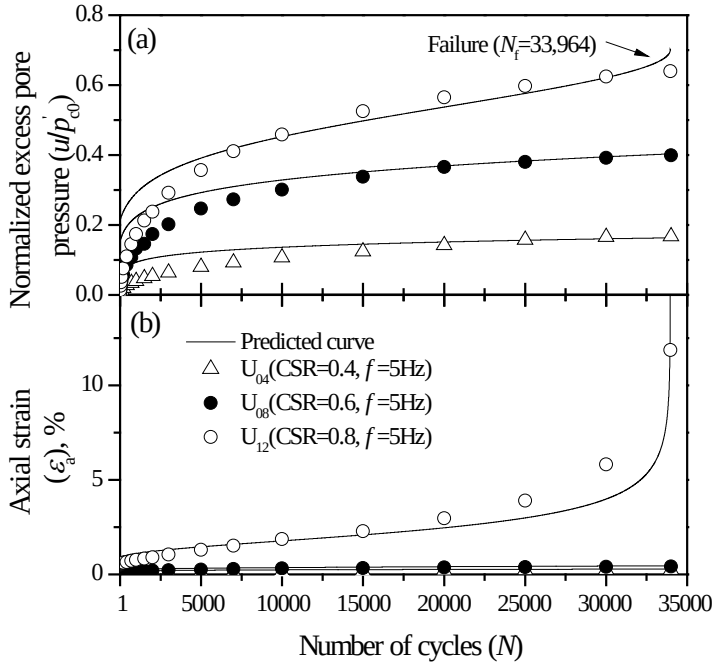

Fig. 4.9 Comparison of predicted results and test data under f = 5Hz : (a) Excess pore pressure, (b) Axial strain

This proposed undrained cyclic model was also used to predict the generation of excess pore pressure within undisturbed specimens of silty clay under cyclic loading (Sakai et al. 2003). Soil had the following properties: natural water content $w_n = 71\%$, liquid limit $w_L = 63\%$, plastic index $I_p = 32\%$, and compression index $C_c = 0.89$. The major and minor consolidation stresses are $\sigma_{1c}^{'} = 98\,\text{kPa}$ and $\sigma_{3c}^{'} = 49\,\text{kPa}$, respectively. A cyclic failure envelope $M_c = 1.75$ was determined from a series of undrained cyclic loading tests. The values of cyclic degradation parameters ξ_1 and ξ_2 from back calculation are 1.5 and 310, respectively. The simulation and the test data of normalised excess pore pressure are given in Fig. 4.10. When $q_{cyc} / p_{c0}^{'} = 0.743$, the excess pore pressure increased so quickly that the specimen failed after only 7 cycles. When specimens were subjected to a lower value of $q_{cyc} / p_{c0}^{'}$, less excess pore pressure generated and specimens were more stable. The comparison indicates a good agreement between the predictions and measurments.

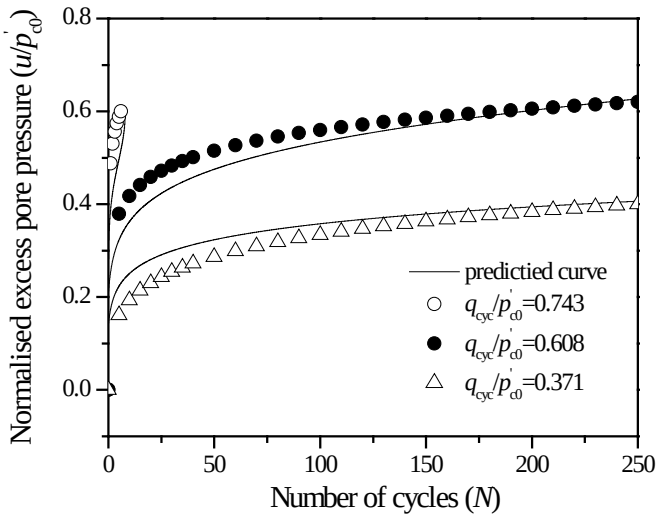

Fig. 4.10 Comparison of predicted results and test data obtained by Sakai et al. (2003)

4.5 Analysis of the new undrained cyclic model

In this section, the effects of cyclic stress ratio, anisotropic consolidation condition and cyclic degradation parameters ξ_1 and ξ_2 on the development of excess pore pressure and axial strains are investigated using the new cyclic model. The basic soil properties used in the following analysis are given in Table 4.3.

Table 4.3 Parameters for Soil properties and initial states

λ	κ	M_c	p'_{c0} (kPa)	p'_0 (kPa)	e_0	G
0.25	0.05	1.2	30	30	0.6	$200c_{u0}$ [a]

[a] $c_{u0} = p'_{c0}(M/4)(2p'_0/p'_{c0})^{\kappa/\lambda}$

4.5.1 Effect of cyclic stress ratio

To investigate how the cyclic stress level affects the performance of soft soils, the predictions of normalised excess pore pressures and axial strains at various cyclic stress ratios using the proposed model are given in Fig. 4.11. The results shown in Fig. 4.11 (a) indicate that the critical cyclic stress ratio is around 0.5 (shown by the dashed line), given the parameters used in this prediction. When CSR = 0.6, 0.7, and 0.8, the excess pore pressure increases so fast that the value of u_f / p'_{c0} reaches 0.8 in the first few cycles. When CSR = 0.2, 0.3, and 0.4, the generation rates of excess pore pressures decreases and the specimens reach a stable state after an initial stage of rapid development. A determination of the critical cyclic stress ratio is made easier by observing the axial strains, as shown in Fig. 4.11 (b). At a critical cyclic ratio of 0.5, the axial strain at 1,000 cycles is around 7%, which is seven times the value at CSR = 0.4 but only two times if the excess pore pressures are compared.

When ξ_2 increases from 10 to 50, the predictions of normalised excess pore pressures and axial strains are shown in Fig. 4.12. The results shown in Fig. 4.12 indicate that the critical cyclic stress ratio is 0.6. Through the comparison of Fig. 4.11 and Fig. 4.12, an increased critical cyclic stress ratio from 0.5 to 0.6 is found when ξ_2 increases from 10 to 50.

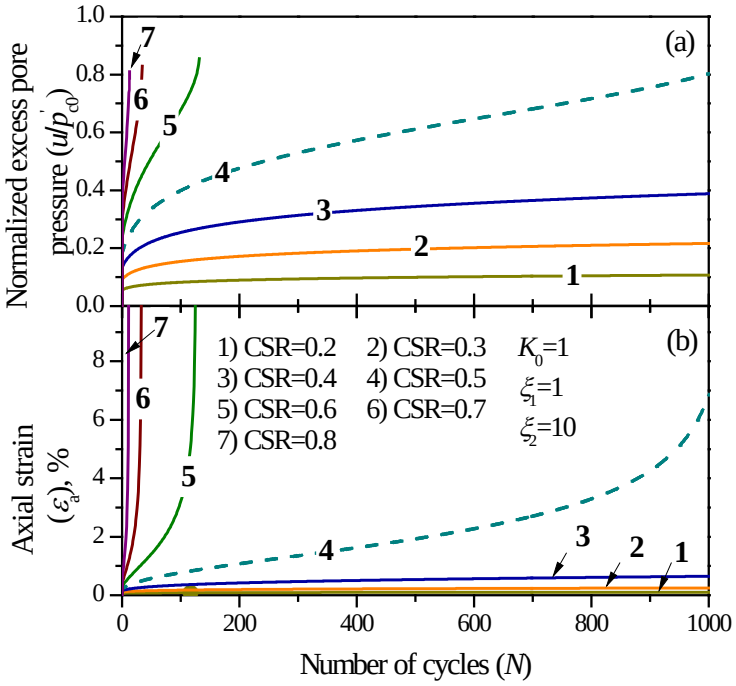

Fig. 4.11 Predictions of the proposed model with different cyclic stress ratios ($K_0 = 1$, $\xi_1 = 1$, $\xi_2 = 10$): (a) Excess pore pressure, (b) Axial strain

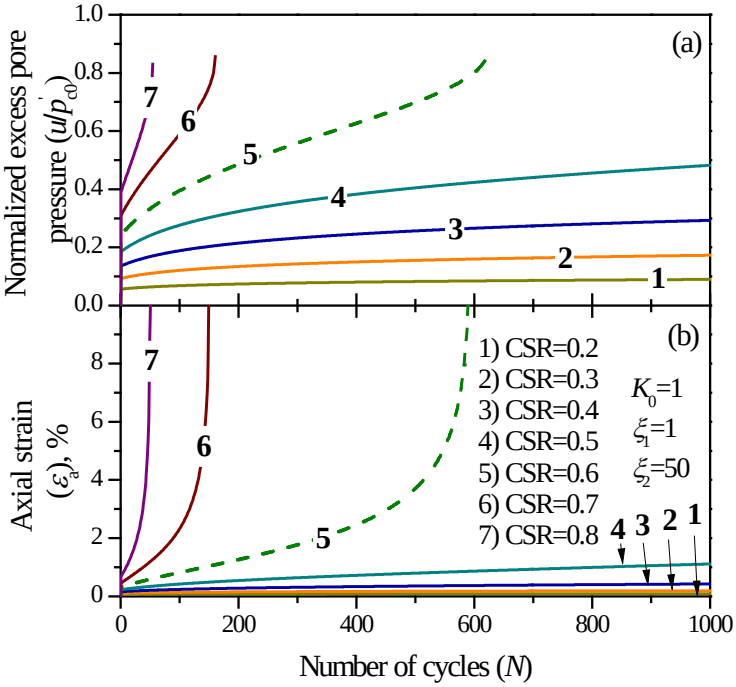

Fig. 4.12 Predictions of the proposed model with different cyclic stress ratios ($K_0 = 1$, $\xi_1 = 1$, $\xi_2 = 50$): (a) Excess pore pressure, (b) Axial strain

4.5.2 Effect of anisotropic consolidation ratio

To investigate how the anisotropic consolidation stress ratio ($K_0 = \sigma'_{3c} / \sigma'_{1c}$) influences the performance of soft soils, the predictions made by the proposed model under various anisotropic consolidation conditions are given in Fig. 4.13 and Fig. 4.14. As shown in Fig. 4.13, five consolidation stress ratios from 0.6 to 1.0 with 0.1 intervals are considered. For a relatively low cyclic stress ratio CSR = 0.3, soft soils behave stably under cyclic loading when K_0 = 0.8, 0.9, and 1.0. When K_0 decreases to 0.7, even at CSR = 0.3, the excess pore pressure and axial strain generate significantly and the failure occurs around 400 cycles. With an even smaller consolidation stress ratio K_0 = 0.6, the excess pore pressure and axial strain increase so rapidly that the soft soil could fail within fewer cycles around 100 cycles. For a medium cyclic stress ratio CSR = 0.5, the effect of different anisotropic consolidation conditions on the behaviour of soft clays under cyclic loading is presented in Fig. 4.14. The predictions in Fig. 4.14 indicate that only the isotropically consolidated soil (K_0 = 1.0) is stable when subjected to cyclic loading. When K_0 decreases to 0.9, great excess pore pressure and axial strain accumulate and the failure occurs around 980 cycles. With a decreasing value of K_0 from 0.8 to 0.6, the number of cycles at failure decreases from 200 to 5 cycles. The comparison of Fig. 4.13 and Fig. 4.14 indicates that while the minimum value of K_0 is 0.8 at CSR = 0.3 to ensure the stability of soft clays under cyclic loading, it increases to 1.0 at CSR = 0.5.

In summary, the anisotropic consolidation stress ratio has an effect on the behaviour of soft clays subjected to cyclic loading. For a given cyclic stress ratio, the excess pore pressure and axial strain increase as the consolidation stress ratio increases. The stable state can be reached at a relatively big value of K_0, while failure could occur at a small value of K_0. The number of cycles at failure decreases with a decreasing value of K_0. When the cyclic stress ratio increases, an increased value of K_0 should be applied during the process of consolidation to ensure that the soft clays behave stably under cyclic loading.

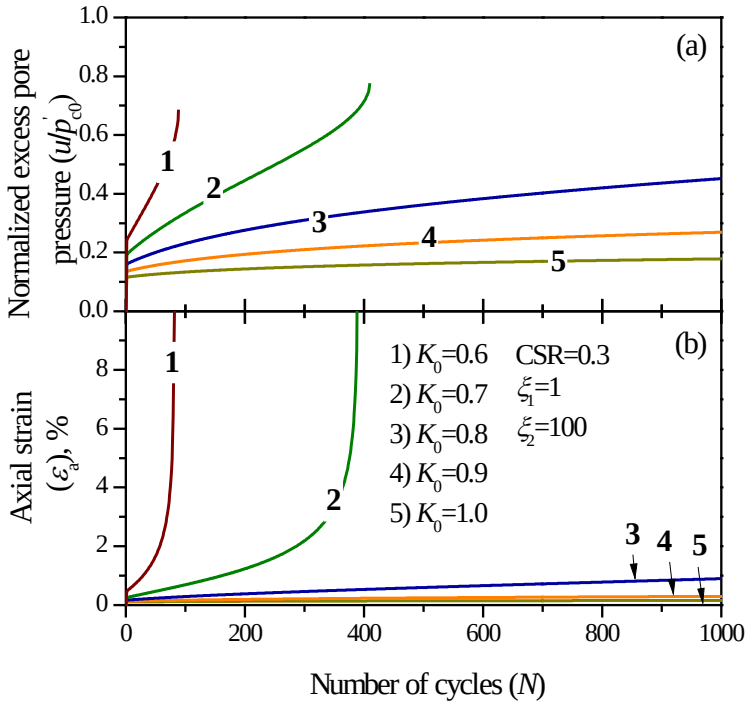

Fig. 4.13 Predictions of the proposed model with different anisotropic consolidation stress ratios ($\mathrm{CSR}=0.3$, $\xi_1=1$, $\xi_2=100$): (a) Excess pore pressure, (b) Axial strain

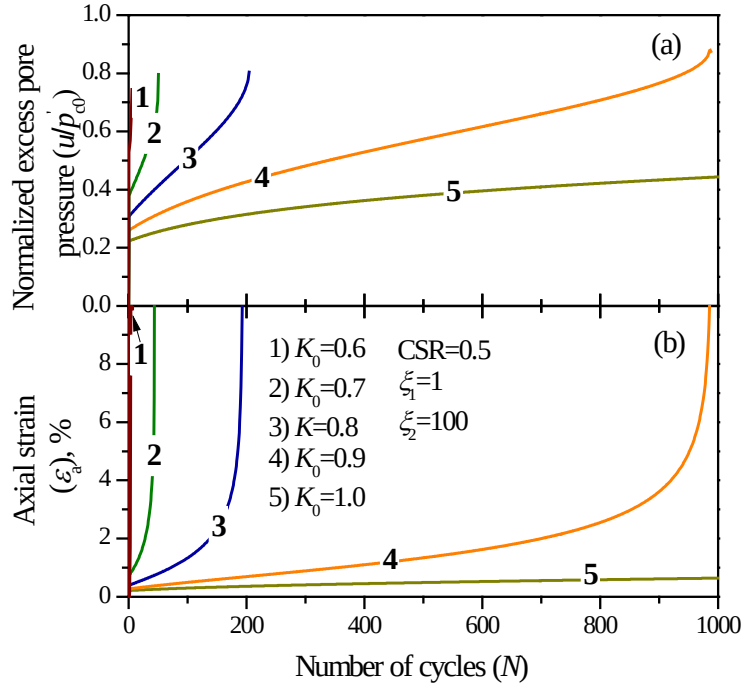

Fig. 4.14 Predictions of the proposed model with different anisotropic consolidation stress ratios ($\mathrm{CSR}=0.5$, $\xi_1=1$, $\xi_2=100$): (a) Excess pore pressure, (b) Axial strain

The effect of the anisotropic consolidation stress ratio on the critical cyclic stress ratio is shown in Fig. 4.15 and Fig. 4.16. For K_0 = 0.82, the development of excess pore pressure and axial strain is shown in Fig. 4.15. The predictions indicate that the critical cyclic stress ratio is 0.4. When the cyclic stress ratio is above the critical level, the excess pore pressure develops rapidly and the value of u_f / p'_{c0} increases to 0.81. When the cyclic stress ratio is below the critical value, the excess pore pressure developed slowly after the initial stage. The axial strain at $CSR > 0.4$ continues to generate at an increasing rate, which causes failure soon after cyclic loading commences. When $CSR < 0.4$, the generation rate of axial strain is quite low, so that the total value is less than 1% at 1,000 cycles.

For a decreased consolidation stress ratio K_0 = 0.68, the development of excess pore pressure and axial strain is shown in Fig. 4.16. As can be seen, a smaller critical cyclic stress ratio of 0.3 is found compared to that under K_0 = 0.82. The comparison of Fig. 4.15 and Fig. 4.16 indicates that a reduced value of u_f / p'_{c0} from 0.81 to 0.78 is observed when consolidation stress ratio decreases from 0.82 to 0.68. When $CSR > 0.3$, the excess pore pressure and axial strain increase significantly and the failure could occur in the initial stage of rapid development. When the cyclic stress ratio is below the critical value $CSR < 0.3$, the excess pore pressure and axial strain develop slowly after the initial stage of rapid development.

In summary, the value of critical cyclic stress ratio is influenced by the anisotropic consolidation stress ratio. Usually the critical cyclic stress ratio decreases with a decreasing value of consolidation stress ratio. Furthermore, the value of u_f / p'_{c0} decreases with a decreasing value of K_0. It is implied that to ensure the stability of the soft clay subgrade, a cyclic load with a smaller q_{cyc} is preferred when the soil is consolidated under a smaller value of $\sigma'_{3c} / \sigma'_{1c}$. This analysis confirms the conclusion mentioned by the researchers (Zimmie and Lien 1986; Andersen 1988; Ishihara et al. 1993) that the lower the value of K_0, the less the cyclic resistance of the soft soils to the cyclic loading.

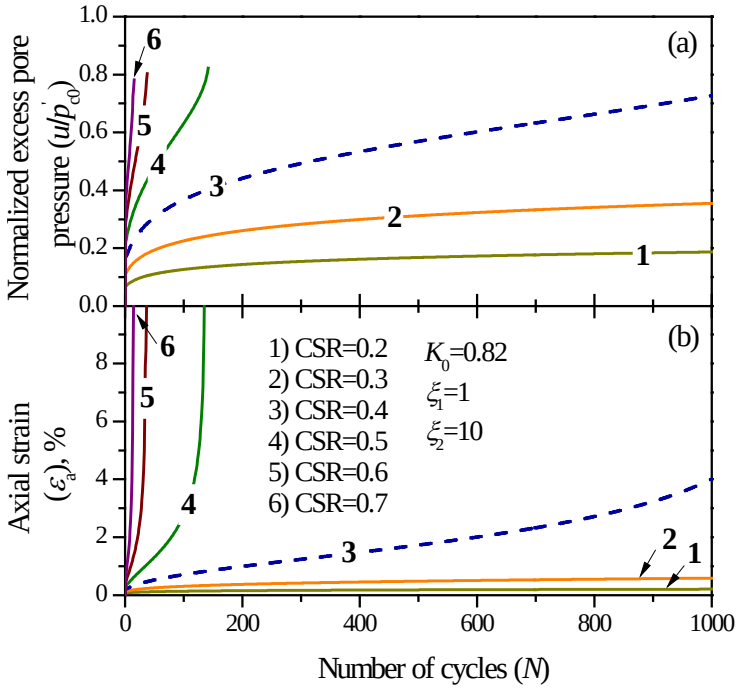

Fig. 4.15 Predictions of the proposed model with initial shear stress $K_0 = 0.82$: (a) Excess pore pressure, (b) Axial strain

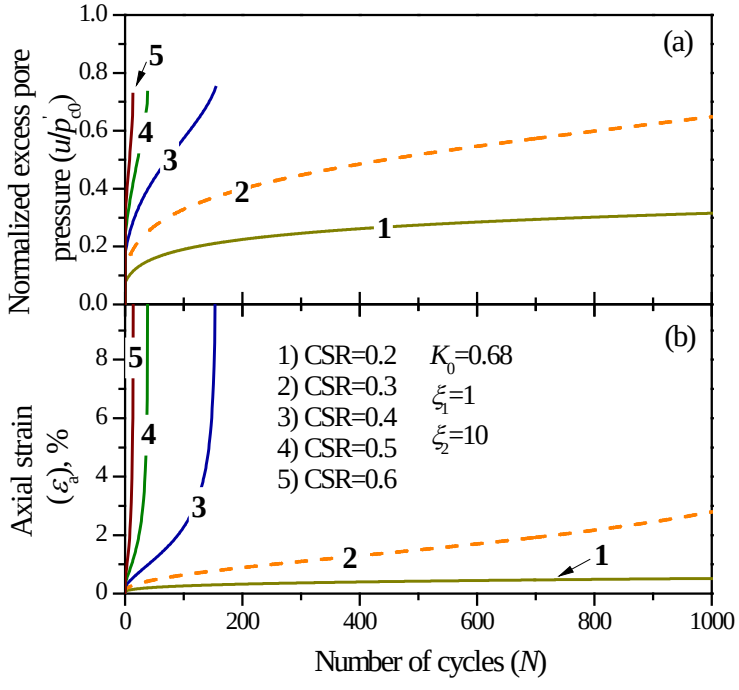

Fig. 4.16 Predictions of the proposed model with initial shear stress $K_0 = 0.68$: (a) Excess pore pressure, (b) Axial strain

4.5.3 Effect of cyclic degradation parameters ξ_1 and ξ_2

The influence of cyclic degradation parameter ξ_1 on the development of excess pore pressures and axial strains for soft soils under cyclic loading is shown in Fig. 4.17. The predicted results indicate that the rate of generation of excess pore pressures and axial strains decreases as the value of ξ_1 increases. When ξ_1 changes from 0, 1, 3, to 5, the number of cycles at failure increases.

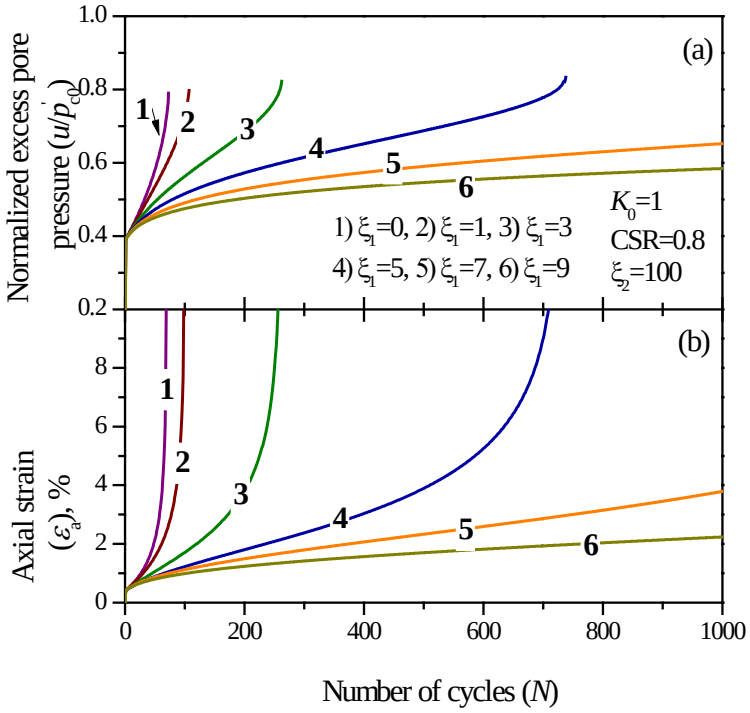

Fig. 4.17 Predictions of the proposed model with different values of ξ_1 : (a) Excess pore pressure, (b) Axial strain

To investigate the influence of cyclic degradation ξ_2 on the performance of soft soils under cyclic loading, two cases will be discussed: (a) $\xi_1 = 0$ which represents the special situation that coincides with the cyclic model of Carter et al. (1982); (b) $\xi_1 \neq 0$.

The development of excess pore pressures and axial strains versus the number of loading cycles for $\xi_1 = 0$ is shown in Fig. 4.18, where the value of ξ_2 ranges from 50 to 300 with 50 intervals. The predicted results indicate that the generation of excess pore pressures and axial strains decreases as the value of ξ_2 increases. The predictions shown in Fig. 4.18(a) indicate that the generation rate of excess pore pressure increases with the increasing number of loading cycles, regardless of the value of ξ_2.

When $\xi_1 = 0$, the effect of the level of cyclic stress on the development of excess pore pressures and axial strains are studied (see Fig. 4.19). The excess pore pressures shown in Fig. 4.19(a) indicate that the generation rate of excess pore pressures does not decrease with an increasing number of loading cycles for a cyclic stress ratio ranging from 0.2 to 0.8. Unfortunately, when $\xi_1 = 0$, the critical cyclic stress ratio could not be predicted because the trends of excess pore pressures are similar to each other, regardless of the cyclic stress ratio. There is no significant difference in excess pore pressures when the cyclic stress ratio changes from one value to another. The critical cyclic stress ratio could not be predicted by the curves of axial strains either, as shown in Fig. 4.19(b).

The relationships between $1/\xi_2$ and number of cycles at failure (N_f) for different cyclic stress ratios are shown in Fig. 4.20. The effect of ξ_1 on the number of cycles at failure is also considered in the way that predictions are made under ξ_1 = 0, 0.1 and 0.5, respectively. It is clear that at a constant cyclic stress ratio, the number of cycles at failure decreases as the value of $1/\xi_2$ increases. In addition, at a constant value of $1/\xi_2$, the number of cycles at failure decreases as the cyclic stress ratio increases. For the identical parameters, the number of cycles at failure increases as ξ_1 increases.

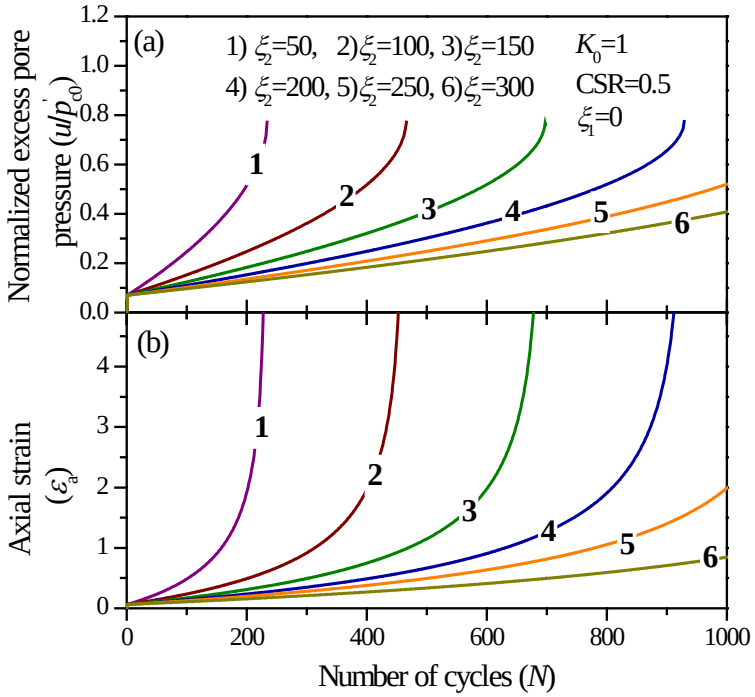

Fig. 4.18 Predictions of the proposed model with different values of ξ_2 : (a) Excess pore pressure, (b) Axial strain

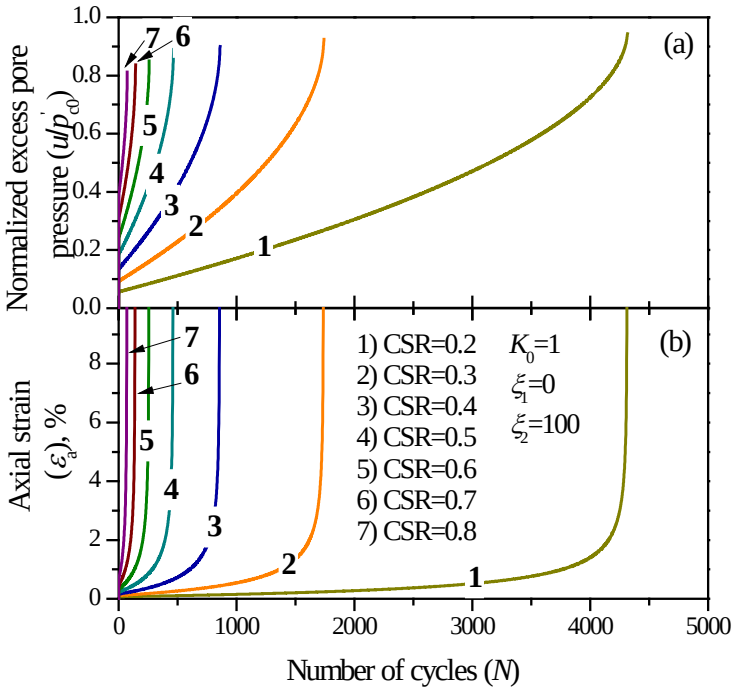

Fig. 4.19 Predictions of the proposed model with different cyclic stress ratios with $\xi_1 = 0$: (a) Excess pore pressure, (b) Axial strain

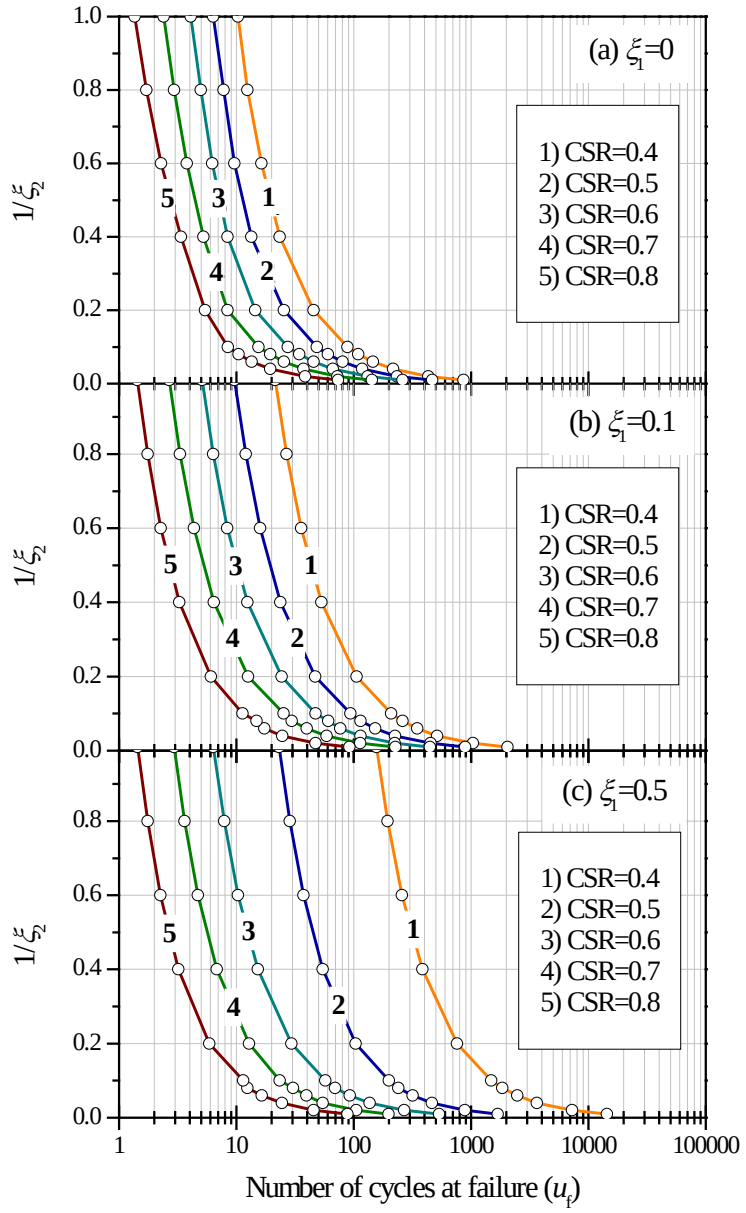

Fig. 4.20 The relationship between $1/\xi_2$ and number of cycles to failure (N_f): (a) $\xi_1 = 0$, (b) $\xi_1 = 0.1$, (c) $\xi_1 = 0.5$

The cyclically generated excess pore pressures and axial strains for $\xi_1 \neq 0$ are shown in Fig. 4.21, with the values of ξ_2 changing from 50 to 300 in increments of 50. As can be seen from Fig. 4.21, the generation of excess pore pressures and axial strains decreases as the value of ξ_2 increases.

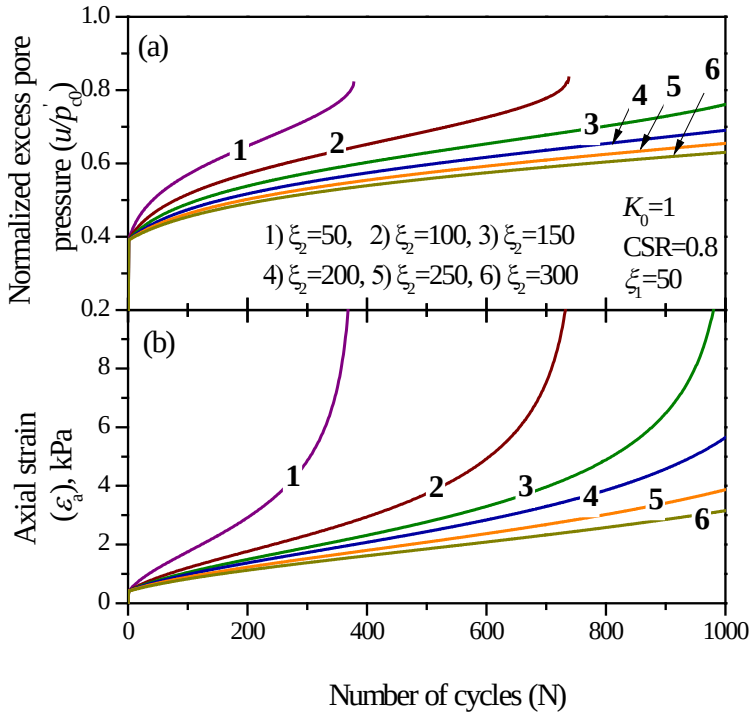

Fig. 4.21 Predictions of the proposed model with different values of ξ_2 : (a) Excess pore pressure, (b) Axial strain

In summary, the excess pore pressure and axial strains decrease as the cyclic degradation parameters ξ_1 and ξ_2 increase in value. When $\xi_1 = 0$ (Carter et al. 1982), the critical cyclic stress ratio is unpredictable by detecting the development of excess pore pressure and axial strains, whereas when $\xi_1 \neq 0$ (the proposed cyclic model), a dramatic increase in both excess pore pressures and axial strains is seen when the cyclic stress ratio increased to a critical value. The critical cyclic stress ratio is affected by the consolidation stress ratio and the cyclic degradation parameters ξ_1 and ξ_2. For a given value of consolidation stress ratio, the critical value decreases as the parameters ξ_1 and ξ_2 increase. For given values of parameters ξ_1 and ξ_2, the critical value increases as the consolidation stress ratio increases.

4.6 Conclusions

A new cyclic model was proposed here, extending the original model of Carter et al. (1982)'s model, to predict the behavior of soft clays under undrained cyclic loading. The theory is developed in terms of the modified Cam-clay soil model and attention is largely restricted to triaxial conditions. State of the soil, normal compression and unloading-reloading lines, critical state line, yield function, and hardening behaviour are the key aspects of this model. A modified yield surface function during elastic unloading is proposed to catch the soil behaviour under cyclic loading while other assumptions remain the same as the modified Cam-clay soil model. There are only two additional parameters needed to characterise the cyclic behaviour together with the traditional parameters associated with the modified Cam-clay soil model. A detailed computational procedure for determining the excess pore pressure and axial strains are demonstrated, including the establishment of parameters (soil properties, initial soil states, and cyclic loading conditions), set-up of steps and sub-steps, and finally the calculation of the excess pore pressure and axial strains.

A comparison is made between the prediction of the proposed model and undrained test results described in Chapter 3, and a good agreement is found in excess pore pressures and axial strains. In this way, the new cyclic model is verified. The values of cyclic degradation parameters ξ_1 and ξ_2 indicate that ξ_1 is a soil property which is independent of the loading frequency, while ξ_2 depends on the loading frequency whereby it increases with an increasing loading frequency.

Furthermore, the proposed model is analysed by investigating many factors which influence the cyclic performance of soft soils such as cyclic stress ratios, pre-shearing, and loading frequencies. The excess pore pressure and axial strains decrease as the cyclic degradation parameters ξ_1 and ξ_2 increase in value. When $\xi_1 = 0$ (Carter et al. 1982), the critical stress ratio is not predictable by detecting the development of excess pore pressure and axial strains, whereas when $\xi_1 \neq 0$ (proposed cyclic model), a dramatic increase in both excess pore pressures and axial strains was observed when the cyclic stress ratio increased to a critical value.

5 Partially Drained Cyclic Triaxial Test with Single PVD

This Chapter describes the partially drained cyclic triaxial tests conducted on soft clay specimens. A single PVD was installed in the centre of the cylinder to allow for radial drainage during and after the cyclic tests. Three types of tests were carried out: (a) cyclic loading without a rest period, (b) cyclic loading with a rest period, and (c) cyclic loading with a changing loading frequency. Changing cyclic stress ratios (CSR = 0.4, 0.6 and 0.8) and frequencies (f = 0.1, 1, 2, and 5 Hz) were chosen as the experimental variables. The development of excess pore pressure was analysed and compared with an undrained condition, and then the usefulness of PVDs in dissipating excess pore pressure during and after cyclic loading were investigated.

5.1 Preparation of PVD

In practice the equivalent diameter of a soil cylinder corresponding to a drain spacing is approximately 1 to 1.5 m and correspondly the radii of influence zone are from 0.56 to 0.85 m and from 0.53 to 0.79 m for rectangular and triangular patterns, respectively. However, the available large scale triaxial equipment for laboratory tests is 300 mm in diameter, which means that if a single drain is installed at the centre, then the drain spacing is 0.3 m, which is much smaller than the actual drain spacing in the field. Therefore the PVDs with a modified size are preferred rather than those with a full size.

This modification in size is based on the concept that for a given time factor (T_{h}), the average degrees of consolidation for two soil cylinders should be the same. It is noted that for simplicity, an ideal drain has been used to calculate the size of the modified PVD. For the actually soil cylinder in the field, the average degree of consolidation can be calculated by:

$$U_{\mathrm{h,re}} = 1 - \exp\left(-8T_{\mathrm{h}} / \mu_{\mathrm{I}}\right) \tag{5.1}$$

where $\mu_{\mathrm{I,re}} = \ln\left(\dfrac{r_{\mathrm{e}}}{r_{\mathrm{w,re}}}\right) - 0.75$, $r_{\mathrm{e}} = 600$ mm is assumed to be the radius of influence zone in the field, and $r_{\mathrm{w,re}}$ is the equivalent radius of the full size PVD which can be calculated by Hansbo (1979):

$$r_{w,re} = 2\frac{(a_{re} + b_{re})}{\pi} \tag{5.2}$$

where $a_{re} = 100$ mm and $b_{re} = 4$ mm, they are respectively the width and thickness of the full size PVD.

The average degree of consolidation of the soil cylinder used in the laboratory tests can be calculated by:

$$U_{h,ex} = 1 - \exp(-8T_h / \mu_{I,ex}) \tag{5.3}$$

where $\mu_{I,ex} = \ln\left(\frac{r_{e,ex}}{r_{w,ex}}\right) - 0.75$, and $r_{e,ex} = 150$ mm is the radius of influence zone for the soil cylinder in laboratory, and $r_{w,ex}$ is the equivalent radius of the PVD in a modified size which can be calculated by:

$$r_{w,ex} = 2\frac{(a_{ex} + b_{ex})}{\pi} \tag{5.4}$$

where $b_{ex} = 4$ mm is the thickness of the PVD and b_{ex} is the width of the PVD which is to be calculated.

As stated previously, for any time factor (T_h), there is a relationship between $U_{h,re}$ and $U_{h,ex}$ which can be expressed by:

$$U_{h,re} = U_{h,ex} \tag{5.5}$$

Then the following equation holds:

$$\mu_{I,re} = \mu_{I,ex} \tag{5.6}$$

Thus, the equivalent radius of the PVD in a modified size can be expressed by:

$$r_{w,ex} = r_{e,ex} / \left(\frac{r_{e,re}}{r_{w,re}}\right) \tag{5.7}$$

Finally, it can be obtained that $r_{w,ex} = 16.55$ mm and $a_{ex} = 22$ mm. So the size of the modified PVDs is 22 mm $\times$ 4 mm.

5.2 Large scale triaxial equipment

The large scale cylindrical dynamic triaxial equipment which was designed and built at the University of Wollongong was used for the partially drained cyclic loading tests (see Fig. 5.1 (a)). This apparatus is capable of accommodating 300 mm diameter by 600 mm high samples and utilises a hydraulic type dynamic actuator to apply load cycles onto the soil specimens. A schematic illustration of the components of this equipment is shown in Fig. 5.1 (b), i.e., the triaxial chamber, the axial loading unit, the air pressure and the water control unit, the pore pressure measurement system, and the volumetric change measurement device. The equipment was modified by the author to measure excess pore pressure at different locations inside the soil sample. Miniature type pore pressure transducers were fitted through the base of the triaxial rig and then through the specimen pedestal to the soil sample.

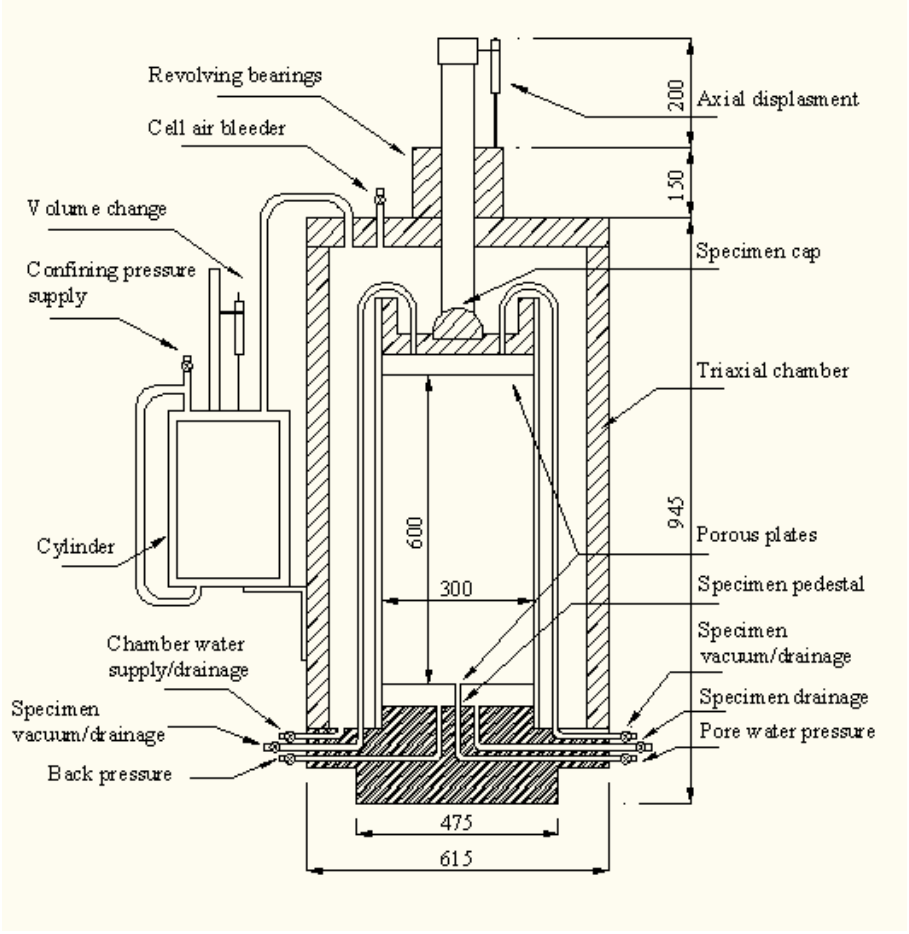

(a)

(b)

Fig. 5.1 Large scale triaxial equipment: (a) Schematic, (b) Photo

5.3 Preparation of the specimens

The specimens used in the partially drained cyclic loading tests were made of clay (kaolinite) powder. The detailed properties of the soil are given elsewhere in Chapter 3 and not repeated here. Reconstituted specimens were prepared from this reconstituted clay for testing. The preparation procedures have been detailed by Attya and Indraratna (2006) and is summarised below:

- Commercial kaolinite (46 kg) was first placed in a mixing bowl with de-aired water (27 kg) and mixed until a uniform clay paste with a water content ($w = 58\%$) slightly above the liquid limit was obtained.

- A rubber membrane was clamped into the base of the triaxial equipment and a geosynthetic filter layer was placed at the bottom to prevent the drainage line from clogging. To ensure there was only radial flow in the specimen, the bottom of the specimen was handled such that the geosynthetic layer was covered by impermeable plastic with a hole in the centre so that the water can only flow out through the drain (see Fig. 5.2(a)).

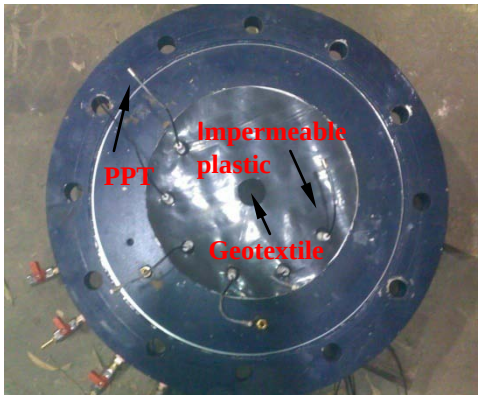

(a)

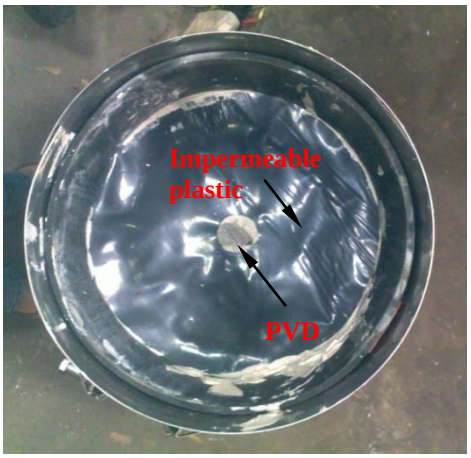

(b)

Fig. 5.2 The boundary condition of the specimen: (a) The bottom of the specimen, (b) The top of the specimen

- Subsequently, clay slurry was placed and lightly compacted in four layers (150 mm each) inside the membrane to a unit weight of about 15.5 kN/m^3.

- While the clay was being loaded into the membrane, four miniature pore pressure transducers T1 to T4 were inserted from the base plate through cable adapters and fixed at predetermined radial (20, 60, and 130 mm from the drain) and vertical distances (150 and 450 mm from the bottom) (see Fig. 5.3).

- A prefabricated vertical drain was driven through the centre of the soil using a rectangular mandrel ($35\,mm \times 6\,mm$) and then removed. Care was taken during installation of the PVD, and the removal of the mandrel, to avoid any excessive

disturbance of the soil. Water was then poured through the centre of the PVD to prevent drain unsaturation.

- To ensure that the pore water in the specimen only drained out through the PVD, the top of the specimen was handled in the same way as at the bottom. At the top of the specimen, the clay was covered by impermeable plastic with the PVD through the hole (see Fig. 5.2). Then a geosynthetic layer was placed on the impermeable plastic before placing the top loading cap, in order to protect the top drainage holes from clogging.

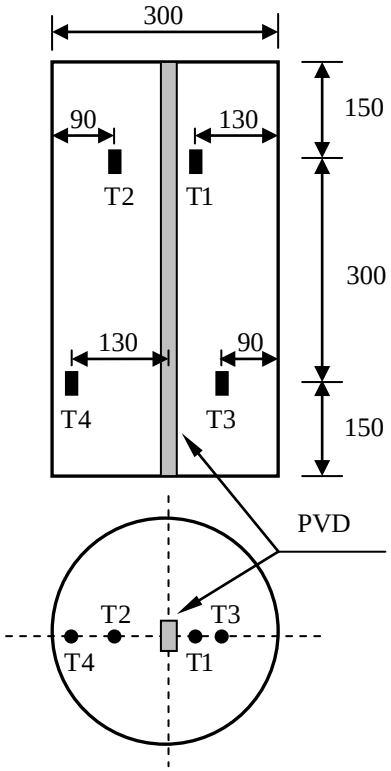

Fig. 5.3 The installation of the excess pore pressure transducers (all units are in millimetres)

5.4 Test conditions

Three types of partially drained cyclic triaxial tests were conducted on specimens of soft kaolin (see Fig. 5.4): (a) cyclic loading without a rest period, (b) cyclic loading with a rest period, and (c) cyclic loading with a changing loading frequency. The usefulness of PVDs in dissipating the excess pore pressure during and after cyclic loading was investigated.

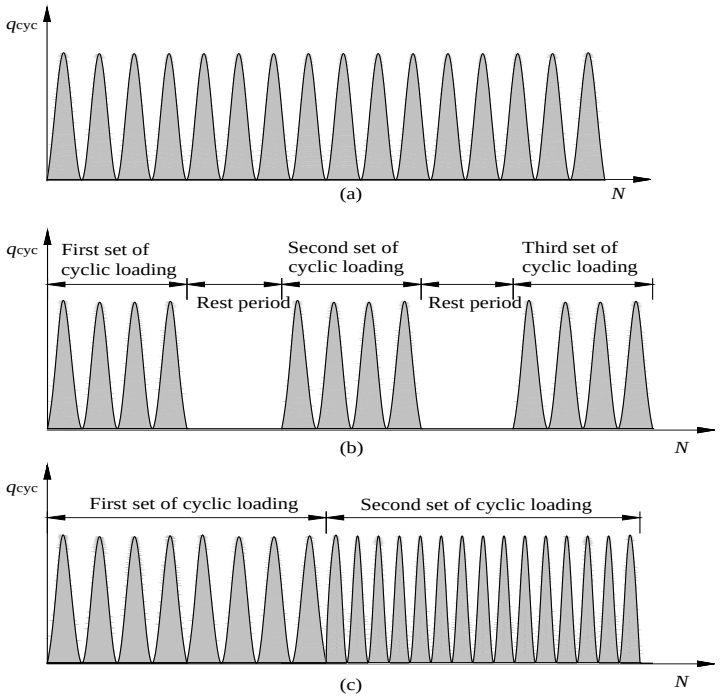

Fig. 5.4 Large scale cyclic triaxial tests: (a) Cyclic loading without a rest period, (b) Cyclic loading with a rest period, (c) Cyclic loading with a changing loading frequency

The main purpose of the first type of test is to validate the effect of radial drainage on reducing the development of excess pore pressure during cyclic loading. Therefore a series of partially drained tests without a rest period were carried out on specimens of soft clay (see Fig. 5.4(a)). All the test conditions, including the name of the specimen, cyclic stress ratio, and loading frequency are given in Table 5.1. The cyclic stress ratio ranged from 0.4 to 0.8 and the loading frequency ranged from 0.1 to 5 Hz. These tests were stopped when either failure occurred or it reached 15,000 cycles. Failure is considered to occur when the excess pore pressure increases to a critical value which is obtained in Chapter 3.

Table 5.1 Test conditions for partially drained cyclic loading (without a rest period)

Specimen	σ_{1c}, kPa	σ_{3c}, kpa	Loading frequency (f), Hz	Cyclic stress ratio (CSR)	Loading cycles (N)	Failed?
D_{01}	40	24	1	0.4	15,000	No
D_{02}	40	24	2	0.6	15,000	No
D_{03}	40	24	5	0.6	15,000	No
D_{04}	40	24	0.1	0.8	3,024	Yes

For the second type of test, the specimens were subjected to several series of partially drained cyclic loading (see Fig. 5.4(b)). The aim of this study was to investigate how partially drained cyclic loading followed by drainage would influence the resistance of a normally consolidated clay specimen to later partially drained cyclic loading. The test condition is given in Table 5.2. The specimen of soft soil was subjected to a 5 Hz cyclic load of 15,000 cycles with a CSR of 0.6, followed by a rest period of 48 hours. This process was repeated again and followed by the last series of cyclic loading.

Table 5.2 Test condition for partially drained cyclic loading (with a rest period)

Specimen	σ_{1c}, kPa	σ_{3c}, kpa	Loading frequency (f), Hz	Cyclic stress ratio (CSR)	Loading cycles (N)	Failed?
D_{05}	40	24	1	0.6	15,000 cycles +rest period[a] +15,000 cycles +rest period[a] +15,000 cycles	No

[a]Rest period was two days.

For the third type of test a changing frequency rather than a constant frequency was used for the partially drained cyclic loading test (see Fig. 5.4(c)). The test condition is given in Table 5.3. The specimen was subjected to a 5 Hz cyclic load of 15,000 cycles, followed by a 10 Hz cyclic load of 15,000 cycles. For the purpose of comparison, a partially drained cyclic loading test under $f = 10$ Hz was conducted as well. The purpose of the two tests was to examine whether a very high frequency can be applied directly to a soft soil, and whether a method of applying a lower frequency followed by a higher frequency could be an alternative.

Table 5.3 Test condition for partially drained cyclic loading (with rest period)

Specimen	σ_{1c}, kPa	σ_{3c}, kpa	Loading frequency (f), Hz	Cyclic stress ratio (CSR)	Loading cycles (N)	Failed?
D_{06}	40	24	10	0.6	3,500	Yes
D_{07}	40	24	5 and 10	0.6	1,5000 cycles (5 Hz) +15,000 cycles (10 Hz)	No

5.5 Test results

5.5.1 Partially drained cyclic loading without a rest period

Some of the test results are given in Table 5.1. Only one specimen ($D_{0.4}$) with CSR = 0.8 failed at 3,024 cycles while it failed at only 1,794 cycles if radial drainage was not allowed during the cyclic loading. Other specimens D_{01} to D_{03} with lower values of cyclic stress ratio did not fail.

Detailed test results for partially drained cyclic loading without a rest period are given in Fig. 5.5 (a) to (d). For each loading condition the development of excess pore pressures against the number of cycles obtained from the four miniature pore pressure transducers is provided, along with the corresponding undrained curves. The details for specimen D_{04} are shown in Fig. 5.5 (d). As expected, the values of all the four pore pressure transducers were lower than the undrained value obtained from the undrained cyclic triaxial test described in Chapter 3. T1 has the lowest value as it has the shortest drainage path, followed by T2, T3, and T4. However, the sample failed after 3,024 cycles when a critical level of excess pore pressure of 0.68 was detected at T4. This indicates that more loading cycles can run before failure occurs at a high cyclic stress ratio with a centrally installed PVD.

For the stable specimens D_{01} to D_{03}, the patterns of excess pore pressures are quite similar to each other. For example, the excess pore pressure at all locations in D_{01} developed rapidly up to 4,000 cycles and then gradually increased at a lower rate of generation. The excess pore pressure response under undrained condition is the highest, followed by T4 which has the longest drainage path. The failure of specimen was not observed during the test.

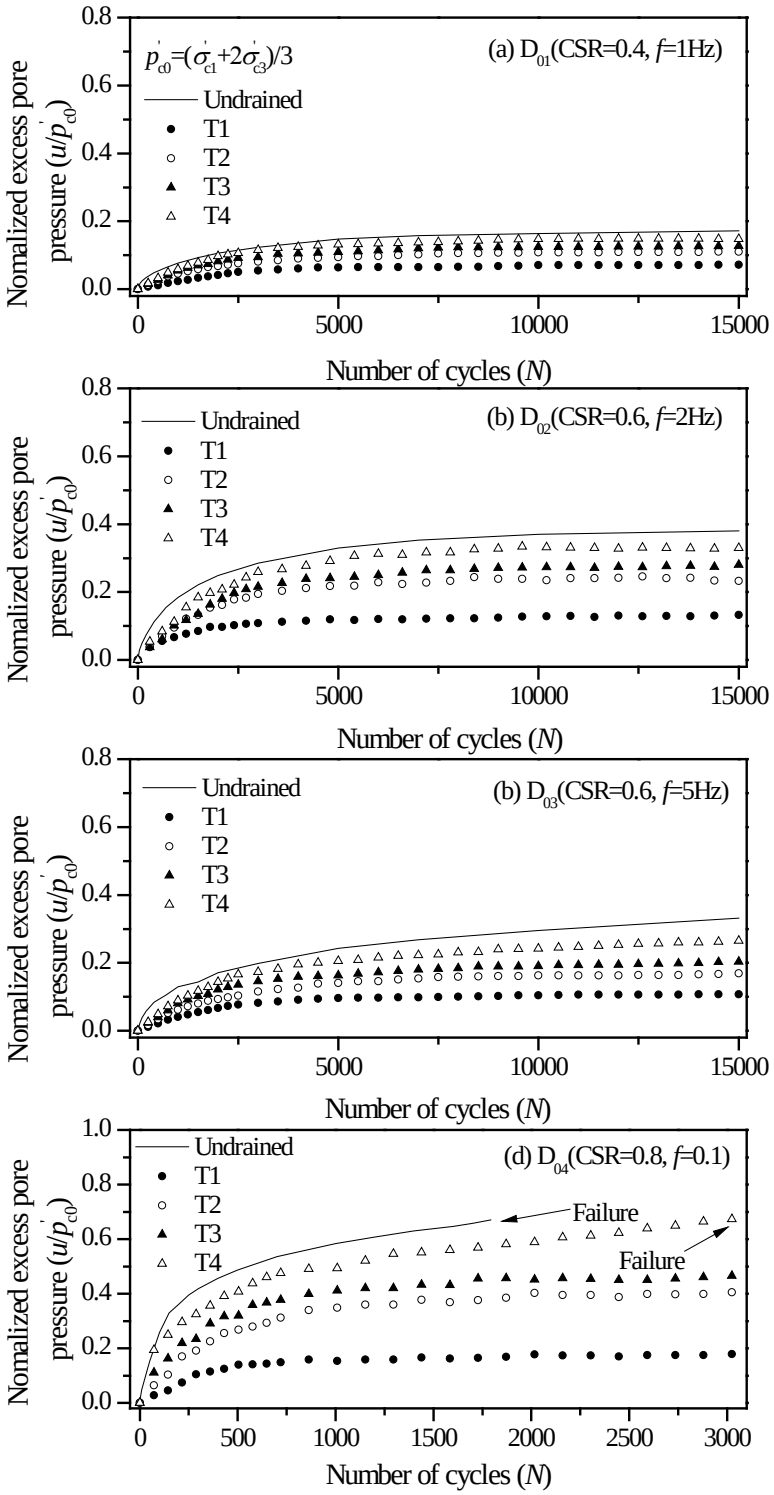

Fig. 5.5 Generation of excess pore pressures at different locations: (a) D_{01}, (b) D_{02}, (c) D_{03}, (d) D_{04}

If the excess pore pressures at the end of the tests for partially drained cyclic loading and undrained cyclic loading are compared, the ratio of excess pore pressures can be

determined at different locations (see Fig. 5.6). The ability of the PVD to prevent the development of excess pore pressure to high values is significant, as all the values are smaller than a unit. Furthermore, the dissipation of excess pore water pressure is more obvious closer to the PVD. When the drainage path is only 13% of the total drainage path, the ratio of excess pore pressure is reduced significantly from 1.0 to approximately 0.2 to 0.4. When the drainage paths become larger (i.e. x/r = 0.4 and 0.86), the excess pore water pressure reduced from 0.6 to 0.8.

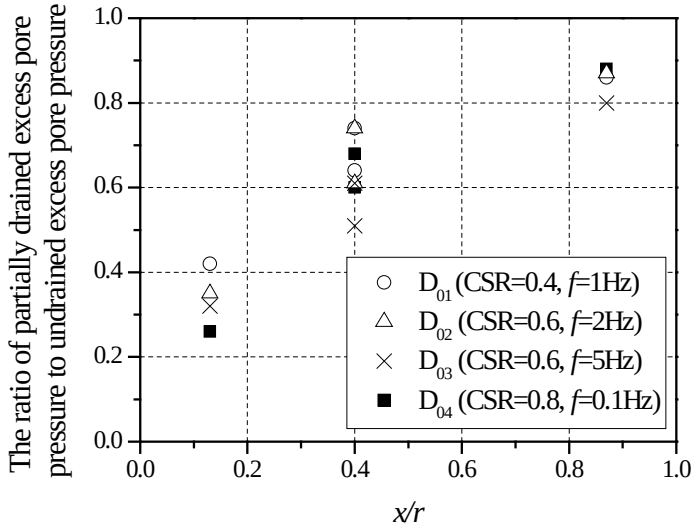

Fig. 5.6 The effectiveness of the drainage during cyclic loading (r = the radius of the specimen, and x = the radial distance from the prefabricated vertical drain)

5.5.2 Partially drained cyclic loading with rest period

The generation and dissipation of excess pore pressures for specimen D_{05} under partially drained cyclic loading with rest periods are given in Fig. 5.7. After the first 15,000 cycles of cyclic loading, the excess pore pressure ratio increased to 0.4 for T4 which is furthest from the drain, followed by 0.35 for T3, 0.3 for T3, and 0.2 for T1. The first rest period of 2 days was allowed for the excess pore pressure to dissipate. After the pore water flowed out of the specimen the excess pore pressure ratios decreased to 0.3, 0.25, 0.1, and 0.05 for T4, T3, T2, and T1 respectively.

Upon the application of the second 15,000 cycles of cyclic loading, the incremental excess pore pressure ratio due to the second set of cyclic shear decreased compared to the first set due to a decreased void ratio caused by the dissipation of excess pore pressure during and after the first set of cyclic loading. The increments in the excess pore pressure ratio were 0.25, 0.18, 0.15, and 0.08 for T4, T3, T2, and T1 respectively. However, with

the residual excess pore pressure, the accumulated excess pore pressure ratios after the second set of cyclic loading for T4 and T3 were higher than the values obtained after the first set, while the accumulated values for T2 and T1 were smaller compared to the first set. Then another rest period of 2 days was allowed for drainage, during which the void ratio decreased further due to the drainage of pore water. After the second rest period of two days, the last 15,000 cycles of cyclic loading was imposed on the specimen. The incremental excess pore pressure ratios were even smaller and the accumulated excess pore pressure ratios were smaller than those after the second application of cyclic loading for all the pore pressure transducers.

To summarise, the prefabricated vertical drains assist the dissipation of the excess pore pressures both during and after cyclic loading. A reduced void ratio due to the drainage of the pore water can prevent the generation of excess pore pressure in the following cyclic loading. After three sets of cyclic loading, the accumulated excess pore pressure began to reduce. This suggests that no substantial excess pore pressure will be observed if more sets of cyclic loading are applied. This study shows that drainage during cyclic loading provides dissipation of excess pore pressure and increases shear strength and therefore normally consolidated clays are more resistant to the following cyclic shear stress.

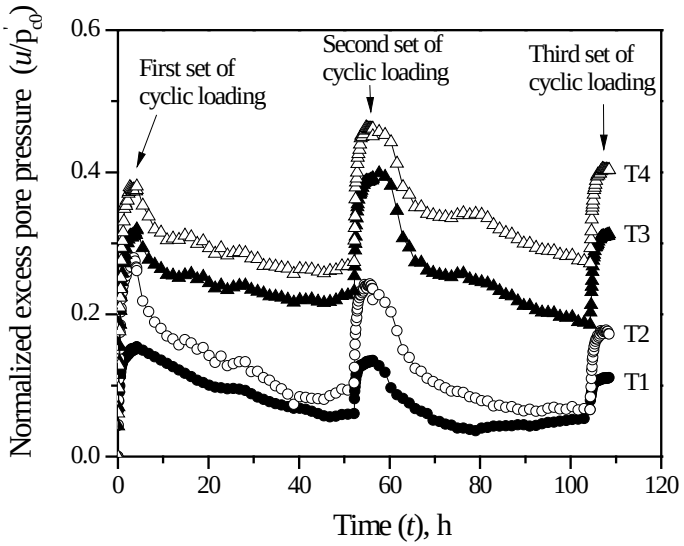

Fig. 5.7 Generation and dissipation of excess pore pressures of specimen D_{05} under partially drained cyclic loading with a rest period

5.5.3 Partially drained cyclic loading with a changing frequency

Some unexpected things happened to specimen D_{07} during the testing period and the test was manually stopped. As shown in Fig. 5.8, the settlement increased gradually in the first 200 cycles up to less than 1 mm, followed by a sharp increase that reached 10 mm. Then 100 cycles ran before another dramatic increase in settlement was observed. After the settlement reached a maximum value of 25 mm, it went back to 20 mm and remained relatively stable afterwards. The test was stopped anyway since the specimen was considered to have already failed in the first 500 cycles. This is probably because the effect of frequency is only negligible for the soft clay tested within the range from 0.1 to 5 Hz in this research work. When the loading frequency was increased to 10 Hz, the soil was too soft to stand this high speed load and consequently failed.

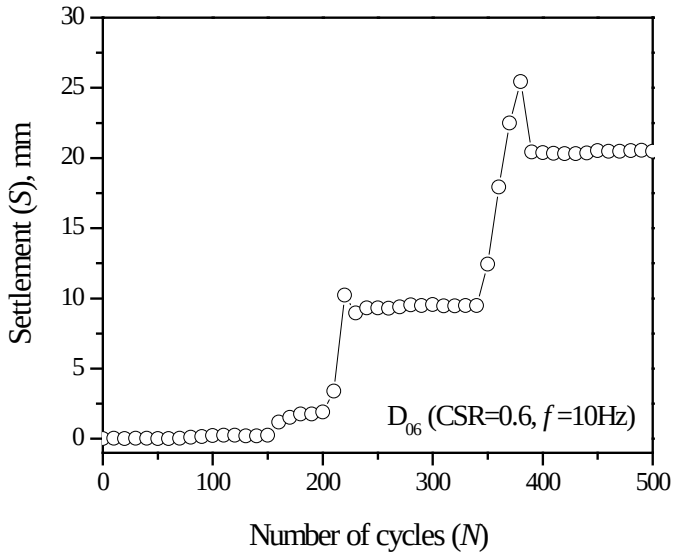

Fig. 5.8 Settlement of specimen D_{06}

The development of excess pore pressures for specimen D_{07} is shown in Fig. 5.9. Instead of applying a direct 10 Hz cyclic load the specimen was first subjected to a 5 Hz cyclic load for 15,000 cycles, followed by 15,000 cycles of cyclic loading under $f = 10$ Hz. The specimen did not fail and no significant settlement suddenly occurred at this time. It is hard to say whether this is because the soil was further consolidated or the soil structure had adjusted itself to the cyclic load before the 10 Hz cyclic load was applied, since there is a lack of data of undrained cyclic loading under $f = 5$ Hz followed by 10 Hz. However,

the test results clearly suggest that the train at lower speed is recommended for newly constructed railway.

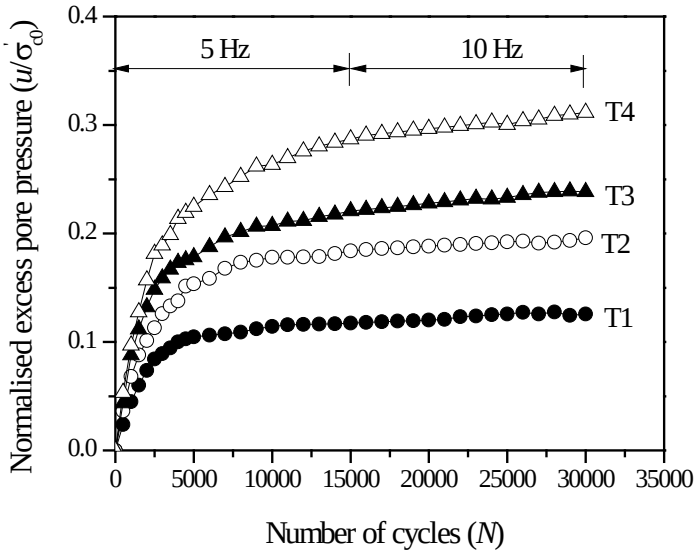

Fig. 5.9 Generation of excess pore pressure for specimen D_{07}

5.6 Conclusions

Partially drained cyclic triaxial tests were conducted on specimens of soft clay using the large scale cylindrical dynamic triaxial equipment designed and built at the University of Wollongong. To allow the dissipation of excess pore prsssure, a single PVD was installed in the centre of the soil cylinder.

The details of the preparation of the specimens and installation of the pore pressure transducers were presented first, and then the test conditions of partially drained cyclic triaxial were described and the test results analysed. The main conclusions are as follows:

- For the first series of test "cyclic loading without a rest period", it was found that the values of all the four pore pressure transducers were lower than the undrained value. T1 showed the lowest value as it had the shortest drainage path, followed by T2, T3, and T4. Only one specimen with a CSR of 0.8 failed at 3,024 cycles (The value was 1,794 if radial drainage was not allowed during the cyclic loading), while the failure of other specimens with a lower CSR was not observed.

- For the second type of test “cyclic loading with a rest period”, it has been found that the incremental excess pore pressure for each set of cyclic loading decreased due to a reduced void ratio caused by the dissipation of excess pore pressure during and after the previous cyclic loading. After three sets of cyclic loading, the accumulated excess pore pressure began to reduce, which suggested that no substantial excess pore pressure would be observed if more sets of cyclic loading were applied. This study showed that partially drained cyclic loading and drainage made normally consolidated clay more resistant to subsequent cyclic loading.

- For the last type of test “cyclic loading with a changing loading frequency”, it has been found that in order to avoid a failure which could occur at a high loading frequency, a cyclic load at a lower frequency could be applied first followed by a higher frequency. It is not clear whether this is because the soil was further consolidated or the soil structure had adjusted itself to the cyclic load before a high frequency cyclic load was applied. However, the test results clearly suggest that for newly constructed railway lines, the train at a lower speed is preferred.

6 Radial Consolidation Model under Cyclic Loading

6.1 Introduction

In this Chapter, a radial consolidation model under cyclic loading is proposed. This model combines the theory of radial consolidation with the undrained cyclic model presented in Chapter 4. When radial drainage is allowed during the application of cyclic load, the dissipation and generation of excess pore pressure occurs simultaneously. The determination of the latter determines how accurate the model can be. The existing model simply assumes that the generation of excess pore pressure is not influenced by the dissipation and stress history, but these effects are considered in this proposed model. To verify this model, the prediction is compared with the test results which are given earlier in Chapter 5. A good agreement is found between them.

6.2 Framework of the radial consolidation model under cyclic loading

6.2.1 Governing equation

For soils under cyclic loading and with radial drainage, excess pore pressure is generated at a reduced rate compared to undrained conditions. Therefore, the generation of excess pore pressure due to partially drained cyclic loading can be due to the combined effect of generated undrained excess pore pressure and dissipation. Based on this concept, a radial consolidation model under cyclic loading will be presented. The axi-symmetric soil cylinder adopted is shown in Fig. 6.1, here, r_w is the equivalent radius of the vertical drain, r_e is the radius of the influence zone, and l is the length of the drain.

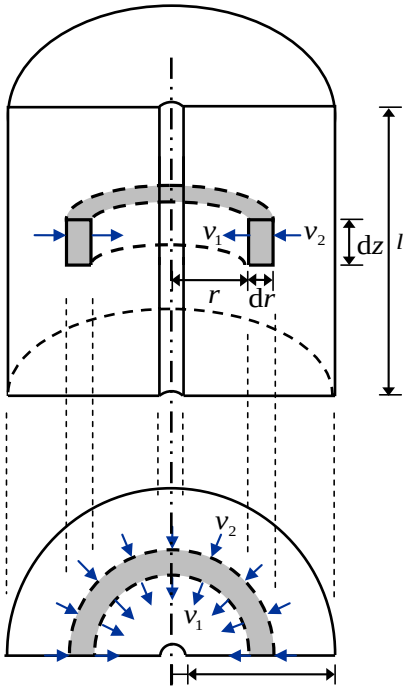

Fig. 6.1 Axi-symmetric soil cylinder (ideal drain)

The flow velocities at a radial distance r and $(r+\mathrm{d}r)$ are given by Darcy's law as:

$$v_1 = \frac{k_\mathrm{h}}{\gamma_\mathrm{w}} \frac{\partial u}{\partial r} \tag{6.1}$$

and

$$v_2 = \frac{k_\mathrm{h}}{\gamma_\mathrm{w}} \left(\frac{\partial u}{\partial r} + \frac{\partial^2 u}{\partial r^2} \mathrm{d}r \right) \tag{6.2}$$

The pore water flowing into and out of the hollow cylindrical slice with an internal radius of r, outer radius $(r+\mathrm{d}r)$, and thickness is:

$$\mathrm{d}Q_1 = -2\pi r \frac{k_\mathrm{h}}{\gamma_\mathrm{w}} \frac{\partial u}{\partial r} \mathrm{d}z\mathrm{d}t \tag{6.3}$$

and

$$\mathrm{d}Q_2 = -2\pi (r+\mathrm{d}r) \frac{k_\mathrm{h}}{\gamma_\mathrm{w}} \left(\frac{\partial u}{\partial r} + \frac{\partial^2 u}{\partial r^2} \mathrm{d}r \right) \mathrm{d}z\mathrm{d}t \tag{6.4}$$

The change in volume in this hollow cylindrical slice is:

$$\mathrm{d}Q = \mathrm{d}Q_1 - \mathrm{d}Q_2 = 2\pi r \frac{k_\mathrm{h}}{\gamma_\mathrm{w}} \frac{\partial^2 u}{\partial r^2} \mathrm{d}r\mathrm{d}z\mathrm{d}t + 2\pi \mathrm{d}r \frac{k_\mathrm{h}}{\gamma_\mathrm{w}} \left(\frac{\partial u}{\partial r} + \frac{\partial^2 u}{\partial r^2} \mathrm{d}r \right) \mathrm{d}z\mathrm{d}t \tag{6.5}$$

The change in volume can be expressed in terms of the change in the void ratio:

$$\mathrm{d}V = \left\lfloor \pi (r + \mathrm{d}r)^2 - \pi r^2 \right\rfloor \varepsilon_\mathrm{v} \mathrm{d}z \tag{6.6}$$

Then the condition of continuity can therefore be expressed as:

$$\mathrm{d}Q = -\mathrm{d}V \tag{6.7}$$

Therefore,

$$2\pi r \frac{k_\mathrm{h}}{\gamma_\mathrm{w}} \frac{\partial^2 u}{\partial r^2} \mathrm{d}r\mathrm{d}z\mathrm{d}t + 2\pi \mathrm{d}r \frac{k_\mathrm{h}}{\gamma_\mathrm{w}} \frac{\partial u}{\partial r} \mathrm{d}z\mathrm{d}t = -2\pi r \mathrm{d}r \varepsilon_\mathrm{v} \mathrm{d}z \tag{6.8}$$

or

$$\frac{k_\mathrm{h}}{\gamma_\mathrm{w}} \frac{\partial^2 u}{\partial r^2} \mathrm{d}t + \frac{k_\mathrm{h}}{\gamma_\mathrm{w}} \frac{1}{r} \frac{\partial u}{\partial r} \mathrm{d}t = -\varepsilon_\mathrm{v} \tag{6.9}$$

6.2.2 A procedure for evaluating excess pore pressure

The procedure for evaluating excess pore pressure in partially drained cyclic loading is demonstrated below (see Fig. 6.2): During the time interval $\mathrm{d}t = t_{i+1} - t_i$, excess pore pressure ($\mathrm{d}u_\mathrm{p}$) is induced due to cyclic shear stress. Assuming that the process of generating excess pore pressure, and its dissipation, traces along the *CDF*, then the excess pore pressure ($\mathrm{d}u + \mathrm{d}u_\mathrm{p}$) can be dissipated during the loading period $\mathrm{d}t$. Then the volumetric strain can be given by the following equation (Seed and Booker 1976):

$$\varepsilon_\mathrm{v} = -m_{\mathrm{vp'}} \left(\mathrm{d}u + \mathrm{d}u_\mathrm{p} \right) = -m_{\mathrm{vp'}} \frac{\partial u}{\partial t} \mathrm{d}t - m_{\mathrm{vp'}} \frac{\partial u_\mathrm{p}}{\partial t} \mathrm{d}t \tag{6.10}$$

where $m_{\mathrm{vp'}}$ which is the coefficient of compressibility in a triaxial condition.

Then the equation of radial consolidation under cyclic loading can be written as:

$$\frac{k_{\mathrm{h}}}{\gamma_{\mathrm{w}}}\frac{\partial^2 u}{\partial r^2}+\frac{k_{\mathrm{h}}}{\gamma_{\mathrm{w}}}\frac{1}{r}\frac{\partial u}{\partial r}=m_{\mathrm{vp'}}\frac{\partial u}{\partial t}+m_{\mathrm{vp'}}\frac{\partial u_{\mathrm{p}}}{\partial t} \tag{6.11}$$

or

$$\bar{c}_{\mathrm{h}}\left(\frac{\partial^2 u}{\partial r^2}+\frac{1}{r}\frac{\partial u}{\partial r}\right)=\frac{\partial u}{\partial t}+\frac{\partial u_{\mathrm{p}}}{\partial t} \tag{6.12}$$

where $\bar{c}_h=\dfrac{k_{\mathrm{h}}}{\gamma_{\mathrm{w}}m_{\mathrm{vp'}}}$ is the coefficient of consolidation during partially drained cyclic loading.

This way of evaluating $\mathrm{d}u_{\mathrm{p}}$ was proposed earlier by Sakai et al. (2003) , where for simplicity, it was assumed that the change in excess pore pressure generated during partially drained cyclic loading was the same as during undrained cyclic loading ($\mathrm{d}u_{\mathrm{p}}=\mathrm{d}u_{\mathrm{u}}$). However, the magnitude of excess pore pressure generated during partially drained cyclic loading, which is affected by the stress history and dissipation of excess pore pressure, would differ from that obtained from undrained cyclic loading, i.e. $\mathrm{d}u_{\mathrm{p}}\neq\mathrm{d}u_{\mathrm{u}}$. For example, in Fig. 6.2, one experiences undrained cyclic loading from o to B with no change in volume while the other experiences partially drained cyclic loading from o to C with a reduced void ratio. It has been recognised that less excess pore pressure can be generated due to a reduced void ratio, therefore, if identical cycles of undrained cyclic loading are applied afterwards, the generation of excess pore pressure under partially drained cyclic loading should be less than under undrained cyclic loading, $\mathrm{d}u_{\mathrm{p}}\leq\mathrm{d}u_{\mathrm{u}}$. For the model proposed in this paper, $\mathrm{d}u_{\mathrm{p}}$ was obtained from partially drained cyclic loading rather than undrained cyclic loading.

The other limitation of Sakai et al. (2003) was the number of cycles which the model could handle. For example, if the soil failed at point G at time t_{f}, it would be impossible to use $\mathrm{d}u_{\mathrm{u}}$ to predict the excess pore pressure caused by partially drained cyclic loading afterwards, however by using the proposed procedure, $\mathrm{d}u_{\mathrm{p}}$ can be determined as long as the soil does not fail during partially drained cyclic loading.

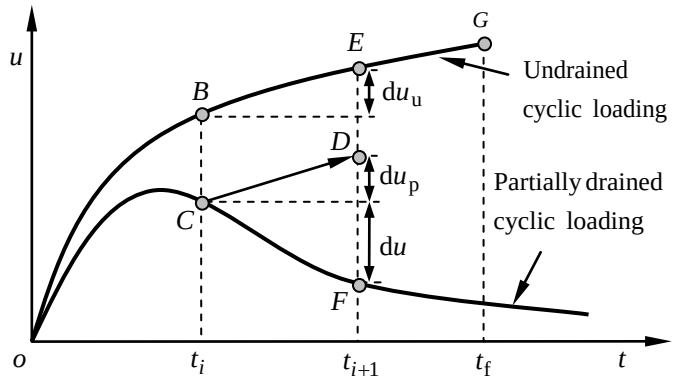

Fig. 6.2 A procedure for evaluating the performance of soils under partially drained cyclic loading with radial drainage

6.2.3 Stress paths

Once the generation of excess pore pressure ($\mathrm{d}u_\mathrm{p}$) was obtained, the build up of excess pore pressure in partially drained cyclic loading conditions can be calculated. The stress path for the soil element under partially drained cyclic loading is shown in Fig. 6.3. $p'_{\mathrm{cl},i}$ (i=1, 2……, n) is the yield stress after the loading part of each cycle, $p'_{\mathrm{cu},i}$ (i=1, 2……, n) is the yield stress after the unloading part of each cycle, and $p'_{\mathrm{y},i}$ (i=1, 2……, n) is the loading parameter after each cycle. When the soil element starts from point A' to point A during the first loading period, the effective mean stress decreases and $p'_{\mathrm{cl},1} = p'_A + \left(q_A / M\right)^2 p'_A$ is the yield stress corresponding to point A. During the following unloading period, the stress path travels from point A to point A^*, the effective mean stress increases and $p'_{\mathrm{y},1}$ is the loading parameter corresponding to point A^*. Then the yield stress for the second cycle can be calculated as $p'_{\mathrm{cu},1} = p'_{\mathrm{cl},1}\left(p'_{\mathrm{y},1} / p'_{\mathrm{cl},1}\right)^{\theta^*}$. For the second cycle the stress path travels from point A^* to point B' and the effective mean stress increases when the soil element behaves elastically ($q < q_{\mathrm{yielding}}$, $q_{\mathrm{yielding}} = \sqrt{\left(p'_{\mathrm{cu},1} - p'_{\mathrm{y},1}\right) M^2 p'_{\mathrm{y},1}}$). Afterwards, the stress path moves from point B' to point B ($q_{\mathrm{yielding}} < q < q_{\mathrm{cyc}}$) with a decrease in the effective mean stress.

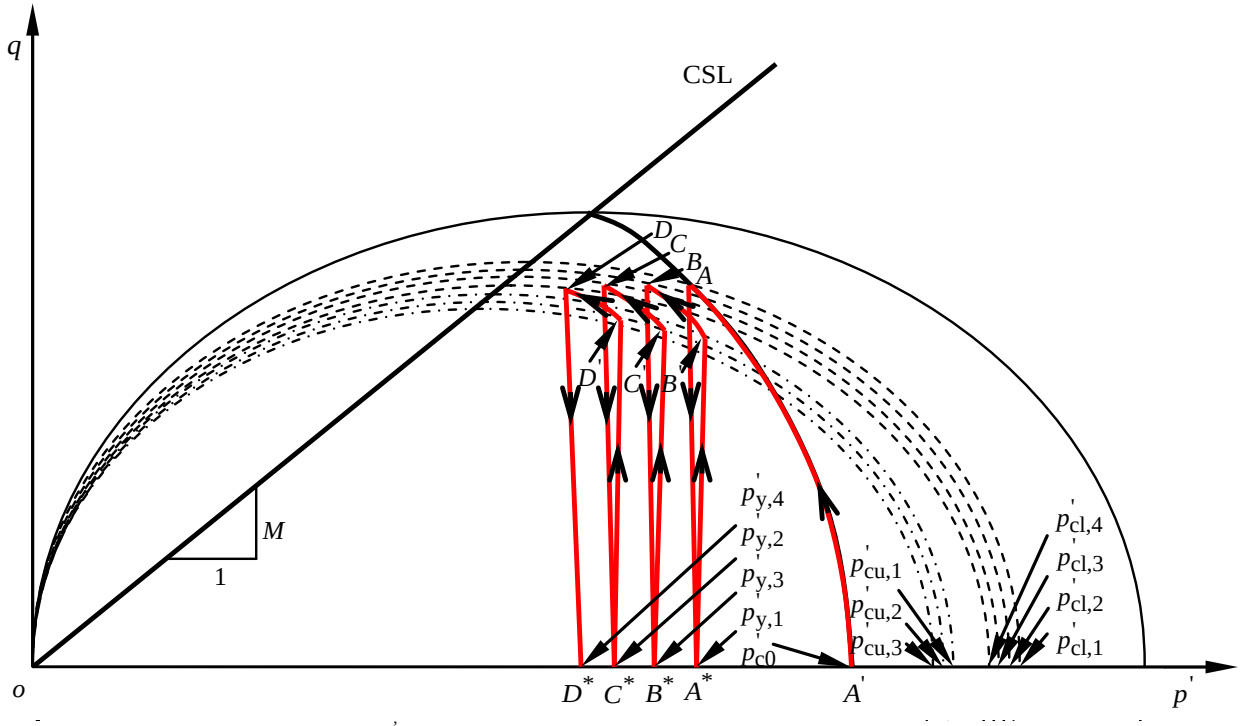

Fig. 6.3 Stress path in p'-q space for soil element under partially drained cyclic loading

6.2.4 Finite difference method

A schematic is given in Fig. 6.4 to show how the finite difference method is conducted.

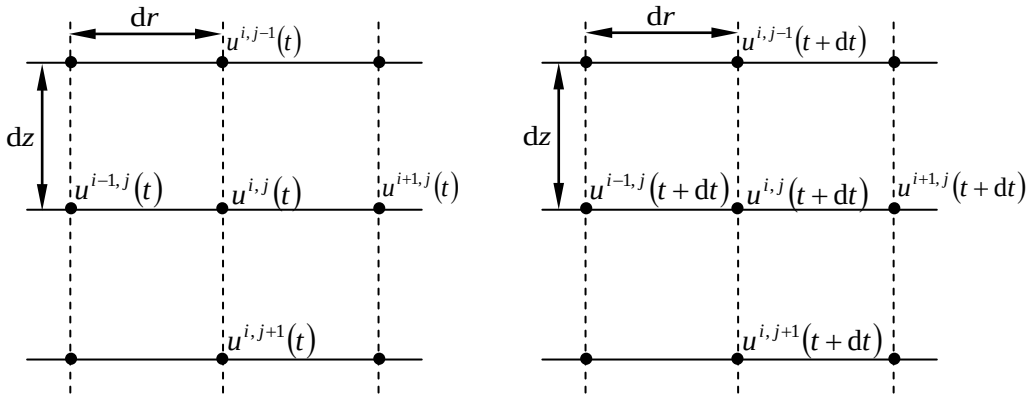

(a) (b)

Fig. 6.4 The finite difference method for combined vertical and radial drainage: (a) Excess pore pressure at time t, (b) Excess pore pressure at time $t+\Delta t$

For combined vertical and radial flow in a unit soil cylinder, the average rate of change of excess pore pressure over the time period is given below:

$$\begin{aligned}\frac{u^{i,j}(t+\mathrm{d}t)-u^{i,j}(t)}{\mathrm{d}t} = c_{\mathrm{h}}&\left[\begin{array}{l}\frac{1}{2}\left(\frac{u^{i-1,j}(t+\mathrm{d}t)-2u^{i,j}(t+\mathrm{d}t)+u^{i+1,j}(t+\mathrm{d}t)}{\mathrm{d}r^2}\right)\\ +\frac{1}{2}\left(\frac{u^{i-1,j}(t)-2u^{i,j}(t)+u^{i+1,j}(t)}{\mathrm{d}r^2}\right)\\ +\frac{1}{2}\frac{1}{i\mathrm{d}r}\frac{\left(u^{i+1,j}(t+\mathrm{d}t)-u^{i-1,j}(t+\mathrm{d}t)\right)}{2\mathrm{d}r}\\ +\frac{1}{2}\frac{1}{i\mathrm{d}r}\frac{\left(u^{i+1,j}(t)-u^{i-1,j}(t)\right)}{2\mathrm{d}r}\end{array}\right]\\ &+c_{\mathrm{v}}\left[\begin{array}{l}\frac{1}{2}\left(\frac{u^{i,j-1}(t+\mathrm{d}t)-2u^{i,j}(t+\mathrm{d}t)+u^{i,j+1}(t+\mathrm{d}t)}{\mathrm{d}z^2}\right)\\ +\frac{1}{2}\left(\frac{u^{i,j-1}(t)-2u^{i,j}(t)+u^{i,j+1}(t)}{\mathrm{d}z^2}\right)\end{array}\right]\\ &+\frac{u(t+\mathrm{d}t)-u(t)}{\mathrm{d}t}\end{aligned} \tag{6.13}$$

Then the excess pore pressure at time $(t+\mathrm{d}t)$ can be given by:

$$\begin{aligned} u^{i,j}(t+\mathrm{d}t) = u^{i,j}(t) &+ \mathrm{d}t c_h \left[\begin{array}{l} \frac{1}{2}\left(\frac{u^{i-1,j}(t+\mathrm{d}t) - 2u^{i,j}(t+\mathrm{d}t) + u^{i+1,j}(t+\mathrm{d}t)}{\mathrm{d}r^2} \right) \\ + \frac{1}{2}\left(\frac{u^{i-1,j}(t) - 2u^{i,j}(t) + u^{i+1,j}(t)}{\mathrm{d}r^2} \right) \\ + \frac{1}{2}\frac{1}{i\mathrm{d}r}\frac{\left(u^{i+1,j}(t+\mathrm{d}t) - u^{i-1,j}(t+\mathrm{d}t)\right)}{2\mathrm{d}r} \\ + \frac{1}{2}\frac{1}{i\mathrm{d}r}\frac{\left(u^{i+1,j}(t) - u^{i-1,j}(t)\right)}{2\mathrm{d}r} \end{array} \right] \\ &+ \mathrm{d}t c_v \left[\begin{array}{l} \frac{1}{2}\left(\frac{u^{i,j-1}(t+\mathrm{d}t) - 2u^{i,j}(t+\mathrm{d}t) + u^{i,j+1}(t+\mathrm{d}t)}{\mathrm{d}z^2} \right) \\ + \frac{1}{2}\left(\frac{u^{i,j-1}(t) - 2u^{i,j}(t) + u^{i,j+1}(t)}{\mathrm{d}z^2} \right) \end{array} \right] \\ &+ \left[u(t+\mathrm{d}t) - u(t)\right] \end{aligned} \tag{6.14}$$

After rearrangement,

$$\begin{aligned} u^{i,j}(t+\mathrm{d}t) = (1-\lambda_h-\lambda_z)u^{i,j}(t) &+ \frac{\lambda_h}{2}\left[\begin{array}{l} \left(1-\frac{1}{2i}\right)\left(u^{i-1,j}(t) + u^{i-1,j}(t+\mathrm{d}t)\right) \\ + \left(1+\frac{1}{2i}\right)\left(u^{i+1,j}(t) + u^{i+1,j}(t+\mathrm{d}t)\right) \end{array} \right] \\ &+ \frac{\lambda_z}{2}\left[\begin{array}{l} u^{i,j-1}(t) + u^{i,j-1}(t+\mathrm{d}t) \\ + u^{i,j+1}(t) + u^{i,j+1}(t+\mathrm{d}t) \end{array} \right] \\ &- (\lambda_h+\lambda_z)u^{i,j}(t+\mathrm{d}t) + \left[u(t+\mathrm{d}t) - u(t)\right] \end{aligned} \tag{6.15}$$

After rearrangement:

$$\begin{aligned} u^{i,j}(t+\mathrm{d}t) = &\frac{(1-\lambda_h-\lambda_z)}{1+\lambda_h+\lambda_z}u^{i,j}(t) \\ &+ \frac{\lambda_h}{2(1+\lambda_h+\lambda_z)}\left[\begin{array}{l} \left(1-\frac{1}{2i}\right)\left(u^{i-1,j}(t) + u^{i-1,j}(t+\mathrm{d}t)\right) \\ + \left(1+\frac{1}{2i}\right)\left(u^{i+1,j}(t) + u^{i+1,j}(t+\mathrm{d}t)\right) \end{array} \right] \\ &+ \frac{\lambda_z}{2(1+\lambda_h+\lambda_z)}\left[u^{i,j-1}(t) + u^{i,j-1}(t+\mathrm{d}t) + u^{i,j+1}(t) + u^{i,j+1}(t+\mathrm{d}t)\right] \\ &+ \frac{1}{1+\lambda_h+\lambda_z}\left[u(t+\mathrm{d}t) - u(t)\right] \end{aligned} \tag{6.16}$$

where $\lambda_{\mathrm{h}} = \dfrac{c_{\mathrm{h}}\mathrm{d}t}{\mathrm{d}r^2}$

$$\lambda_z = \frac{c_{\mathrm{v}}\mathrm{d}t}{\mathrm{d}z^2}$$

For a vertical flow only ($\lambda_h = 0$), the following equation can be obtained:

$$\begin{aligned} u^j(t+\mathrm{d}t) = {} & \frac{(1-\lambda_z)}{1+\lambda_z}u^j(t) + \frac{\lambda_z}{2(1+\lambda_z)}\begin{bmatrix} u^{j-1}(t)+u^{j-1}(t+\mathrm{d}t) \\ +u^{j+1}(t)+u^{j+1}(t+\mathrm{d}t) \end{bmatrix} \\ & + \frac{1}{1+\lambda_z}\left[u(t+\mathrm{d}t)-u(t)\right] \end{aligned} \tag{6.17}$$

For a vertical flow only ($\lambda_z = 0$), the following equation can be obtained:

$$\begin{aligned} u^i(t+\mathrm{d}t) = {} & \frac{(1-\lambda_h)}{1+\lambda_h}u^i(t) + \frac{\lambda_h}{2(1+\lambda_h)}\begin{bmatrix} \left(1-\dfrac{1}{2i}\right)\left(u^{i-1}(t)+u^{i-1}(t+\mathrm{d}t)\right) \\ +\left(1+\dfrac{1}{2i}\right)\left(u^{i+1}(t)+u^{i+1}(t+\mathrm{d}t)\right) \end{bmatrix} \\ & + \frac{1}{1+\lambda_h}\left[u(t+\mathrm{d}t)-u(t)\right] \end{aligned} \tag{6.18}$$

6.2.5 The calculation of time interval d*t* *for each loading step* d*q*

6.2.5.1 The first half of the first cycle

The cyclic stress for the first half of the first cycle is given in Fig. 6.5 to calculate the time interval dt for each loading step dq.

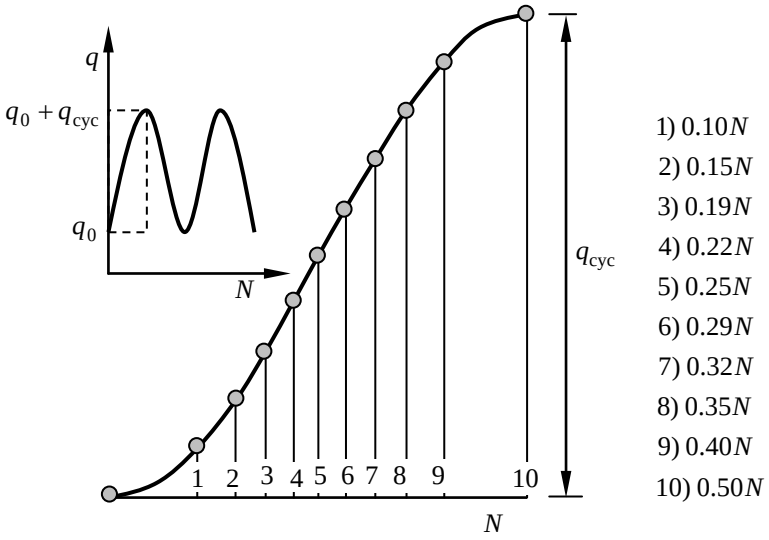

Fig. 6.5 The calculation of the time interval for the first half of the first cycle

The deviator stress (q_i) can be expressed by:

$$q_i = q_0 + \frac{q_{cyc}}{2}\left(1 + \sin\left(\omega t_i - \frac{\pi}{2}\right)\right) \tag{6.19}$$

where ω is the angular velocity which can be expressed by:

$$\omega = 2\pi f \tag{6.20}$$

where f is the loading frequency which can be expressed by:

$$f = \frac{1}{T} \tag{6.21}$$

where T is the period for each cycle.

If q_{cyc} is divided into a number of equal increments (say n), then the deviator stress (q_i) can also be expressed by:

$$q_i = q_0 + i\frac{q_{cyc}}{n} \tag{6.22}$$

Then the following equation can be obtained:

$$t_i = \frac{\arcsin\left(i\frac{2}{n}-1\right)+\frac{\pi}{2}}{2\pi}T, \quad 1 \le i \le n \tag{6.23}$$

Then the number of cycles (N_i) corresponding to the deviator stress q_i can be obtained by:

$$N_i = \frac{\arcsin\left(i\frac{2}{n}-1\right)+\frac{\pi}{2}}{2\pi}, \quad 1 \le i \le n \tag{6.24}$$

Then the time interval $\mathrm{d}t_{i+1}$ corresponding to each incremental deviator stress ($\mathrm{d}q_{i+1}$) can be calculated by:

$$\mathrm{d}t_{i+1} = t_{i+1} - t_i = \frac{\left[\arcsin\left((i+1)\frac{2}{n}-1\right)-\arcsin\left(i\frac{2}{n}-1\right)\right]}{2\pi}T, \quad 1 \le i \le n \tag{6.25}$$

6.2.5.2 The first half of the following cycles:

The cyclic stress for the first half of the following cycles is given in Fig. 6.6 to calculate the time interval $\mathrm{d}t$ for each loading step $\mathrm{d}q$.

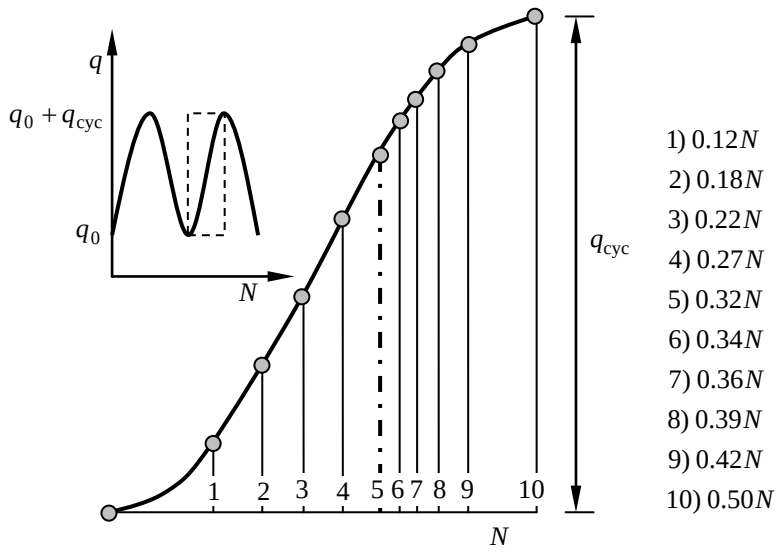

Fig. 6.6 The calculation of the time interval for the first half of the following cycle

Since the soil behaves elastically first, and then plastically, q_{cyc} is divided into two parts: $q_{\text{yielding}} - q_0$ and $q_{\text{cyc}} - \left(q_{\text{yielding}} - q_0\right)$.

- For $q_i \le q_{\text{yielding}}$

  If $q_{\text{yielding}} - q_0$ is divided into a number of equal increments (say n_1), then the deviator stress (q_i) can also be expressed by:

$$q_i = q_0 + i\frac{q_{\text{yielding}} - q_0}{n_1}, \quad 1 \le i \le n_1 \tag{6.26}$$

  Then the following equation can be obtained:

$$t_i = \frac{\arcsin\left(i\dfrac{2\left(q_{\text{yielding}} - q_0\right)}{n_1 q_{\text{cyc}}} - 1\right) + \dfrac{\pi}{2}}{2\pi} T, \quad 1 \le i \le n_1 \tag{6.27}$$

Then the number of cycles (N_i) corresponding to the deviator stress (q_i) can be obtained by:

$$N_i = \frac{\arcsin\left(i\frac{2\left(q_{\text{yielding}} - q_0\right)}{n_1 q_{\text{cyc}}} - 1 \right) + \frac{\pi}{2}}{2\pi}, \quad 1 \le i \le n_1 \tag{6.28}$$

Then the time interval ($\mathrm{d}t_{i+1}$) corresponding to each incremental deviator stress ($\mathrm{d}q_{i+1}$) can be calculated by:

$$\begin{aligned} \Delta t_{i+1} &= t_{i+1} - t_i \\ &= \frac{\left[\begin{array}{l} \arcsin\left((i+1)\frac{2\left(q_{\text{yielding}} - q_0\right)}{n_1 q_{\text{cyc}}} - 1 \right) \\ -\arcsin\left(i\frac{2\left(q_{\text{yielding}} - q_0\right)}{n_1 q_{\text{cyc}}} - 1 \right) \end{array} \right]}{2\pi} T, \quad 1 \le i \le n \end{aligned} \tag{6.29}$$

- For $q_{i+n_1} \ge q_{\text{yielding}}$

  If $q_{\text{cyc}} - \left(q_{\text{yielding}} - q_0\right)$ is divided into a number of equal increments (say n_2), then the deviator stress (q_{i+n_1}) can also be expressed by:

$$q_{i+n_1} = q_{\text{yielding}} + i\frac{q_{\text{cyc}-}\left(q_{\text{yielding}} - q_0\right)}{n_2}, \quad 1 \le i \le n_2 \tag{6.30}$$

Then the following equation can be obtained:

$$t_{i+n_1} = \frac{\arcsin\left(\frac{2\left(n_2 - i\right)\left(q_{\text{yielding}} - q_0\right)}{n_2 q_{\text{cyc}}} + \frac{2i}{n_2} - 1 \right) + \frac{\pi}{2}}{2\pi} T, \quad 1 \le i \le n_2 \tag{6.31}$$

Then the number of cycles (N_{i+n_1}) corresponding to the deviator stress (q_{i+n_1})can be obtained by:

$$N_{i+n_1} = \frac{\arcsin\left(2\frac{\left(n_2 - i\right)\left(\mathrm{q}_{\text{yielding}} - q_0\right)}{n_2 q_{\text{cyc}}} + \frac{2i}{n_2} - 1 \right) + \frac{\pi}{2}}{2\pi}, \quad 1 \le i \le n_2 \tag{6.32}$$

Then the time interval ($\mathrm{d}t_{i+1+n_1}$) corresponding to each incremental deviator stress ($\mathrm{d}q_{i+1+n_1}$) can be calculated:

$$\begin{aligned}\Delta t_{i+1+n_1} &= t_{i+1+n_1} - t_{i+n_1} \\ &= \frac{\arcsin\left(\dfrac{2\left(n_2-(i+1)\right)\left(q_{\text{yielding}}-q_0\right)}{n_2 q_{\text{cyc}}}+\dfrac{2(i+1)}{n_2}-1\right)}{2\pi}T \\ &\quad -\frac{\arcsin\left(\dfrac{2\left(n_2-i\right)\left(q_{\text{yielding}}-q_0\right)}{n_2 q_{\text{cyc}}}+\dfrac{2i}{n_2}-1\right)}{2\pi}T,\quad 1\le i\le n_2\end{aligned} \tag{6.33}$$

There is an example given in Table 6.1, where for the first half of the first cycle, q_{cyc} is divided evenly into ten parts ($n=10$) and for the first half of the following cycle, $\left(q_{\text{yielding}}-q_0\right)$ which is 70% of q_{cyc} is divided evenly into five parts ($n_1=5$) and $\left(q_{\text{cyc}}-\left(q_{\text{yielding}}-q_0\right)\right)$ which is 30% of q_{cyc} is divided evenly into five parts ($n_2=5$). The number of cycles (N) corresponding to the deviator stress (q), for the first half of the first and second cycle, are also shown in Fig. 6.5 and Fig. 6.6 respectively.

Table 6.1 Relationship between the number of cycles (N) corresponding to the deviator stress (q)

The first half of the first cycle		The first half of the following cycle	
q	N	q	N
$q_0+10\%\times q_{\text{cyc}}$	0.10	$q_0+20\%\times\left(q_{\text{yielding}}-q_0\right)$	0.12
$q_0+20\%\times q_{\text{cyc}}$	0.15	$q_0+40\%\times\left(q_{\text{yielding}}-q_0\right)$	0.18
$q_0+30\%\times q_{\text{cyc}}$	0.19	$q_0+60\%\times\left(q_{\text{yielding}}-q_0\right)$	0.22
$q_0+40\%\times q_{\text{cyc}}$	0.22	$q_0+80\%\times\left(q_{\text{yielding}}-q_0\right)$	0.27
$q_0+50\%\times q_{\text{cyc}}$	0.25	$q_0+100\%\times\left(q_{\text{yielding}}-q_0\right)$	0.32
$q_0+60\%\times q_{\text{cyc}}$	0.29	$q_{\text{yielding}}+20\%\times\left(q_{\text{cyc}}-\left(q_{\text{yielding}}-q_0\right)\right)$	0.34
$q_0+70\%\times q_{\text{cyc}}$	0.32	$q_{\text{yielding}}+40\%\times\left(q_{\text{cyc}}-\left(q_{\text{yielding}}-q_0\right)\right)$	0.36
$q_0+80\%\times q_{\text{cyc}}$	0.35	$q_{\text{yielding}}+60\%\times\left(q_{\text{cyc}}-\left(q_{\text{yielding}}-q_0\right)\right)$	0.39
$q_0+90\%\times q_{\text{cyc}}$	0.40	$q_{\text{yielding}}+80\%\times\left(q_{\text{cyc}}-\left(q_{\text{yielding}}-q_0\right)\right)$	0.42
$q_0+100\%\times q_{\text{cyc}}$	0.50	$q_{\text{yielding}}+100\%\times\left(q_{\text{cyc}}-\left(q_{\text{yielding}}-q_0\right)\right)$	0.50

6.2.6 Computational procedures

The procedure for calculating excess pore pressure under cyclic loading with radial drainage is summarised in Fig. 6.7. The detailed procedure is as follows.

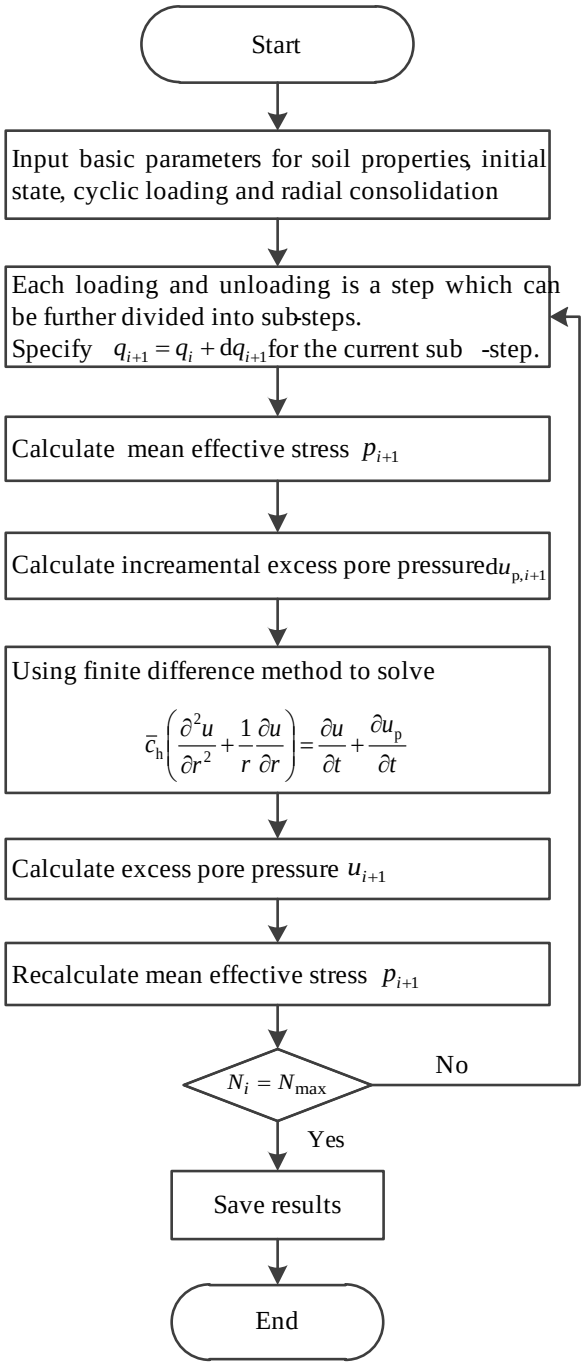

Fig. 6.7 The procedure of calculation

6.2.6.1 Establish parameters for the proposed model

It should be noted that ideal conditions (no smear and no well-resistance) are assumed in the analysis in this section. Except for the parameters for the soil properties (λ, κ, M, G, and $p_{c0}^{'}$), the initial soil state ($p_0^{'}$, $q_0^{'}$, and v_0), and cyclic loading (q_{cyc}, f, ξ_1, and ξ_2), which have been mentioned for the proposed undrained cyclic model, additional parameters for radial consolidation and finite difference method are required to predict the behavior of soft clays.

- Establish the parameters for radial consolidation (PVD):
  - Equivalent radius of PVD (r_w)
  - Radius of influence zone (r_e)
  - Coefficient of consolidation in a horizontal direction under cyclic loading ($\bar{c}_h$)
- Finite difference method:
  - Number of horizontal parts in which the radius of influence is divided into (n_r)
  - The length of each part ($dr = r_e / n_r$)
  - The time interval (dt)
  - Radial consolidation parameter ($\lambda_h = (\bar{c}_h dt)/dr^2$)

6.2.6.2 Calculation procedures

Each loading and unloading can be deemed to be a step which can be further divided into sub-steps, e.g., q_{cyc} can be divided into a number of increments (say n), where each step has an incremental deviator stress (dq_i) (i =1, 2, 3… n). The detailed procedures for calculating the excess pore pressure are given below:

- Calculate the deviator stress q_{i+1} and $p_{i+1}^{'}$ in the $(i+1)th$ step
- Calculate the generation of excess pore water pressure $du_{p,i+1}$ during the time interval dt_{i+1}:

$$du_{p,i+1} = \left(p_i^{'} - p_{i+1}^{'}\right) + \frac{dq_{i+1}}{3} \tag{6.34}$$

- The finite difference method has been used to incorporate the generation of excess pore water pressure $\mathrm{d}u_{p,i+1}$ into the radial consolidation. The excess pore water pressure at different locations $u^{*}_{j+1,i+1}$ after the $(i+1)th$ step when $(\mathrm{d}u+\mathrm{d}u_{\mathrm{p}})$ is dissipated can be calculated as:

$$u^{*}_{j+1,i+1}=\frac{1-\lambda_{h,i+1}}{1+\lambda_{h,i+1}}u^{*}_{j+1,i}+\frac{\lambda_{h,i+1}}{2(1+\lambda_{h,i+1})}\left[\begin{array}{l}\left(1-\frac{1}{2j}\right)\left(u^{*}_{j,i}+u^{*}_{j,i+1}\right)\\+\left(1+\frac{1}{2j}\right)\left(u^{*}_{j+2,i}+u^{*}_{j+2,i+1}\right)\end{array}\right]+\frac{1}{1+\lambda_{h+1}}\left(p_i^{'}-p_{i+1}^{'}+\frac{\mathrm{d}q_{\mathrm{i+1}}}{3}\right),\quad r_w/\mathrm{d}r\le j\le n_r \tag{6.35}$$

The boundary conditions are:

$$u_{j,i}=0,\quad r_w/\mathrm{d}r+1\le j\le n_r+1,\quad i=1 \tag{6.36}$$

$$u_{j,i}=0,\quad j=r_w/\mathrm{d}r+1,\quad 1\le i\le n \tag{6.37}$$

- The average excess pore pressure after the $(i+1)th$ step can be given by:

$$u_{i+1}=\sum_{j=r_w/\mathrm{d}_r+1}^{n_r}\frac{2\frac{\left(u_{j,i+1}+u_{j+1,i+1}\right)}{2}\mathrm{d}r\times\left((j-1)\mathrm{d}r+j\mathrm{d}r\right)}{2\left(r_e^{2}-r_w^{2}\right)},\quad r_{\mathrm{w}}/\mathrm{d}r\le j\le n \tag{6.38}$$

- Then the effective mean stress ($p_{i+1}^{'}$) can be recalculated by:

$$p_{i+1}^{'}=p_i^{'}+\left(u_i-u_{i+1}\right)+\frac{\mathrm{d}q_{i+1}}{3} \tag{6.39}$$

6.3 Model verification

The normalized excess pore pressures predicted in the partially drained cyclic loading tests, with and without a rest period, are given in Fig. 6.8 and Fig. 6.9, respectively. The recorded values of two transducers are provided along with the values predicted for each test condition. The basic soil properties used in the following analysis are: $\lambda=0.17$, $\kappa=0.04$, $M=1.87$, $p_{\mathrm{c0}}^{'}=30$ kPa, $p_0^{'}=30$ kPa, $q_0=16$ kPa, $e_0=1.32$, $r_{\mathrm{e}}=0.15$ m,

$r_w = 0.01\text{m}$, $G = 1.24\,\text{MPa}$, and $\bar{c}_h = 9.46\,\text{m}^2/\text{year}$. It can be seen that acceptable agreement was achieved between the test data and predictions. This study clearly suggests that under cyclic loading conditions such as high speed rail, the failure of soft subgrade soil can be prevented by the use of vertical drains.

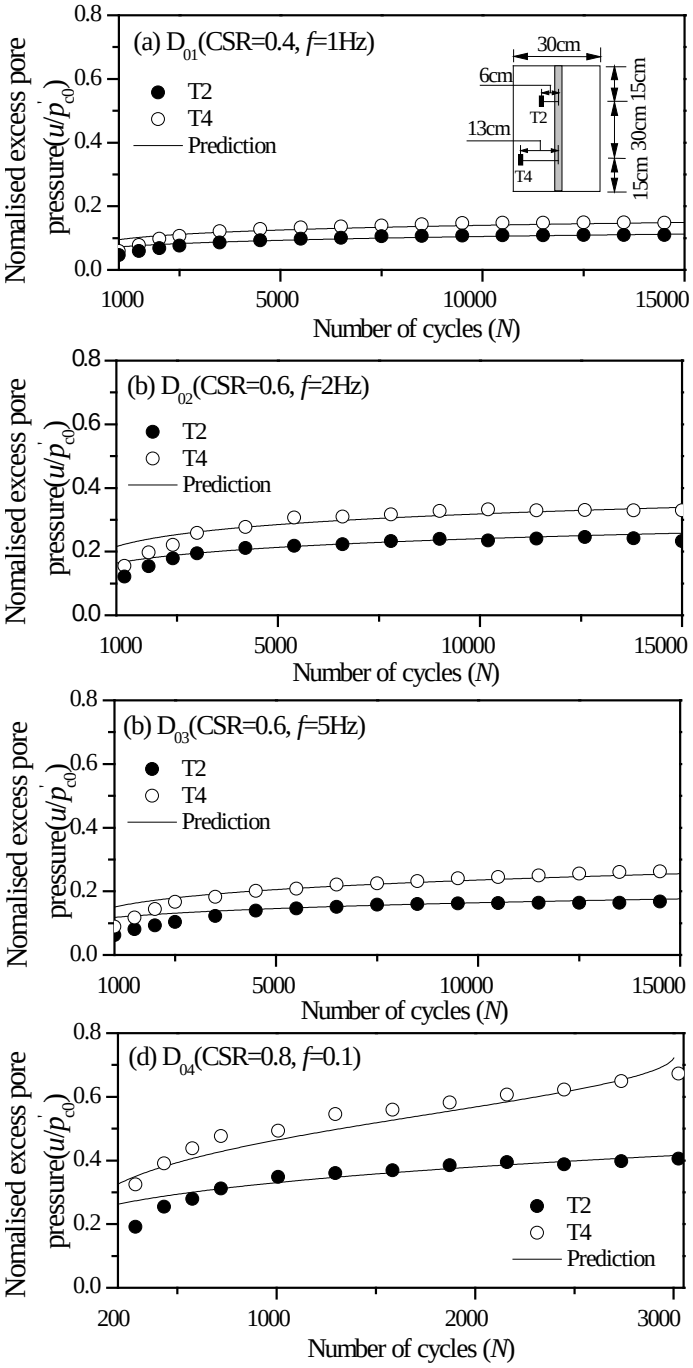

Fig. 6.8 Prediction of the proposed model for partially drained cyclic loading test without a rest period

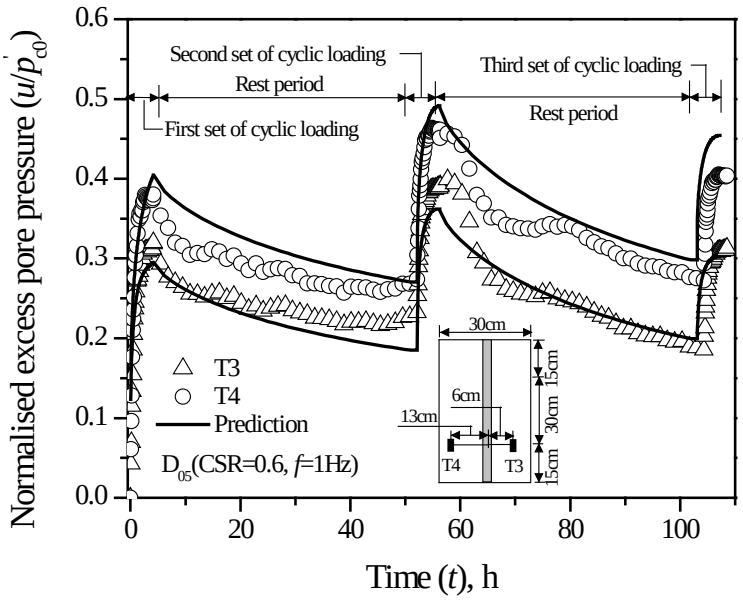

Fig. 6.9 Prediction of the proposed model for partially drained cyclic loading test with a changing loading frequency

6.4 Analysis of the model of radial consolidation under cyclic loading

In this section the effects of the cyclic stress ratio, coefficient of consolidation, and cyclic degradation parameters ξ_1 and ξ_2, on the development of normalized excess pore pressure were investigated using the new model of radial consolidation under cyclic loading. The basic soil properties used in the following analysis are: $\lambda = 0.25,\ \kappa = 0.05,$ $M = 1.2,\quad p'_{c0} = 30\ \text{kPa},\quad p'_0 = 30\ \text{kPa},\quad k_0 = 1,\quad e_0 = 0.6,\quad r_e = 0.15\ \text{m},\quad r_w = 0.01\ \text{m},$ $G = 200c_{u0}$, and $c_{u0} = p'_{c0}(M/4)(2p'_0/p'_{c0})^{\kappa/\lambda}$.

6.4.1 Effect of cyclic stress ratio

For $\xi_1 = 0$ the details of excess pore pressure under partially drained cyclic loading are shown in Fig. 6.10, where eight cyclic stress ratios from 0.3 to 0.65 with 0.5 interval have been calculated. The results given in Fig. 6.10(a) show that at a low cyclic stress ratio ranging from 0.3 to 0.4, the accumulation of excess pore pressure is negligible. For $\text{CSR} = 0.45 \text{ and } 0.5$, the excess pore pressure starts to accumulate. When CSR increases to 0.55, the excess pore pressure develops substantially and u_f / p'_{c0} reaches 0.9 at about 900 cycles. At a high cyclic stress ratio above the critical cyclic stress ratio such as

$\mathrm{CSR} = 0.6$ and 0.65, the number of cycles at failure decreases as CSR increases. When ξ_2 decreases from 50 to 25, the corresponding predictions are given in Fig. 6.10(b). When the cyclic stress ratio is relatively low ($\mathrm{CSR} = 0.35$ and 0.4), the excess pore pressure develops stably at a low rate of generation. Once the CSR reaches 0.4, the excess pore pressure increases significantly and u_f / p'_{c0} has the value of 0.9 at approximately 950 cycles. The comparison of Fig. 6.10(a) and Fig. 6.10(b) indicates that given the identical parameters, the critical cyclic stress ratio in a partially drained condition decreases from 0.55 to 0.4 when ξ_2 decreases from 50 to 25.

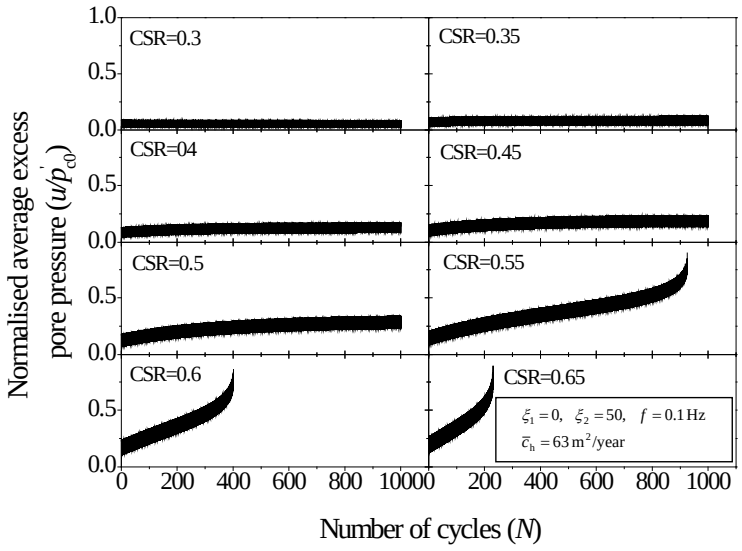

(a)

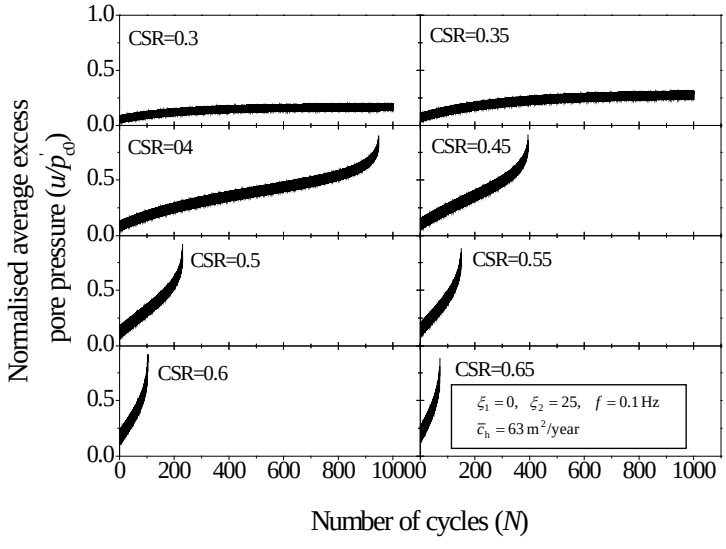

(b)

Fig. 6.10 Detailed development of average excess pore pressure with the number of cycles: (a) $\xi_2 = 50$, (b) $\xi_2 = 25$

A comparison of excess pore pressures between partially drained and undrained conditions is shown in Fig. 6.11, where eight cyclic stress ratios and two values of ξ_2 are considered. The results given in Fig. 6.11(a) indicate that for a high cyclic stress ratio ranging from 0.55 to 0.65, radial drainage decelerates the rate of excess pore pressure build up to its critical value $u_f / p'_{c0} = 0.9$, so the soil can undergo more loading cycles before failure. For a low cyclic stress ratio ranging from 0.3 to 0.5, radial drainage can prevent the excess pore pressure from accumulating to its critical value and no failure would occur. When ξ_2 changes from 50 to 25, the trend of excess pore pressure build up is shown in Fig. 6.11(b) which is similar as that in Fig. 6.11(a). When soil is subjected to a cyclic stress ratio ranging from 0.4 to 0.65, the failure of the soil is inevitable and radial drainage can only increase the number of cycles before the failure occurs. When the cyclic stress ratio varies from 0.3 to 0.35, the radial drainage effectively prevents the soil from failing.

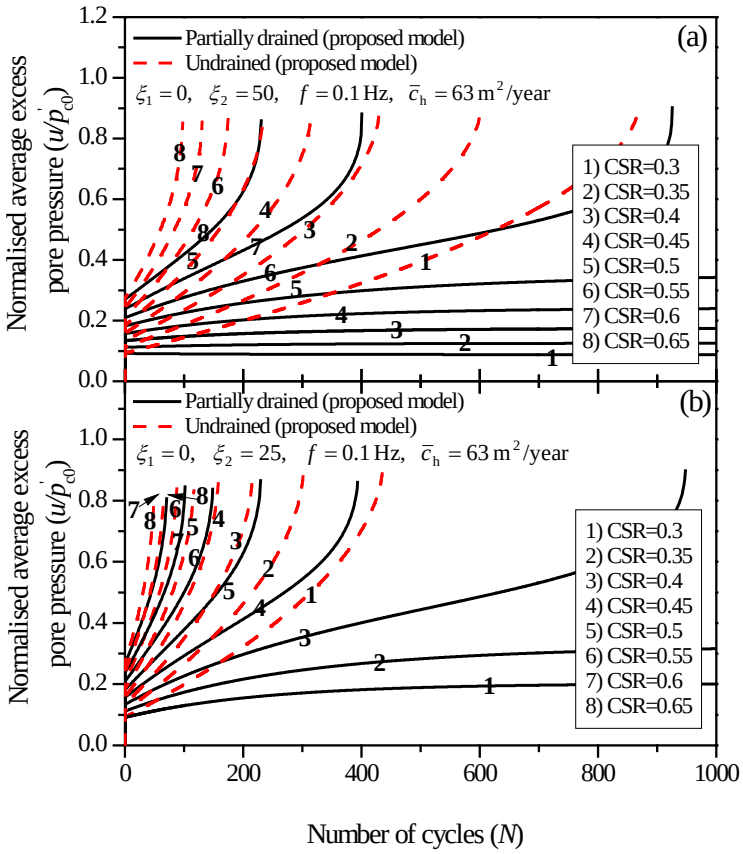

Fig. 6.11 Comparison of excess pore pressure between partially drained and undrained conditions: (a) $\xi_2 = 50$, (b) $\xi_2 = 25$

For $\xi_1 \neq 0$ a similar comparison of excess pore pressure between partially drained and undrained conditions is shown in Fig. 6.13, while the details of excess pore pressure under partially drained cyclic loading are shown in Fig. 6.12. The results given in Fig. 6.12(a) indicate that at a relatively low cyclic stress ratio ranging from 0.3 to 0.45, the excess pore pressure increases at the initial stage and then decreases after certain number of cycles. The effective stress increases as the excess pore pressure decreases, and therefore the failure of the soil would not occur. When the cyclic stress ratio increases to 0.5, the excess pore pressure develops dramatically and the failure occurs at 300 cycles. When the cyclic stress ratio is above the critical level, failure occurs after certain loading cycles which is related to the value of CSR. When ξ_2 increases from 10 to 50, the corresponding predictions are given in Fig. 6.12(b). The accumulation of the excess pore pressure can be neglected at CSR equal 0.3 to 0.35. When CSR varies from 0.4 to 0.55, the excess pore pressure increases stably and generates at a relatively low speed. Once CSR reaches 0.6, substantial accumulation of excess pore pressure is observed and the failure of the soil occurs around 500 cycles. When CSR increases to 0.65, the failure occurs even more quickly around 200 cycles. The comparison of Fig. 6.12(a) and Fig. 6.12(b) indicates that an increased critical cyclic stress ratio from 0.5 to 0.6 is observed when ξ_2 increases from 10 to 50.

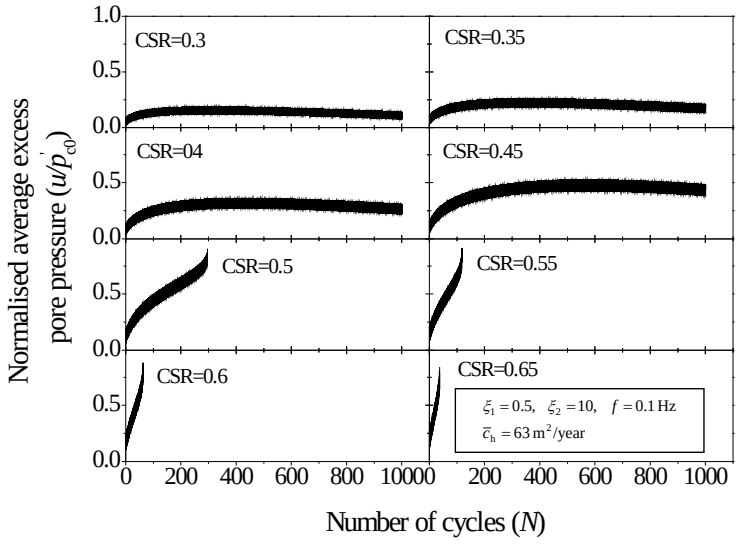

(a)

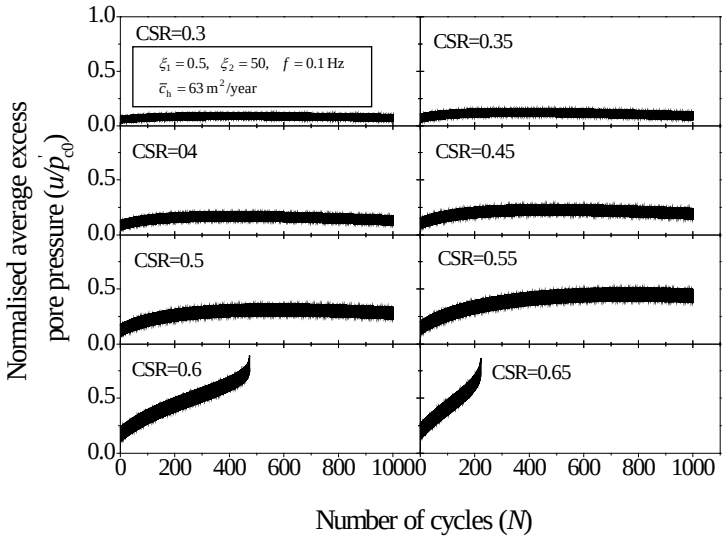

(b)

Fig. 6.12 Detailed development of average excess pore pressure with the number of cycles: (a) $\xi_2 = 10$, (b) $\xi_2 = 50$

A comparison of excess pore pressures between partially drained and undrained conditions is shown in Fig. 6.13. The results given in Fig. 6.13(a) indicate that the effectiveness of radial drainage in stabilising the soil can be considered in three aspects: (a) When soil is subjected to a low cyclic stress ratio ($\mathrm{CSR} = 0.3,\ 0.35,\ \text{and}\ 0.4$) at which soil would not fail even under the undrained condition, the radial drainage can help to reduce the excess pore pressure to a smaller value, (b) When soil is subjected to a medium cyclic stress ratio ($\mathrm{CSR} = 0.45$), radial drainage can prevent the excess pore pressure from accumulating to its critical value, and therefore no failure would occur, and (c) When soil is loaded under a relatively high cyclic stress ratio varying from 0.5 to 0.65, the radial drainage can only decelerate the rate of generation of excess pore pressure to its critical value. However, the soil would fail but can undergo more loading cycles prior to failure compared with undrained conditions. Similarly, the behaviour of the soil depends on the cyclic stress ratio when ξ_2 increases from 10 to 50 (see Fig. 6.13(b)). At CSR equal to 0.3, 0.35, 0.4, and 0.45, with the radial drainage the excess pore pressure is reduced to an even smaller value compared with the undrained condition. At CSR equal to 0.5 and 0.55, the failure of the soil can be prevented due to the radial drainage and therefore the soil can be stabilised. At CSR equal to 0.6 and 0.65, the excess pore pressure generates so fast that even with the radial drainage, the failure of the soil occurs.

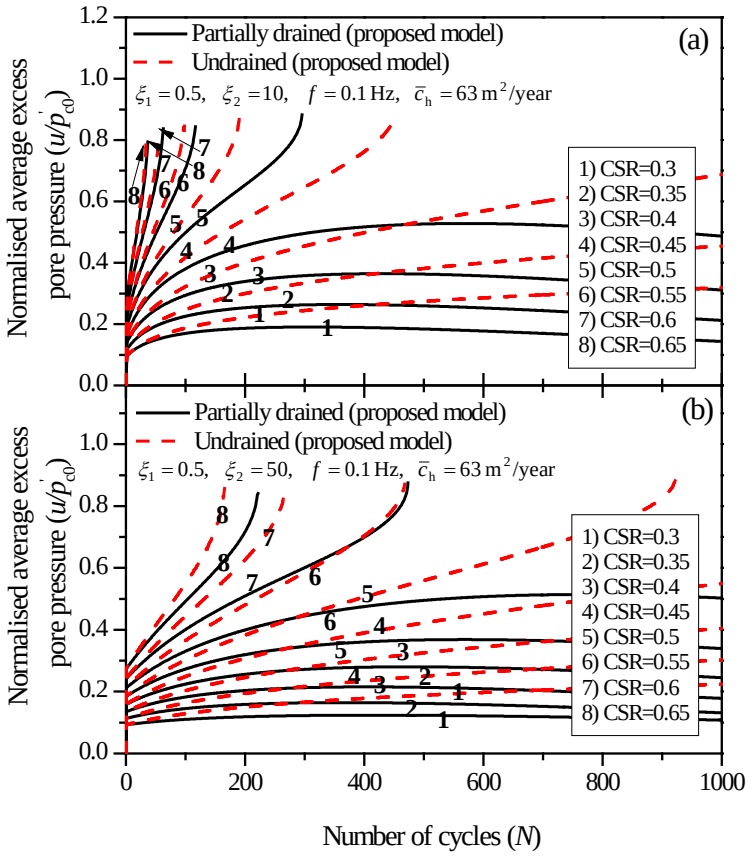

Fig. 6.13 Comparison of excess pore pressure between partially drained and undrained conditions: (a) $\xi_1 = 10$, (b) $\xi_2 = 50$

6.4.2 Effect of cyclic degradation parameters ξ_1 and ξ_2

The effect of the cyclic degradation parameter ξ_2 on the generation of excess pore pressure is shown in Fig. 6.14. The excess pore pressures versus the number of loading cycles under three cyclic stress ratios (CSR =0.4, 0.5, and 0.6) are given in Fig. 6.14(a), (b), and (c) respectively. Generally the shapes of u/p'_{c0} curves for undrained conditions are similar to each other, while those for partially drained conditions depends on the values of ξ_2. The results shown in Fig. 6.14(a) indicate that when the value of ξ_2 is relatively high ranging from 60 to 100, the excess pore pressure decreases after the initial stage of development, therefore the soil would not fail. With $\xi_2 = 40$, the excess pore pressure increases stably at a low rate of generation and the soil would not fail either. When ξ_2 decreases to 20, the excess pore pressure increases significantly and the value

of u_f / p'_{c0} reaches 0.9 around 400 cycles. A similar trend is shown in Fig. 6.14(b) for $\mathrm{CSR} = 0.5$. When ξ_2 ranges from 80 to 100, a decrease in excess pore is observed after the initial stage of development. When ξ_2 equals to 60, the excess pore pressure increases slowly and the accumulation of the excess pore pressure is negligible. When the value of ξ_2 is relatively low ranging from 20 to 40, the excess pore pressure develops dramatically and the failure of the soil occurs irrespective of the radial drainage. The results given in Fig. 6.14 (c) indicate that soils are stable at ξ_2=80 and 100, while the failure would occur at ξ_2=20, 40, and 60.

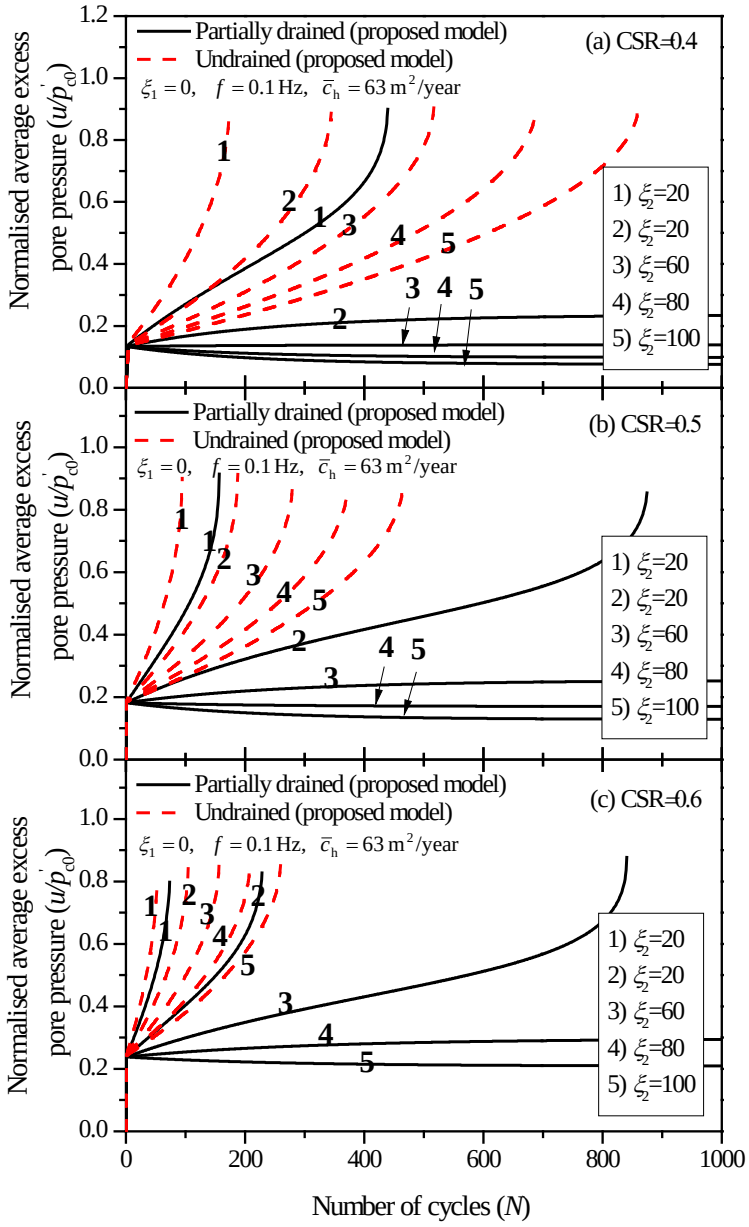

Fig. 6.14 Comparison of excess pore pressure between partially drained and undrained conditions ($\xi_1 = 0$): (a) $\mathrm{CSR} = 0.4$, (b) $\mathrm{CSR} = 0.5$, (c) $\mathrm{CSR} = 0.6$

When $\xi_1 \neq 0$, the excess pore pressures versus the number of loading cycles are given in Fig. 6.15(a), (b), and (c) for CSR =0.4, 0.5, and 0.6, respectively. The results shown in Fig. 6.15(a) indicate that at a low cyclic stress ratio (CSR =0.4) when the failure would not occure even under the undrained conditions, the radial drainage reduces the excess pore pressure and further stabilises the soil. When the cyclic stress ratio increases (CSR =0.5 and 0.6), the generation of excess pore pressure is retarded and the failure of the soil can be prevented with a high value of ξ_2, while the failure of the soil would occur with a low value of ξ_2 (see Fig. 6.15(b) and (c)).

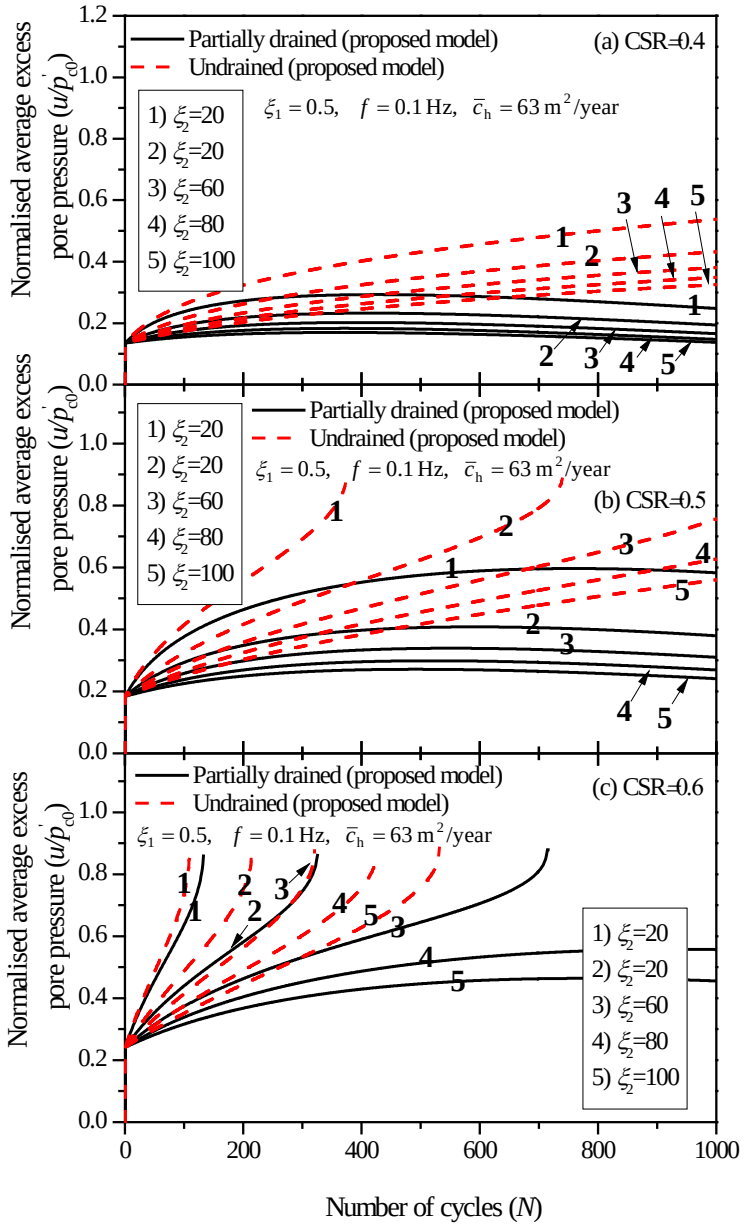

Fig. 6.15Comparison of excess pore pressure between partially drained and undrained conditions ($\xi_1 = 0.5$): (a) CSR = 0.4, (b) CSR = 0.5, (c) CSR = 0.6

6.4.3 Effect of the coefficient of consolidation

Two values of the coefficient of consolidation have been used to examine how the coefficient of consolidation affects the stability of soft clays. To take into account the effect of ξ_2 as well, one comparison is made under $\xi_2 = 50$ (see Fig. 6.16), and the other under $\xi_2 = 10$ (see Fig. 6.17). The results illustrated in Fig. 6.16 indicate that for $\xi_1 = 0.5$ and $\xi_2 = 50$, the critical cyclic stress ratio in partially drained conditions decreases from 0.6 (see Fig. 6.16(a)) to 0.55 (see Fig. 6.16(b)) when $\bar{c}_h$ decreases from $63\,m^2$/year to $9.46\,m^2$/year. As expected, a similar result is obtained when ξ_2 decreases from 50 to 10. The prediction given in Fig. 6.17 indicates that for $\xi_1 = 0.5$ and $\xi_2 = 10$, the critical cyclic stress ratio in partially drained conditions decreases from 0.5 (see Fig. 6.17(a)) to 0.45 (see Fig. 6.17(b)) when $\bar{c}_h$ decreases from $63\,m^2$/year to $9.46\,m^2$/year.

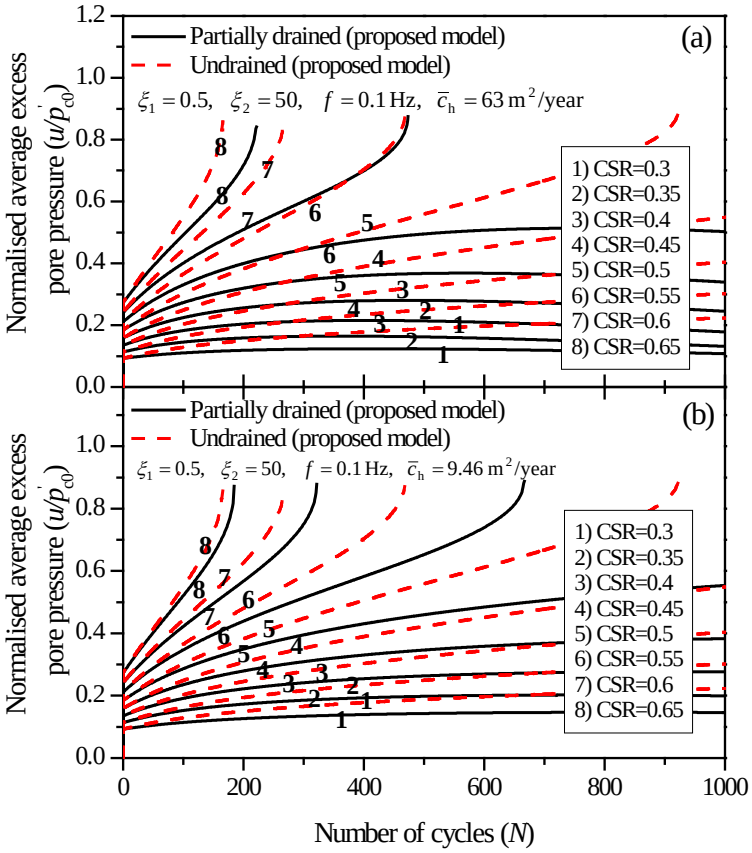

Fig. 6.16 Comparison of excess pore pressure between partially drained and undrained conditions ($\xi_1 = 0.5$ and $\xi_2 = 50$) : (a) $63\,m^2$/year, (b) $9.46\,m^2$/year

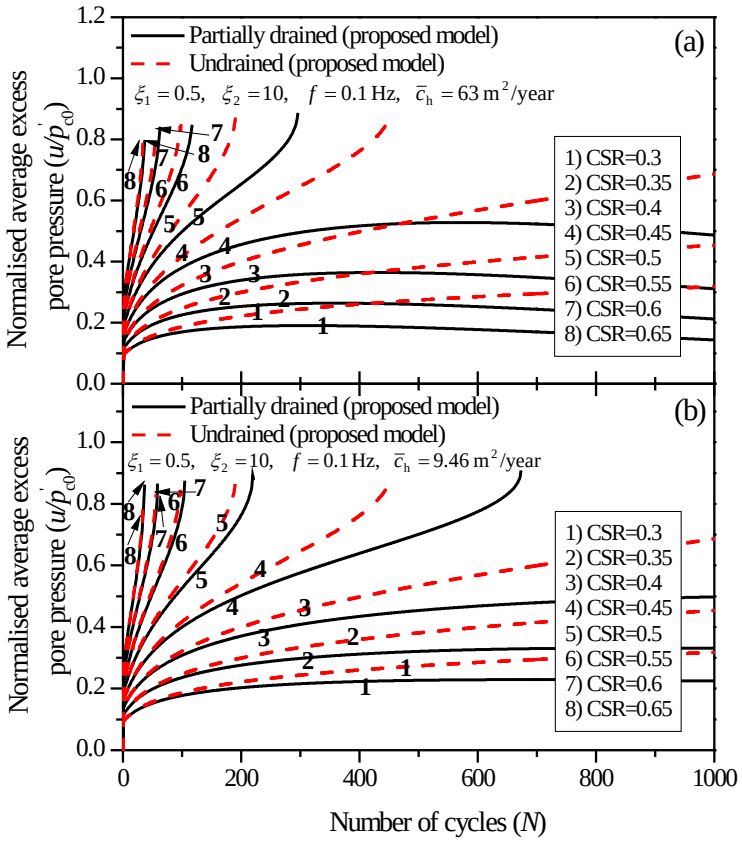

Fig. 6.17 Comparison of excess pore pressure between partially drained and undrained conditions ($\xi_1 = 0.5$ and $\xi_2 = 10$): (a) $63\ m^2$/year, (b) $9.46\ m^2$/year

6.5 Conclusions

A new model of radial consolidation under cyclic loading was proposed in this Chapter. This model can simulate a condition where soft soil subgrade is installed with vertical drains and is subjected to train loads. This is achieved through the application of radial consolidation theory and generation of excess pore pressure predicted by the undrained cyclic model, which has already been presented in Chapter 4. The framework of this model is presented first, including a derivation of the governing equations, the procedure for evaluating the excess pore pressure, and the finite difference method used to solve the governing equations. A detailed computational procedure is summarized, where the parameters are established, the computational steps and sub-steps are set up, a calculation of the time interval according to each loading step is presented, and the procedure for

calculating the excess pore pressure for each increment in the load are finally demonstrated.

A comparison was made between the prediction of this new model and the test results given in Chapter 5. An acceptable agreement was found between them and therefore the proposed model is verified. Furthermore the model has been analysed by investigating the effects of the cyclic stress ratio, the parameters ξ_1 and ξ_2, and the coefficient of consolidation. The specify conclusions are as follows:

(a) At a high cyclic stress ratio, the radial drainage decelerates the rate at which the excess pore pressure builds up to its critical value, so the soil can undergo more loading cycles prior to failure. At a low cyclic stress ratio, radial drainage can prevent the excess pore pressure from accumulating to its critical value and consequently no failure would occur.

(b) Given the identical parameters, the critical cyclic stress ratio increases when ξ_1 and ξ_2 increase because ξ_1 and ξ_2 govern the rate of development of excess pore pressure. The larger values of ξ_1 and ξ_2 are, the lower the rate of generation of excess pore pressure, and therefore a higher cyclic stress ratio can be applied to obtain the same excess pore pressure compared to smaller values of ξ_1 and ξ_2.

(c) Given the identical parameters, a higher critical cyclic stress ratio can be obtained as the coefficient of consolidation increases, because, the coefficient of consolidation controls how fast the pore water flows out. The larger the coefficient of consolidation, the faster the rate at which the excess pore pressure dissipates, and therefore, a higher cyclic stress ratio can be applied to achieve the same excess pore pressure compared to a smaller coefficient of consolidation.

This study clearly suggests that under cyclic loading conditions, the failure of soft subgrade soil can be prevented by the use of vertical drains. It should be noted that the assumptions such as no smear effects and no well-resistance are applied to all the analysis in this chapter. In addition, the average excess pore pressure is used in the parametric analysis.

7 Application to Case History

7.1 General

This Chapter presents the application of the theoretical developments of Chapter 6 to a field study. This case history in Sandgate includes two new railway lines that have been constructed adjacent to the existing track. The model of combined vertical and radial consolidation under cyclic loading has been used to compare the predicted settlement and lateral displacement with the field data.

7.2 Sandgate Rail Grade Separation Project

The Sandgate Rail Grade Separation Project is located at Sandgate, between Maitland and Newcastle, in the lower Hunter Valley of New South Wales (see Fig. 7.1). This project is the result of Kooragang Island becoming a major export terminal, and the coal trains need to cross the main lines at Sandgate to enter Kooragang Island. The existing track capacity cannot meet the demanding freight and passenger train schedules, which often results in delays throughout the entire Hunter Valley Coal network. Therefore, the construction of two new lines has been a top priority.

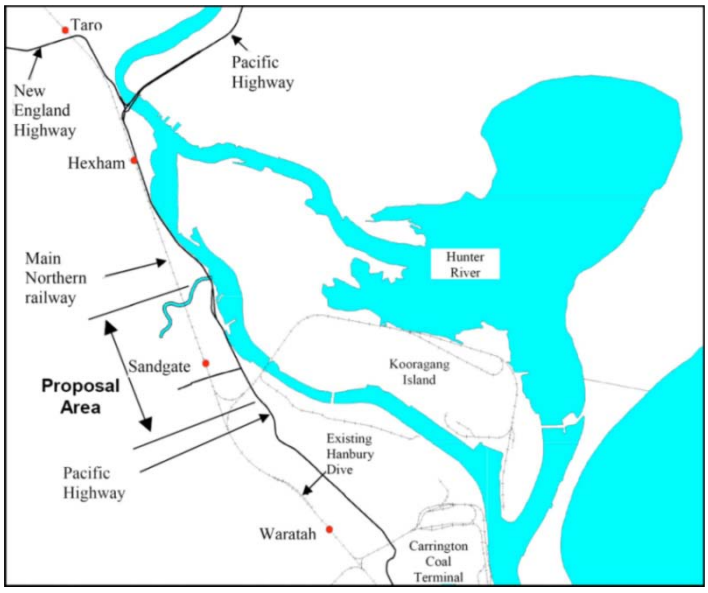

Fig. 7.1 Site location plan (after Indraratna et al. 2010)

7.2.1 Site investigation

A site investigation was carried out through extensive in situ and laboratory testing to ascertain the soil profile along the proposed route. These tests included two in situ vane shear tests, six boreholes, two test pits, and 14 piezocone and piezometric cone penetration tests.

The soil profile of the proposed area is shown in Fig. 7.2. The existing embankment fill overlies soft compressible soil (soft clay) to a depth that varies from 4 to 30 m. The soil profile consists of soft compressible clay, soft sandy clay, stiff sandy clay, medium dense sand, stiff clay, and stiff to very stiff clay, followed by shale bedrock.

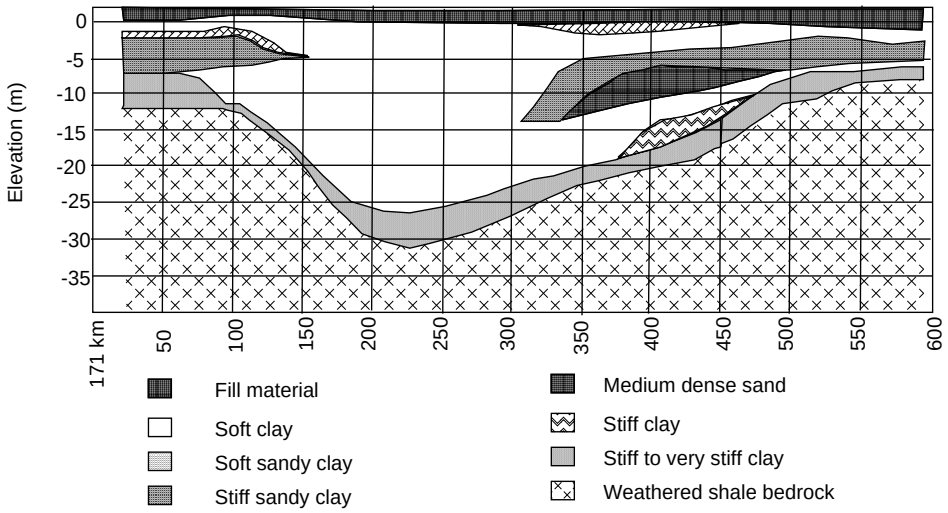

Fig. 7.2 Typical soil profile at the Sandgate Rail Grade Separation Project (after Indraratna et al. 2010)

The soil properties at depths varying from 0 to 30 m are illustrated in Fig. 7.3. The groundwater level is located at the ground surface. The water content of the soil layers is very close to their liquid limits. The unit weight of soils varies from 14 to 16 kN/m^3. The undrained shear strength obtained from the in situ vane tests varies from 10 to 40 kPa. The oedometer tests indicate that the overconsolidation ratio (OCR) varies from 1 to 1.2, thus all the clay deposits can be considered as normally consolidated to lightly overconsolidated.

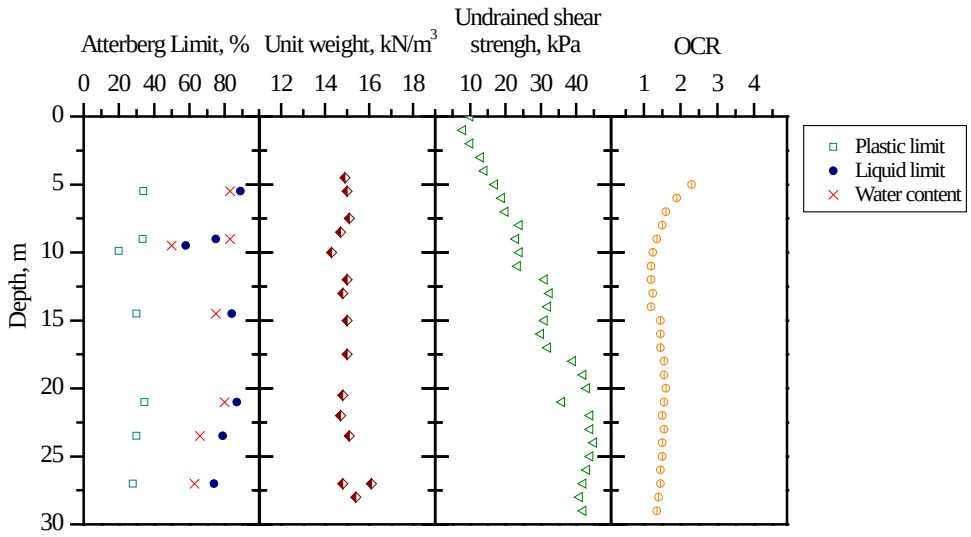

Fig. 7.3 Soil properties at Sandgate Rail Grade Separation Project (original data from Indraratna et al. 2010)

The consolidation properties obtained from the oedometer and CPTU tests are shown in Fig. 7.4 where it can be seen that the horizontal coefficient of consolidation (c_h) is approximately 2-10 times the vertical coefficient of consolidation (c_v).

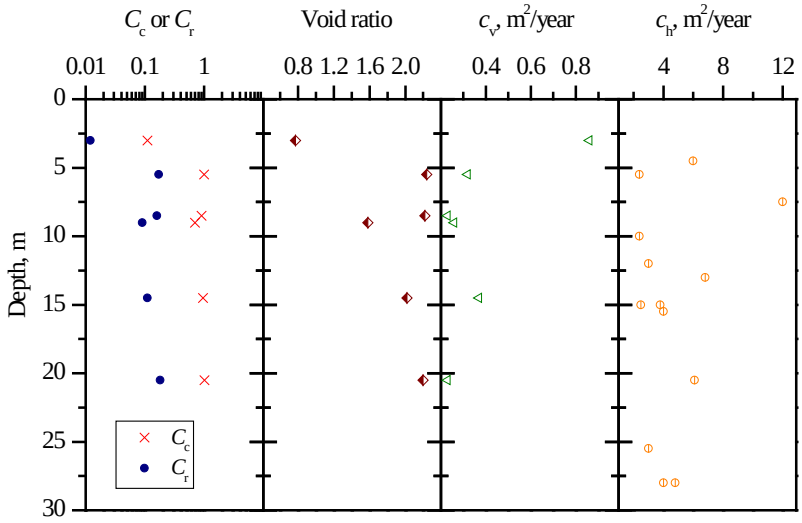

Fig. 7.4 Soil consolidation properties at Sandgate Rail Grade Separation Project (original data from Indraratna et al. 2010)

7.2.2 The use of short PVDs under the railway track

Due to the stringent time constraints placed on this project, only an initial train load at very low speed was considered to be the external surcharge instead of preloading with a conventional surcharge embankment. The installation of PVDs was chosen as a useful technique to effectively accelerate the dissipation of excess pore pressure due to the train load, curtail the excessive lateral displacement, and thus enhance the stability of the newly constructed (0.3 m high) rail track. The PVDs were determined to be 8 m long because the train load was restricted to a depth of 5-8 m.

7.3 Combined vertical and radial consolidation under cyclic loading

7.3.1 Loading condition

For a previously executed fully instrumented track at Bulli (near Wollongong), a cyclic deviatoric stress of 50–100 kPa and a load frequency of 5–10 Hz was typically obtained at the subgrade when a freight train approaches a speed of 100 km/h. For Australian standard gauge operations (longitudinal distance between adjacent wheels is 2.02 m and the width between the rails is 2.55 m), the ratio of the speed of the train (km/h) to its frequency (Hz) is approximately 7. Therefore 5 Hz typically simulates the loading frequency of a cyclic load in the subgrade at a train speed of less than 40 km/h. The maximum amplitude of the cyclic load conforms to 25 t axle loads. The corresponding design axle load (P_{d}) can then be obtained from the Australian standards [AS 1085.14-1997 (Australia Standards 1997)] as follows:

$$P_{\mathrm{d}} = \left(1 + 5.4\frac{V}{D}\right)P_{\mathrm{s}} \tag{7.1}$$

where $V = 40$ km/h is the train speed, $D = 860$ mm is the diameter of the wheel, and $P_{\mathrm{s}} = 25$ tons is the axle load. Based on Australian Standards AS 1085.14-1997, the sleeper to ballast contact pressure p_{d} can be determined by:

$$p_{\mathrm{d}} = \frac{P_{\mathrm{d}} \times 9810}{4BL} \tag{7.2}$$

where $B = 0.3$ m is the width of the sleeper and $L = 2.55$ m is the length of the sleeper. Considering the attenuation of dynamic stress within the subgrade caused by a passing

train, the dynamic stress is assumed to be distributed linearly with its maximum value (contact pressure) at the top of the subgrade and zero at the bottom of the subgrade.

7.3.2 Selection of soil parameters and numerical analysis

A soil cylinder with a combined vertical and radial consolidation under equal strain conditions was considered. The soil was divided into three layers, namely, ballast and fill, Soil 1, and Soil 2 (see Fig. 7.5(a)). Each layer can then be further divided into several sub-layers (see Fig. 7.5 (b)).

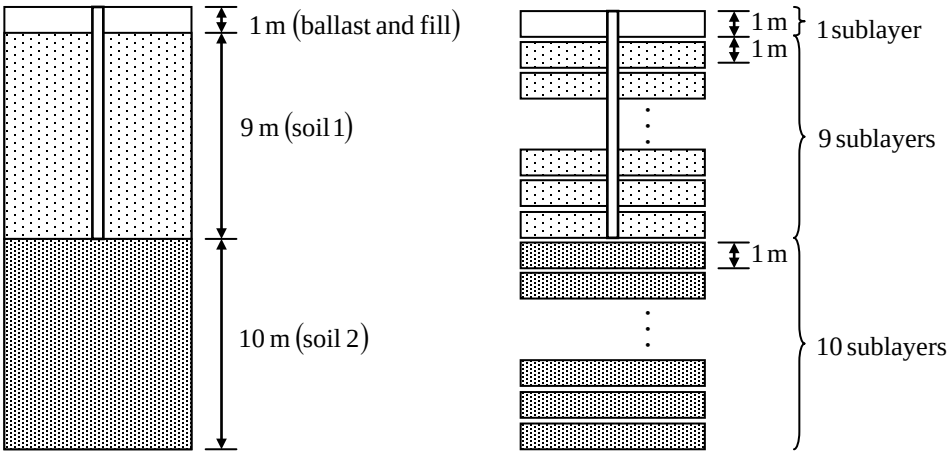

Fig. 7.5 Unit cell with combined vertical and radial consolidation: (a) Three layers of the formation, (b) Sub-layers.

The parameters obtained from an oedometer test, a field vane shear test, and CPTU for each layer of soil are given in Table 7.1.

Table 7.1 Parameters for fill and Soil 1 layer at Sandgate Rail Grade Separation

Sub-layer		Sub-layer thickness (m)	k_v ($\times 10^{-4}$ m/day)	k_h ($\times 10^{-4}$ m/day)	C_c	C_s	p_0' (kPa)	p_{c0}' (kPa)	e_0
Ballast and fill	1	1	0.7	1.4	0.91	0.105	6.20	15.49	2.26
Soil 1	2	1	0.7	1.4	0.92	0.11	11.99	29.98	2.26
	3	1	0.7	1.4	0.93	0.115	17.78	44.46	2.26
	4	1	0.7	1.4	0.94	0.12	23.58	58.94	2.26
	5	1	0.7	1.4	0.95	0.125	29.37	73.43	2.26
	6	1	0.7	1.4	0.96	0.13	35.16	87.91	2.26
	7	1	0.7	1.4	0.97	0.135	40.96	90.10	2.26
	8	1	0.7	1.4	0.98	0.14	46.75	88.83	2.26
	9	1	0.7	1.4	0.99	0.145	52.54	84.07	2.26
	10	1	0.7	1.4	1	0.15	58.34	75.84	2.26
Soil 2	11	1	0.75	1.5	1	0.15	64.34	64.34	2.04
	12	1	0.75	1.5	1.01	0.155	70.54	71.95	2.04
	13	1	0.75	1.5	1.02	0.16	76.74	79.81	2.04
	14	1	0.75	1.5	1.03	0.165	82.95	87.92	2.04
	15	1	0.75	1.5	1.04	0.17	89.15	96.28	2.04
	16	1	0.75	1.5	1.05	0.175	95.36	104.90	2.04
	17	1	0.75	1.5	1.06	0.18	101.56	113.75	2.04
	18	1	0.75	1.5	1.07	0.185	107.76	122.85	2.04
	19	1	0.75	1.5	1.08	0.19	113.97	132.20	2.04
	20	1	0.75	1.5	1.09	0.195	120.17	141.80	2.04

7.4 Comparison of settlement and lateral displacement

The field results were made available to the writers by the owner of the track (ARTC). In the field, a spacing of 2 m was adopted for the 8 m long PVDs based on based on previous trials conducted by ARTC. Mebra (MD88) wick vertical drains ($100\ \text{mm} \times 4\ \text{mm}$) were installed at this site. In this section the field measurements and the predictions are compared and discussed. A comparison of the settlement at the centre line of the rail tracks between the prediction and field data is shown in Fig. 7.6. The predicted settlement agrees well with the measured data. The variation in the time-dependent settlement at different drain spacing is shown in Fig. 7.7. It is observed that 90% consolidation due to PVDs may be encountered within 1 year, whereas it will take much longer to achieve the same degree of consolidation without PVD.

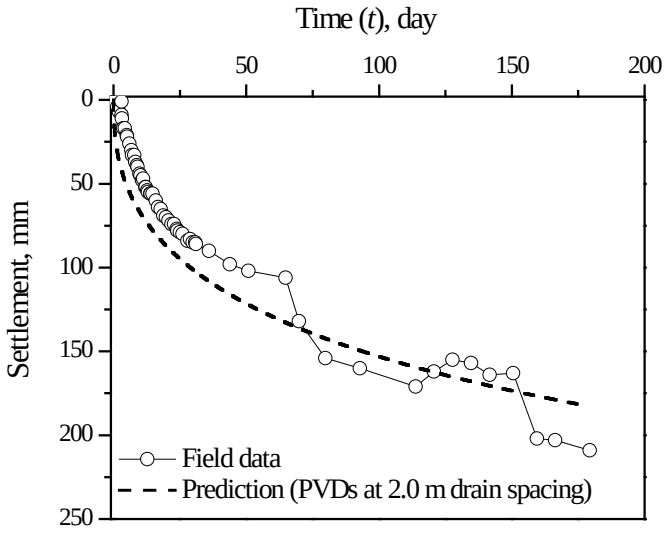

Fig. 7.6 Comparison of settlements at the centre line of rail tracks between the predictions and field data

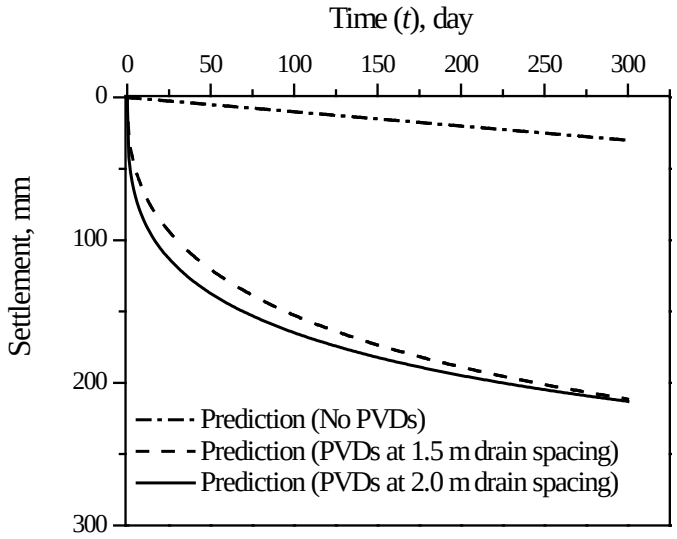

Fig. 7.7 Surface settlements at the centre line of the rail load

The variation of in situ lateral displacement after 180 days at the toe of the rail embankment is presented in Fig. 7.8. As expected, maximum displacements were measured within the top layer of clay, i.e., the softest soil below the 1 m crust. As expected, lateral displacement was restricted to the topmost compacted fill (0-1 m deep). The predicted lateral displacement agrees well with the measurements. A comparison of lateral displacement at the 2.0 and 1.5 m drain spacing is given in Fig. 7.9, where the condition of no PVDs is also presented. In terms of excess pore pressure dissipation, little advantage was gained by a closer drain spacing of 1.5 m compared to a spacing of 2.0 m. As anticipated, the lateral displacements are shown to be at their maximum within the layer of soft clay directly beneath the compacted crust, about 1 m in thickness. Lateral displacement at 180 days may be as large as 0.04 m at a depth of around 1.0 m below the surface, however, the PVDs decrease the lateral movements by 25–35% depending on the drain spacing.

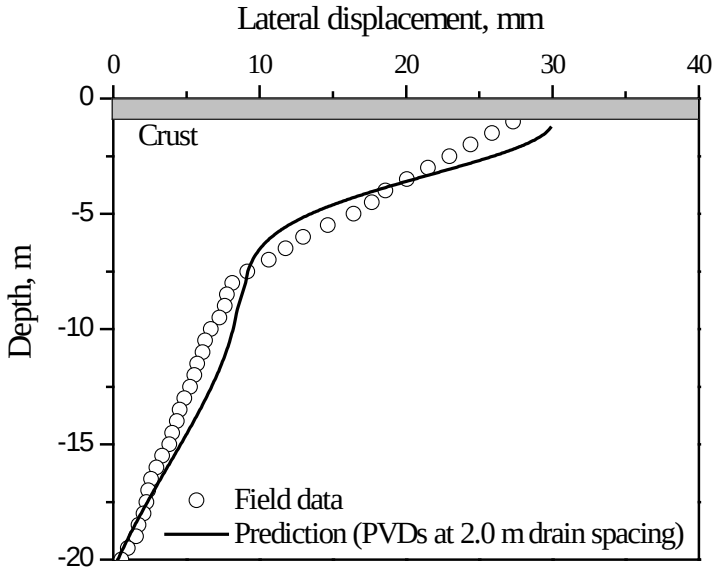

Fig. 7.8 Comparison of lateral displacement near the rail embankment toe at 180 days between predictions and field data

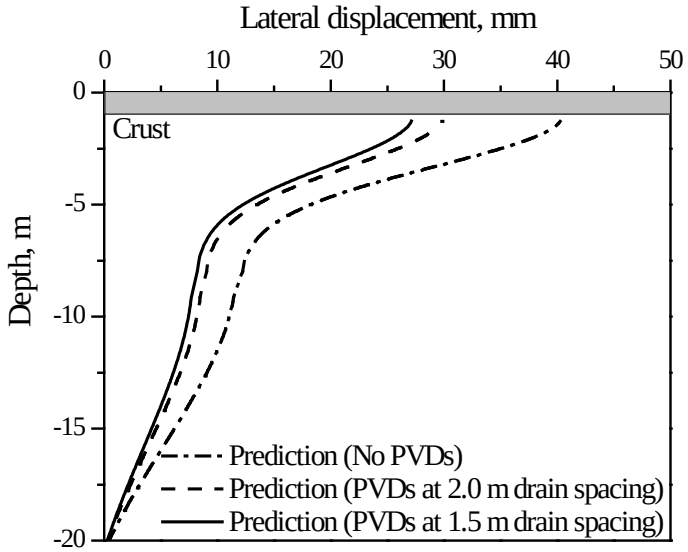

Fig. 7.9 Lateral displacement profiles near the toe of the embankment at 180 days

7.5 Conclusions

This Chapter presented a case history of two new railway lines which were constructed adjacent to the existing working track at Sandgate, between Maitland and Newcastle, in the lower Hunter Valley of New South Wales. The theoretical developments described in Chapter 6 were applied to this case history to analyse the track behaviour. The field settlement data and lateral displacement were compared with the predictions of a multi-layered cyclic consolidation model incorporating both vertical and horizontal drainage, and very good agreement was found between them. This case study demonstrates that the application of short PVDs at 2 m spacing was successfully implemented at the Sandgate Rail Grade Separation Project. In the absence of a conventional preloading embankment, the initial soil compression caused by low speed trains (< 50 km/h) was accompanied by routine ballast packing to maintain the elevation and alignment of the track. Because the excess pore pressure rapidly dissipates through the PVDs during cyclic loading and the subsequent rest period, the track than becomes more stable for the next loading stage. Even with the relatively short PVDs (8 m), both the predictions and field data proved that the lateral displacement could be curtailed effectively by the installation of PVDs. Further investigations will be carried out to study the similarities and differences in soil response to cyclic loading for both artificial clay in laboratory and real clay in the field so that more accuracy can be obtained when the theory derived from the laboratory tests are applied to the field conditions.

8 Conclusions and Recommendations

8.1 Generally summary

As a foundation for the rail track, the soft clay subgrade is deemed to have a significant influence on its performance. The progressive shear failure and excessive plastic deformation caused by train passages are the major concerns when a new rail track is designed or an existing one is under maintenance. Therefore it is important to understand the behaviour of soft clays under train loads. High speed trains with heavy axle loads are inevitable, in order to satisfy the need to transport passengers and freight, both in quantity and speed. Consequently, the magnitude and frequency of the resulting dynamic stress can be increased and the deterioration of the subgrade can be exacerbated. Among a variety of techniques to improve the foundations, the use of prefabricated vertical band drains (PVDs) is increasing in popularity, because their construction is cheaper and their installation poses the least disturbance to the surrounding soils. The installation of PVDs enables the short radial drainage path to accelerate the dissipation of excess pore pressure, effectively transferring the external load from the pore water to the skeleton of the foundation.

With this background, this thesis contributes most to analysing the effect of the level and loading frequency of cyclic stress and radial drainage on the behaviour of soft clay subgrade. Chapter 3 presented a series of undrained cyclic triaxial tests, while Chapter 4 proposed an undrained cyclic model. Chapters 5 and 6 presented the laboratory tests and numerical model respectively, where radial drainage was allowed during the application of cyclic loading.

8.2 Level of cyclic stress

A number of researchers (Seed et al. 1955; Larew and Leonards 1962; Seed and Chan 1966) have noted that a critical level of cyclic stress exists and it is defined as the minimum level of cyclic stress that will lead to failure. Sangrey et al. (1969) confirmed this idea by conducting cyclic triaxial tests on normally consolidated specimens of New York clay and found that the critical level of cyclic stress was approximately 0.8 times the maximum static deviator stress. Since then, the cyclic stress ratio, which is defined as the ratio of applied cyclic stress to maximum static deviator stress, has been used to show the influence of cyclic loading. The critical cyclic stress ratio is accordingly defined as

the ratio of critical cyclic stress to maximum static deviator stress. The collected critical cyclic stress ratios in the literature varied from 0.5 to 0.8 (Sangrey et al. 1969; Lashine 1971; France and Sangrey 1977; Sangrey et al. 1978; Ausal and Erken 1989; Zhou and Gong 2001; Pillai et al. 2011).

By conducting a series of undrained cyclic triaxial tests on specimens of soft clay under the current research work, it was found that the critical cyclic stress ratio was not influenced by the loading frequency. Failure occurred after a number of cycles for specimens tested under a CSR of 0.8, irrespective of the loading frequency. The failure mode was found to be barrelling, with numerous slip surfaces that formed a diamond shaped pattern on the surface of the sample. The specimens tested under a CSR of 0.4 and 0.6 did not fail at the end of the tests and behaved in a stable manner. Therefore, the critical cyclic stress ratio was expected to be greater than 0.6.

An increasing cyclic stress ratio increased the normalised excess pore pressure for any given loading frequency. This normalised excess pore pressure increased significantly at the initial stages ($N < 500$) and then gradually increased with the number of cycles. With stable specimens (CSR = 0.4 and 0.6), the normalised excess pore pressure stabilised after an initial rapid development, where the normalised excess pore pressures equalled 0.2 and 0.4 for CSR = 0.4 and 0.6, respectively. With failed specimens (CSR = 0.8), the excess pore pressure developed so quickly that a critical normalised value of 0.65 was reached in the first few cycles, and indeed they failed before they could stabilise. Nevertheless, there was no distinct difference in the shape of the excess pore pressure-cycle curve for both the stable and failed samples. The rate at which the excess pore pressure was generated continued to decrease during the process of cyclic loading for all the cyclic stress ratios.

In contrast, the failed specimens indicated a dramatic rise in axial strain beyond a critical number of cycles. With the stable specimens (CSR = 0.4 and 0.6), the development of axial strain was very small, less than 1.0% at the end of the test, while with the failed specimens (CSR = 0.8), a much larger axial strain of nearly 10% was observed. Apart from the different values of axial strains between the failed and stable specimens, the shapes of the axial strain-cycle curves were also different. The rate of axial stain generated for the stable specimens generally decreased during cyclic loading but with the failed specimens, there was a rapid upward trajectory of axial strain when a normalised excess pore pressure of 0.55 to 0.6 was attained. Indeed this was the cause of their failure.

8.3 Cyclic loading frequency

The cyclic loading frequency had an effect on the number of cycles at failure for specimens tested under a CSR of 0.8. The number of cycles at failure increased from 1,793 to 33,964 after the loading frequency was increased from 0.1 to 5 Hz. This observation was consistent with studies by Andersen (2009) and Takahashi et al. (1980) where more cycles were needed to bring the specimen to failure at a higher frequency. The time to failure can be calculated by $t_f = N_f (1/f)$ where N_f is the number of cycles at failure. In this current study t_f decreased from 299 to 113 min when the loading frequency was increased from 0.1 to 5 Hz. At a given critical CSR where failure was inevitable, the higher the frequency the shorter the time required for failure to occur.

Moreover, the variations of excess pore pressure and axial strains against loading time indicated that the data points of excess pore pressure and axial strains did not deviate significantly from each other as the frequency increased from 0.1 to 5 Hz. This increase in frequency had insignificant effect on the development of excess pore pressure and axial strains. For a given value of CSR, the excess pore pressure of all the specimens tended to converge to the same value, irrespective of the frequency. For a CSR of 0.4 and 0.6, the normalised excess pore pressure after about 200 minutes approached 0.15 and 0.4, respectively. As expected, a significantly higher excess pore pressure exceeding 0.6 was observed for the four failed specimens having a CSR of 0.8.

8.4 Strain rates

As mentioned above, the behaviour of soft clays was influenced mainly by the cyclic stress ratio rather than the loading frequency, which raised the following fundamental question. What is the mechanism that leads to this cyclic stress dependent behaviour? It has been found in the current research work that the strain rate was responsible for this phenomenon and could explain this independent behaviour of the loading frequency.

A number of researchers have noted that the excess pore pressures and undrained shear strength are intimately related to the strain rate (Richardson and Whitman 1963; Ladd et al. 1972; Crooks and Graham 1976; Vaid and Campanella 1977; Vaid et al. 1979; Baracos et al. 1980; Andersen and Stenhamar 1982; Graham et al. 1983; Adachi et al. 1985; Lefebvre and LeBoeuf 1987; Sheahan et al. 1996). However, a comprehensive understanding of the effect of the strain rate in stress controlled cyclic loading has not yet

been obtained. Indeed the only results related to this aspect were made by Lefebvre and LeBoeuf (1987) Lefebvre and Pfendler (1996), who reported that the strain rates for stress-controlled tests under 0.1 Hz were roughly 300 and 3,500 %/h for Eastern Canada clay and St. Lawrence Valley clay, respectively.

The relationship between the strain rate, the cyclic stress ratio, and the loading frequency has been investigated, and the question raised earlier in this section has been answered. To calculate the strain rate for a stress controlled cyclic loading test, it was assumed that during the whole cycle a constant strain rate was applied. The calculated strain rate for each cyclic loading condition seemed to be constant during the whole process of cyclic loading. It was indicated that an increase in the cyclic stress ratio raises the strain rate and this increment was also influenced by the value of the cyclic stress ratio, e.g., the difference in the strain rate was 100 %/h between CSR =0.4 and 0.6, whereas the difference in the strain rate between CSR = 0.6 and 0.8 was 300 %/h. This sharp rise in the strain rate when the CSR increased from 0.6 to 0.8 suggests that the cyclic resistance decreased dramatically at a high cyclic stress level, which further confirmed previous observations that failure would occur at CSR = 0.8. It should be noted that all four plots for f = 0.1 to 5 Hz were close together, indicating that the strain rate did not depend on the frequency. That is why the loading frequency had very little influence on the development of excess pore pressure and axial strains. Therefore, the mechanism that leads to cyclic stress dependent behaviour can be described as, a higher strain rate at CSR = 0.8 would cause a higher strain rate and a subsequently higher excess pore pressures and axial strains.

The calculated strain rate varied from 150 to 550 %.h for all the loading conditions, which was much larger than 0.5 %/h under which the monotonic loading was conducted. Consequently, an increased effective stress friction angle was observed. The slope of q/p' at failure for cyclic loading increased by 24% compared to the condition of monotonic loading. This observation was consistent with the studies by Sheahan et al. (1996) that an increased strain rate resulted in an increased effective stress friction angle, or a combination of decreased shear induced excess pore pressure and an increased effective stress friction angle.

8.5 Critical state based undrained cyclic model

An undrained cyclic model has been proposed based on the Modified Cam-clay model. When normally consolidated soft clays subjected to cyclic loading, the test results of permanent excess pore pressures and axial strains keep increasing during the whole process of cyclic loading. One way of interpreting this behaviour is to assume that the form of the yield surface remains unchanged but with a reduced size in an isotropic manner by the elastic unloading. Therefore a modified yield surface function during elastic unloading was proposed to capture the soil behaviour under cyclic loading, while other assumptions remain the same as the modified Cam-clay model.

In this new model only two additional cyclic degradation parameters were introduced to present the yield surface during elastic unloading, in addition to the parameters adopted in the modified Cam-clay model. These two cyclic degradation parameters controlled how much the size of the yield surface would shrink during an elastic unloading and how this reduction in the size of the yield surface would change with loading cycles. Usually the greater the reduction in the size of the yield surface, the higher the excess pore pressure and axial strain. The key aspects of this model were the state of the soil, normal compression and unloading-reloading lines, the critical state line, yield function, and hardening behaviour. A detailed computational procedure for determining the excess pore pressure and axial strains were demonstrated, including the establishment of parameters (soil properties, initial soil states, and cyclic loading conditions), set-up of steps and sub-steps, and finally the calculation of excess pore pressure and axial strains.

Comparisons were made between the predictions of this proposed model and the test results of undrained cyclic loading at three cyclic stress ratios and four loading frequencies. Good agreement was found and this proposed model has been verified in this way. The cyclic degradation parameters ξ_1 and ξ_2 from the back calculation indicated that ξ_1 is a soil property which is independent of both the cyclic stress ratio and loading frequency, while ξ_2 depends on the loading frequency in the way that ξ_2 increases with an increasing loading frequency.

The cyclic behaviour of anisotropically consolidated soft clays can be predicted by this undrained cyclic model. The effect of the stress ratio for consolidation was examined by considering three conditions, $K_0 = 1$, $K_0 = 0.82$, and $K_0 = 0.68$. It was found that the critical cyclic stress ratio decreased as consolidation stress ratio decreased. Furthermore,

the excess pore pressure at failure (u_f) decreased when the consolidation stress ratio decreased.

It is clear that for a given cyclic stress ratio, the excess pore pressure and axial strains decreased as the cyclic degradation parameters ξ_1 and ξ_2 increased, while the number of cycles at failure increased as the cyclic degradation parameters ξ_1 and ξ_2 increased. The effect of the level of cyclic stress on the development of excess pore pressure and axial strains have been studied for both $\xi_1 = 0$ and $\xi_1 \neq 0$. When $\xi_1 = 0$ (the model proposed by Carter et al. 1982), the generation rate of excess pore pressure did not decrease with an increasing number of loading cycles for all the stress ratios tested, which was inconsistent with the laboratory results. Furthermore, the critical cyclic stress ratio could not be predicted because the trends of excess pore pressure were similar to each other, regardless of the cyclic stress ratio. There was no significant difference when the cyclic stress ratio changed from one value to another. Whereas when $\xi_1 \neq 0$ (the new undrained cyclic model), a dramatic increase in both excess pore pressures and axial strains was observed when the cyclic stress ratio increased to a critical value. In summary, the critical stress ratio is predictable for $\xi_1 \neq 0$ by detecting the development of excess pore pressure and axial strains, but it is unpredictable for $\xi_1 = 0$.

8.6 Laboratory verification of the effect of radial drainage in stabilising soft clays

To investigate the effect of radial drainage in stabilising soft clays, large scale cyclic triaxial tests were conducted on soft clay specimens using the cylindrical dynamic triaxial equipment (accommodating 300 mm diameter and 600 mm height samples) which was designed and built at the University of Wollongong. A single PVD was installed in the centre of the soil cylinder to allow for radial drainage during and after the cyclic tests. Three types of tests were carried out: (a) cyclic loading without a rest period; (b) cyclic loading with rest periods; (c) cyclic loading with a changing frequency.

The dissipation of excess pore water pressure was more obvious at the locations close to the PVD. When the drainage path was only 0.13 of the total drainage path, the excess pore pressure ratio was reduced significantly from 1.0 to approximately 0.2-0.4. When the drainage paths became larger (i.e. x/r = 0.4 and 0.86), the excess pore water pressure reduced to 0.6-0.8. It was found that for a high cyclic stress ratio, the radial drainage

decelerates the rate of excess pore pressure build up to its critical value, so the soil can undergo more loading cycles prior to failure. With a low cyclic stress ratio, radial drainage can prevent the excess pore pressure from accumulating to its critical value, so the soil would not fail. When a rest period was allowed between the two consecutive sets of cyclic loading, the incremental excess pore pressure caused by each set of cyclic loading kept decreasing due to a decreased void ratio caused by the dissipation of excess pore pressure during and after the previous cyclic loading. After three sets of cyclic loading, the accumulated excess pore pressure began to reduce, which suggested that no substantial excess pore pressure would be observed if more sets of cyclic loading were applied. This study demonstrated that drainage made normally consolidated clay more resistant to subsequent cyclic loading. Furthermore, it has been found that in order to avoid failure which could occur at a high loading frequency, a cyclic load at a lower frequency could be applied first followed by a higher frequency. The test results clearly suggest that for newly constructed railway lines, a train with a lower speed is preferred initially, until the track becomes stable for the next loading stage.

8.7 Model for radial consolidation under cyclic loading

When radial drainage was allowed during the application of a cyclic load, the dissipation of existing excess pore pressure and generation of internal excess pore pressure occurred simultaneously. Therefore a radial consolidation model under cyclic loading has been proposed by combining the theory of radial consolidation with the undrained cyclic model.

How accurate this proposed model could be was largely influenced by the generation of internal excess pore pressure. The existing model proposed by Sakai et al. (2003) simply assumed that the incremental internal excess pore pressure generated during a time period in a partially drained cyclic loading test was the same as during an undrained cyclic loading test. However, the magnitude of internal excess pore pressure generated during partially drained cyclic loading, which was affected by the stress history and dissipation of excess pore pressure, would differ from that obtained from undrained cyclic loading, In the current proposed model, the initial state of the soil was always updated for each loading step to predict the increment in excess pore pressure. The other limitation of the model proposed by Sakai et al. (2003) was the number of cycles which the model could handle. For example, if the soil failed at time t_f in an undrained condition, it would be impossible to use the generation of excess pore pressure in this undrained condition to

predict the behaviour under partially drained cyclic loading afterwards. But by using the proposed procedure in the current model, the generation of excess pore pressure was always available as long as the soil did not fail during partially drained cyclic loading.

A comparison was made between the prediction of this new model and the laboratory results. An acceptable agreement was found between them and therefore this proposed model was verified. Given the identical parameters, the critical cyclic stress ratio increased when ξ_1 and ξ_2 increased because ξ_1 and ξ_2 governed the generation rate of internal excess pore pressure. The larger the values of ξ_1 and ξ_2 are, the lower the generation rate of excess pore pressure, and therefore a higher cyclic stress ratio could be applied to obtain the same excess pore pressure compared to smaller values of ξ_1 and ξ_2. Furthermore, for given identical parameters, a higher critical cyclic stress ratio can be obtained as the coefficient of consolidation increases, because, the coefficient of consolidation controls how fast the pore water flows out. The larger the coefficient of consolidation, the faster the rate of dissipation of excess pore pressure, and therefore a higher cyclic stress ratio can be applied to achieve the same excess pore pressure compared to a smaller coefficient of consolidation.

A field case history in Sandgate, between Maitland and Newcastle, was used to verify the theoretical development of the radial consolidation model under cyclic loading. The measured settlement and lateral displacement were compared to the predictions of a multi-layered cyclic consolidation model where both vertical and horizontal drainage were considered. A good agreement was found between them. From this case study, it was demonstrated that the application of short PVDs at 2 m spacing was successfully implemented at the Sandgate Rail Grade Separation Project. In the absence of a conventional preloading embankment, the initial soil compression caused by low speed trains (<50 km/h) was accompanied by routine ballast packing to maintain the track elevation and alignment. Because the excess pore pressure dissipates through the PVDs during the cyclic loading and the subsequent rest period, the track then became more stable for the next loading stage. Even with the relatively short PVDs (8 m), both the predictions and field data proved that lateral displacement could be curtailed, effectively by the installation of PVDs.

8.8 Recommendations for future research work

It is recommended that further research be undertaken in the following areas:

(a) In the current research work, both undrained and partially drained tests were conducted on normally consolidated specimens. It is suggested that the behaviour of lightly to moderately overconsolidated soft clays under cyclic loading be investigated in future studies. The effectiveness of prefabricated vertical drains in dissipating the excess pore pressure in overconsolidated soft clays can be examined. Furthermore, the range of the overconsolidation ratio in which the PVDs are useful can then be investigated.

(b) The values of parameters ξ_1 and ξ_2 were back calculated, and therefore it would be beneficial to assess the values of ξ_1 and ξ_2 for different soil properties.

(c) Future work needs to be carried out to take into account the degradation of the shear modulus in the cyclic models.

(d) It is plausible that the model of radial consolidation under cyclic loading proposed in this thesis could be improved by:
   (1) Including the smear zone,
   (2) Including well resistance, and
   (3) Instead of using the average excess pore pressure over the whole soil cylinder to predict the initial state for the subsequent loading step, the excess pore pressure in each segment could be used to calculate the corresponding initial state.

9 Reference List

Abuel-Naga, H. M., Bergado, D. T., and Chaiprakaikeow, S. (2006). “Innovative thermal technique for enhancing the performance of prefabricated vertical drain system.” *Geotextile and Geomembranes*, 24(6), 359–370.

Adachi, T., Mimura, M., and Oka, F. (1985). “Descriptive accuracy of several existing constitutive models for normally consolidated clays.” *Proc. 5th Int. Conf. Numer. Meth. Geomech.*, Nagoya, 1, 259–266.

Airey, D. W. (1991). “Finite element analyses of triaxial tests with different end and drainage conditions.” *Proceedings of the 7th International Conference on Computer Methods and Advances in Geomechanics*, Vol. 1, ed. G. Beer, J. R. Booker and J. P. Carter. Balkema, Rotterdam, pp. 225–230.

Alberro, J., and Santoyo, E. (1973). “Long term behaviour of Mexico City clay.” *Proc. 8th Int. Conf. on Soil Mech. and Found. Engrg.*, 1, 1–9.

Aldrich, H. P. (1965). “Precompression for support of shallow foundations.” *J. Soil Mech. Found. Div.*, ASCE, 91(2), 5–20.

Andersen, K. H. (1976). “Behavior of clay subjected to undrained cyclic loading.” *Proceedings, International Conference on the Behavior of Off-Shore Structures* ’76, Vol. 1, Trondheim, Norway, 392–403.

Andersen, K. H., Pool, J. H., and Brown, S. F. (1980). “Cyclic and static laboratory tests on Drammen clay.” *J. Geotech. Engrg. Div.*, 106(GT5), 499–529.

Andersen, K. H., and Stenhamar, P. (1982). “Static Plate Loading Tests on Overconsolidated Clay.” *J. Geotech. Engrg. Div.*, 108(GT7), 918–934.

Andersen, K. H. (1988). “Properties of soft clay under static and cyclic loading.” *Proceedings of Int. Conf. Eng. Problems on Reg. Soils*, [S.1]: [s.n.], 7–26.

Andersen, K. H. (2009). “Bearing capacity under cyclic loading – offshore, along the coast, and on land. The 21th Bjerrum Lecture presented in Oslo, 23 November 2007.” *Can. Geotech. J.*, 46(5), 513–535.

Anderson, K. H., Brown, S. F., Foss, I., Pool, J. H., and Rosenbrand, F. W. (1976). “Effect of Cyclic Loading on Clay Behavior.” Proceedings of the Conference on Design and Construction of Offshore Structures, Institution of Civil Engineers, London, UK, 75–79.

Andreasson, B. A. (1979). “Deformation characteristics of soft, highplastic clays under dynamic loading conditions.” Ph.D. thesis, Chalmers Univ. of Technology, Gothenburg, Sweden.

Andreasson, B. A. (1981). “Dynamic deformation characteristics of a soft clay.” *Proc., Int. Conf. on Recent Advances in Geotechnical Earthquake Engineering and Soil Dynamics*, Vol. 1, St. Louis, Univ. of Missouri–Rolla, Rolla, Mo., 65–70.

Andrews, D. C. A., and Martin, G. R. (2002). “Criteria for liquefaction of silty soil.” *Proc., 12th World Conf. on Earthquake Engineering*, Auckland, New Zealand.

Ausal, A. M., and Erken, A. (1989). “Undrained behavior of clay under cyclic shear stresses.” *J. Geotech. Eng.*, 115(7), 968–983.

Babu, G. L. S., Pandian, N. S., and Nagaraj, T. S. (1993). “A re-examination of the permeability index of clays.” *Can. Geotech. J.*, 30, 187–191.

Baldi, G., Hight, D. W. and Thomas, G. E. (1988). “A reevaluation of conventional triaxial test methods.” *Advanced triaxial testing of soil and rock*, ASTM STP 977, 219-263.

Baracos, A., Graham, J., and Domaschuk, L. (1980). “Yielding and rupture in a lacustrine clay.” *Can. Geotech. J.*, 17(4), 559–573.

Barron, R. A. (1948). “Consolidation of fine-grained soils by drain wells.” Trans., 113, 718–742.

Basu, D., Basu, P., and Prezzi, M. (2006). “Analytical solutions for consolidation aided by vertical drains.” *Geomechanics and Geoengineering*, 1(1), 63–71.

Basu, P., Basu, D., and Prezzi, M. (2008). “Equal-strain analysis of PVD-enhanced consolidation considering soil disturbance.” *The 12th International Conference of International Association for Computer Methods and Advances in Geomechanics*, October, Goa, India, 1–6.

Bell, A. L. (1977). “A geotechnical investigation of post glacial estuarine deposits at Kinnegar, Belfast Lough.” PHD thesis, Queen’s University, Belfast.

Bergado, D. T., Balasubramaniam, A. S., Fannin, R. J., and Holts, R. D. (2002). “Prefabricated vertical drains (PVDs) in soft Bangkok clay: a case study of the new Bangkok International Airport project.” *Can. Geotech. J.*, 39, 304–315.

Berre, T., and Bjerrum, L. (1973). “Shear strength of normally consolidated clays.” *Proc. 8th Int. Conf. on Soil Mech. and Found. Engrg.*, 1, 39–49.

Bishop, A. W., and Green, G. E. (1965). “The influence of end restraint on the compression strength of a cohesionless soil.” *Geotechnique*, 15, 243–266.

Bishop, A. W., and Henkel, D. J. (1962). “The measurement of soil properties in the triaxial test.” Arnold, London, (2nd. ed.)

Boulanger, R. W., and Idriss, I. M. (2006). “Liquefaction susceptibility criteria for silts and clays.” *J. Geotech. Geoenviron. Eng.*, 132(11), 1413–1426.

Boulanger, R. W., Idriss, I. M., Stewart, D. P., Hashash, Y., and Schmidt, B. (1998). “Dranage capacity of stone columns or gravel drains for mitigating liquefaction.” *ASCE Geotechnical Special Publication*, 75(1), 678–690.

Bray, J. D., Sancio, R. B., Durgunoglu, T., Onalp, A., Youd, T. L., Stewart, J. P., Seed R. B., Cetin, O. K., Bol, E., Baturay, M. B., Christensen, C., and Karadayilar, T. (2004a). “Subsurface characterization at ground failure sites in Adapazari, Turkey.” *J. Geotech. Geoenviron. Eng.*, 130(7), 673–685.

Bray, J. D., Sancio, R. B., Riemer, M. F., and Durgunoglu, T. (2004b). “Liquefaction susceptibility of fine-grained soils.” *Proc., 11th Int. Conf. on Soil Dynamics and Earthquake Engineering and 3rd Int. Conf. on Earthquake Geotechnical Engineering*, D. Doolin et al., eds., Stallion Press, Singapore, 655–662.

Brown, S. F. (1996). “Soil mechanics in pavement engineering.” *Geotechnique*, 46(3), 383–426.

Brown, S. F., Lashine, A. K. F., and Hyde, A. F. L. (1975). “Repeated load triaxial testing of silty clay.” *Geotechnique*, 25(1), 95–114.

Cai, Y., and Cao, X. W. (1996). “Study of the critical dynamic stress and permanent strain of the subgrade-soil under the repeated load.” *Journal of Southwest Jiaotong University*, 31(1), 1–5. (in Chinese)

Cai, Z., and Raymond, G. P. (1994). “Moddelling the dynamic response of railway track to wheel/rail impact loading.” *Structural Engineering Mechanics*, 2(1), 95–112.

Carrillo, N. (1942). “Simple two- and three-dimensional cases in the theory of consolidation of soils.” *Journal of Mathematics and Physics*, 21(1), 1–5.

Carter, J. P. (1982). “Predictions of the non-homogeneous behaviour of clay in the triaxial test.” *Geotechnique*, 32, 55–58.

Carter, J. P., Booker, J. R., and Wroth, C. P. (1982). “A critical state soil model for cyclic loading.” Soil mechanics-transient and cyclic loading, Chichester: John Wiley & Sons, 219–252.

Casagrande, A., and Poulos, S. J. (1964). “Investigation of stress-deformation and strength characteristics of compacted clay.” In: Havard soil mechanics series, Cambridge, MA: Harvard University.

Casagrande, A., and Wilson, S. D. (1951). “Effect of rate of loading on the strength of clays and shales at constant water content.” *Geotechnique*, 2(3), 251–263.

Chai, J., Miura, N., and Bergado, D. T. (2008). “Preloading clayey deposit by vacuum pressure with cap drain: analyses versus performance.” *Geotextiles and Geomembranes*, 26(3), 220–230.

Chu, D. B., Stewart, J. P., Lee, S., Tsai, J. S., Lin, P. S., Chu, B. L., Seed, R. B., Hsu, S. C., Yu, M. S., and Wang, M. C. H. (2004). “Documentation of soil conditions at liquefaction and non-liquefaction sites from 1999 Chi-Chi (Taiwan) earthquake.” *Soil Dyn. Earthquake Eng.*, 24(9–10), 647–657.

Chu, J., Bo, M. W., and Choa, V. (2004). “Practical considerations for using vertical drains in soil improvement projects.” *Geotextiles and Geomembranes*, 22(1–2), 101–117.

Crooks, J. H. A., and Graham, J. (1976). “Geotechnical properties of Belfast estuarine deposits.” *Geotechnique*, 26(2), 293–315.

Degrande, G. (2001). “Free field vibrations during the passage of a Thalys high- speed train at variable speed.” *J. Sound Vib.*, 247(1), 131–144.

Dobry, R., Ladd, R. S., Yokel, F. Y., Chung, R. M., and Powell, D. (1982). “Prediction of pore-water pressure buildup and liquefaction of sands during earthquakes by the cyclic strain method.” National Bureau of Standards Building Science Series No. 138, July.

Dobry, R., Yokel, F. Y., and Ladd, R. S. (1981). “Liquefaction potential of overconsolidated sands in moderately seismic areas.” *Proc., Conf. on Earthquakes and Earthquake Engineering in the Eastern U.S.*, Knoxville, Tenn., J. E. Beavers, ed., Vol. 2, Ann Arbor Science, Inc./ The Butterworth Group, Ann Arbor, Mich.

Duncan, J. M., and Dunlop, P. (1968). “The significance of cap and base restraint.” *J Soil Mech Found Div*, 94(1), 271–290.

Dyvik, R., Dobry, R., Thomas, G. E., and Pierce, W. G. (1984). “Influence of consolidation shear stresses and relative density on threshold strain and pore pressure during cyclic straining of saturated sands.” Miscellaneous Paper, GL-84-15, Dept. of the Army, U.S. Army Corps of Engineers, Washington, D.C.

Erten, D., and Maher, M. H. (1995). “Cyclic undrained behaviour of silty sand.” *Soil Dynamics and Earthquake Engineering*, 14, 115–123.

Fellenius, B. H., and Wager, O. (1977). “Discussion of ‘Theoretical and practical aspects of the bahavior of vertical drains with special reference to geodrains.” *Proc., 9th Int. Conf. on Soil Mech. and found. Engrg.*, Tokyo, 3, 395–396.

France, J. W., and Sangrey, D. A. (1977). “Effects of drainage in repeated loading of clays.” *J. Geotech. Eng. Div.*, Proceedings of the American Society of Civil Engineers, 103(GT7), 769–785.

Frost, M. W., Fleming, P. R., and Rogers, C. D. F. (2004). “Cyclic triaxial tests on clay subgrades for analytical pavement design.” *Journal of Transportation Engineering*, 130(3), 378–386.

Geng, D. X., and Zhong, C. G. (2007) “Study on influence of embankment height on residual deformation under action of traffic load.” *Subgrade Engineering*, 6, 117–118. (in Chinese)

Geng, D. X., Zhong, C. G., and Zheng, M. X. (2007). “Study on residual deformation of soft foundation under vehicle load.” *Journal of East China Jiaotong University*, 24(4), 46–50. (in Chinese)

Gibson, R. E. (1963). “An analysis of system flexibility and its effect on time-Lag in pore-water pressure measurements.” *Geotechnique*, 13(1), 1–11.

Gong, Q. M., Liao, C. F., and Zhou, S. H. (2001). “Testing study of dynamic pore water perssure under train loading.” *Chinese Journal of Rock Mechanics and Engineering*, 20(S1), 1154–1157. (in Chinese)

Goulois, A. M., Whitman, R. V., and Hoeg, K. (1985). "Effects of sustained shear stresses on the cyclic degradation of clay."*Strength testing of marine sediments; ASTM STP 883*, R. C. Chaney and K. R. Demars, eds., ASTM, Philadelphia, Pa., 336–351.

Graham, J. (1969). “Laboratory results from Mastemyr quick clay after reconsolidation to the in situ stresses.” Internal Report F372-5. Oslo: Norwegian Geotechnical Institute.

Graham, J. (1974). “Laboratory testing of sensitivity clay from Lyndhurst, Ontario.” Civil Engineering Research Report CE74-2. Kingston, Ontario: Royal Military College of Canada.

Graham, J., Crooks, J. H. A., and Bell, A. L. (1983). “Time effects on the stress-strain behavior of soft natural clays.” *Geotechnique*, 33(3), 327–340.

Han, Z. L., and Zhang, Q. L. (2005). “Dynamic stress analysis on speed-increase subgrade of existing railway.” *China Railway Science*, 26(5), 1–5.

Hannon, J. B. (1986). “Wick drain selection and design.” *Transp. Circular No. 309*, National Research Council, Washington, D. C., 6–7.

Hansbo, S. (1981). “Consolidation of fine-grained soils by prefabricated drains.” *In Proceedings of the 10th International Conference on Soil Mechanics and Foundation Engineering*, Stockholm, Sweden, 15–19 June. Balkema, Rotterdam, the Netherlands, 3, 677–682.

Hansbo, S. (1993). “Band drains.” *Ground improvement*, M. P. Moseley, ed., CRC Press Inc., Boca Raton, Fla., 40–62.

Hansbo, S., and Torstensson, B. A. (1977). “Geodrain and other vertical drain behaviour.” *Proc., 9th Int. Conf. on Soil Mech. and found. Engrg.*, Tokyo, 1, 533–540.

Hausmann, M. R. (1990). “Preloading and the use of vertical drains.” *Engineering principles of ground modifications*. McGraw-Hill Inc., New York, N. Y., 245–271.

Huang, M. S., Li, J. J., and Li, X. Z. (2006). “Cumulative deformation behaviour of soft clay in cyclic undrained tests.” *Chinese Journal of Geotechnical Engineering*, 28(7), 891–895. (in Chinese).

Hight, D. W. (1983). “Laboratory investigations of sea bed clays.” Ph.D. thesis, Imperial College, London, U. K.

Hsu, C. C., and Vucetic, M. (2006). “Threshold shear strain for cyclic pore-water pressure in cohesive soils.” *J. Geotech. Geoenviron. Eng.*, 132(10), 1325–1335.

Hvorslev, M. J. (1951). “Time-lag and soil permeability in ground-water observations.” *Bull. No. 36, U.S. Waterways Expt Statn, Vicksburg.*

Hyde, A. F. L., and Brown, S. F. (1976). “The plastic deformation of a silty clay under creep ad repeated loading.” *Geotechnique*, 26(1), 173–184.

Hyde, A. F. L., and Ward, S. J. (1986). “The effect of cyclic loading on the undrained shear strength of a silty clay.” *Marine Geotechnology*, 6(3), 299–314.

Hyde, A. F. L., Yasuhara, K., and Hirao, K. (1993) “Stability cariteria for marine clay under one-way cyclic loading.” *J. Geotech. Engrg.*, 119(11), 1771–1789.

Hynes-Griffin, M. E. (1988) “Pore pressure generation characteristics of gravel under undrained cyclic loading.” Ph.D. dissertation, Univ. of California, Berkeley, Calif.

Hyodo, M., Yamamoto, Y., and Sugiyama, M. (1994). “Undrained cyclic shear behaviour of normally consolidated clay subjected to initial static shear stress.” *Soils and Foundations*, 34(4), 1–11.

Idriss. I. M., Dobry. R., Doyle. E. H., and Singh. R. D. (1976). "Behavior of soft clays during earthquake loading conditions." *Proc. Offshore Tech. Conf.*, Dallas. Tex ., 3.

Idriss. I. M., Dobry. R., and Singh. R. D. (1978). “Nonlinear behavior of soft clays during cyclic loading.” J. Geotech. Engrg. Div., 104(12), 1427–1447.

Indraratna, B., Balasubramaniam, A. S. and Balachandran, S. (1992). “Performance of test embankment constructed to failure on soft marine clay.” *J. Geotech. Engrg.*, 118(1), 12–33.

Indraratna, B., Rujikiatkamjorn, C., Ewers, B., and Adams, M. (2010). "Class A prediction of the behavior of soft estuarine soil foundation stabilized by short vertical drains beneath a rail track." *J. Geotech. Geoenviron. Eng.*,136(5), 686-696.

Indraratna, B., and Redana, I. W. (1998). "Laboratory determination of smear zone due to vertical drain installation." *J. Geotech. Geoenviron. Eng*., 124(2), 180–185.

Indraratna, B., and Redana, I. W. (1999). "Closure: Plane strain modeling of smear effects associated with vertical drains." *J. Geotech. Engrg*., 123(5), 474–478.

Ishibashi, I., Kawamura, M., and Bhatia, S. K. (1985). "Effect of initial shear on cyclic behaviour of sand." *J. Geotech. Engrg*., 111(12), 1395–1412.

Ishihara, K. (1993). "Dynamic Properties of Soils and Gravels from Laboratory Tests." Soil Dynamics and Geotechnical Engineering, Seco e Pinto ed., Balkema, Rotterdam, 1–17.

Jamiolkowski, M., Lancellotta, R., and Wolski, W. (1983). "Precompression and speeding up consolidation." *Proc., 8th ECSMFE*, A. A. Balkema, The Netherlands, 3, 1201–1226.

Jamiolkowski, M., Ladd, C. C., Germaine, J. T., and Lancelotta, R. (1985). 'New developments in field and laboratory testing of soils." *Proceedings of the 11th international conference on soil mechanics and foundation engineering*, San Fransisco, CA: A.A. Balkema, 57–153.

Jiang, H. W., and Zhao, X. H. (1997). "Study on anisotropic undrained shear strength of K_0-consolidated clays." *Rock and soil Mechanics*, 18(2), 1–7. (in Chinese)

Jiang, Y., Lei, H. Y., Zheng, G., and Yang, X. J. (2010). "Fractal study of microstructure variation of structured clays under dynamic laoding." *Rock and Soil Mechanics*, 31(10), 3075–3080. (in Chinese)

Johnson, S. J. (1970). "Precompression for improving foundation soils." *J. Soil. Mech. Found. Div*., ASCE, 96(1), 111–144.

Kallstenius, T., and Wallgren, A. (1956). "Pore-water pressure measurements in field investigations." *Proc. Roy. Swed. Geotech. Inst., No. 13*.

Katti, D. R., Tang, J. P., and Yazdani, I. (2003). "Undrained response of clays to varying strain rate." *J. Geotech. Geoenviron. Eng*., 129(3), 278–282.

Keedwell, M. J. (1984). "Rheology and soil mechanics." Elsevier Applied Science Publishers, London.

Koerner, R. M. (1994). "Wick drains." *Design with geosynthetics*, 3rd Ed., Prentice-Hall, Inc., Englewood Cliffs, N. J., 734–745.

Koester, J. P. (1992). “The influence of test procedure on correlation of Atterberg limits with liquefaction in fine-grained soils.” *Geotech. Test. J.*, 15(4), 352–360.

Konrad, J. M., and Wagg, B. T. (1993). “Undained cyclic loading of anisotropically consolidated clayey silts.” *J. Geotech. Engrg.*, 119(5), 929–947.

Kutara, K., Miki, H., Mashita, Y., and Seki, K. (1980). ‘‘Settlement andcountermeasures of the road with low embankment on soft ground.’’ Tech. Rep. of Civil Eng., 22(8), 13–16. (in Japanese)

Kutter, B. L., and Sathialingam, N. (1992). “Elastic-viscoplastic modelling of the rate-depent behaviour of clays.” *Geotechnique*, 42(3), 427–441.

Ladd, C. C., William, C. E., Connell, D. H., and Edgers, L. (1972). “Engineering properties of soft foundation clays at two south Louisiana levee sutes.” *Res. Resp. No. R72-26*, Massachusetts Inst. of Technol., Cambridge, Mass.

Ladd, R. S., Dobry, R., Dutko, P., Yokel, F. Y., and Chung, R. M. (1989). “Pore-water pressure buildup in clean sands because of cyclic straining.” *Geotech. Test. J.*, 12(1), 77–86.

Ladd, C. C. (1991). “Stability evaluation during staged construction.” *J. Geotech. Engrg.*, 117(4), 540–615.

Ladd, C. C., and Foott, R. (1974). “New design procedure for stability of soft clays.” *J. Geotech. Engrg. Div.*, 100(7), 763–786.

Ladd, C. C., Foott, R., Ishihara, K., Schlosser, F., and Poulos, H. G. (1977). “Stress deformation and strength characteristics.” *Proceedings of the ninth international conference on soil mechanics and foundation engineering*, 421–494.

Landau, R. E. (1966). “Method of installation as a factor in sand drain stabilization design.” *Hwy. Res. Rec., 133*, Hwy. Res. Board, Washington, D.C., 75–97.

Larew, H. G., and Leonards, G. A. (1962). “A strength criterion for repeated loads.” *Highway Research Board Proceedings*, 41, 529–556.

Lashine, A. K. (1971). “Some aspects of the characteristics of Keuper marl under repeated loading.” Ph.D. thesis, University of Nottingham, Nottingham, U. K.

Lee, K. L. (1978). “End restraint effects on undrained static triaxial strength of sand.” *Journal of Geotechnical Engineering Divisions*, 104, 687–703.

Lee, K. L., and Focht, J. A. (1976). “Strength of a clay subjected to cyclic loading.” *Mar. geotech.*, 1(3), 165–185.

Lefebvre, G., and LeBoeuf, D. (1987). “Rate effects and cyclic loading of sensitive clays.” *J. Geotech. Engrg.*, 113(5), 476–489.

Lefebvre, G., and Pfendler, P. (1996). “Strain rate and preshear effects in cyclic resistance of soft clay.” *J. Geotech. Engrg.*, 122(1), 21–26.

Lei, H. Y., Jiang, Y., and Lu, P. Y. (2007). “Experimental study of dynamic stress-strain relation of structural soft soil under traffic load.” *Chinese Journal of Rock Mechanics and Engineering*, 27(S1), 3052–3057. (in Chinese)

Leo, C. J. (2004). "Equal strain consolidation by vertical drains." *J. Geotech. Geoenviron. Eng.*, 130(3), 316–327.

Leroueil, S. (1996). “Compressibility of clays: fundamental and practical aspects.” *J. Geotech. Engrg.*, 122(7), 534–543.

Li, D. (1994). “Railway track granular layer thickness design based on subgrade performance under repeated loading.” Ph.D. dissertation, Department of Civil Engineering, University of Massachusetts, Amherst, Mass.

Li, T., and Meissner, H. A. (2002). “two-surface plasticity model for cyclic undrained behavior of clays.” *J. Geotech. Geoenviron. Eng.*, 128(7), 613–626.

Li, A. L., and Rowe, R. K. (2001). “Combined effects of reinforcement and prefabricated vertical drains on embankment performance.” *Can. Geotech. J.*, 38, 1266–1282.

Li, D. Q, and Selig, E. T. (1996). “Cumulative plastic deformation for fine grained subgrade soils.” *J. Geotech. Engrg.*, 122(12), 1006–1013.

Li, D. Q., and Selig, E. T. (1998a). “Method for railroad track foundation design. I: development.” *J. Geotech. Geoenviron. Eng.*, 124(4), 316–322.

Li, D. Q., and Selig, E. T. (1998b). “Method for railroad track foundation design. II: application.” *J. Geotech. Geoenviron. Eng.*, 124(4), 323–329.

Lin, H. D., and Wang, C. C. (1998). “Stress-strain-time function of clay.” *J. Geotech. Geoenviron. Eng.*, 124(4), 289–296.

Ling, J. M., Wang, W., and Wu, H. B. (2002). “On residual deformation of saturated clay subgrade under vehicle load.” *Journal of Tongji University*, 30(11), 1315–1320. (in Chinese)

Liu, J. K. (2006). Subgrade engineering, The Architecture and Building Industry Publishing House of China, Beijing.

Liu, T. J., and Mo, H. H. (2008). “Strain rate of saturated soft clay under long term cyclic loading.” *Journal of South China University of Technology (Natural Science Edition)*, 36(10), 37–42. (in Chinese)

Liu, J. K., and Xiao, J. H. (2010). “Experimental study on the stability of railroad silt subgrade with increasing train speed.” *J. Geotech. Geoenviron. Eng*., 136(6), 833–841.

Lo, D. O. K., and Mesri, G. (1994). “Settlement of test fills for Chek Lap Kok airport.” *Vertical and horizontal deformations of foundations and embankments*, A. T. Yeung and G. Y. Felio, eds., *Geotech. Spec. Publ*. No. *40*, ASCE, New York, N. Y., 2, 1082–1099.

Lorenzo, G. A., Bergado, D. T., Bunthai, W., Hormdee, D., and Phothiraksanon, P. (2004). “Innovations and performances of PVD and dual function geosynthetic applications.” *Geotextile and Geomembranes*, 22(1–2), 75–99.

Madhav, M. R., Park, Y. –M., and Miura, N. (1993). “Modelling and study of smear zones around band shaped drains.” *Soils and Foundations*, 33(4), 135–147.

Matasovic, N., and Vucetic, M. (1995). “Generalized cyclic-degradation-pore-pressure generation model for clays.” *J. Geotech. Engrg*., 121(1), 33–42.

Matsui, T., Ito, T., and Ohara, H. (1980). “Cyclic stress–strain history and shear characteristics of clay.” *J. Geotech. Eng. Div*., 106(10), 1101–1120.

McGown, A., and Hughes, F. H, (1981). “Practical aspects of the design and installation of deep vertical drains.” *Geotechnique*, 31(1), 67–90.

Mesri, G., and Choi, Y. K. (1985). “The uniqueness of the end-of-primary (EOP) void ratio-effective stress relationships.” *Proceedings of international conference of soil mechanics and foundation engineering (ICSMFE)*, 587–590.

Miller, G. A., Ten, S. Y., and Li, D. (2000). “Cyclic shear strength of soft railroad subgrade.” *J. Geotech. Geoenviron. Eng*., 126(2), 139–147.

Ohara, S., and Matsuda, H. (1988). “Study on the settlement of saturated clay layer induced by cyclic shear.” *Soils and Foundations*, 28(3), 103–113.

Olson, R. E., Daniel, D. E., and Liu, T. K. (1974). “Finite difference analyses for sand drain problem.” *Proc., ASCE Specialty Conf. on Anal. And Des. In Geotech. Engrg.*, ASCE, New York, N.Y., 1, 85–110.

Onoue, A. (1988). “Consolidation by vertical drains taking well resistance and smear into consideration.” *Soils and Foundations*, 28(4), 165–174.

Onoue, A., Ting, N. -H., Germaine, J. T., and Whitman, R. V. (1991). “Permeability of disturbed zone around vertical drains.” *In Proceeding of the Geotechnical Engineering*

Congress, Boulder, Colo., 10–12 June. Edited by F. G. Mclean, D. A. Campbell, and D. W. Harris. American Society of Civil Egineering, New York, 879–890.

O'Reilly, M. P., Brown, S. F., and Overy, R. F. (1991). "Cyclic oading of silty clay with drainage periods." *J. Geotech. Engrg*., 117(2), 354–362.

Peacock, W. H., and Seed, H. B. (1969). "Sand liquefaction under cyclic loading simple shear conditions." *J. soil Mech. Foundation Div*., 94(3), 689–709.

Penman, A. D. M. (1961). "A study of the response time of various types of piezometer." *Proc. Conf. Pore Pressure and Suction in Soils*, Buttevworths. London, pp. 53–58.

Perzyna, P. (1966). "The constitutive equations for rate sensitive plastic materials." *Q. Appl. Math*., 20, 321–332.

Pillai, R. J., Robinson, R. G., and Boominathan, A. (2011). "Effect of microfabric on undrained static and cyclic behaviour of kaolin clay." *J. Geotech. Geoenviron. Eng*., 137(4), 421–429.

Prashant, A., and Penumadu D. (2004). "Effect of intermediate principal stress on overconsolidated Kaolin clay." *J. Geotech. Geoenviron. Eng*., 130(4), 284–292.

Priest, J. A., and Powrie, W. (2009). "Determination of cyclic track modulus from measurement of track velocity during train passage." *J. Geotech. Geoenviron. Eng*., 135(11), 1732–1740.

Procter, D. C., and Khaffaf, J. H. (1984). "Cyclic triaxial tests on remoulded clays." *J. Geotech. Engrg*., 110(10), 1431–1445.

Puppala, A. J., Mohammad L. N., and Allen, A. (1999). "Permanent deformation characterization of subgrade soils from RLT test." *Journal of Materials in Civil Engineering*, 11(4), 274–282.

Qiu, Y. J. (1998). "Permanent deformation of subgrade soils: Laboratory investigation and application in mechanistic-based pavement design." Ph.D. thesis, Univ. of Arkansas, Ark.

Ramsamooj, D. V., and Alwash, A, J. (1990). "Prediction of cyclic response of soils." *Journal of Geotechnical Engineering*, 116(7), 1053–1072.

Richardson, J. M., and Whitman R. V. (1963). "Effect of strain-rate upon undrained shear resistance of a saturated remolded fat clay." *Geotechnique*, 13(4), 310–324.

Richart, F. E. Jr. (1959). "Review of the theories for sand draind." *Trans*., 124, 709–736.

Rixner, J. J., Kraener, S. R., and Smith, A. D. (1986). "Prefabricated vertical drains. Summary of research effort-final report." *Rep. No. FHWA-RD-86-169*, Vol. 2, Federal Highway Administraton, U. S. Dept. of Commerce, Washington, D. C.

Rowe, P. W. (1964). "The calculation of the consolidation of laminated varved or layered clays, with particular reference to sand drains." *Geotechnique*, 14(4), 321–340.

Rowe, P. W., and Barden, L. (1964). "Importance of free ends in triaxial. testing." *J Soil Mech Found*, 90(SM1), 1–27.

Rowe, R. K., and Li, A. L. (2005). "Geosynthetic-reinforced embankments over soft foundations." *Geosynthetics International*, 12(1), 50–85.

Rowe, R. K., and Taechakumthorn, C. (2008). "Combined effect of PVDs and reinforcement on embankment over rate sensitive soils." *Geotextile and Geomembranes*, 26(3), 239–249.

Rujikiatkamjorn, C., and Indraratna, B. (2009). "Design procedure for vertical drains considering a linear variation of lateral permeability within the smear zone." *Can. Geotech. J.*, 46, 270–280.

Saada, A. S., and Townsend, F. C. (1981). "Laboratory strength testing of soils, state of the art." *In Laboratory Shear Strength of Soil, ASTM. Special Technical Publication 740*, ed. R. N. Yong and F. C. Townsend. ASTM, Philadelphia, pp. 7–77.

Sakai, A., Samang, L., and Miura, N. (1996). "Behaviour of soft soils under undrained cyclic loading with initial shear stress." *Geotech. Engrg., J. of Southeast Asian Geotech. Society*, 27(2), 1–22.

Sakai, A., Samang, L., and Miura, N. (2003). "Partially-drained cyclic behavior and its application to the settlement of a low embankment road on silty-clay." *Soil and Foundations*, 43(1), 33–46.

Samarasinghe, A. M., Huang, Y. H., and Drnevich, V. P. (1982). "Permeability and consolidation of normally consolidated soils." *J. Geotech. Eng. Div.*, 108, 835–840.

Sangrey, D. A., Henkel, D. J., and Esrig, M. I. (1969). "The effective stress response of a saturated clay soil to repeated loading." *Can. Geotech. J.*, 6, 241–252.

Sangrey, D. A., Polard, W. S., and Egan, J. A. (1978). "Errors associated with rate of undrained cyclic testing of clay soils. In Cyclic geotechnical testing." American Society for Testing and Materials, Special Technical Publication STP 654, 280–294.

Sathananthan, I. and Indraratna, B. (2006). "Laboratory evaluation of smear zone and correlation between permeability and moisture content." *J. Geotech. Geoenviron. Eng.*, 132(7), 942–945.

Schanz, T., and Gussman, P. (1994). “The influence of geometry and end restraint on the strength in triaxial compression in numerical simulation.” *In Numerical Methods in Geotechnical Engineering*, ed. I. M. Smith. Balkema, Rotterdam, pp. 129–133.

Seed, H. B., and Booker, J. R. (1976). “Stabilisation of potentially liquefiable sand deposits using gravel drain systems.” Report No. EERC 76-10, Earthquake Engineering Research Center, University of California, Berkeley, Calif., Apr.

Seed, R. B., Cetin, K. O., Moss, R. E. S., Kammerer, A. M., Wu, J., Pestana, J. M., Riemer, M. F., Sancio, R. B., Bray, J. D., Kayen, R. E., and Faris, A. (2003). “Recent advances in soil liquefaction engineering: a unified and consistent framework.” Keynote Presentation, 26th Annual ASCE Los Angeles Geotechnical Spring Seminar, Long Beach, Calif.

Seed, H. B., and Chan, C. K. (1966). “Clay Strength under Earthquake Loading Conditions.*” Proc. Amer. Soc. Civil Eng*., 92(SM2), 53–78.

Seed, H. B., Chan, C. K., and Monismith, C. L. (1955). “Effects of repeated loading on the strength and deformation of compacted clays.” *Proc. Hwy. Res. Bd., #34*, 541–558.

Seed, H B., and Idriss, I. M. (1982). *Ground motions and soil liquefaction during earthquakes*, Earthquake Engineering Research Institute, Berkeley, Calif.

Shahu, J. T., Yudhbir, and Kameswara Rao, N. S. V. (1999). “A simple test methodology for soils under transportation routes.” *Geotechnique*, 49(5), 639–649.

Sharma, J. S., and Xiao, D. (2000). “Characterization of a smear zone around vertical drains by large-scale laboratory tests.” *Can. Geotech. J.*, 37(6), 1265–1271.

Sheahan, T. C., Ladd, C. C., and Germaine, J. T. (1996). “Rate-dependent undrained shear behaviour of saturated clay *J. Geotech. Engrg*., 122(2), 99–108.

Shen, S. L., Chai, J. C., Hong, Z. S., and Cai, F. X. (2005). “Analysis of field performance of embankments on soft clay deposit with and without PVD-improvement.” *Geotextiles and Geomembranes*, 23(6), 463–485.

Sheng, D., Westerberg, B., Mattsson, H., and Axelsson, K. (1997). “Effects of end restraint and strain rate in triaxial tests.” *Computers and Geotechnics*, 21(3), 163–182.

Singh, A., and Mitchell, L. K. (1968). “General stress-strain-time function for soils.” *J. Soil Mech. Div. Am. Soc. Civ. Engrs*., SM1, 21–46.

Sinha, A. K., Havanagi, V. G., and Mathur, S. (2007). “Inflection point method for predicting settlement of PVD improved soft clay under embankments.” *Geotextiles and Geomembranes*, 25(6), 336–345.

Soga, K., and Mitchell, J. K. (1996). “Rate dependent deformation of structured natural clays.” *Proceedings of Am Soc. Civ. Eng. Geotech.*, [S.1]: [s.n.], 243–257.

Sonu, C. J., Ito, K., and Osishi, H. (1993). “Harry Seed, liquefaction and the gravel drain.” *Civil Engng. (NY)*, 63(12), 58–60.

Stamatopoulos, A. C., and Kotzias, P. C. (1985). *Soil improvement by preloading*. Wiley Interscience, New York, N. Y.

Suiker, A. S. J., Selig, E. T., and Frenkel, R. (2005). “Static and cyclic triaxial testing of ballast and subballast.” *J. Geotech. Geoenviron. Eng.*, 131(6), 771–782.

Takahashi, M., Hight, D. W., and Vaughan, P. R. (1980). “Effective stress changes observed during undrained cyclic triaxial tests on clay.” International Symposium on Soils under Cyclic and Transient Loading, Swansea, 7-11 January, 201–209.

Takemiya, H. (2003). “Simulation of track-ground vibrations due to a high-speed train: the case of X-2000 at Ledsgard.” *J. Sound Vib.*, 261(3), 503–526.

Tang, X.W., and Onitsuka, K. (2000). “Consolidation by vertical drains under time dependent loading.” *International Journal for Numerical and Analytical Methods in Geomechanics*, 24(9), 739–751.

Tatsuoka, F. (1988). “Some recent developments in triaxial testing systems for cohesionless soils.” *Advanced Triaxial Testing of Soil and Rock*, ASTM STP 977, 7–67.

Tavenas, F., Jean, P., Leblond, P., and Leroueil, S. (1983a). “The permeability of natural soft clays, Part I: Methods of laboratory permeability measurement.” *Can. Geotech. J.*, 20, 629–644.

Tavenas, F., Jean, P., Leblond, P., and Leroueil, S. (1983b). “The permeability of natural soft clays, Part II: Permeability characteristics.” *Can. Geotech. J.*, 20, 645–660.

Taylor, D. W. (1948). Fundamentals of soil mechanics, Wiley, New York,

Terzaghi, K. (1943). *Theoretical Soil Mechanics*. New York, John Wiley and Sons.

Thomas, C. S., Charles, C. L., and John, T. G. (1996). “Rate-dependent undrained shear behaviour of saturated soil.” *J. Geotech. Engrg.*, 122(2), 99–108.

Turan, A. S., Hinchberger, D., and El Naggar, M. H. (2011). “influence of pore fluid viscosity on the dynamic properties of an artificial clay.” *J. Geotech. Geoenviron. Eng.*, 137(12), 1190–1201.

Vaid, Y. P., and Campanella, R. G. (1977). “Time-dependent behaviour of undisturbed clay.” *J. Geotech. Engrg. Div.*, 103(7), 693–709.

Vaid, Y. P., Robertson, P. K., and Campanella, R. G. (1979). "Strain rate behavior of St. Jean Viannery clay." *Can. Geotech. J.*, 16(1), 34–42.

Vucetic, M., et al. (1985). "Cyclic simple shear behavior of overconsolidated offshore clay." *Proceedings, Second International Conference on Soil Dynamics and Earthquake Engineering*, On board the liner Queen Elizabeth II, 107–116.

Vucetic, M., and Dobry, R. (1988). "Degradation of marine clays under cyclic loading." *J. Geotech. Engrg.*, 114(2), 133–149.

Vucetic, M., Lanzo, G., and Doroudian, M. (1998). "Damping at small strains in cyclic simple shear test." *J. Geotech. Geoenviron. Eng.*, 124(7), 585–594.

Walker, R. (2006). "Analytical solutions for modeling soft soil consolidation by vertical drains." Ph.D. thesis, University of Wollongong, Wollongong, Australia.

Walker, R., and Indraratna, B. (2006). "Vertical drain consolidation with parabolic distribution of permeability in smear zone." *J. Geotech. Geoenviron. Eng.*, 132(7), 937–941.

Walker, R., and Indraratna, B. (2007). "Vertical drain consolidation with overlapping smear zones." *Geotechnique*, 57(5), 463–467.

Wang, C. J., and Chen, Y. M. (2007). "Study on effect of traffic loading induced static deviator stress on undrained cyclic properties of saturated soft clay." *Chinese Journal of Geotechnical Engineering*, 29(11), 1742–1747. (in Chinese)

Wang, J. (2005). "The Stress-Strain and Strength Characteristics of Portaway Sand." Ph.D. dissertation, University of Nottingham.

Wang, J., and Cai, Y. Q. (2008). "Coupling effects of initial shear stress and loading rate on strength behaviours of saturated soft clay." Chinese Journal of Rock Mechanics and Engineering, 27(Supp. 2), 3321–3327. (in Chinese)

Whitman, R. V., Richardson, A. M., and Healy, K. A. (1961). "Time-lags in pore pressure measurements." *Proc. 5th Int. Conf. Soil Mech.*, 1, 407–411.

Wilson, N. E., and Greenwood, J. R. (1974). "Pore pressures and strains after repeated loading of saturated clay." *Can. Geotech. J.*, 11(2), 269–277.

Wood, D. M. (1990). "Soil behaviour and critical state soil mechanics." Cambridge, England/New York: Cambridge University Press, p. 462.

Woods, R. D. (1991). "Field and laboratory determination of soil properties at low and high strains." *Proc. 2nd Int. Conf. on Recent Advances in Geotech. Earthquake Engrg.* and Soil Dynamics, Vol. 2, Univ. of Missouri-Rolla, Rola, Mo., 1727–1741.

Woods, R. D. (1994). “Laboratory measurements of dynamic soil properties.” *Dynamics Geotechnical Testing II, ASTM STP1213,* ASTM, West Conshohocken, Pa., 165–190.

Yamanouchi, T., and Yasuhara, K. (1975). “Settelement of clay subgrade after opening to traffic.” *Proceedings of 2nd Australia and New Zealand Conference Geomechanics*, Brisbane, 1, 115–200.

Yang, G. Q. (2003). “Study of dynamic performance of cement improved soil.” *Chinese Journal of Rock Mechanics and Engineering*, 22(7), 1156–1160. (in Chinese)

Yang. G. Q., and Guan, Z. X. (2001). “Experimental study on improved soil for high-speed railway subgrade.” *Chinese Journal of Geotechnical Engineering*, 23(6), 659–662. (in Chinese)

Yang, L.A., Powrie, W., and Priest, J. A. (2009). “Dynamic stress analysis of a ballasted railway track bed during train passage.” *J. Geotech. Geoenviron. Eng*., 135(5), 680–689.

Yang, P., Tang, Y. Q., and Shen, F. (2007). “Deformation characteristics of hydraulic fill under traffic loading in Shanghai.” *Journal of Engineering Geology*, 15(6), 823–827. (in Chinese)

Yang, P., Tang, Y. Q., and Zhou, N. Q. (2008). “Study on pore water pressure of hydraulic fill under traffic loading.” *Chinese Journal of Underground Space and Engineering*, 4(2), 253–258. (in Chinese)

Yao, H. L., Ma, S. D., and Lu, Y. F. (1994). “Some properties of normally-consolidated soild and overconsolidated aoils and determination of its stress history.” *Pock and Soil Mechanics*, 15(3), 38–45. (in Chinese)

Yasuda, S., Ishihara, K., Harada, K., and Sinkawa, N. (1996). “Effect of soil improvement on ground subsidence due to liquefaction.” *Soils Foundations*, 99–108. Special issue on the geotechnical aspects of the January, 17, 1995, Hyogoken-Nanbu earthquake.

Yasuhara, K. (1985). “Undrained and drained cyclic triaxial tests on a marine clay.” *Proc. 11th International Conf. Soil Mech. and Founds. Eng.*, San Francisco, USA, 2, 1095–1098.

Yasuhara, K. (1995). “Consolidation and settlement under cyclic loading.” *Proceedings of the international symposium on compression and consolidation of clayey soils*, Hiroshima.

Yasuhara, K., and Andersen, K. H. (1991). “Recompression of normally consolidated clay after cyclic loading.” *Soils and Foundations*, 31(1), 83–94.

Yasuhara, K., Hirao, K., and Hyodo, M. (1988). “Partially-drained behaviour of clay under cyclic loading.” *Proc. 6th Intn’l. Conf. Numerical Methods in Geomechanics*, 659–664.

Yasuhara, K., and Hirao, K. (1989). “Changes in undrained strengrh of clay after cyclic loading.” Technical Report of Geotechnical Research Institute, Nishinippon Institute of Technology, 5, 15–30.

Yasuhara, K., Murakami, S., Song, B. W., Yokokawa, S., and Hyde, A. F. L. (2003). “Postcyclic degradation of strength and stiffness for low plasticity silt.” *J. Geotech. Geoenviron. Eng.*, 129 (8), 756–769.

Yasuhara, K., Ue, S., and Fujiwara, H. (1983). “Undrained shear behaviour of quasi-overconsolidated clay.” *Proc. IUTAM Symp. On Seabed Mechanics*, Graham and trotman, London, England, 17–24.

Yasuhara, K., Yamanouchi, T., and Hirao, K. (1982). “Cyclic strength and deformation of normally consolidated clay.” *Soils and Foundations*, 22(3), 77–91.

Yeung, A. T. (1997). “Design curves for prefabricated vertical drains.” *J. Geotech. Geoenviron. Eng.*, 123(8), 755–759.

Yildirim, H., and Ersan, H. (2007). “Settlements under consecutive series of cyclic loading.” *Soil Dynamics and Earthquake Engineering*, 27(6), 577–585.

Yoshikuni, H., and Nakanodo, H. (1974). “Consolidation of fine-grained soils by drain wells with finite permeability.” *Japan Soc. Soil Mechanics and Foundation Engineering*, 14(2), 35–46.

Zeng, G. X., and Xie, K. H. (1989). “New development of the vertical drain theories.” *Proc., 12th ICSMFE*, A. A. Balkema, The Netherlands, 2, 1435–1438.

Zhang, H., and Garga, V. K. (1997). “Quasi-steady state: a real behavior?” *Can Geotech J*, 34, 749–61.

Zhao, J. M., Liu, S. Y., and Shi, M. L. (2007). “Experimental study on dynamic response of low embankment under traffic load.” *Journal of Southeast University (Natural Science Edition)*, 37(5), 921–925. ,(in Chinese)

Zhou, J., and Gong, X. N. (2001). “Strain degradation of saturated clay under cyclic loading.” *Can. Geotech. J.*, 38(1), 208–212.

Zhou, J., Tu, H. Q., and Yaswhara, K. (1996). “A model for predicting the cyclic behaviour of soft clay.” *Rock and Soil Mechanics*, 17(1), 54–60. (in Chinese)

Zhu, Z. Y., Ling, X. C., and Hu, Q. L. (2007). “Experimental study on dynamic strain rate of frozen soil from railway embankment of Qinghai-Tibet railway in China.” *Chinese Journal of Geotechnical Engineering*, 29(10), 1472–1476. (in Chinese)

Zhu, Z. Y., Ling, X. Z., Chen, S. J., Zhang, F., Wang, Z. Y., Wang, L. N., and Zou, Z. Y. (2011). “Analysis of dynamic compressive stress induced by passing trains in permafrost subgrade along Qinghai-Tibet railway.” *Cold Regions Science and Technology*, 65, 465–473.

Zhu, G., and Yin, J. -H. (2001). “Consolidation of soil with vertical and horizontal drainage under ramp load.” *Geotechnique*, 51(4), 361–367.

Zhu, G., and Yin, J. –H. (2004). “Consolidation analysis of soil with vertical and horizontal drainage under ramp loading considering smear effects.” *Geotextiles and Geimembranes*, 22(1–2), 63–74.

Zhu, Z. T., Zhou J., and Hu, X. Y. (1998) “Analysis on dynamic settlement of a saturated soft clay under the action of a long term dynamic load.” *Harbor Engineering*, 6, 1–5. (in Chinese)

Zimmie, T. F., and Lien, C. Y. (1986). “Response of clay subjected to combined cyclic and initial static shear stress.” *Proceedings of the 3rd Can. Conf. on Marine Geotech. Engrg.*, [S.l.]：[s.n.], 655–675.

10 Appendix A: The Newton-Raphson Method

The Newton-Raphson method, or Newton Method, is a powerful technique for solving equations numerically. Like so much of the differential calculus, it is based on the simple idea of linear approximation. The Newton Method, properly used, usually homes in on a root with devastating efficiency.

Let $f(x)$ be a well-behaved function, and let x^* be a root of the equation $f(x)=0$. We start with an estimate x_0 of x^*. From x_0, we produce a new estimate x_1. From x_1, we produce a new estimate x_2. From x_2, we produce a new estimate x_3. We go on until we are close enough to x^*. The above general style of proceeding is called iterative. The details are described below.

Let x_0 be a good estimate of x^* and let $x^* = x_0 + h$. Since the true root is x^*, and $h = x^* - x_0$, the number h measures how far the estimate x_0 is from the truth. Since h is small, we can use the linear (tangent line) approximation to conclude that:

$$0 = f(x^*) = f(x_0 + h) \approx f(x_0) + hf'(x_0) \tag{A.1}$$

and therefore, unless $f'(x_0)$ is close to 0, the following equation holds:

$$h \approx -\frac{f(x_0)}{f'(x_0)} \tag{A.2}$$

It follows that:

$$x^* = x_0 + h \approx x_0 - \frac{f(x_0)}{f'(x_0)} \tag{A.3}$$

Our new improved estimate x_1 of x^* is therefore given by:

$$x_1 = x_0 - \frac{f(x_0)}{f'(x_0)} \tag{A.4}$$

The next estimate x_2 is obtained from x_1 in exactly the same way as x_1 was obtained from x_0:

$$x_2 = x_1 - \frac{f(x_1)}{f'(x_1)} \tag{A.5}$$

Continue in this way. If x_n is the current estimate, then the next estimate x_{n+1} is given by:

$$x_{n+1} = x_n - \frac{f(x_n)}{f'(x_n)} \tag{A.6}$$

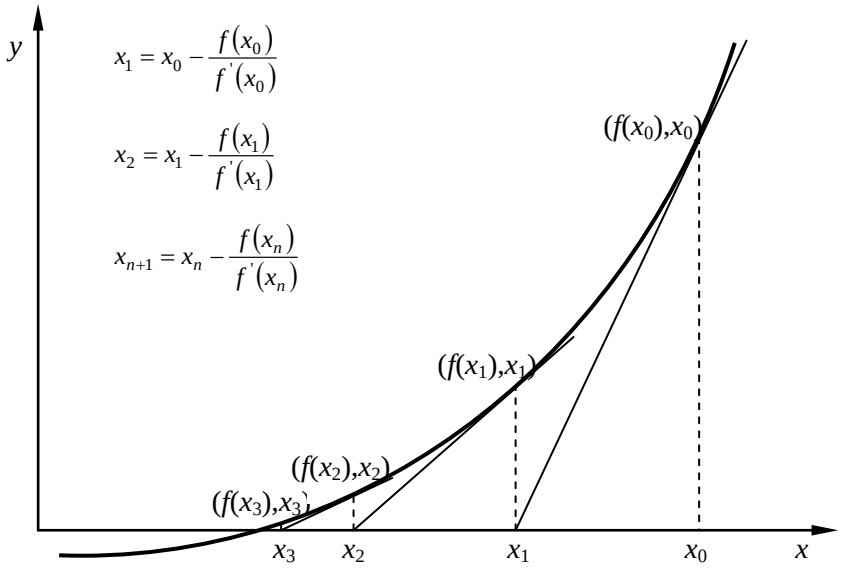

Fig. 10.1 The Newton-Raphson Method